
Doctoral Dissertations

Student Theses and Dissertations

Spring 2019

Provenance and depositional environments of the upper Permian-lowermost Triassic fluvial and lacustrine sandstones, Wutonggou low-order cycle, Bogda Mountains, NW China

Dongyu Zheng

Follow this and additional works at: https://scholarsmine.mst.edu/doctoral_dissertations



Part of the [Geology Commons](#), and the [Sedimentology Commons](#)

Department: Geosciences and Geological and Petroleum Engineering

Recommended Citation

Zheng, Dongyu, "Provenance and depositional environments of the upper Permian-lowermost Triassic fluvial and lacustrine sandstones, Wutonggou low-order cycle, Bogda Mountains, NW China" (2019). *Doctoral Dissertations*. 2800.

https://scholarsmine.mst.edu/doctoral_dissertations/2800

This thesis is brought to you by Scholars' Mine, a service of the Missouri S&T Library and Learning Resources. This work is protected by U. S. Copyright Law. Unauthorized use including reproduction for redistribution requires the permission of the copyright holder. For more information, please contact scholarsmine@mst.edu.

PROVENANCE AND DEPOSITIONAL ENVIRONMENTS OF THE UPPER
PERMIAN-LOWERMOST TRIASSIC FLUVIAL AND LACUSTRINE
SANDSTONES, WUTONGGOU LOW-ORDER CYCLE, BOGDA MOUNTAINS, NW
CHINA

by

DONGYU ZHENG

A DISSERTATION

Presented to the Faculty of the Graduate School of the
MISSOURI UNIVERSITY OF SCIENCE AND TECHNOLOGY

In Partial Fulfillment of the Requirements for the Degree

DOCTOR OF PHILOSOPHY

in

GEOLOGY AND GEOPHYSICS

2019

Approved by

Wan Yang, Advisor
John P. Hogan
David J. Wronkiewicz
Andreas Eckert
Jonathan Obrist-Farner
Mingli Wan

© 2019

Dongyu Zheng

All Rights Reserved

PUBLICATION DISSERTATION OPTION

This dissertation consists of the following two articles which have been submitted for publication, or will be submitted for publication as follows:

Paper I, pages 3 to 48, is titled “Provenance of Upper Permian-Lowermost Triassic Sandstones, Wutonggou Low-Order Cycle, Bogda Mountains, NW China: Implications on the Unroofing History of the Eastern North Tianshan Suture,” has been submitted to the Journal of Asian Earth Sciences.

Paper II, pages 49 to 82, is titled “Textural Characteristics and Their Controlling Processes of Upper Permian-Lowermost Triassic Sandstones, Wutonggou Low-Order Cycle, Bogda Mountains, NW China,” and are intended for submission to the Journal of Paleogeography.

ABSTRACT

This work integrates petrographic and fieldwork studies and documents the spatial and temporal distributions of compositions and textures of the upper Permian-lowermost Triassic fluvial-lacustrine sandstones, Wutonggou low-order cycle (WTG LC), Bogda Mountains, NW China. In the first part, three petrofacies are identified on the basis of the relative abundances of quartz, feldspar, and lithics and conglomerate compositions and paleocurrent directions are documented. These data indicate that rocks of the eastern North Tianshan Suture (ENTS) and rift shoulders were the provenance lithology. Moreover, the upsection changes of petrofacies and conglomerate compositions suggest that the lithology of ENTS changed. During approximately Wuchiapingian, the eastern part of ENTS included the subduction complex, whereas the western part contained the undissected volcanic arc. During approximately Changhsingian to early Induan, the eastern part of ENTS was dominated with the transitional volcanic arc and subordinate with the subduction complex, whereas the subduction complex was exposed in the western part of ENTS. The second part documents the textural characteristics of the sandstones of WTG LC. Textures of different petrofacies are different in grain size, sorting, roundness, and textural maturity, indicating provenance is a major control factor in sandstone textures. Moreover, each petrofacies is subdivided into littoral/beach, deltaic, and fluvial sedimentary facies, of which the textural characteristics are similar. This work improves our understanding of the nature and the unroofing history of ENTS and factors in controlling compositions and textures of fluvial-lacustrine sandstones.

ACKNOWLEDGEMENTS

I would like to express my deep gratitude to my advisor, Dr. Wan Yang for his tremendous help, both in my research and in my life. He is my idol who motivates me to be generous, perseverant, and energetic. I would like to thank my committee members, Drs. Jonathan Obrist-Farner, Mingli Wan, David Wronkiewicz, John Hogan, and Andreas Eckert for their help to share their ideas and to improve this study. I thank all the faculty and staff in GGPE for their help. I thank the Alfred Sprend Award for funding a part of this study.

I would like to thank Yiran Lu, Jing Duan, Xin Zhan, Jaimeson Fredericks, Ziyue Ju, Xiaokaiti Nilufar and Mr. J.J. Li for their help in the field and Xiaowei Peng, Bin Sun, Dr. Zhixin Li, Muneer Abdalla, Dr. Walaa Award, Yuxing Wu, Dr. Xin Jiao, Qiuwan Yu, Yizuo Shi, Leixin Ouyang, Cheng Zhang, Jie Xu, Le Lin, and Xiang Lu for their ideas, help, and suggestions.

I would like to thank Sixuan Wu for for her support, encouragement, and love.

I would like to thank my parents for their unconditional love and support for so many years. Their love is always my motivation to conquer challenges. Without them, I could not complete this work. This is for them.

TABLE OF CONTENTS

	Page
PUBLICATION DISSERTATION OPTION	iii
ABSTRACT.....	iv
ACKNOWLEDGEMENTS.....	v
LIST OF ILLUSTRATIONS.....	ix
LIST OF TABLES.....	xi
 SECTION	
1. INTRODUCTION	1
 PAPER	
I. PROVENANCE OF UPPER PERMIAN-LOWERMOST TRIASSIC SANDSTONES, WUTONGGOU LOW-ORDER CYCLE, BOGDA MOUNTAINS, NW CHINA: IMPLICATIONS ON THE UNROOFING HISTORY OF THE EASTERN NORTH TIANSHAN SUTURE	3
ABSTRACT.....	3
1. INTRODUCTION	4
2. GEOLOGICAL BACKGROUND.....	6
3. DATA AND METHODOLOGY.....	11
4. RESULTS	13
4.1. FRAMEWORK GRAINS.....	14
4.1.1. Quartz.....	14
4.1.2. Feldspars.....	14
4.1.3. Lithic Fragments.....	16
4.1.4. Accessory Minerals.....	16
4.2. MATRIX, CEMENT, AND SANDSTONE CLASSIFICATION	16

4.3. COMPOSITION OF GRAVELS AND PALEOCURRENT MEASUREMENTS.....	18
4.4. PETROFACIES AND IMPLICATIONS ON LITHOLOGY AND TECTONIC SETTINGS OF SOURCE AREAS.....	19
4.4.1. Petrofacies 1.....	19
4.4.2. Petrofacies 2.....	26
4.4.3. Petrofacies 3.....	27
5. STRATIGRAPHIC DISTRIBUTION OF PETROFACIES AND EVOLUTION OF PROVENANCE.....	28
5.1. PROVENANCE OF ZHAOBISHAN SECTION.....	28
5.2. PROVENANCE OF NORTH TARLONG SECTION.....	31
5.3. PROVENANCE OF TAODONGGOU SECTION.....	31
5.4. PROVENANCE OF DALONGKOU SECTION.....	32
5.5. SPATIAL CORRELATION OF PETROFACIES.....	33
6. THE UNROOFING HISTORY OF THE EASTERN NORTH TIANSHAN SUTURE.....	36
7. CONCLUSIONS.....	39
ACKNOWLEDGEMENTS.....	41
REFERENCES.....	41
II. TEXTURAL CHARACTERISTICS AND THEIR CONTROLLING PROCESSES OF UPPER PERMIAN-LOWERMOST TRIASSIC SANDSTONES, WUTONGGOU LOW-ORDER CYCLE, BOGDA MOUNTAINS, NW CHINA.....	49
ABSTRACT.....	49
1. INTRODUCTION.....	50
2. GEOLOGICAL BACKGROUND.....	51
3. DATA AND METHODOLOGY.....	56
4. RESULTS.....	58

4.1. TEXTURAL CHARACTERISTICS OF PETROFACIES 1	59
4.2. TEXTURAL CHARACTERISTICS OF PETROFACIES 2	61
4.3. TEXTURAL CHARACTERISTICS OF PETROFACIES 3	66
5. CONTROLS ON TEXTURE CHARACTERISTICS	70
5.1. PROVENANCE.....	70
5.2. DEPOSITIONAL ENVIRONMENTS	73
6. CONCLUSIONS.....	76
ACKNOWLEDGEMENTS	77
REFERENCES	77
SECTION	
2. CONCLUSIONS.....	83
APPENDICES	
A. ZHAOBISHAN SECTION.....	85
B. GRAIN SIZE DISTRIBUTION.....	152
BIBLIOGRAPHY.....	168
VITA.....	171

LIST OF ILLUSTRATIONS

PAPER I	Page
Figure 1. Tectonic map of the Central Asian Orogenic Belt.. .. .	6
Figure 2. Tectonic map of eastern Xinjiang.	9
Figure 3. Geological maps of Zhaobishan (A), Tarlong-Taodonggou (B), and Dalongkou (C) areas.	10
Figure 4. Chrono-, litho-, and cyclostratigraphy of upper Carboniferous-Middle Triassic strata in Bogda Mountains.	11
Figure 5. Highly-simplified lithological columns, sample names and locations, paleocurrent data, compositions of gravels, and petrofacies.	13
Figure 6. Photomicrographs of sandstones in the Wutonggou low-order cycle (WTG)..	17
Figure 7. Ternary diagrams with mean compositions and classifications of petrofacies of Wutonggou sandstones.	25
Figure 8. Correlation of petrofacies distribution of Wutonggou sandstones in five sections in the study area.	30
Figure 9. QFL ternary diagram of upper Permian-lowermost Triassic sandstones in Bogda Mountains and Turpan Basin.	34
Figure 10. Unroofing trends of sources area in eastern North Tianshan Suture, as interpreted from petrofacies of WTG sandstones in Bogda Mountains.....	38
Figure 11. Schematic maps showing the reconstruction of lithologic distributions in the source areas in the eastern North Tianshan Suture during late Permian- earliest Triassic.....	40
 PAPER II	
Figure 1. Tectonic map of study areas.	53
Figure 2. Geological maps of Zhaobishan (A), Tarlong-Taodonggou (B), and Dalongkou (C) areas	54
Figure 3. Chrono-, litho-, and cyclostratigraphy of upper Carboniferous-Middle Triassic strata in Bogda Mountains.	55

Figure 4. Sedimentary facies and descriptions	57
Figure 5. QFL ternary diagram and petrofacies	59
Figure 6. Simplified stratigraphic column of ZBS section showing compositions and textures of sandstones of Wutonggou low-order cycle	63
Figure 7. Simplified stratigraphic column of NTRL section showing compositions and textures of sandstones of Wutonggou low-order cycle.	64
Figure 8. Simplified stratigraphic column of TDG section showing compositions and textures of sandstones of Wutonggou low-order cycle.	65
Figure 9. Simplified stratigraphic column of DLK section showing compositions and textures of sandstones of Wutonggou low-order cycle.	67
Figure 10. Box and whisker plot of graphic means and inclusive standard deviations of PF1, PF2, and PF3.	72
Figure 11. Bivariate plot of standard deviation versus skewness of petrofacies 1 sandstones.	74
Figure 12. Bivariate plot of standard deviation versus skewness of petrofacies 2 sandstones.....	74
Figure 13. Bivariate plot of standard deviation versus skewness of petrofacies 3 sandstones	75

LIST OF TABLES

PAPER I	Page
Table 1. Raw and recalculated grain types and categories for point-counting and petrofacies classification	15
Table 2. Percentages of different types of framework grains derived from raw point-counting data.....	21
Table 3. Conglomerate compositions	24
PAPER II	
Table 1. Compositional and textural characteristics of petrofacies 1	62
Table 2. Compositional and textural characteristics of petrofacies 2	68
Table 3. Compositional and textural characteristics of petrofacies 3	69

1. INTRODUCTION

The Central Asian Orogenic Belt (CAOB) is one of the largest accretionary orogen on Earth and formed by many episodes of accretion and collision (Sengör et al., 1993; Sengör and Natl'in, 1996; Windley, 2007; Xiao et al., 2013). The eastern North Tianshan Suture was one of the key element in the southern CAOB and marked the closure of the southern segment of the Paleo-Asian Ocean (Xiao et al., 2009, 2013). Therefore, ENTS is critical to understand the final assembly of the southern CAOB. Most studies work on the rocks exposed in the present ENTS (e.g., Allen et al., 1993; Gao et al., 1998; Xiao et al., 2004; Charvet et al., 2011). However, as the ENTS was formed during Late Paleozoic, abundant rocks of the ancient ENTS were eroded and deposited in the adjacent basins and detailed works on these rocks are necessary to reconstruct the ancient ENTS. Sandstones in the greater Turpan-Junggar basin, about 100 km north of ENTS, provide clues on reconstructing the eroded ENTS. The reconstruction cannot be achieved by previous petrographic studies of sandstones in the greater Turpan-Junggar basin due to the out-of-date stratigraphy, large sampling spacing, and limited studied sections (Carroll et al., 1995; Shao et al., 2001; Greene et al., 2005; Guan et al., 2010; Guan, 2011). Therefore, a detailed provenance study of the sandstones are required.

In addition, the composition and texture of sandstones record the tectonic, climatic, transportation and depositional processes on Earth's surface (Suttner, 1974; Ingersoll, 1984; Johnsson, 1993). Although numerous studies have been conducted to investigate the relationships between composition and texture of sandstones and their controlling factors, these relationships are still not well understood, especially the

relationship between the texture and depositional environments. Many studies suggest that textures of sandstones are good criteria to distinguish different lithofacies, whereas others demonstrates that the textural characteristics should be restricted to the purpose of description (Folk and Ward, 1957; Friedman, 1962, 1967; Enrlich, 1983; Ehrlich and Full, 1987; Hartmann, 2007).

This study focuses on the upper Permian-lowermost Triassic fluvial-lacustrine sandstones of Wutonggou low-order cycle in Bogda Mountains, NW China to document a comprehensive analysis of compositions and textures of these sandstones. The aim of this study is to present the temporal and spatial trends of the composition and texture of sandstones of Wutonggou low-order cycle, to interpret the provenance of sandstones in Bogda Mountains and the unroofing history of the provenance, and to investigate the controlling factors on the composition and texture of fluvial-lacustrine sandstones. The compositional and textural characteristics of sandstones of Wutonggou low-order cycle indicate that rocks in both ENTS and rift shoulders were the provenance lithology, two unroofing trends exist in ENTS, and provenance is a dominant control in sandstone textures. This study improves our understanding of the nature and unroofing process of ENTS during late Permian-earliest Triassic and provides clues on the controlling processes on compositional and textural characteristics of fluvial-lacustrine sandstones.

PAPER

I. PROVENANCE OF UPPER PERMIAN-LOWERMOST TRIASSIC SANDSTONES, WUTONGGOU LOW-ORDER CYCLE, BOGDA MOUNTAINS, NW CHINA: IMPLICATIONS ON THE UNROOFING HISTORY OF THE EASTERN NORTH TIANSHAN SUTURE

Dongyu Zheng and Wan Yang

ABSTRACT

The upper Permian-lowermost Triassic sandstones in Wutonggou low-order cycle (WTG) exposed in Bogda Mountains, NW China, provide clues to reconstruct the eroded lithologies of the eastern North Tianshan Suture (ENTS). Petrographic point counting data, compositions of conglomerates and paleocurrent directions from Zhaobishan (ZBS), North Tarlong (NTRL), Taodonggou (TDG) sections in the southern, and Dalongkou (DLK) section in the northern foothills of Bogda Mountains are used to interpret the provenance and to reconstruct the unroofing history of ENTS. Three petrofacies are defined by the relative abundance of quartz, feldspar, and lithic framework grains. Petrofacies 1 (PF1) has mean compositions of $Q_{51}F_{30}L_{19}$ and $Qm_{21}F_{30}Lt_{49}$ and occurs in the lower ZBS, upper NTRL and middle TDG sections. Petrofacies 2 (PF2) has mean compositions of $Q_{28}F_{36}L_{36}$ and $Qm_{14}F_{36}Lt_{50}$ and occurs in the upper ZBS section. Petrofacies 3 (PF3) has mean compositions of $Q_8F_{13}L_{79}$ and $Qm_2F_{13}Lt_{85}$ and occurs in the lower NTRL, lower and upper TDG, and DLK sections. The upsection change from PF1 to PF2, the occurrence of quartzite and granite gravels in the upper part and northward

paleocurrent directions in ZBS section indicate that the sources changed from an undissected volcanic arc, accretionary wedge and trench to predominant transitional volcanic arc and subordinate accretionary wedge and trench in ENTS. The upsection changes from PF3 to PF1 in NTRL and TDG sections and the occurrence of granitic gravels in the upper part indicate that the sources shifted from an undissected volcanic arc in ENTS and local rift shoulders to transitional volcanic arc, accretionary wedge and trench. The occurrence of PF3 and variable paleocurrent directions in DLK section suggest that the sediments were derived from the undissected volcanic arc in ENTS and rift shoulders.

An approximately coeval provenance shift of the WTG sandstones suggest persistent unroofing and probably uplift of ENTS during late Permian-earliest Triassic. During Wuchiapingian, the eastern part of ENTS consisted of the undissected volcanic arc, accretionary wedge and trench, and the western part an undissected volcanic arc. During Changhsingian to early Induan, a transitional volcanic arc in the eastern part of ENTS, and transitional volcanic arc, accretionary wedge and trench in the western part were exposed. The different unroofing trends for the eastern and western parts of ENTS indicate that the ENTS was an amalgamated complex with spatial and temporal variations in lithology during late Permian-earliest Triassic.

1. INTRODUCTION

The Central Asian Orogenic Belt (CAOB) is one of the accretionary orogens that were the main sites of continental growth since Phanerozoic and resulted from the

accretion and collision of magmatic arcs, accretionary complexes, trapped oceanic plates, and trailing continental plates (Sengör et al., 1993; Sengör and Natl'in, 1996; Windley, 2007; Xiao et al., 2013). The eastern North Tianshan Suture (ENTS), located in the southern part of CAO (Figure 1), marks the closure of the North Tianshan Ocean, which was the major southern segment of the Paleo-Asian Ocean (e.g., Xiao et al., 2009, 2013). Detailed studies of the ENTS can provide critical information on the final assembly of the southern parts of CAO (e.g., Charvet et al., 2007; Han et al., 2010). Most studies of ENTS focus on its tectonic evolution based on regional tectonics, structures, and geochemical and geochronological data of the rocks exposed in ENTS (e.g., Allen et al., 1993; Gao et al., 1998; Xiao et al., 2004, 2013; Wang et al., 2007; Han et al., 2010; Charvet et al., 2011). However, the eroded rocks in ENTS during late Permian-earliest Triassic are not well understood.

Provenance studies of sandstones in basins adjacent to orogens are useful to reconstruct the eroded parts of the orogens (e.g., Dickinson and Suczek, 1979; Ingersoll and Suczek, 1979; Dickinson, 1985; Dorsey, 1988; Garzanti et al., 1996, 2007; Trop and Ridgway, 1997; Ingersoll, 2012). However, detailed reconstruction of rocks in ENTS during late Permian-earliest Triassic cannot be achieved by previous petrographic studies. Limitations of previous studies include the out-of-date chronostratigraphy (Carroll et al., 1995), large sampling spacing (Shao et al., 2001; Greene et al., 2005), or limited study areas (Guan et al., 2010; Guan, 2011). This study focuses on the sandstones of the upper Permian-lowermost Triassic Wutonggou (WTG) low-order cycle exposed in the northern and southern foothills of Bogda Mountains, the greater Turpan-Junggar intracontinental rift basin (Yang et al., 2010), to document high-resolution temporal and spatial variations

of sandstone compositions, in order to interpret the provenance of these sandstones and reconstruct the unroofing history of ENTs. The results provide insights on the nature and tectonic evolution of ENTs as an amalgamated complex of the volcanic arc, accretionary wedge, and trench during late Permian-earliest Triassic.

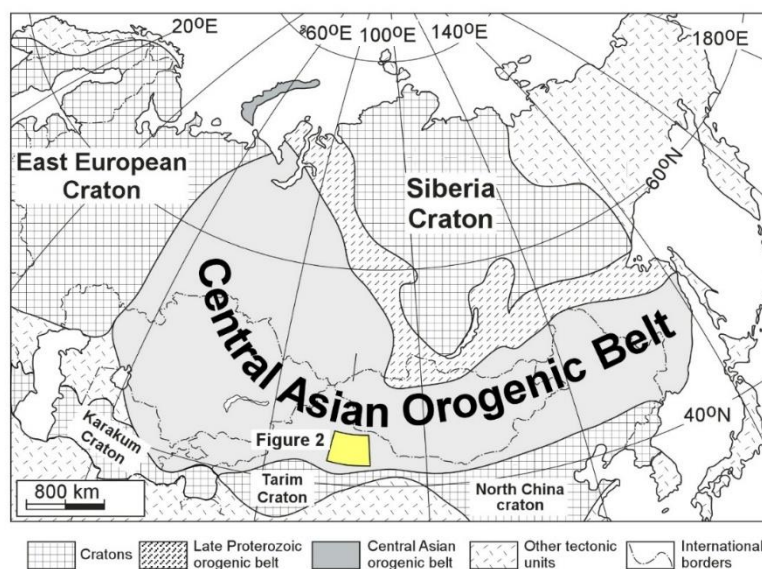


Figure 1. Tectonic map of the Central Asian Orogenic Belt. This orogenic belt is bordered by the East European Craton to the west, Siberia Craton to the east, and North China, Tarim, and Karakum Craton to the south. Modified from Sengör et al. (1993) and Jahn et al. (2000). The yellow box is the location of Figure 2.

2. GEOLOGICAL BACKGROUND

This study focuses on the upper Permian-lowermost Triassic fluvial-lacustrine sandstones of WTG low-order cycle in Zhaobishan (ZBS), North Tarlong (NTRL), and Taodonggou (TDG) sections in the southern and Dalongkou (DLK) section in the northern foothills of Bogda Mountains, NW China (Figures. 2, 3). The Bogda Mountains is an E-W striking giant anticline with Devonian to Quaternary sedimentary and igneous

rocks, located between the Junggar Basin to the north and Turpan-Hami Basin to the south (Figure 2). It was a part of the greater Turpan-Junggar basin during late Carboniferous-Jurassic (Shao et al., 1999, 2001; Greene et al., 2001, 2005; Yang et al., 2007, 2010). The type of the greater Turpan-Junggar basin is speculated to be a back-arc basin (Hsü, 1988), a transitional basin from rift to foreland basin (Carroll et al., 1990; Hendrix et al., 1992; Shao et al., 1999, 2001; Greene et al., 2001, 2005), or a rift basin (Allen et al., 1991; Allen et al., 1993; Shu et al., 2005, 2011; Yang et al., 2010, 2013). The seismic profiles (Yang et al., 2010), mixed tholeiitic volcanism and marine sedimentation in the uppermost basement (Yang et al., 2013), the bimodal volcanic rocks (Shu et al., 2005, 2011), continental rift-type geochemical signatures (Allen et al., 1991; Shu et al., 2005, 2011), and regional scale strike-slip shear zones (Laurent-Charvet et al., 2002, 2003; Shu et al., 2005, 2010) support that the greater Turpan-Junggar basin was an intracontinental rift basin with a Carboniferous volcanic arc or back-arc basement (Shu et al., 2005; Yang et al., 2010; Yang et al., 2013). Regional dextral strike-slip triggered the rifting starting in the latest Carboniferous (Laurent-Charvet et al., 2002, 2007; Yang et al., 2010, 2013; Shu et al., 2011). The rifting formed a series of grabens and half-grabens in the greater Turpan-Junggar basin, resemble the Basin and Range Province in the western United States (Yang et al., 2010).

The Chinese Tianshan separates the Junggar Basin to the north from the Tarim Basin to the south and has been created since the Cenozoic collision between the Indian and Asian Plates (e.g., Windley et al., 1990; Hendrix et al., 1994; Yin et al., 1998). Before the Cenozoic collision, a series of suture zones were formed in Chinese Tianshan during Paleozoic, one of which is the North Tianshan Suture. The North Tianshan Suture

is further divided into the western and eastern segments in terms of their relative locations to the city of Urumqi (Figure 2). This study focuses on the eastern segment of North Tianshan Suture, which is situated about 100 km south of Bogda Mountains and north of Central Tianshan Suture. The formation of ENTS is not fully understood, but the southward subduction of North Tianshan Ocean beneath the Central Tianshan Suture, and the collision between the Central Tianshan Suture and the trailing Junggar Plate are widely accepted (Windley et al., 1990; Gao et al., 1998; Xiao et al., 2004, 2013; Charvet et al., 2011).

The timing of the collision is in the debate, varying from Middle Ordovician (Gao et al., 1998), Devonian-early Carboniferous (Xiao et al., 2004, 2013) to Late Devonian-Carboniferous (Charvet et al., 2011). Similarly, the closure time varies from the end of Early Carboniferous (Gao et al., 1998), late Carboniferous (Windley et al., 1990; Xiao et al., 2004, 2013; Han et al., 2010), to late Carboniferous-early Permian (Allen et al., 1993; Carroll et al., 1995). The current ENTS consists of Ordovician to Devonian-Carboniferous volcanic-arc rocks and associated submarine volcanic-sedimentary rocks (Allen et al., 1993; Xiao et al., 2004). The fragmental ophiolites, radiolarian chert, turbidites, and high-pressure schists mark the subduction of the oceanic crust between the Junggar Plate and Central Tianshan Suture (Carroll et al., 1990; Gao et al., 1998; Shu et al., 1999; Xiao et al., 2004; Charvet et al., 2007).

The WTG low-order cycle is an informal cyclostratigraphic unit defined by Yang et al. (2007, see also Yang et al., 2010) and approximately correlates to the Wutonggou and Guodikeng formations (Figure 3; XBGMR, 1993; Yang et al., 2007, 2010). A low-order cycle formed during a period of long-term stable tectonic and/or climatic conditions

and contains high and intermediate-order cycles. The high-order cycle (HC) is the smallest unit that records the environmental changes caused by the transgression and regression of lakes or erosion and deposition of rivers. The intermediate-order cycle (IC) includes several HCs, representing longer trends of transgression and regression or erosion and deposition than the HCs. The WTG LC records an overall persistently uplifting history of the source areas and humid to subhumid climate conditions (Yang et al., 2007, 2010; Thomas et al., 2011).

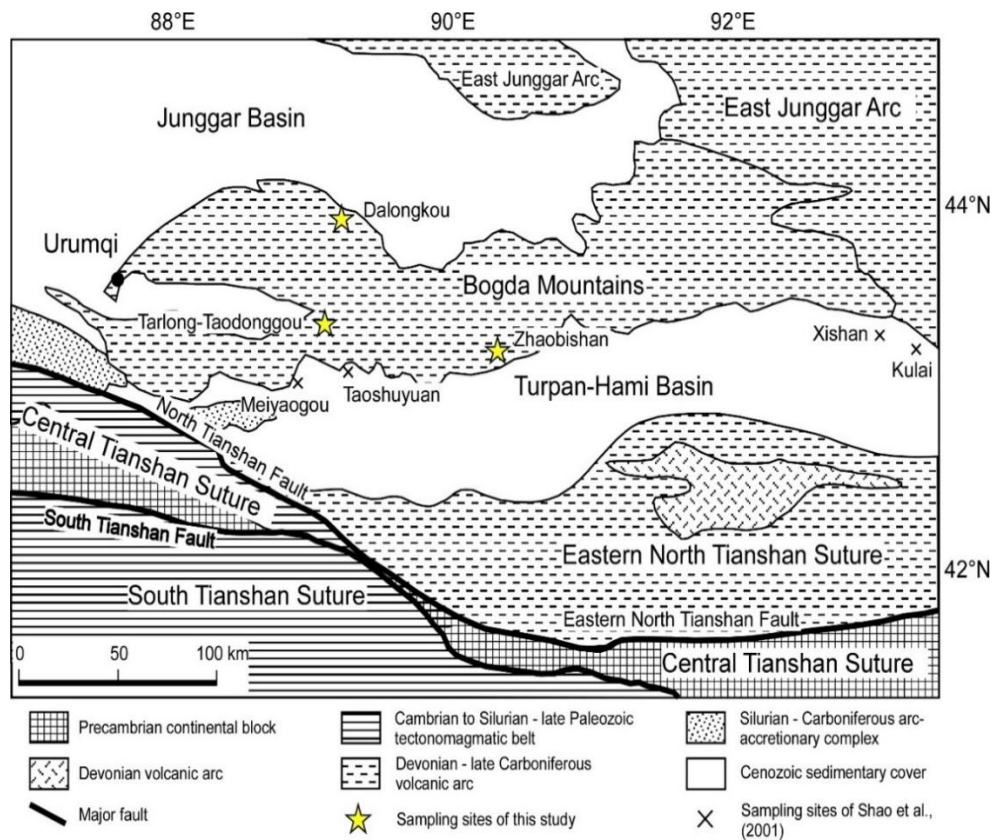


Figure 2. Tectonic map of eastern Xinjiang. This map shows the locations of the eastern North Tianshan Suture, Central Tianshan Suture, Bogda Mountains, and measured sections. Modified from Xia et al. (2004).

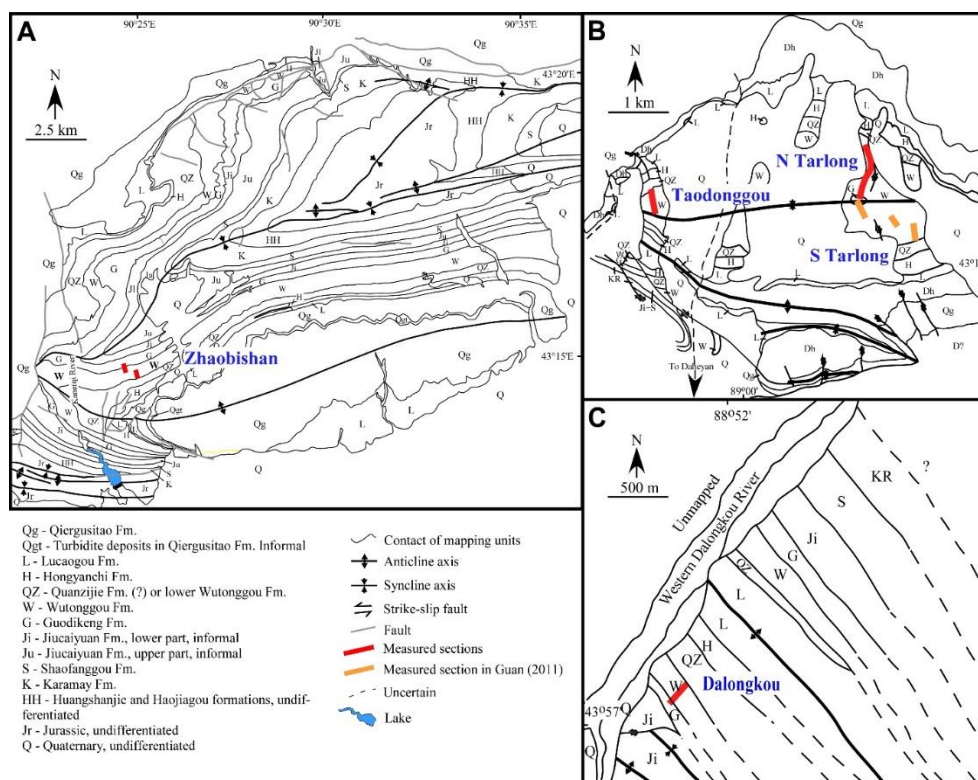


Figure 3. Geological maps of Zhaobishan (A), Tarlong-Taodonggou (B), and Dalongkou (C) areas. This map shows names and locations (red lines) of measured sections. Modified from Yang et al. (2010), Obrist-Farner and Yang (2015), and Fredericks (2017).

Stratigraphic correlation has largely based on lithostratigraphy, biostratigraphy, and cyclostratigraphy (Zhang, 1981; Liao et al., 1987; Wartes et al., 2002; Yang et al., 2007, 2010). The chronostratigraphy in the greater Turpan-Junggar basin is not well constrained. Yang et al. (2010) placed the Permo-Triassic boundary in a 90 m-thick interval in NTRL section. Based on stratigraphic correlation and petrographic studies, the strata in Tarlong and Taodonggou area were interpreted as being deposited within one half-graben, termed the Tarlong-Taodonggou half graben (Yang et al., 2010; see also Guan, 2011; Peng, 2016; Obrist-Farner and Yang, 2017; Fredericks, 2017). The basin

geometry of the ZBS and DLK areas is not clear due to a limited number of measured sections and is speculated to be similar to that of Tarlong-Taodonggou half-graben.

System	Series	Lithostratigraphy	Cyclostratigraphy Low-order Cycles (Yang et al., 2010; Obriest-Farmer and Yang, 2015)	Revised chronostratigraphy (Yang et al., 2010, 2013)			
				New dates	Stages		
Triassic	Middle	Karamay	Karamay	247.2	Anisian		
	Lower	Shaofanggou	Shaofanggou	251.2	Olenekian		
		Jiucaiyuan	Jiucaiyuan	251.9	Induan		
Permian	Lopingian	Guodikeng	Wutonggou	253.11	Changhsingian		
		Wutonggou		253.63	254.1		
	Guadalupian	Quanzijie	Upper Quanzijie	?	265.1	Capitanian	
		?	Lower Quanzijie		?	268.8	Wordian
		?	?		?	273.0	Roadian
	Cisuralian	Hongyanchi	Lucaogou	Tarlong	283.5	Kungurian	
					290.1	Artinskian	
		Daheyan	Upper Daheyan	?	293.5	Sakmarian	
			Middle Daheyan		298.9	Asselian	
	Carboniferous	Upper	Qiergusitao	-	301.26 ? 0.05	Gzhelian	
301.37 ? 0.07							
304.1							
				305.50 ? 0.11	Kasimovian		
				306.48 ? 0.32			
					307.0		

Figure 4. Chrono-, litho-, and cyclostratigraphy of upper Carboniferous-Middle Triassic strata in Bogda Mountains. Wavy lines are major unconformities; dashed lines disconformity; and hachured areas missing strata. The studied Wutonggou low-order cycle is shown in the shaded box. Modified from Yang et al. (2010) and Obriest and Yang (2015).

3. DATA AND METHODOLOGY

Sixty sandstones from four sections were studied to observe the compositional and textural characteristics (Figure 5; see Yang et al., 2007, 2010 for detailed measured sections). Three hundred framework grains in each thin section were counted using both Suttner's (Suttner, 1974) and Gazzi-Dickinson's methods (Gazzi, 1966; Dickinson,

1970). The Gazzi-Dickinson method counts sand-size (0.063 mm) mineral crystals within large rock fragments as individual grains, whereas the Suttner's method does not count the mineral crystals, only as the rock fragments (Ingersoll et al., 1984). As most of the counted lithic grains in the studied sandstones contain minerals smaller than sand, the results of these two methods are similar. Definitions of raw and recalculated parameters of point counting categories are tabulated in Table 1. The interpretations of volcanic lithic fragments follow the descriptions of Dickinson (1970) and Marsaglia and Ingersoll (1992). The interpretation of polycrystalline quartz grains follows those of Basu et al. (1975), Young (1976), and Blatt and Tracy (2006). Point counting data in recalculated parameters are presented in Table 2 in terms of Gazzi-Dickinson method so that petrofacies can be defined by composition and compared with the tectonic fields in templates from previous studies (Dickinson and Suczek, 1979; Dickinson et al., 1983; Dickinson, 1985; Marsaglia and Ingersoll et al., 1992; Critelli et al., 1995).

1914 gravels in 17 conglomeratic beds were counted and described in the field to obtain the spatial and temporal trends in clast composition. Fresh surfaces were used to identify lithologies. A rectangular grid on the outcrop surface was laid out as a guide for counting. About 100 clasts were counted in each location. In addition, 168 attitudes of nine tabular cross beds of fluvial sandstones were measured in the field. They were later corrected using the method of Davis et al. (1996, pp. 710-714). The correction, rose diagrams, and mean vectors were performed using the software StereoNet of Allmendinger (2005).

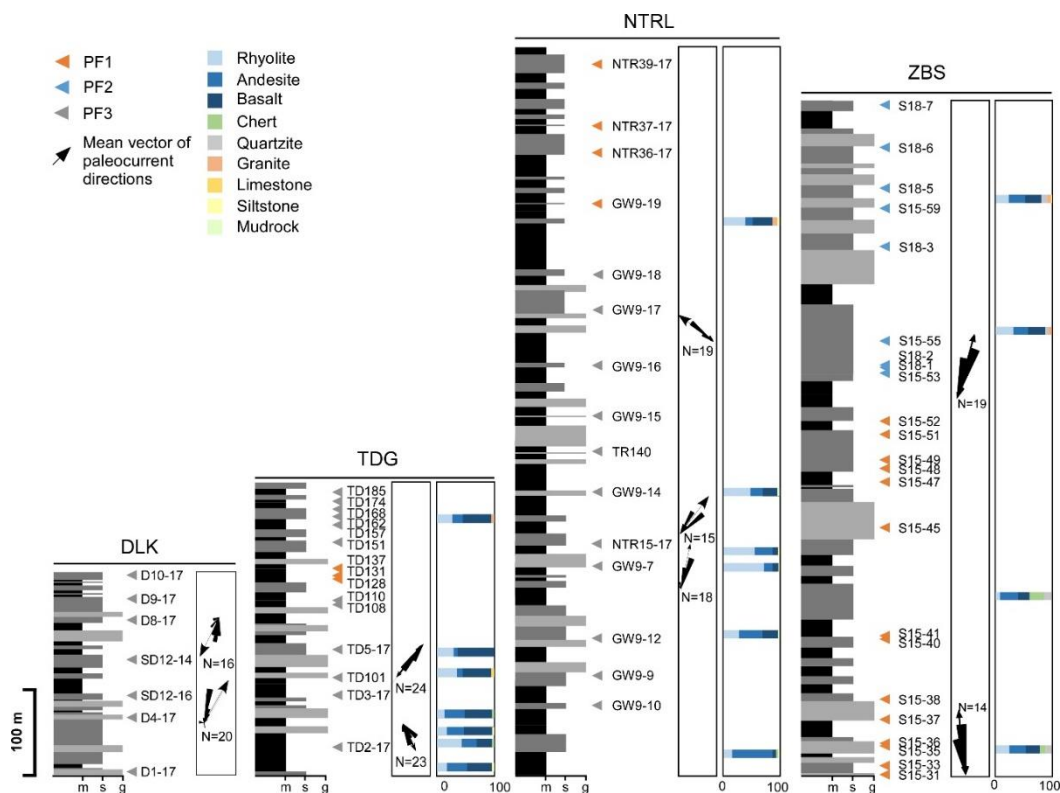


Figure 5. Highly-simplified lithological columns, sample names and locations, paleocurrent data, compositions of gravels, and petrofacies. See Figure 3 for locations of measured sections. See Yang et al., (2010) for detailed measured sections. DLK, Dalongkou section; TDG, Taodonggou section; NTRL, North-Tarlong section; ZBS, Zhaobishan section.

4. RESULTS

Sandstone compositions are used to classify petrofacies, of which the lithology and tectonic settings of the source areas can be interpreted. The results of clast compositions of conglomerates and paleocurrent directions supplement the classification of petrofacies and provenance interpretation. The stratigraphic distributions of petrofacies, clast compositions, and paleocurrent directions in individual sections show the temporal changes of sandstone compositions. Finally, the spatial variations of

sandstone compositions are interpreted on the basis of correlations among sections in the study areas.

4.1. FRAMEWORK GRAINS

The major framework grains in sandstones of WTG low-order cycle (WTG LC) include quartz, feldspar, and lithic fragment. They are further differentiated on the basis of optical mineralogic characteristics, such as extinction, twinning, and relict textures (Tables 1, 2). Accessory minerals, including micas and heavy and opaque minerals, are of a trace amount.

4.1.1. Quartz. Quartz occurs as monocrystalline crystals (Qm) and polycrystalline (Qp) and microcrystalline aggregates (Cht). Qm grains are clear, inclusion-free, and subangular-angular, and are subdivided into nonundulatory (Qnu; Figure 6A) and undulatory types (Qu). Qnu grains exhibit straight extinctions, whereas Qu grains are strained with undulose extinction at an angle between 5-10 degrees. Qp grains are subdivided into polycrystalline ones with metamorphic deformed texture (Qpt; Figure 6B) and polycrystalline ones without such texture (Qpw). Qpt grains contain more than five sutured, elongate quartz crystals. In contrast, Qpw grains contain two to five monocrystalline quartz grains without sutured contacts. Cht grains are aggregates of microcrystalline quartz and interpreted as fragments of chert (Figure 6C).

4.1.2. Feldspars. This group includes plagioclase (P; Figure 6A) and potassium feldspar (K; Figure 6A). Plagioclase grains usually exhibit polysynthetic twinning. The plagioclase grains in NTRL and TDG areas are common with albite twinning. They occur as discrete angular-subangular grains and lath or mosaic phenocrysts in volcanic

Table 1. Raw and recalculated grain types and categories for point-counting and petrofacies classification

Symbol	Definition
Raw	
Qnu	Nonundulose monocrystalline quartz
Qu	Undulose monocrystalline quartz
Qpt	Polycrystalline quartz with metamorphic textures
Qpw	Polycrystalline quartz without metamorphic textures
Cht	Chert and chalcedony
K	Potassium feldspar
P	Plagioclase
Lvf	Volcanic lithic with felsic texture
Lvmi	Volcanic lithic with microlitic texture
Lvl	Volcanic lithic with lathwork texture
Lvv	Volcanic lithic with vitric texture
Lvun	Unidentified volcanic lithic
Lmd	Mudrock fragment
Lslt	Siltstone fragment
Lsd	Sandstone fragment
Lm	Metamorphic lithic
Carb	Carbonate
AM	Accessory transparent minerals
OM	Opaque minerals
Bio	Bioclastic grains
Uni	Unidentified grain
Recalculated	
Qm	Qnu+Qu
Qp	Qpt+Qpw+Cht
Q	Qm+Qp
F	K+P
Lv	Lvf+Lvmi+Lvl+Lvv+Lvun
Ls	Lmd+Lslt+Lsd
Lmt	Lm+Qpt
Lst	Ls+Cht
L	Lv+Ls+Lm
Lt	Lv+Lmt+Lst

lithic fragments. Potassium feldspar includes microcline and orthoclase. The microclines exhibit tartan twinning and only occur in ZBS and TDG sections. The orthoclase is

usually Carlsbad twinned or untwinned. Clear, inclusion-free orthoclase are common in the studied thin sections.

4.1.3. Lithic Fragments. Lithic fragments include volcanic (Lv), sedimentary (Ls), and metamorphic (Lm). Lv and Ls grains dominate and account for over 99% of the total lithics. Lm grains are rare.

The Lv grains are subdivided into four types based on their textures, including felsic (Lv_f; Figure 6D), microlitic (Lv_{mi}; Figure 6E, F), lathwork (Lv_l; Figure 6E), and vitric (Lv_v; Figure 6F). Lv_f, Lv_{mi}, Lv_l, and Lv_v grains are interpreted to be derived from felsic (Lv_f), intermediate (Lv_{mi}), and mafic (Lv_l) igneous rocks and volcanic glass (Lv_v), respectively (Dickinson, 1970). The Ls grains are subdivided into three types based on their textures, including mudrock (Lm_d; Figure 6E), siltstone (Ls_{lt}), and sandstone fragments (Ls_d). The Lm_d grains account for more than 95% of the total sedimentary lithics. Finally, a trace amount of Lm grains, mainly schist fragments, are identified on the basis of their foliations.

4.1.4. Accessory Minerals. Accessory mineral grains are the minor framework grains in WTG sandstones and account for 2% of the total detrital grains. Muscovite, biotite, zircon, tourmaline, amphibole, and opaque minerals are observed.

4.2. MATRIX, CEMENT, AND SANDSTONE CLASSIFICATION

WTG sandstones contain 1% matrix, grains smaller than 0.031 mm, on average. Based on the sandstone classification of Dott (1964), sandstones in this study include forty-six litharenites, eleven feldspathic arenites, and three lithic wackes (Table 2). The

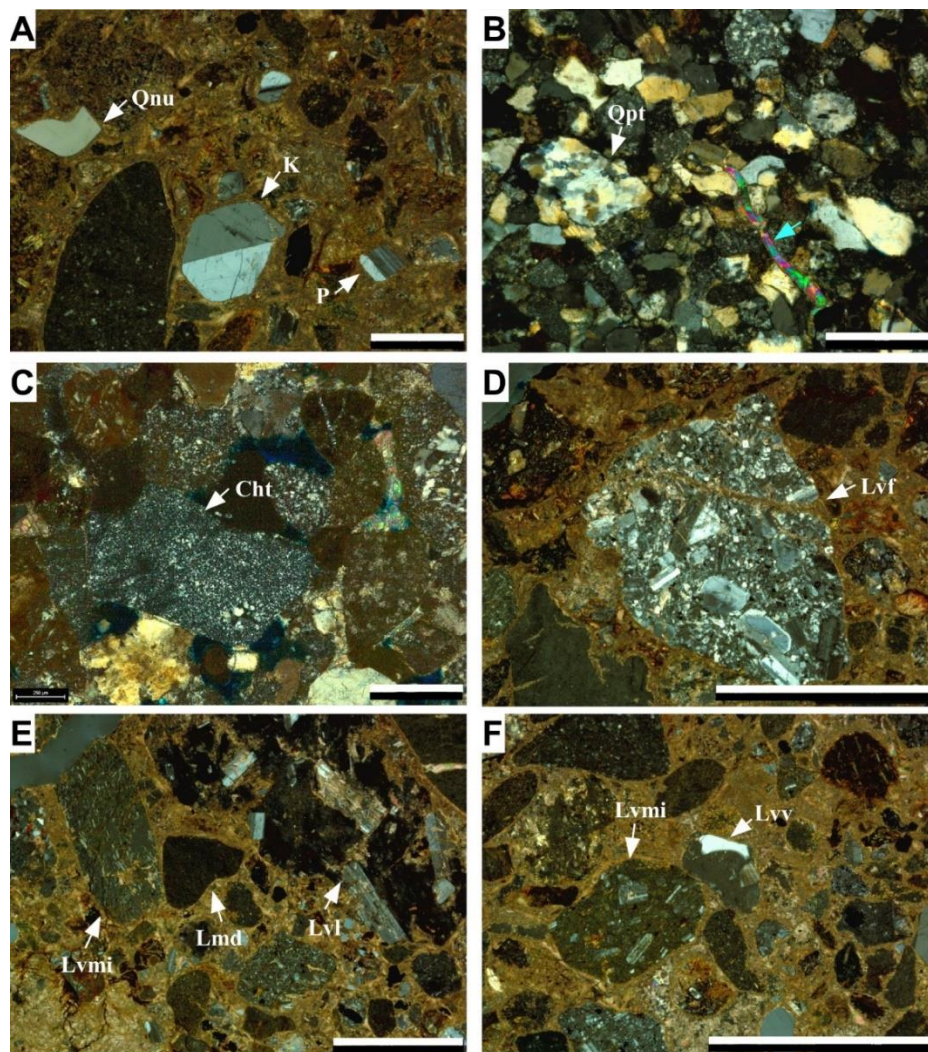


Figure 6. Photomicrographs of sandstones in the Wutonggou low-order cycle (WTG). A) A nonundulatory monocrystalline quartz grain (Qnu) with embayment, a potassium feldspar with Carlsbad twinning, and a plagioclase with albite twinning. Sample TD110, lower WTG in Taodonggou (TDG) section. B) A polycrystalline quartz grain with sutured quartz crystals, indicating its metamorphic origin. The blue arrow points to an elongate muscovite grain. S15-36, lower WTG in Zhaobishan section. C) A slightly clay coated chert grain. NTR39-17, upper WTG in NTRL section. D) A volcanic lithic fragment with felsic texture. The phenocrysts are mainly feldspar grains. TD110, lower WTG in TDG section. E) A volcanic lithic fragment with microlitic texture, an angular mudrock fragment, and a volcanic lithic with lathwork texture showing large feldspar laths. These grains suggest sedimentary and volcanic origins. TD108, lower WTG in TDG section. F) A volcanic lithic fragment with microlitic texture and a volcanic lithic with vitric texture, suggesting a volcanic origin. TD168, upper WTG in TDG section. All micrographs are taken under XPL. Scale bar is 1 mm long in all photos. See Table 1 for the abbreviations of grain categories.

cements in the sandstones are predominately calcite, clays, and iron oxides and sulfides. Zeolite and silica are rare. As matrix is not further studied and cements are largely controlled by diagenesis rather than provenance lithology (Dickinson and Suczek, 1979), they are not included in the classification of petrofacies.

4.3. COMPOSITION OF GRAVELS AND PALEOCURRENT MEASUREMENTS

Conglomerates in the WTG low-order cycle are typically polymictic, either clast- or matrix-supported. Compositions of gravels are described below (Figure 5; Table 3). The compositions of individual conglomeratic beds are summarized in Section 5 to facilitate the interpretations of source lithology.

The gravels are igneous, sedimentary, or metamorphic. Igneous gravels are volcanic and plutonic clasts, including white or gray rhyolite, dark green or dark purple andesite, and dark green, dark purple or black basalt, and reddish granite. Sedimentary gravels are mudrock and chert, including green, purple, brown soft clasts of mudrock and massive or laminated gray chert. Metamorphic gravels include white quartzite, of which the boundaries of single quartz crystals are interlocking with each other.

The paleocurrent directions were only measured from cross-beddings within point bar sandstones to remove the possible errors induced by the bed-form hierarchies (Allen, 1968; Miall, 1974). The mean vectors of paleocurrent directions provide qualitative estimates of the locations of the surrounding highs. These results are further discussed in Section 5 to aid the interpretations of source locations (Figure 5).

4.4. PETROFACIES AND IMPLICATIONS ON LITHOLOGY AND TECTONIC SETTINGS OF SOURCE AREAS

Three petrofacies are classified for sandstones of the WTG low-order cycle on the basis of relative abundance of quartz, feldspar, and lithic fragment. The distributions of the petrofacies are shown in the QFL and QmFLt ternary diagrams (Figure 7; Table 2). All quartz grains are grouped together in QFL diagram to emphasize the variations of grain stability among quartz, feldspar, and lithic fragments. In contrast, polycrystalline and microcrystalline quartz grains are counted as lithic fragments in QmFLt diagram to emphasize the grain size of the source rocks because fine-sized source rocks produce more lithic fragments than monocrystalline grains (Dickinson and Suczek, 1979). Moreover, ternary diagrams of QmPK, QpLvLs, LmtLvLst, and LvFLvmiLvL use subgroups of QFL to show the characteristics of monocrystalline, polycrystalline, lithic, and volcanic lithic grains, respectively (Figure 7; Dickinson and Suczek, 1979; Dickinson et al., 1983). These diagrams are used to further classify the petrofacies for detailed interpretation of source lithology. Finally, ternary diagrams of QFL, QmFLt, and QpLvLs are used to interpret the tectonic settings of source areas using the templates of Dickinson and Suczek (1979) and Dickinson et al. (1983).

4.4.1. Petrofacies 1. Petrofacies 1 (PF1) has mean compositions of $Q_{51}F_{30}L_{19}$ and $Qm_{21}F_{30}Lt_{49}$ and occurs in eleven lithic arenites, nine feldspathic arenites, and one lithic wacke (Figure 7; Table 2). Quartz grains dominate and consist of monocrystalline, polycrystalline, and chert grains, which account for 21%, 13%, and 17% of the total grains, respectively. Feldspars account for 30% of the total grains and are slightly more enriched with plagioclase than potassium feldspars with an average plagioclase/feldspar (P/F) ratio of 0.55 and a mean composition of $Qm_{43}P_{33}K_{24}$ (Figure 7). Polycrystalline and

lithic grains are mainly polycrystalline quartz and chert with mean compositions of $Qp_{61}Lv_{25}Ls_{14}$ and $Lmt_{19}Lv_{29}Lst_{52}$ (Figure 7). Other lithic fragments include volcanic and mudrock, which account for 12% and 7% of the total grains, respectively. The volcanic lithic fragments are the minor component and are mainly felsic volcanic lithics with a mean composition of $Lvf_{66}Lvmi_{25}Lv_{19}$ (Figure 7).

The mean composition of PF1 suggests that its source rocks are probably a suite of felsic igneous rocks, quartzite, chert, and mudrocks. The common monocrystalline quartz and feldspar grains and the occurrence of felsic volcanic lithic sandy and gravelly clasts (see also Section 5) indicate a felsic plutonic and volcanic origin of this petrofacies. The undulatory quartz grains and polycrystalline quartz with deformed texture indicate a metamorphic origin. Finally, chert and mudrock fragments were originated from sedimentary rocks. from QFL and QmFLt distributions are different because the polycrystalline quartz and chert grains are incorporated as quartz in QFL diagram but as lithic fragments in QmFLt diagram. The chert-rich sandstones from Klamath Mountains within Cordilleran with known magmatic arc and associated accretionary wedge and trench sources fall in the recycled orogen in QFL and lithic recycled field in QmFLt (Dickinson and Suczek, 1979; Dickinson et al., 1983). Similarly, PF1 of WTG sandstones is also enriched in polycrystalline quartz and chert and falls in the recycled orogen in QFL and transitional arc in QmFLt plots. Hence, PF1 was likely derived from sources of a transitional arc and associated accretionary wedge and trench, which, as a whole, is termed as subduction complex by Dickinson and Suczek (1979). The QpLvLs plot

Table 2. Percentages of different types of framework grains derived from raw point-counting data

Sample Number	ZBS Section																		Matrix	Classificaiton	Petrofacies
	Q	F	L	Qm	F	Lt	Qm	P	K	Qp	Lv	Lv	Ls	Lm	Lv	Ls	Lvf	Lvmi			
S15-31	55	32	13	29	32	39	47	43	9	27	32	41	22	34	44	90	10	0	2	FA	PF1
S15-33	48	13	39	20	13	67	61	28	11	16	45	39	15	45	40	69	24	6	0	LA	PF1
S15-35	49	32	19	15	32	53	34	39	27	55	21	23	42	28	30	77	19	3	0	FA	PF1
S15-36	56	24	19	19	24	56	44	43	13	27	23	50	21	25	54	65	26	9	3	LA	PF1
S15-37	63	17	20	22	17	60	56	18	26	16	25	58	12	27	62	71	29	0	3	LA	PF1
S15-38	58	31	10	32	31	37	50	17	33	14	23	63	9	24	66	78	22	0	3	LA	PF1
S15-40	53	37	10	34	37	29	48	18	34	25	25	49	21	27	52	65	29	6	2	FA	PF1
S15-41	44	45	11	17	45	38	29	43	28	36	23	41	28	25	46	96	0	4	0	FA	PF1
S15-45	64	21	15	30	21	49	59	17	24	33	18	50	27	19	54	59	41	0	0	LA	PF1
S15-47	53	46	1	32	46	21	44	24	31	16	4	80	6	4	90	100	0	0	0	FA	PF1
S15-48	51	7	42	25	7	68	77	10	13	14	24	62	13	25	63	47	37	16	0	LA	PF1
S15-49	49	41	10	21	41	38	36	47	17	45	18	37	29	23	48	75	25	0	1	FA	PF1
S15-51	42	37	21	16	37	47	30	45	24	16	38	46	6	43	51	43	18	39	0	LA	PF1
S15-52	38	23	39	21	23	57	48	42	10	15	51	34	11	54	36	56	36	9	0	LA	PF1
S15-53	20	43	37	7	43	50	15	53	32	14	71	15	6	77	17	69	18	13	0	LA	PF2
S18-1	32	39	29	18	39	42	32	45	23	17	67	16	17	67	16	83	8	8	0	FA	PF2
S18-2	26	39	35	13	39	48	25	60	15	14	67	19	13	67	20	84	12	4	0	LA	PF2
S15-55	32	30	38	15	30	55	37	46	18	20	54	26	7	62	30	71	22	8	0	LA	PF2
S18-3	29	17	54	18	17	65	51	40	9	8	76	16	5	78	17	81	16	4	0	FA	PF2
S15-59	31	43	26	11	43	46	24	47	30	14	57	29	4	64	33	75	11	14	1	LA	PF2
S18-5	33	33	33	18	33	48	35	47	17	15	63	23	14	64	23	80	15	5	0	LA	PF2
S18-6	24	39	36	13	39	47	25	41	34	11	70	19	9	71	19	80	15	6	1	LA	PF2
S18-7	23	37	40	9	37	54	19	44	37	12	61	27	8	64	29	81	14	4	1	LA	PF2

Table 2. Percentages of different types of framework grains derived from raw point-counting data (cont.)

NTRL Section																					
gw9-10*	7	32	62	4	32	64	14	79	6	0	87	13	0	87	13	30	55	15	0	LA	PF3
gw9-9*	12	14	74	2	14	84	16	80	5	4	46	51	0	47	53	52	28	20	0	LA	PF3
gw9-12*	10	3	87	0	3	97	25	75	0	1	67	31	0	68	32	47	48	4	0	LA	PF3
gw9-7*	18	1	80	1	1	98	33	67	0	1	25	74	0	25	75	67	33	0	4	LA	PF3
NTR15-17	6	3	91	3	3	94	44	44	13	0	57	43	0	57	43	68	17	15	0	LA	PF3
gw9-14*	13	16	70	1	17	83	4	92	4	4	45	51	0	47	53	50	25	25	2	LA	PF3
TR140	6	3	91	0	3	97	13	63	25	0	35	65	0	35	65	46	41	13	3	LA	PF3
GW9-15*	5	11	84	0	11	89	0	94	6	1	69	29	0	70	30	55	35	10	2	LA	PF3
GW9-16*	10	6	84	1	6	93	15	85	0	0	30	70	0	30	70	50	33	18	2	LA	PF3
GW9-17*	3	6	91	1	6	93	9	86	5	1	54	44	0	55	45	43	17	40	1	LA	PF3
GW9-18*	9	28	63	0	28	71	1	96	3	4	74	22	1	77	23	59	22	19	1	LA	PF3
GW9-19*	55	23	22	16	29	56	37	38	25	33	22	45	19	27	54	64	30	6	2	FA	PF1
NTR36-17	49	27	24	18	33	49	40	27	34	31	18	51	21	20	59	75	14	11	2	LA	PF1
NTR37-17	56	29	15	25	38	37	44	38	18	46	6	47	18	10	73	33	22	44	6	LW	PF1
NTR39-17	39	33	28	16	38	45	33	53	14	25	34	41	12	40	48	49	33	18	4	LA	PF1
TDG Section																					
TD2-17	1	2	96	0	2	98	0	100	0	0	70	30	0	70	30	6	87	7	0	LA	PF3
TD3-17	2	4	94	1	4	95	17	58	25	0	84	16	0	84	16	15	63	23	0	LA	PF3
TD101	7	17	76	3	17	79	17	53	30	3	70	26	1	72	27	51	25	24	1	LA	PF3
TD5-17	0	10	90	0	10	90	5	86	10	0	72	28	0	72	28	25	46	29	0	LA	PF3
TD108	2	8	89	0	8	91	4	63	33	0	56	44	0	56	44	49	38	13	1	LA	PF3
TD110	0	12	87	0	12	88	0	38	63	0	60	40	0	60	40	51	36	12	0	LA	PF3
TD128	49	37	14	22	45	33	35	40	25	40	15	46	32	17	51	72	28	0	2	FA	PF1
TD131	36	42	22	17	46	37	28	23	50	21	42	37	10	47	42	85	15	0	1	FA	PF1
TD137	56	34	9	24	42	34	40	36	24	43	5	53	30	6	64	100	0	0	0	LA	PF1
TD151	3	5	92	0	5	94	8	75	17	0	75	25	0	75	25	38	52	10	0	LA	PF3

Table 2. Percentages of different types of framework grains derived from raw point-counting data (cont.)

TD157	12	19	69	3	19	77	14	38	48	2	84	14	0	85	15	47	44	9	5	LW	PF3
TD162	7	17	75	4	17	78	20	45	34	0	87	13	0	87	13	58	31	11	0	LA	PF3
TD168	8	21	72	2	21	77	9	57	34	3	88	9	0	91	9	50	27	23	8	LW	PF3
TD174	7	9	84	2	9	89	17	63	20	0	57	43	1	56	43	34	47	19	0	LA	PF3
TD185	8	20	71	6	20	73	23	49	28	2	54	44	0	55	45	63	25	13	0	LA	PF3
DLK Section																					
D1-17	9	21	70	5	22	74	21	45	34	7	41	53	4	42	55	47	24	29	0	LA	PF3
D4-17	6	17	77	3	17	80	17	41	43	4	59	37	2	61	37	60	37	2	2	LA	PF3
SD12-16	3	16	81	2	16	82	13	56	31	1	47	51	0	48	52	54	43	3	0	LA	PF3
SD12-14	11	21	69	7	21	72	27	51	22	5	50	46	0	52	48	45	45	10	0	LA	PF3
D8-17	7	6	87	6	6	88	50	26	24	1	41	58	0	41	58	51	45	4	0	LA	PF3
D9-17	7	9	84	5	9	86	38	49	14	2	38	60	1	38	61	44	56	0	0	LA	PF3
D10-17	4	35	61	2	35	62	7	65	28	3	57	40	2	58	40	23	59	18	3	LA	PF3

* Samples that were point counted in Guan (2011), and they are re-counted in this study to make the volcanic lithic fragments differentiated under same standard with other sandstones, and to obtain the textural information. All numbers are in percentage. See Table 1 for the explanation of the grain categories. LA, litharenite; FA, feldspathic arenite; LW, lithic wacke; FW, feldspathic wacke; PF1, petrofacies 1; PF2, petrofacies 2; PF3, petrofacies 3.

Table 3. Conglomerate compositions

Section	Thickness (m)	Lithology (%)								
		Rhyolite	Andesite	Basalt	Chert	Quartzite	Granite	Limestone	Sandstone	Mudstone
ZBS	26	24	30	25	10	11	0	0	0	0
ZBS	204	8	32	21	25	14	0	0	0	0
ZBS	501	32	26	30	0	6	6	0	0	0
ZBS	865	23	29	29	0	10	6	3	0	0
Ave		22	29	26	9	10	3	1		
TDG	5	17	35	43	0	0	0	0	4	0
TDG	29	43	26	26	4	0	0	0	0	0
TDG	38	17	30	50	0	0	0	0	3	0
TDG	80	13	35	48	4	0	0	0	0	0
TDG	113	35	10	50	0	0	0	5	0	0
TDG	139	29	7	64	0	0	0	0	0	0
TDG	281	27	18	50	0	0	5	0	0	0
Ave		26	23	47	1		1	1	1	
NTRL	35	16	72	6	3				3	
NTRL	160	28	41	28	0					3
NTRL	232	72	16	10	0				2	
NTRL	247	56	32	9	0				3	
NTRL	322	48	22	26	0					4
NTRL	523	39	13	35	0		9		4	
Ave		43	33	19	1		9		3	4

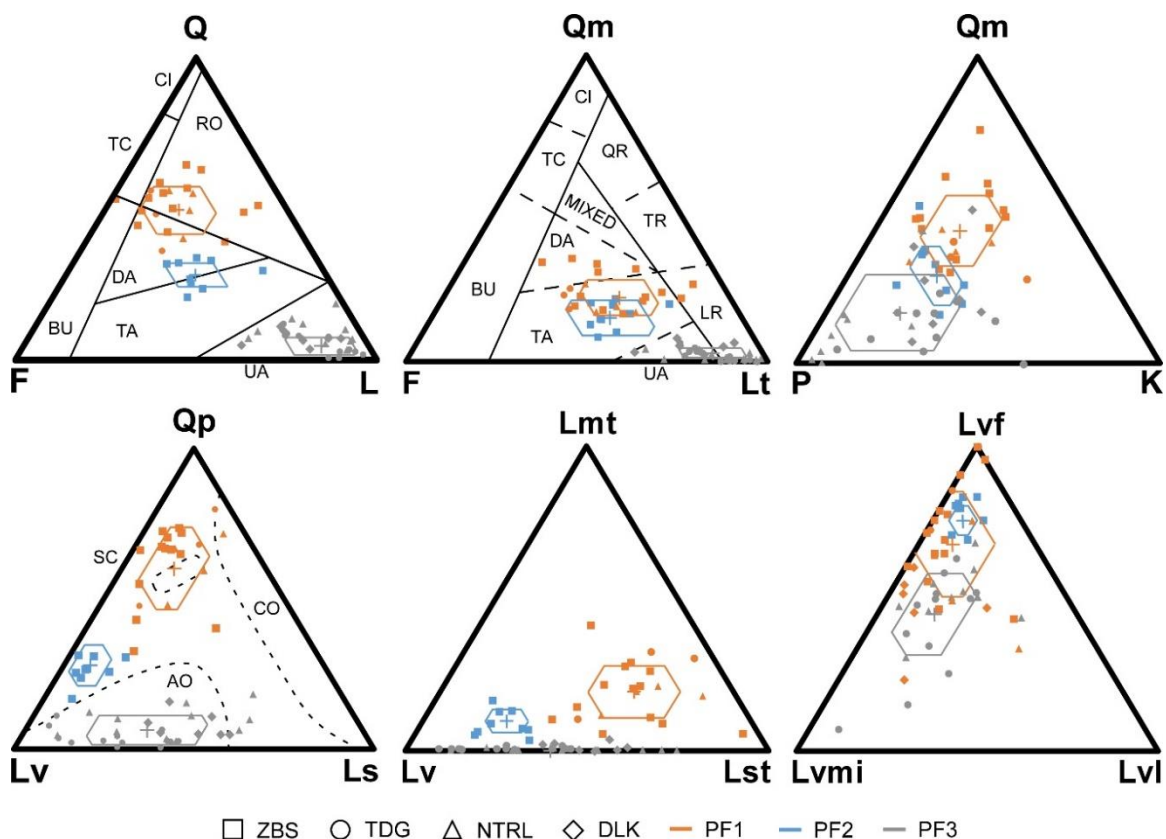


Figure 7. Ternary diagrams with mean compositions and classifications of petrofacies of Wutonggou sandstones. Sandstones of Petrofacies 1 (n=21), Petrofacies 2 (n=9), and Petrofacies 3 (n=30) are shown as orange, blue, and gray symbols, respectively. See Table 1 for definitions of grain categories and end-members. Fields of tectonic settings are adapted from Dickinson and Suczek (1979) and Dickinson et al., (1983). CI, craton interior; TC, transitional continent; BU, basement uplift; RO, recycled orogeny; DA, dissected arc; TA, transitional arc; UA, undissected arc; QR, quartzose recycled; TR, transitional recycled; LR, lithic recycled; SC, subduction complex; CO, collision orogen; AO, arc orogen.

plot substantiates the interpretation that PF1 falls in the subduction complex field (Figure 7). Overall, these three diagrams indicate that the sources of PF1 include felsic volcanic and plutonic rocks from a transitional volcanic arc, and quartzite, chert and mudrock from the associated accretionary wedge and trench.

4.4.2. Petrofacies 2. Petrofacies 2 (PF2) has mean compositions of $Q_{28}F_{36}L_{36}$ and $Q_{m14}F_{36}L_{t50}$ and consists of seven litharenites and two feldspathic arenites (Figure 7; Table 2). Quartz is still the major component but less enriched than PF1. The monocrystalline and polycrystalline quartz and chert account for 14%, 7%, and 7% of the total grains, respectively. Feldspars are slightly enriched than PF1 and account for 36% of the total grains. Plagioclase is dominant with an average P/F ratio of 0.65 and a mean composition of $Q_{m29}P_{47}K_{24}$ (Figure 7). The polycrystalline grains and lithic fragments include mainly volcanic lithic fragments and subordinate polycrystalline quartz, chert and mudrock fragments with mean compositions of $Q_{p28}L_{v65}L_{s7}$ and $L_{mt9}L_{v68}L_{st23}$. Similar to PF1, the felsic volcanic lithic fragments are the major components of volcanic lithic fragments with a mean composition of $L_{vf78}L_{vmi15}L_{vl7}$.

The composition of PF2 suggests that the sources include predominant felsic volcanic and plutonic rocks and subordinate quartzite, chert, and mudrocks. The occurrence of large amounts of volcanic lithic fragments, especially felsic volcanic ones, is indicative of felsic volcanic and plutonic source rocks. The common occurrence of monocrystalline quartz and feldspar grains and rhyolitic and granitic gravels (see Section 5) support the interpretation. The content of polycrystalline quartz, chert, and mudrock fragments is markedly lower than that of volcanic lithic fragments, suggesting that the metamorphic and sedimentary rocks are the subordinate sources.

The mean compositions of samples of PF2 on the QFL, Q_mFL_t , and $Q_pL_vL_s$ ternary diagrams fall within the tectonic fields of the transitional arc and the mixed zone between subduction complex and arc orogen (Figure 7). Mean compositions fall in the field of transitional arc in both QFL and Q_mFL_t diagrams, indicating the transitional

volcanic arc origin of these sandstones. In addition, mean composition falls in the mixed zone rather than the arc orogen field in the QpLvLs diagram indicates that the sources are mixed rocks from the volcanic arc and accretionary wedge and trench. The sources of accretionary wedge and trench are not reflected in the QFL and QmFLt diagrams due to the relatively low content of chert and polycrystalline quartz grains. Overall, the three diagrams indicate that the transitional or dissected volcanic arc rocks are the major sources, and the accretionary wedge and trench metamorphic and sedimentary rocks the secondary sources.

4.4.3. Petrofacies 3. Petrofacies 3 (PF3) has mean compositions of $Q_8F_{13}L_{79}$ and $Qm_2F_{13}Lt_{85}$ and occurs in twenty-eight litharenites and two lithic wackes (Figure 7; Table 2). Quartz is no longer the major component. Monocrystalline, polycrystalline, and chert grains only account for 2%, 1%, and 5% of the total grains, respectively. Similarly, feldspars decrease significantly and only account for 13% of the total grains. Plagioclase is still more than K-feldspars with an average P/F ratio of 0.69 and a mean composition of $Qm_{16}P_{64}K_{20}$ (Figure 7). In contrast to PF1 and PF2, the polycrystalline grains and lithic fragments are the major components and largely consist of volcanic and sedimentary fragments with mean compositions of $Qp_6Lv_{60}Ls_{34}$ and $Lmt_0Lv_{60}Lst_{40}$ (Figure 7D, E). Finally, although felsic volcanic lithic fragments still dominate in PF3, the proportion of microlitic volcanic lithic fragments increases significantly as indicated by the mean composition of volcanic lithic fragments $Lvf_{46}Lv_{mi39}Lv_{l15}$ (Figure 7).

The mean compositions of PF3 indicate that the sources of PF3 are rhyolites, andesites, and mudrocks. Moreover, the mean compositions of PF3 fall within the fields of undissected volcanic arc in QFL and QmFLt diagrams and arc orogen in the QpLvLs

diagram, indicating undissected volcanic arc rocks in the sources. However, although the mean composition is in the undissected arc field in QmFLt diagram, fifteen sandstones of PF3 fall within the lithic recycled field (Figure 7). The recycled lithics may be derived from uplifted older sedimentary strata (Dickinson et al., 1983; Dickinson, 1985). Thus, these sandstones may have mixed sources of sedimentary and volcanic rocks. The sedimentary sources are unlikely the trench-fill sedimentary rocks because the mudrocks fragments of PF3 include abundant angular rip-up clasts and the concurrent chert fragments are rare. As a result, the mudrock fragments were more likely derived from a nearby source area, such as the rift shoulders, the uplifted hanging wall of the graben (Yang et al., 2010; Guan, 2011; Obrist-Farner and Yang, 2017).

5. STRATIGRAPHIC DISTRIBUTION OF PETROFACIES AND EVOLUTION OF PROVENANCE

The stratigraphic distributions of petrofacies along each section provide clues on the evolution of provenance. Clast compositions of conglomerates and paleocurrent directions are used to substantiate provenance interpretations. Finally, the correlation of the four studied sections demonstrates the spatial variations of sandstone compositions and source areas.

5.1. PROVENANCE OF ZHAOBISHAN SECTION

Petrofacies of sandstones of the WTG low-order cycle in ZBS section change upsection, suggesting that the lithology and tectonic setting of the source areas of the lower and upper WTG sandstones are different. PF1 occurs in fourteen sandstones in the

lower 420 m, whereas PF2 occurs in nine sandstones in the upper 350 m of ZBS section (Figures. 6, 8; Table 2). The occurrence of PF1 suggests that the sandstones in the lower WTG were derived from the transitional volcanic arc and associated accretionary wedge and trench. As the ENTS was the collisional product of oceanic plate, volcanic arc, and continental plates (Allen et al., 1991; Gao et al., 1998; Xiao et al., 2004, 2013; Charvet et al., 2011), it should contain volcanic, metamorphic, and sedimentary rocks. Rhyolites, fragmental radiolarian chert and high-pressure metamorphic rocks are still exposed in current ENTS (Xiao et al., 2004; Wang et al., 2006), indicating that ENTS was the available source area of ZBS section during late Permian-earliest Triassic.

Clast composition of WTG conglomerates and paleocurrent directions support the provenance interpretation. Two conglomeratic beds at the 26 and 204 m thickness points in the lower ZBS section consist of abundant volcanic and a few quartzite and chert gravels (Figure 5; Table 3). The paleocurrent direction is northward at the bottom of ZBS section (Figure 5). These data indicate that the ENTS, located ~100 km south of the section, served as the volcanic, metamorphic, and sedimentary sources to the lower WTG sandstones in ZBS section. Finally, the absence of plutonic gravels in the conglomerates suggests that the volcanic arc might be undissected or slightly dissected without major exposure of plutons.

In contrast, the occurrence of PF2 in the upper WTG sandstones indicates that the sources are mainly transitional volcanic arc and subordinately accretionary wedge and trench. The ENTS is still interpreted as the available source areas containing igneous, metamorphic and sedimentary rocks. The northward paleocurrent direction identified in

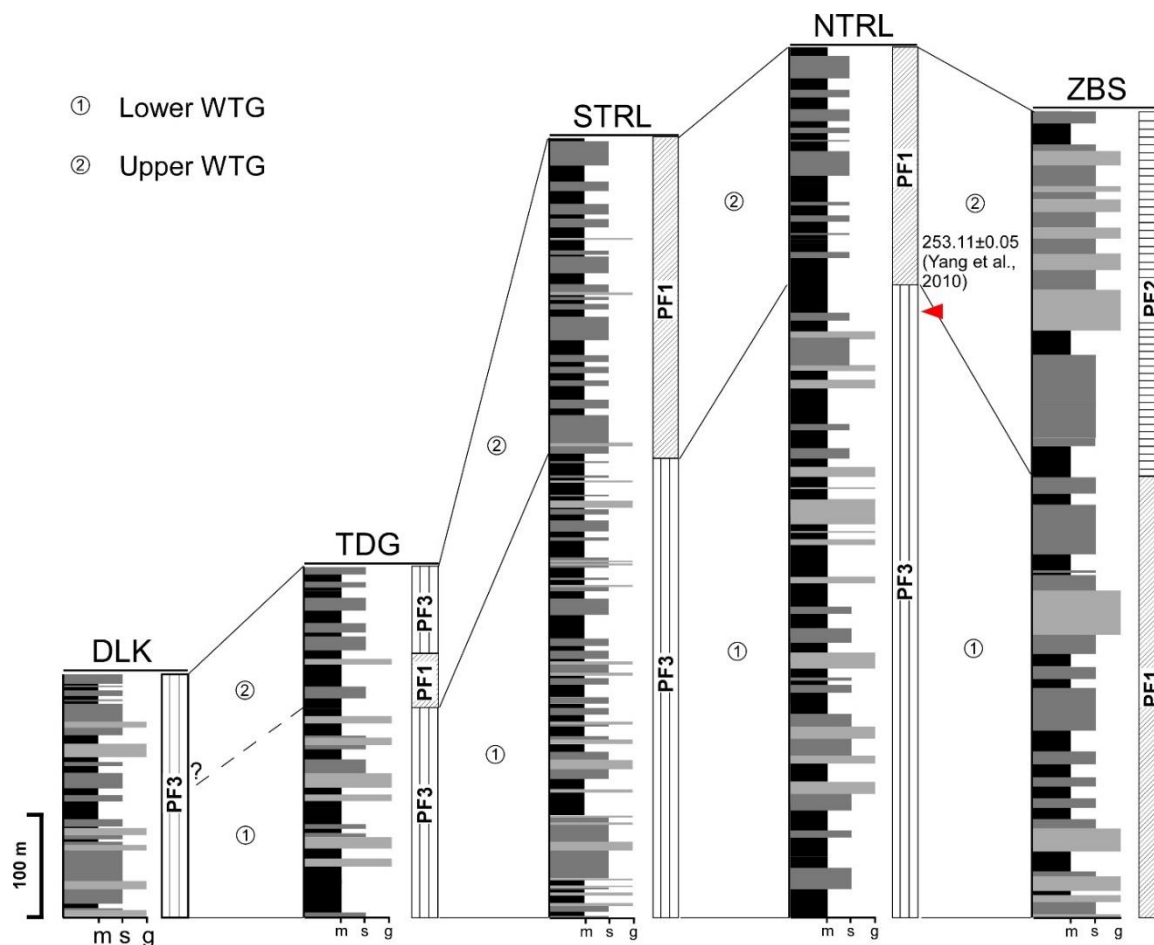


Figure 8. Correlation of petrofacies distribution of Wutonggou sandstones in five sections in the study area. The correlation assumes that the changes of petrofacies in the sections are approximately coeval. The correlation with DLK section is uncertain because there is no compositional change in the section. PF1, Petrofacies 1; PF2, Petrofacies 2; PF3, Petrofacies 3.

the bed at 450 m in the upper half section, supports the interpretation (Figure 5). The significant decrease of polycrystalline quartz and chert fragments and the occurrence of granitic gravels in conglomeratic beds at the thickness of 501 and 765 m (Figure 5; Table 3) indicate that the source lithology contains a significant amount of granites along with rhyolites from the transitional volcanic arc and diminishing quartzite and chert from the accretionary wedge and trench.

5.2. PROVENANCE OF NORTH TARLONG SECTION

The distribution of petrofacies of sandstones of the WTG low-order in NTRL section also indicates different provenances for lower and upper WTG sandstones. PF3 occurs in eleven sandstones in the lower 600 m, whereas PF1 occurs in four sandstones in the upper 220 m of NTRL section. The occurrence of PF3 in the lower WTG sandstones indicates that the sources were an undissected volcanic arc and rift shoulders. The overall northward paleocurrent directions documented in the beds at 5, 29, and 38 m suggest a highland to the south, likely the ENTS (Figure 5; Table 3). Abundant volcanic clasts are present in the lower five conglomeratic beds (Figure 5). Thus, rhyolites and andesites probably covered a large area in the ENTS as the main source. In addition, the large number of mudrock fragments in the lower sandstones may have been derived from local rift shoulders.

In contrast, the occurrence of PF1 in the upper WTG sandstones suggests that the source changed to the transitional volcanic arc and associated accretionary wedge and trench of ENTS. The change is also evidenced by the granitic gravels in the uppermost conglomeratic bed in NTRL section (Figure 5; Table 3).

5.3. PROVENANCE OF TAODONGGOU SECTION

Sandstone petrofacies of the WTG low-order cycle also vary in the TDG section, indicating changes of provenance. PF3 occurs in six sandstones in the lower 200 m and six sandstones in the upper 90 m of the section, whereas PF1 occurs in three sandstones in the middle 50 m of TDG section (Figures. 5 and 8). The occurrence of PF3 in the lower and upper parts of TDG section suggests volcanic and sedimentary sources. The

rift shoulders are likely the sources for mudrock fragments. In addition, the basement in the Taodonggou-Tarlong area contains upper Carboniferous basaltic, andesitic, and sedimentary rocks (Yang et al., 2010; Yang et al., 2013). Thus, the rift shoulders, if the basement rocks were exposed, might also supply basaltic and andesitic fragments. The abundant volcanic clasts in WTG conglomerates and southward paleocurrent directions documented in TDG section (Figure 5; Table 3) support a rift-shoulder source. However, the rhyolitic fragments might come from some other sources. Therefore, the ENTS might have provided fragments of rhyolites and likely, andesites.

In contrast, the occurrence of PF1 in the middle part of TDG section suggests that the sediments were derived from rocks in a transitional volcanic arc and the associated accretionary wedge and trench. ENTS might have been the likely source to supply the felsic volcanic and plutonic, metamorphic, and sedimentary rocks in the sandstones of the middle TDG section.

5.4. PROVENANCE OF DALONGKOU SECTION

Only PF3 occurs in the seven sandstones in DLK section, suggesting a persistent provenance. PF3 indicates volcanic and sedimentary sources from rift shoulders and ENTS, as discussed above. In addition, the paleocurrent directions are either northward or southward (Figure 5), which suggest a complex dispersal pattern, probably originated from surrounding rift shoulders. No basement rocks are exposed in the DLK area at the present time. Thus, the volcanic clasts may have been derived from either ancient rift shoulders and/or undissected volcanic arc in ENTS. A dominant rift-shoulder source

conforms to that for the sandstones of the underlying Quanzijie low-order cycle (Obrist-Farner and Yang, 2017).

5.5. SPATIAL CORRELATION OF PETROFACIES

The distributions of petrofacies in the four studied sections are correlated to identify spatial variations of sandstone compositions and provenance. Petrofacies of NTRL section is correlative with those of South Tarlong (STRL) section (Figure 8; Guan, 2011). These sections are the northern and southern limbs of a syncline and both converge toward the axis and were deposited in the same graben (Figure 3; Yang et al., 2010; Guan, 2011). Twenty-three WTG sandstones were divided into the lower lithic-rich and upper quartz- and feldspar-rich petrofacies, which resemble the distribution of petrofacies in NTRL section (Guan, 2011; Figures. 8, 9). The good correlation between these two sections suggests that they shared the same provenance during the deposition of the WTG low-order cycle.

Correlation between petrofacies of NTRL and STRL sections and those of TDG section shows a slight difference. The petrofacies of the three sections shift from PF3 to PF1 upsection, suggesting a similar trend of provenance evolution. However, PF1 occurs only in a thin interval in the middle part of the TDG section, about one-seventh of the total thickness, and abruptly changes to PF3 again. TDG section is 6 km away from the NTRL-STRL sections and located in the same half-graben as NTRL-STRL sections (Yang et al., 2010). However, the thickness and types of high-order cycles change significantly; TDG section was at the ramp of the half-graben and NTRL-STRL sections were at the depocenters (Yang et al., 2010). Thus, they do not have the same depositional

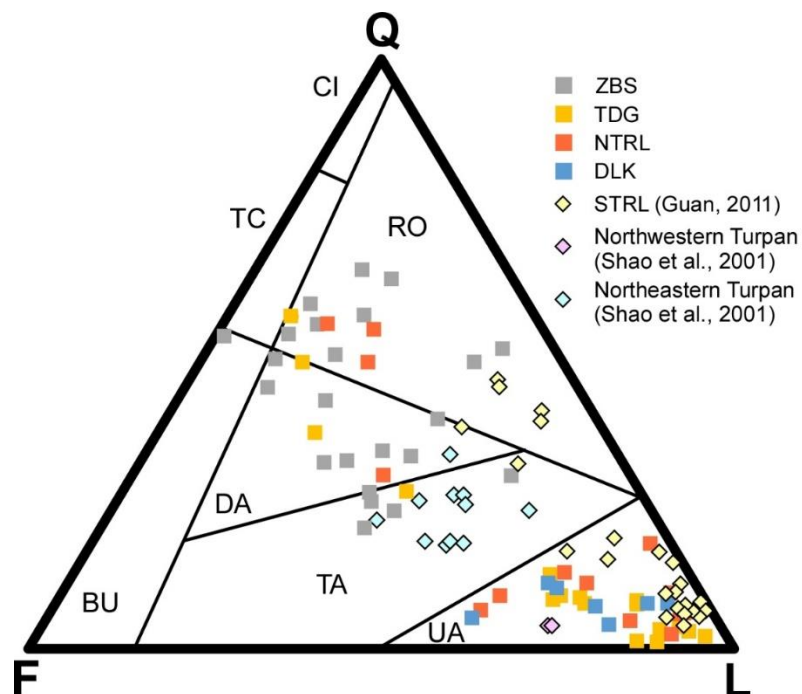


Figure 9. QFL ternary diagram of upper Permian-lowermost Triassic sandstones in Bogda Mountains and Turpan Basin. Data of South Tarlong (STRL) section are from Guan (2011); and data of Turpan Basin from Shao et al. (2001). See Figures 2 and 3 for locations of measured sections, STRL section and Turpan Basin. See Figure 7 for explanations of grain categories and tectonic fields.

environments and even might not have the same drainage areas (e.g., Soreghan and Cohen, 1993). These factors may have caused the abrupt shift of petrofacies in the upper TDG section.

Additionally, the correlation between petrofacies of Tarlong-Taodonggou areas and that of the northwestern Turpan Basin has variations. The northwestern Turpan Basin is about 30 km south of Tarlong-Taodonggou areas (Figure 2), where two Wutonggou Formation sandstones are lithic-rich, resemble the lower WTG sandstones in NTRL, STRL, and TDG sections (Shao et al., 2001; Figure 9). However, the upper quartz- and feldspar-rich sandstones are not documented in the northwestern Turpan Basin.

The trend of petrofacies evolution of ZBS section cannot be correlated with those of NTRL, STRL, and TDG sections because PF3 is absent in ZBS section. On the other hand, the petrofacies shifts in these sections all occur in the middle parts of the sections (Figure 8), which suggests an approximately coeval tectonic event in both source areas of ZBS and Tarlong-Taodonggou areas in ENTS. The shift in NTRL section occurred at a bed 10 m below a bentonite with an age of 253.11 ± 0.05 Ma (Yang et al., 2010; Figure 8). Therefore, the petrofacies shift of the studied sections occurred probably during Wuchiapingian-early Changhsingian transition.

Moreover, the petrofacies of ZBS section may be similar to that of sandstones of the Wutonggou Formation in the northeastern part of the Turpan Basin as documented by Shao et al. (2001). Eleven sandstones of the Wutonggou Formation from Xishan and Kulai sections in northeastern Turpan Basin are quartz- and feldspar-rich, similar to PF2 in this study (see Figure 2 for the section locations; Figure 9). This suggests that the two areas may share a similar provenance.

The petrofacies trend of DLK section cannot be correlated with those in the other sections, because the section contains only PF3. The DLK section was interpreted to be in a separated drainage system (see above). This interpretation fits the tectonic setting of the greater Turpan-Junggar basin as a highly-partitioned rift basin (Yang, 2008; Yang et al., 2010), where the abundant rift shoulders might have hampered the transport of sediments from the ENTS. Alternatively, rivers originating from ENTS might have been persistently draining an area rich in volcanic and sedimentary rocks during the deposition of the entire WTG low-order cycle.

Previous studies suggest the WTG low-order cycle sandstones in the southern Junggar Basin and Northern Turpan Basin are uniformly volcanic-rich with slight variations in compositions based on limited numbers of point-counting data (Carroll et al., 1995; Hendrix, 2000; Greene et al., 2005). The petrofacies distribution and correlation among multiple detailed stratigraphic sections present a clear spatial and temporal pattern of provenance evolution during the deposition of WTG sandstones.

6. THE UNROOFING HISTORY OF THE EASTERN NORTH TIANSHAN SUTURE

The interpreted provenance lithology and tectonic setting and their evolution for WTG low-order cycle sandstones can be used to reconstruct of the unroofing history of the ENTS. Overall, ENTS had been persistently unroofed during late Permian-earliest Triassic to provide a large amount of siliciclastic sediments northward into the greater Turpan-Junggar basin. Uplifting of ENTS is likely but the rate of uplifting cannot be confirmed. During approximately the Wuchiapingian Stage when the lower WTG sandstones in ZBS section was deposited, the source area in the eastern part of ENTS was composed of rocks of the undissected volcanic arc, accretionary wedge, and trench (Figure 10). During approximately Changhsingian-early Induan stages when the upper WTG sandstone were deposited, the source area was covered by rocks mainly of the transitional volcanic arc and subordinately of accretionary wedge and trench, where deep-seated granitic plutons started to expose (Figure 10). The unroofing trend indicates the amalgamation of accretionary wedge, trench, and volcanic arc rocks caused by the collision between Junggar Plate and Central Tianshan Suture (Allen et al., 1993; Gao et

al., 1998; Xiao et al., 2004, 2013; Charvet et al., 2011). The southward subduction of North Tianshan Ocean formed the accretionary wedge and trench and North Tianshan volcanic arc, which were accreted together by later continuous movement. A similar trend was reported from the Eocene-Middle Miocene sandstones in the collisional zone between Izu Arcs and the Honshu Arc in central Japan (Okuzawa and Hisada, 2008), of which the older sources are volcanoclasts, and the younger sources are accretionary wedge and trench rocks. The unroofing trend of ENTS continued through Triassic as indicated by increasingly quartzose compositions of Triassic sandstones in Turpan-Hami Basin (Shao et al., 2001; Greene et al., 2005), as a consequence of progressive dissection of the volcanic arc in ENTS.

In contrast to the source area of the ZBS section in the eastern part of the ENTS, that of the Tarlong-Taodonggou sections is located in the western part of the ENTS, probably ~90 km west of the ZBS source area, which is the present-day distance between Zhaobishan and Tarlong-Taodonggou areas. The Tarlong-Taodonggou source area in ENTS has a different unroofing history. It was covered by an undissected volcanic arc during Wuchiapingian during the deposition of the lower WTG sandstones. However, the area was covered with complex lithologies of the amalgamated transitional volcanic arc, accretionary wedge, and trench rocks during Changhsingian-early Induan during the deposition of the upper WTG sandstones. This unroofing trend is similar to those of the continental arc within the Turan Plate, Western Turkmenistan (Garzanti and Gaetani, 2002) and the Andes in North America (Ingersoll, 2012), where the contents of quartz and feldspar in the studied sandstones increase at the expense of volcanic lithic fragments. During continuous plate consumption, sandstones may also show an increase

of polycrystalline quartz and chert fragments derived from the accretionary wedge and trench (Dickison and Suczek, 1979; Dickinson et al., 1983; Garzanti et al., 2007).

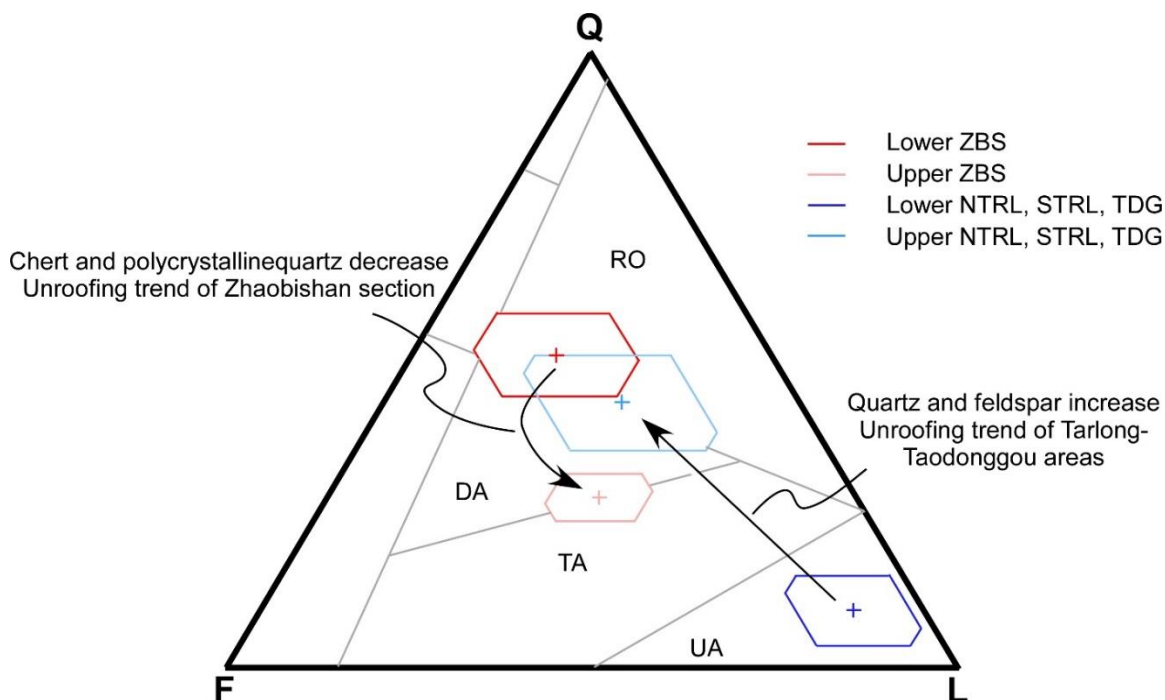


Figure 10. Unroofing trends of sources area in eastern North Tianshan Suture, as interpreted from petrofacies of WTG sandstones in Bogda Mountains. The trend for the ZBS section shows that the sources changed from the undissected volcanic arc, accretionary wedge and trench rocks to the transitional volcanic arc rocks. The trend for NTRL, STRL, and TDG sections shows that the sources shifted from the undissected volcanic arc rocks to the transitional volcanic arc, accretionary wedge and trench rocks. See Figure 7 for the explanations of the tectonic fields.

The two different unroofing trends between the source areas for ZBS and Tarlong-Taodonggou sections indicate that ENTS was an amalgamated complex with spatial and temporal variations in lithology during late Permian-earliest Triassic. During Wuchiapingian, the source areas of ZBS section in the eastern part of ENTS contained amalgamated rocks of the undissected volcanic arc, accretionary wedge and trench,

whereas the source areas of Tarlong-Taodonggou areas in the western part of ENTS contained assemblages of undissected volcanic arcs. During Changhsingian-early Induan, the eastern part of ENTS contained mainly rocks of volcanic arcs that were dissected, whereas the western part of ENTS contained rocks of the transitional volcanic arc, accretionary and trench (Figure 11).

7. CONCLUSIONS

Sandstones of the upper Permian-lowermost Triassic WTG low-order cycle in Bogda Mountains, NW China, provide critical information on the provenance and unroofing history of the ENTS. The source of the ZBS section to the east changed from the rocks of the undissected volcanic arc, accretionary wedge and trench to those of transitional volcanic arc with subordinate accretionary wedge and trench. The source of the NTRL and Taodongou (TDG) sections to the west shifted from the undissected volcanic arc and sedimentary rocks from ENTS and rift shoulders to rocks in the transitional volcanic arc, accretionary wedge and trench. The sources of the DLK section 70 km north of the NTRL and TDG sections are the undissected volcanic arc and sedimentary rocks from ENTS and rift shoulders. Unroofing history differs between the source areas for ZBS and NTRL-TDG sections, indicating that the ENTS was an amalgamated complex of the volcanic arc, accretionary wedge and trench with spatial and temporal variations in lithology during late Permian-earliest Triassic.

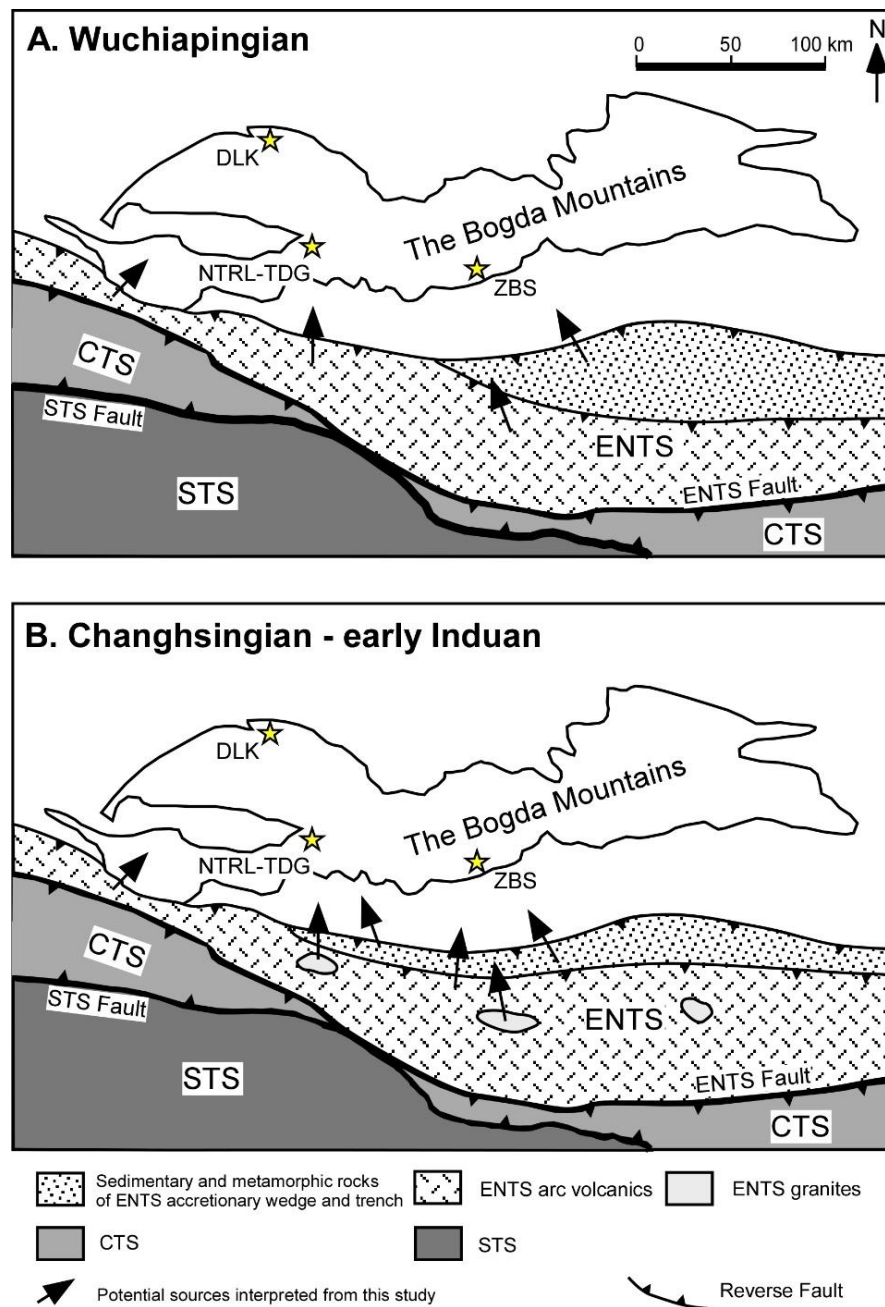


Figure 11. Schematic maps showing the reconstruction of lithologic distributions in the source areas in the eastern North Tianshan Suture during late Permian-earliest Triassic. A) During Wuchiapingian, most parts of eastern North Tianshan Suture were covered by undissected arc volcanic rocks and sedimentary and metamorphic rocks were exposed in the eastern parts of the eastern North Tianshan Suture. B) During Changhsingian to early Induan, the exposure of sedimentary and metamorphic rocks expanded to the western part of eastern North Tianshan Suture and the deep-seated granites were initially exposed. See text for details. ENTS, eastern North Tianshan Suture; CTS, Central Tianshan Suture; STS, South Tianshan Suture.

ACKNOWLEDGEMENTS

This work is a part of the dissertation research of D. Y. Zheng at Missouri University of Science and Technology, U.S.A. We would like to thank Drs. J. Wang, M. L. Wan and Mr. S. W. Mei of Nanjing Institute of Geology and Paleontology of Chinese Academy of Sciences and Y. R. Lu, X. Zhan, J. Duan, J. Fredericks, Z.Y. Ju, S.X. Wu and J.J. Li for their field assistance and financial support. D. Y. Zheng would like to thank Drs. J. Obrist-Farner, D. Wronkiewicz, J. P. Hogan, and A. Eckert of Missouri University of Science and Technology for serving in the dissertation committee and improving this manuscript. This research was partially supported by Alfred Spreng Graduate Research Grant from Geology and Geophysics Program of Missouri University of Science and Technology to D. Y. Zheng and by a research grant (EAR-1714749) from National Science Foundation to W. Yang.

REFERENCES

- Allen, J., 1968, The nature and origin of bed - form hierarchies: *Sedimentology*, v. 10, no. 3, p. 161-182.
- Allen, M., Windley, B., Chi, Z., Zhong, Y. Z., and Guang, R. W., 1991, Basin evolution within and adjacent to the Tien Shan Range, NW China: *Journal of the Geological Society*, v. 148, no. 2, p. 369-378.
- Allen, M. B., Windley, B. F., and Zhang, C., 1993, Palaeozoic collisional tectonics and magmatism of the Chinese Tien Shan, central Asia: *Tectonophysics*, v. 220, no. 1, p. 89-115.
- Allmendinger, R., 2005, Stereonet: Program for stereographic projection.

- Basu, A., Young, S. W., Suttner, L. J., James, W. C., and Mack, G. H., 1975, Re-evaluation of the use of undulatory extinction and polycrystallinity in detrital quartz for provenance interpretation: *Journal of Sedimentary Research*, v. 45, no. 4, p. 873-882.
- Blatt, H., Tracy, R., and Owens, B., 2006, *Petrology: igneous, sedimentary, and metamorphic*, Macmillan.
- Carroll, A., Graham, S., Hendrix, M., Ying, D., and Zhou, D., 1995, Late Paleozoic tectonic amalgamation of northwestern China: sedimentary record of the northern Tarim, northwestern Turpan, and southern Junggar basins: *Geological Society of America Bulletin*, v. 107, no. 5, p. 571-594.
- Carroll, A. R., Yunhai, L., Graham, S. A., Xuchang, X., Hendrix, M. S., Jinchi, C., and McKnight, C. L., 1990, Junggar basin, northwest China: trapped Late Paleozoic ocean: *Tectonophysics*, v. 181, no. 1-4, p. 1-14.
- Charvet, J., Shu, L., Laurent-Charvet, S., Wang, B., Faure, M., Cluzel, D., Chen, Y., and De Jong, K., 2011, Palaeozoic tectonic evolution of the Tianshan belt, NW China: *Science China Earth Sciences*, v. 54, no. 2, p. 166-184.
- Charvet, J., Shu, L. S., and Laurent-Charvet, S., 2007, Paleozoic structural and geodynamic evolution of eastern Tianshan (NW China): welding of the Tarim and Junggar plates: *Episodes*, v. 30, no. 3, p. 162-186.
- Critelli, S., and Ingersoll, R. V., 1995, Interpretation of neovolcanic versus palaeovolcanic sand grains: an example from Miocene deep - marine sandstone of the Topanga Group (Southern California): *Sedimentology*, v. 42, no. 5, p. 783-804.
- Davis, G. H., Reynolds, S. J., Kluth, C. F., and Kluth, C., 2011, *Structural geology of rocks and regions*, John Wiley & Sons.
- Dickinson, W. R., 1970, Interpreting detrital modes of graywacke and arkose: *Journal of Sedimentary Research*, v. 40, no. 2.
- Dickinson, 1985, Interpreting provenance relations from detrital modes of sandstones, *Provenance of arenites*, Springer, p. 333-361.
- Dickinson, W. R., Beard, L. S., Brakenridge, G. R., Erjavec, J. L., Ferguson, R. C., Inman, K. F., Knepp, R. A., Lindberg, F. A., and Ryberg, P. T., 1983, Provenance of North American Phanerozoic sandstones in relation to tectonic setting: *Geological Society of America Bulletin*, v. 94, no. 2, p. 222-235.

- Dickinson, W. R., and Suczek, C., 1979, Plate tectonics and sandstone composition: American Association of Petroleum Geologists Bulletin, v. 63, no. 12, p. 2164-2182.
- Dorsey, R. J., 1988, Provenance evolution and unroofing history of a modern arc-continent collision; evidence from petrography of Plio-Pleistocene sandstones, eastern Taiwan: Journal of Sedimentary Research, v. 58, no. 2, p. 208-218.
- Fang, S., Song, Y., Jia, C., Wang, X., and Yuan, Q., 2007, The Mesozoic-Cenozoic clastic composition of Bogda Area, Xinjiang: implications on the evolution of basin-range pattern: Acta Geologica Sinica, v. 81, no. 9, p. 1229-1237.
- Fredericks, J. G., 2017, Provenance and depositional environments of fluvial-lacustrine deposits in a non-marine rift basin, Lower-Triassic Jiucayuan and Shaofanggou low-order cycles Bogda Shan, NW China.
- Garzanti, E., Critelli, S., and Ingersoll, R. V., 1996, Paleogeographic and paleotectonic evolution of the Himalayan Range as reflected by detrital modes of Tertiary sandstones and modern sands (Indus transect, India and Pakistan): Geological Society of America Bulletin, v. 108, no. 6, p. 631-642.
- Garzanti, E., Doglioni, C., Vezzoli, G., and Ando, S., 2007, Orogenic belts and orogenic sediment provenance: The Journal of Geology, v. 115, no. 3, p. 315-334.
- Garzanti, E., and Gaetani, M., 2002, Unroofing history of Late Paleozoic magmatic arcs within the "Turan plate"(Tuarkyr, Turkmenistan): Sedimentary Geology, v. 151, no. 1-2, p. 67-87.
- Garzanti, E., Vezzoli, G., Andò, S., and Castiglioni, G., 2001, Petrology of Rifted - Margin Sand (Red Sea and Gulf of Aden, Yemen): The Journal of Geology, v. 109, no. 3, p. 277-297.
- Gawthorpe, R., and Leeder, M., 2000, Tectono-sedimentary evolution of active extensional basins: Basin Research, v. 12, no. 3-4, p. 195-218.
- Gazzi, P., 1966, Le arenarie del flysch sopracretaceo dell'Appennino modenese; correlazioni con il flysch di Monghidoro: Mineral. Petrogr. Acta, v. 12, no. 6, p. 69-97.
- Greene, T. J., Carroll, A. R., Hendrix, M. S., Graham, S. A., Wartes, M. A., and Abbink, O. A., 2001, Sedimentary record of Mesozoic deformation and inception of the Turpan-Hami basin, northwest China: Paleozoic and Mesozoic tectonic evolution of central and eastern Asia, v. 194, p. 317.

- Greene, T. J., Carroll, A. R., Wartes, M., Graham, S. A., and Wooden, J. L., 2005, Integrated provenance analysis of a complex orogenic terrane: Mesozoic uplift of the Bogda Shan and inception of the Turpan-Hami Basin, NW China: *Journal of Sedimentary Research*, v. 75, no. 2, p. 251-267.
- Guan, W., 2011, Provenance analysis of Upper Permian-basal Triassic fluvial-lacustrine sedimentary rocks in the greater Turpan-Junggar Basin, southern Bogda Mountains, NW China: Wichita State University.
- Guan, W., Yang, W., Jeffrey, B., Feng, Q., Liu, Y., Zhao, W., and Wang, Q., Distinguishing source areas of Upper-Permian fluvial-lacustrine deltaic sediment fills of a half-graben through petrographic study, southern Bogda Mountains, the Greater Turpan-Junggar basin, NW China: Abstract Volume, Am. Asso. Petrol, in *Proceedings Geologists Annual Meeting, New Orleans 2010*.
- Han, B. F., Guo, Z. J., Zhang, Z. C., Zhang, L., Chen, J. F., and Song, B., 2010, Age, geochemistry, and tectonic implications of a late Paleozoic stitching pluton in the North Tian Shan suture zone, western China: *Bulletin*, v. 122, no. 3-4, p. 627-640.
- Hendrix, M. S., 2000, Evolution of Mesozoic sandstone compositions, southern Junggar, northern Tarim, and western Turpan basins, northwest China: a detrital record of the ancestral Tian Shan: *Journal of Sedimentary Research*, v. 70, no. 3, p. 520-532.
- Hendrix, M. S., Dumitru, T. A., and Graham, S. A., 1994, Late Oligocene-early Miocene unroofing in the Chinese Tian Shan: An early effect of the India-Asia collision: *Geology*, v. 22, no. 6, p. 487-490.
- Hendrix, M. S., Graham, S. A., Carroll, A. R., Sobel, E. R., McKnight, C. L., Schulein, B. J., and Wang, Z., 1992, Sedimentary record and climatic implications of recurrent deformation in the Tian Shan: Evidence from Mesozoic strata of the north Tarim, south Junggar, and Turpan basins, northwest China: *Geological Society of America Bulletin*, v. 104, no. 1, p. 53-79.
- Hsü, K. J., 1988, Relict back-arc basins: principles of recognition and possible new examples from China, *New perspectives in basin analysis*, Springer, p. 245-263.
- Ingersoll, R. V., 2012, Composition of modern sand and Cretaceous sandstone derived from the Sierra Nevada, California, USA, with implications for Cenozoic and Mesozoic uplift and dissection: *Sedimentary Geology*, v. 280, p. 195-207.
- Ingersoll, R. V., Bullard, T. F., Ford, R. L., Grimm, J. P., Pickle, J. D., and Sares, S. W., 1984, The effect of grain size on detrital modes: a test of the Gazzi-Dickinson point-counting method: *Journal of Sedimentary Research*, v. 54, no. 1, p. 103-116.

- Ingersoll, R. V., and Suczek, C. A., 1979, Petrology and provenance of Neogene sand from Nicobar and Bengal fans, DSDP sites 211 and 218: *Journal of Sedimentary Research*, v. 49, no. 4.
- Jahn, Bor-ming, Fuyuan Wu, and Bin Chen., 2000, Granitoids of the Central Asian Orogenic Belt and continental growth in the Phanerozoic: *Earth and Environmental Science Transactions of the Royal Society of Edinburgh*, v. 91, no. 1-2: 181-193.
- Jun, G., Maosong, L., Xuchang, X., Yaoqing, T., and Guoqi, H., 1998, Paleozoic tectonic evolution of the Tianshan Orogen, northwestern China: *Tectonophysics*, v. 287, no. 1, p. 213-231.
- Laurent - Charvet, S., Charvet, J., Monié, P., and Shu, L., 2003, Late Paleozoic strike - slip shear zones in eastern Central Asia (NW China): New structural and geochronological data: *Tectonics*, v. 22, no. 2.
- Laurent - Charvet, S., Charvet, J., Shu, L., Ma, R., and Lu, H., 2002, Palaeozoic late collisional strike - slip deformations in Tianshan and Altay, eastern Xinjiang, NW China: *Terra Nova*, v. 14, no. 4, p. 249-256.
- Liao, Z., Lu, L., Jiang, N., Xia, F., Sung, F., Zhou, Y., Li, S., and Zhang, Z., Carboniferous and Permian in the western part of the east Tianshan Mountains: Beijing, in *Proceedings Eleventh Congress of Carboniferous Stratigraphy and Geology, Guide Book Excursion, 1987, Volume 4*, p. 50.
- Liu, S., Guo, Z., Zhang, Z., Li, Q., and Zheng, H., 2004, Nature of the Precambrian metamorphic blocks in the eastern segment of Central Tianshan: constraint from geochronology and Nd isotopic geochemistry: *Science in China Series D: Earth Sciences*, v. 47, no. 12, p. 1085-1094.
- Marsaglia, K. M., and Ingersoll, R. V., 1992, Compositional trends in arc-related, deep-marine sand and sandstone: a reassessment of magmatic-arc provenance: *Geological Society of America Bulletin*, v. 104, no. 12, p. 1637-1649.
- Miall, A. D., 1974, Paleocurrent analysis of alluvial sediments; a discussion of directional variance and vector magnitude: *Journal of Sedimentary Research*, v. 44, no. 4, p. 1174-1185.
- Obrist-Farner, J., and Yang, W., 2015, Nonmarine time-stratigraphy in a rift setting: An example from the Mid-Permian lower Quanzijie low-order cycle Bogda Mountains, NW China: *Journal of Palaeogeography*, v. 4, p. 27-51.

- Obrist-Farner, J., and Yang, W., 2017, Provenance and depositional conditions of fluvial conglomerates and sandstones and their controlling processes in a rift setting, mid-Permian lower and upper Quanzijie low order cycles, Bogda Mountains, NW China: *Journal of Asian Earth Sciences*, v. 138, p. 317-340.
- Okuzawa, K., and Hisada, K. i., 2008, Temporal changes in the composition of Miocene sandstone related to collision between the Honshu and Izu Arcs, central Japan: *Special Papers, Geological Society of America*, v. 436, p. 185.
- Peng, X., 2016, Provenance and depositional environments of fluvial-lacustrine sandstones of lower Permian Lucaogou low-order cycle, Bogda Mountains, NW China: Missouri University of Science and Technology.
- Şengör, A., Natal'in, B., and Burtman, V., 1993, Evolution of the Altiid tectonic collage and Palaeozoic crustal growth in Eurasia: *Nature*, v. 364, no. 6435, p. 299.
- Sengör, A., and Natalin, B., 1996, Paleotectonics of Asia: fragments of a synthesis.
- Shao, L., Stattegger, K., Li, W., and Haupt, B. J., 1999, Depositional style and subsidence history of the Turpan Basin (NW China): *Sedimentary Geology*, v. 128, no. 1, p. 155-169.
- Shao, L., Stattegger, K., and Garbe-Schoenberg, C. D., 2001, Sandstone petrology and geochemistry of the Turpan basin (nw china): Implications for the tectonic evolution of a continental basin: *Journal of Sedimentary Research*, v. 71, no. 1, p. 37-49.
- Shu, L., Charvet, J., Guo, L., Lu, H., and Laurent-Charvet, S., 1999, A large-scale Palaeozoic dextral ductile strike-slip zone: the Aqqikkudug–Weiya Zone along the Northern margin of the Central Tianshan Belt, Xinjiang, NW China: *Acta Geologica Sinica (English edition)*, v. 73, no. 2, p. 148-162.
- Shu, L., Wang, B., Zhu, W., Guo, Z., Charvet, J., and Zhang, Y., 2011, Timing of initiation of extension in the Tianshan, based on structural, geochemical and geochronological analyses of bimodal volcanism and olistostrome in the Bogda Shan (NW China): *International Journal of Earth Sciences*, v. 100, no. 7, p. 1647-1663.
- Shu, L. S., Zhu, W., Wang, B., Faure, M., Charvet, J., and Cluzel, D., 2005, The post-collision intracontinental rifting and olistostrome on the southern slope of Bogda Mountains, Xinjiang: *Acta Petrologica Sinica*, v. 21, p. 1, 25-36.
- Soreghan, M. J., and Cohen, A. S., 1993, The effects of basin asymmetry on sand composition: examples from Lake Tanganyika, Africa: *Special Papers-Geological Society of America*, p. 285-285.

- Suttner, L. J., 1974, Sedimentary petrographic provinces: an evaluation.
- Tang, W., Zhang, Z., Li, J., Li, K., Chen, Y., and Guo, Z., 2014, Late Paleozoic to Jurassic tectonic evolution of the Bogda area (northwest China): Evidence from detrital zircon U-Pb geochronology: *Tectonophysics*, v. 626, no. 1, p. 144-156.
- Thomas, S. G., Tabor, N. J., Yang, W., Myers, T. S., Yang, Y., and Wang, D., 2011, Palaeosol stratigraphy across the Permian-Triassic boundary, Bogda Mountains, NW China: Implications for palaeoenvironmental transition through earth's largest mass extinction: *Palaeogeography, Palaeoclimatology, Palaeoecology*, v. 308, no. 1-2, p. 41-64.
- Trop, J. M., and Ridgway, K. D., 1997, Petrofacies and provenance of a Late Cretaceous suture zone thrust-top basin, Cantwell Basin, central Alaska Range: *Journal of Sedimentary Research*, v. 67, no. 3, p. 469-485.
- Wang, B., Faure, M., Cluzel, D., Shu, L., Charvet, J., Meffre, S., and Ma, Q., 2006, Late Paleozoic tectonic evolution of the northern West Chinese Tianshan belt: *Geodinamica Acta*, v. 19, no. 3-4, p. 237-247.
- Wang, B., Shu, L. S., Cluzel, D., Faure, M., and Charvet, J., 2007, Geochronological and geochemical studies on the Borohoro plutons, north of Yili, NW Tianshan and their tectonic implication: *Acta Petrologica Sinica*, v. 8, p. 1885-1900.
- Wartes, M. A., Carroll, A. R., and Greene, T. J., 2002, Permian sedimentary record of the Turpan-Hami basin and adjacent regions, northwest China: Constraints on post-amalgamation tectonic evolution: *Geological Society of America Bulletin*, v. 114, no. 2, p. 131-152.
- Windley, B., Allen, M., Zhang, C., Zhao, Z., and Wang, G., 1990, Paleozoic accretion and Cenozoic red formation of the Chinese Tien Shan range, central Asia: *Geology*, v. 18, no. 2, p. 128-131.
- Windley, B. F., Alexeiev, D., Xiao, W., Kröner, A., and Badarch, G., 2007, Tectonic models for accretion of the Central Asian Orogenic Belt: *Journal of the Geological Society*, v. 164, no. 1, p. 31-47.
- XBGMR, 1993. Regional geology of Xinjiang Uygur Autonomous Region. Geological Memoirs, Series 1, No. 32. In: Xinjiang Bureau of Geology and Mineral resources (In Chinese with English abstract). Ministry of Geology and Mineral Resources, Geological Publication House, Beijing, p. 762.
- Xia, L.Q., Xu, X. Y., Xia, Z. C., Li, X. M., Ma, Z. P., and Wang, L. S., 2004, Petrogenesis of Carboniferous rift-related volcanic rocks in the Tianshan, northwestern China: *Geological Society of America Bulletin*, v. 116, no. 3-4, p. 419-433.

- Xiao, W.J., Zhang, L. C., Qin, K. Z., Sun, S., and Li, J. L., 2004, Paleozoic accretionary and collisional tectonics of the Eastern Tianshan (China): implications for the continental growth of central Asia: *American Journal of Science*, v. 304, no. 4, p. 370-395.
- Xiao, W., Windley, B. F., Allen, M. B., and Han, C., 2013, Paleozoic multiple accretionary and collisional tectonics of the Chinese Tianshan orogenic collage: *Gondwana Research*, v. 23, no. 4, p. 1316-1341.
- Yang, W., 2008, Depositional systems analysis within a seismic sequence stratigraphic framework, Turpan-Hami basin, Internal Report, Tu-Ha Petroleum Bureau NW China.
- Yang, W., Crowley, J., Obrist-Farner, J., Tabor, N., Feng, Q., and Liu, Y., 2013, A marine back-arc origin for the Upper Carboniferous basement of intracontinental greater Turpan-Junggar basin-Volcanic, sedimentary, and geochronologic evidence from southern Bogda Mountains, *in Proceedings NW China: Geological Society of America Annual Meeting, GSA Abstract with Programs, Volume 45*.
- Yang, W., Feng, Q., Liu, Y., Tabor, N., Miggins, D., Crowley, J. L., Lin, J., and Thomas, S., 2010, Depositional environments and cyclo- and chronostratigraphy of uppermost Carboniferous–Lower Triassic fluvial–lacustrine deposits, southern Bogda Mountains, NW China — A terrestrial paleoclimatic record of mid-latitude NE Pangea: *Global and Planetary Change*, v. 73, no. 1–2, p. 15-113.
- Yang, W., Liu, Y., Feng, Q., Lin, J., Zhou, D., and Wang, D., 2007, Sedimentary evidence of Early–Late Permian mid-latitude continental climate variability, southern Bogda Mountains, NW China: *Palaeogeography, Palaeoclimatology, Palaeoecology*, v. 252, no. 1, p. 239-258.
- Yin, A., Nie, S., Craig, P., Harrison, T., Ryerson, F., Xianglin, Q., and Geng, Y., 1998, Late Cenozoic tectonic evolution of the southern Chinese Tian Shan: *Tectonics*, v. 17, no. 1, p. 1-27.
- Young, S. W., 1976, Petrographic textures of detrital polycrystalline quartz as an aid to interpreting crystalline source rocks: *Journal of Sedimentary Research*, v. 46, no. 3, p. 595-603.
- Zhang, X., 1981, Regional stratigraphic chart of northwestern China, branch of Xinjiang Uygur Autonomous Region, Beijing, Geological Publishing House.

II. TEXTURAL CHARACTERISTICS AND THEIR CONTROLLING PROCESSES OF UPPER PERMIAN-LOWERMOST TRIASSIC SANDSTONES, WUTONGGOU LOW-ORDER CYCLE, BOGDA MOUNTAINS, NW CHINA

Dongyu Zheng and Wan Yang

ABSTRACT

Textural characteristics of sandstones provide critical information to understand the processes on the Earth's surfaces. This study focuses on the upper Permian-lowermost Triassic sandstones of Wutonggou (WTG) low-order cycle in Bogda Mountains, NW China and conducts a detailed textural analysis of these sandstones. Three petrofacies are identified by their relative compositions of quartz, feldspar, and lithic fragment. Petrofacies 1, with highest quartz content, is overall coarse-sized, moderately well sorted, and submature-mature. Petrofacies 2, with intermediate quartz content, is overall coarse-sized, moderately well sorted, and mature. Petrofacies 3, with lowest quartz content, is overall coarse-sized, moderately sorted, and submature. Variations of textural characteristics of petrofacies 1, 2, and 3 suggest that provenance, including source lithology and location, is a dominant factor in controlling sandstone textures. Petrofacies 1 and petrofacies 2 were derived from a distant source and are finer, better sorted, and more mature than the mixed-sourced petrofacies 3. Moreover, although petrofacies 1 and petrofacies 2 shared the same source location, variations in source lithology make their textures different. In addition, each petrofacies is subdivided into littoral/beach, deltaic, and fluvial facies. These sedimentary facies show limited variations in sorting degree, skewness, and textural maturity, thus these facies cannot be

distinguished on the basis of their textural characteristics. This work documents the textural characteristics of the ancient fluvial-lacustrine sandstones and discusses the controlling factors on sandstone textures.

1. INTRODUCTION

Sedimentary rocks recorded complex processes, involve with the tectonic activities, weathering, transportation, deposition, and diagenesis, and their interactions on the Earth's surfaces (e.g., Suttner, 1974; Ingersoll, 1984; Johnsson, 1993). The provenance is widely accepted as the most determining control on compositions of sedimentary rocks (Dickinson and Suczek, 1979; Johnsson, 1993; Garzanti, 2016), but the relationship between the provenance and textures is less discussed (Folk and Ward, 1957; Boulton, 1978; Arens et al., 2002; Obrist-Farner and Yang, 2017). Moreover, the textural characteristic is one of the widely-discussed attributes of sediments that many publications attempted to understand influences of processes of transportation and deposition on the textures (e.g., Passega, 1957; Visher, 1969; Barndorff-Nielsen, 1977; Folk, 1980; Boggs, 2009; Pettijohn et al., 2012). Different depositional environments, especially the beach, dune, and river, have been successfully distinguished by textural attributes of sediments (Folk and Ward, 1957; Friedman, 1962, 1967). However, skepticism of textural analysis demonstrates that the textural attributes should be restricted to the purpose of description (Ehrlich and Full, 1987; Hartmann, 2007). Therefore, it is intriguing to examine the relationship between textural features of ancient sedimentary rocks and depositional environments.

The upper Permian-lowermost Triassic Wutonggou (WTG) low-order cycle sandstones in Bogda Mountains, NW China provide a great opportunity to investigate the influences of the provenance and depositional environments on sandstone textures. The provenance, high-resolution measured sections and the associated depositional environments of WTG low-order were documented in previous studies (Yang et al., 2007, 2010; Zheng and Yang, submitted manuscript). Therefore, this study focus on the sandstones of WTG low-order cycle exposed in the northern and southern foothills of Bogda Mountains to document their textural characteristics, to interpret their textural maturity, and further to investigate the influences of provenance and depositional environments. The result of this works can improve our understanding of the controlling processes on sandstone textures.

2. GEOLOGICAL BACKGROUND

This study works on the upper Permian-lowermost Triassic fluvial-lacustrine sandstones and conglomerates of Wutonggou (WTG) low-order cycle exposed in Bogda Mountains (Figure1). Four sections, including the Zhaobishan (ZBS), North Tarlong (NTRL) and Taodonggou (TDG) sections, and Dalongkou (DLK) sections, in the southcentral, southwestern, and northern foothills of Bogda Mountains, are the focuses of this study (Figure 2). The Bogda Mountains is a giant E-W directed anticlines with Devonian to Quaternary sedimentary and igneous rocks and located between Junggar Basin to the north and Turapn-Hami Basin to the south in NW China. Before the Mesozoic uplift (Shao et al., 2001; Greene et al., 2005), Bogda Mountains was a part of

the greater Turpan-Junggar basin, which was an intracontinental rift basin caused by regional dextral strike-slip (Laurent-Charvet et al., 2002, 2007; Shu et al., 2011) and included a series of grabens and half-grabens (Yang et al., 2010; Obrist-Farner and Yang, 2015, 2016). The Bogda Mountains has a volcanic basement which is with either volcanic arc or back-arc origins (Shu et al., 2005, 2011; Yang et al., 2010, 2013). The Bogda Mountains was bordered by the eastern Chinese North Tianshan Suture to the south. The eastern Chinese North Tianshan is an amalgamated complex involves with the subduction of the North Tianshan Ocean and the collision between the Junggar Plate and the Central Tianshan Suture (Gao et al., 1998; Xiao et al., 2004, 2013; Charvet et al., 2011). The rocks of the eastern Chinese North Tianshan Suture and the volcanic and sedimentary rocks of the rift shoulders are interpreted as the main sources of the sandstones of WTG low-order cycle (Guan, 2011; Zheng and Yang, submitted manuscript).

The WTG low-order cycle is an informal cyclostratigraphic unit defined by overall long-term trends of subhumid-humid conditions and persistently uplifting history of the source areas (Yang et al., 2007, 2010; Thomas et al., 2011) and approximately correlates to Wutonggou and Guodikeng Formations (XBGMR, 1993; Figure3). The stratigraphy is correlated based on the lithostratigraphy, biostratigraphy, and cyclostratigraphy (Zhang, 1981; Liao et al., 1987; Wartes et al., 2002; Yang et al., 2007, 2010). The chronostratigraphy in Bogda Mountains is not well constrained that a Permo-Triassic boundary was placed within a 90 m-thick interval in North Tarlong section (Yang et al., 2010). Based on the stratigraphic correlation and petrographic studies (Yang et al., 2007, 2010; Guan, 2011; Peng, 2016; Fredericks, 2017; Obrist-Farner and Yang,

2017; Zheng and Yang, submitted manuscript), the strata in NTRL and TDG are interpreted as being deposited in one half-graben, named as Tarlong-Taodonggou half graben. The basin geometry of ZBS and DLK section is uncertain and is speculated to be similar to that of Tarlong-Taodonggou half-graben (Yang et al., 2010; Zheng and Yang, submitted manuscript).

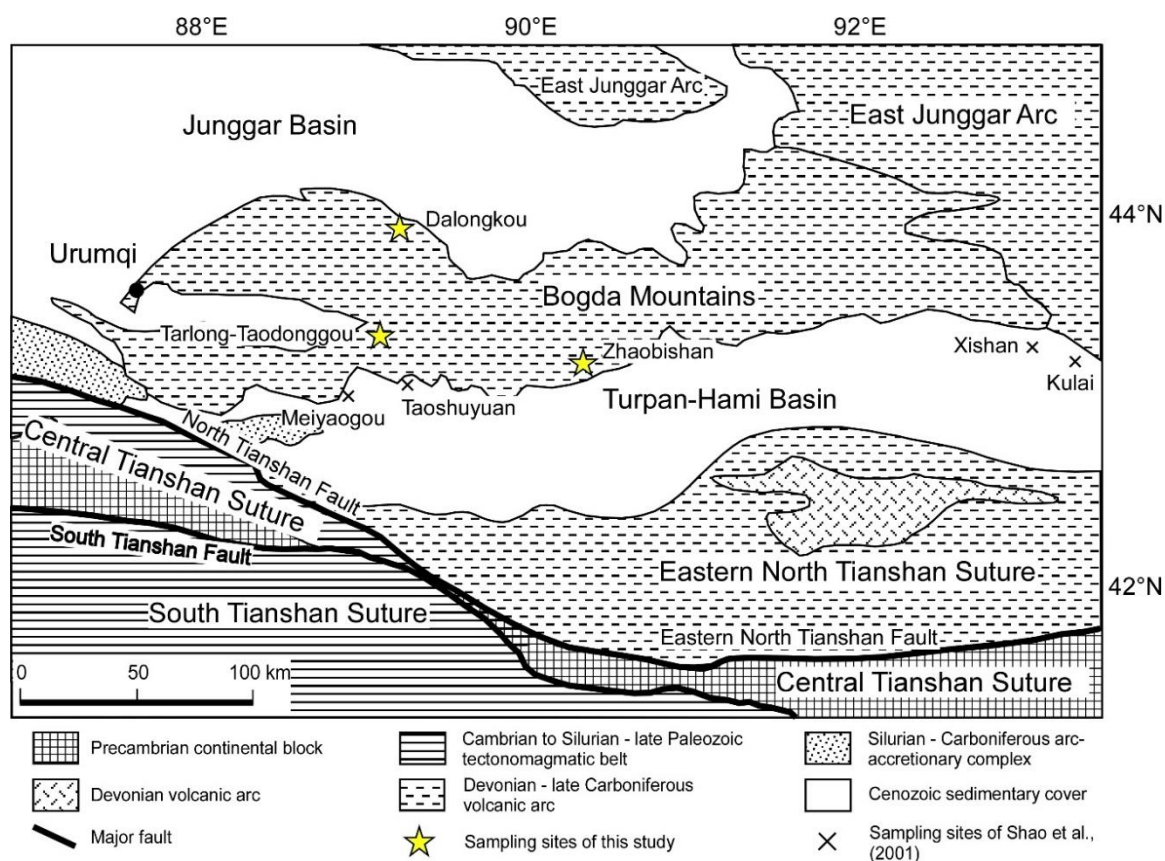


Figure 1. Tectonic map of study areas. This map shows the locations of Bogda Mountains and the eastern North Tianshan Suture, and the measured sections. Modified from Xia et al. (2004).

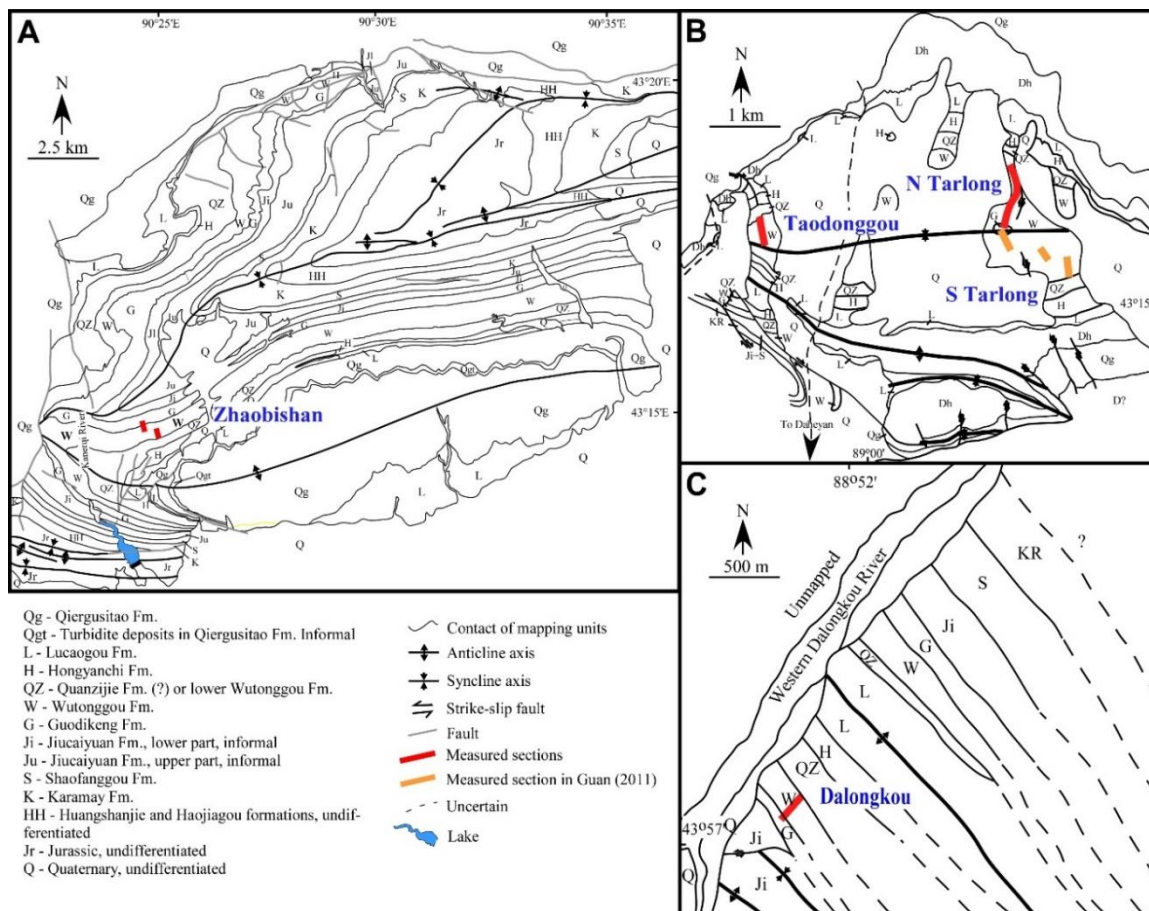


Figure 2. Geological maps of Zhaobishan (A), Tarlong-Taodonggou (B), and Dalongkou (C) areas. This map shows names and locations (red lines) of measured sections. Modified from Yang et al. (2010), Obrist-Farner and Yang (2015), and Fredericks (2017).

Three depositional environments, including fluvial, delta, and littoral-beach environments, have been interpreted within WTG low-order cycle based on the lithology, sedimentary texture and structures, paleontological information, stratal geometry and boundary relationships (Yang et al., 2007, 2010). The fluvial environments are subdivided into braided stream and meandering stream environments. The Braided stream environment is identified by an upward-fining succession of clast-supported conglomerate and/or sandstone on a low-relief erosional base (Figure 4). The meandering stream environment is recognized by an upward-fining succession of channel-fill

System	Series	Lithostratigraphy	Cyclostratigraphy Low-order Cycles (Yang et al., 2010; Obrist-Farner and Yang, 2015)	Revised chronostratigraphy (Yang et al., 2010, 203)		
				New dates	Stages	
Triassic	Middle	Karamay	Karamay		247.2 Anisian	
	Lower	Shaofanggou	Shaofanggou		251.2 Olenekian	
		Jiucaiyuan	Jiucaiyuan		251.9 Induan	
Permian	Lopingian	Guodikeng	Wutonggou	253.11	Changhsingian	
		Wutonggou		253.63	254.1	
	Guadalupian	Quanzijie	Upper Quanzijie		254.22	Wuchiapingian
		?	Lower Quanzijie	?		259.1
		?	?	?		265.1 Capitanian
		?	?	?		268.8 Wordian
	Cisuralian	Hongyanchi	Hongyanchi		273.0 Roadian	
		Lucaogou	Lucaogou		283.5 Kungurian	
		Daheyang	Upper Daheyang		290.1 Artinskian	
		Daheyang	Middle Daheyang		293.5 Sakmarian	
Carboniferous	Upper	Daheyang	Lower Daheyang		298.9 Asselian	
		Qiergusitao		301.26 ? 0.05	Gzhelian	
				301.37 ? 0.07	303.7	
				304.1	Kasimovian	
			305.50 ? 0.11			
			306.48 ? 0.32	307.0		

Figure 3. Chrono-, litho-, and cyclostratigraphy of upper Carboniferous-Middle Triassic strata in Bogda Mountains. Wavy lines are major unconformities; dashed lines disconformity; and hachured areas missing strata. The studied Wutonggou low-order cycle is shown in the shaded box. Modified from Yang et al. (2010) and Obrist and Yang (2015).

conglomerate and/or sandstone on a high-relief erosional base, highly cross-bedded point bar sandstones, and overbank sandstone, siltstone and shale (Figure 4). The deltaic environment is interpreted by the exposure of the upward-coarsening and thickening succession of prodeltaic shale, siltstone, sandstone and delta front siltstone, sandstone and/or conglomerate in the lower part of the succession, and distributary channel-fill and interdistributary deltaplain sandstone, conglomerate, mudrock, and paleosol in the upper

part (Figure 4). The littoral-beach environment is identified by the succession of laterally persistent sandstone and conglomerate, sublittoral shale, and overlying lakeplain muddy and sandy paleosols with high-angle cross-beddings (Figure 4). Transgressive lag deposits are common in WTG low-order cycle (Yang et al., 2007, 2010). The materials of the transgressive lags are derived from shore erosion of the underlying strata during lake transgression, characterizing by coarse-gravelly sandstone and conglomerate with common rip-up clasts. Some littoral-beach deposits are deficient with transgressive lag; the absence of transgressive lag may suggest the low-energy of the transgression (Yang et al., 2010).

3. DATA AND METHODOLOGY

Fifty-two fine- to very coarse-sized sandstones are point counted to record their compositional and textural characteristics. Three hundred framework grains in each thin section are documented with their grain type, size, and roundness using Gazzi-Dickinson's methods (Gazzi, 1966; Dickinson, 1970) and Suttner's method (Suttner, 1974). Gazzi-Dickinson's method counts sand-sized mineral crystals within large lithic fragments as individual mineral grains, whereas Suttner's method counts the mineral crystals as lithic fragments. In this study, the grain composition are recorded follows Gazzi-Dickinson's method to avoid the errors caused by grain size effects (Ingersoll, 1984); the grain textures are documented followed Suttner's method. Details of the grain composition are discussed in Zheng and Yang (Submitted Manuscript). Matrix and

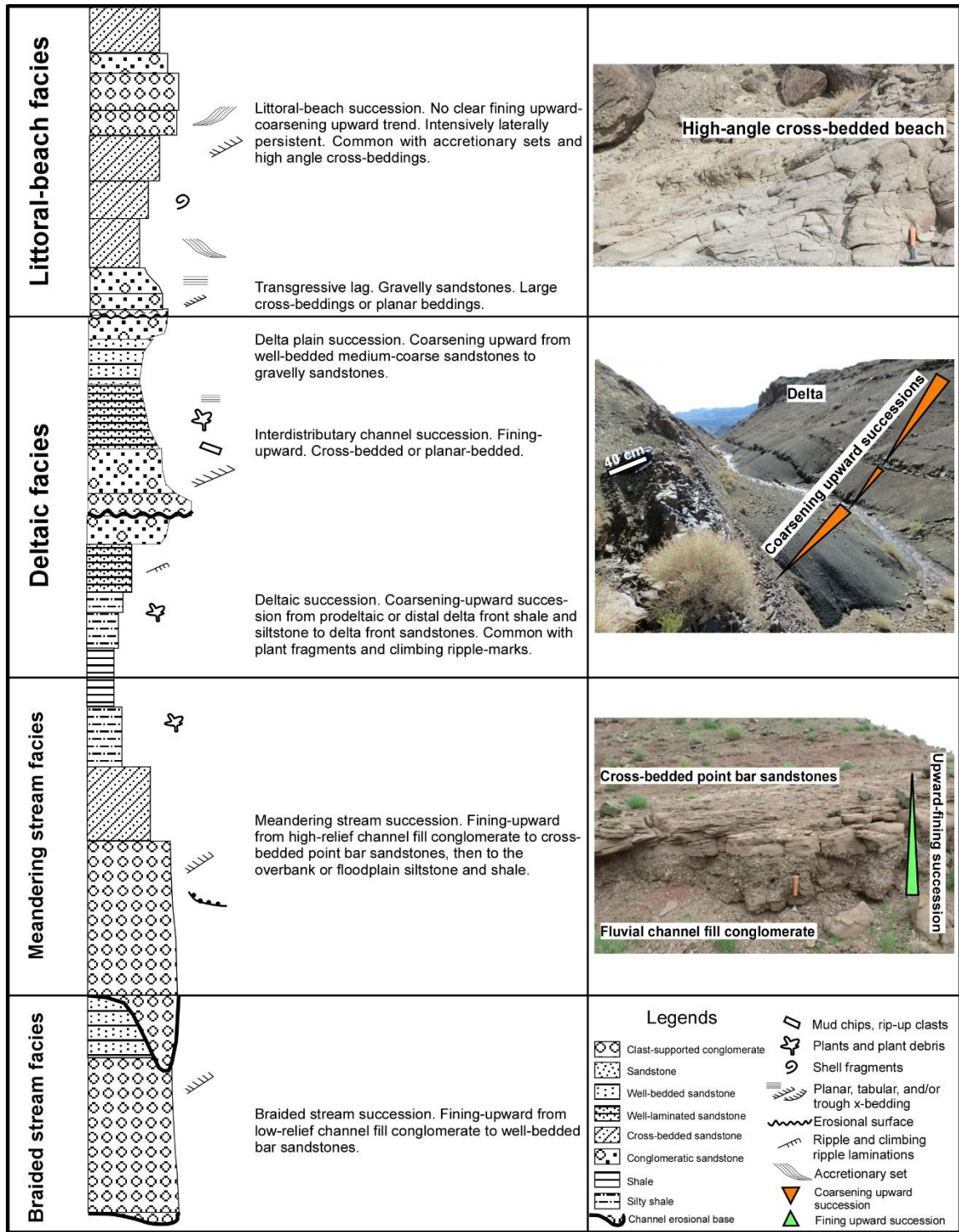


Figure 4. Sedimentary facies and descriptions. The facies include braided stream, meandering stream, deltaic, and littoral-beach successions from lower to upper column.

cements are recorded with their mineralogical type. The classification of sandstones follows Dott's (1964) scheme based on the grain composition and content of matrix. The grain size data in this study are in ϕ scale to overcome the problems caused by the great differences of each size class in the millimeter scale. The measurement of grain sizes of grains in thin sections underestimates the real values by 0.2023ϕ because the spherical grains are observed in the two-dimensional view (Johnson, 1994). In this work, the raw grain-size data are used without corrections.

The grain-size statistical parameters, including the graphic mean (M_z), inclusive graphic standard deviation (σ_i), inclusive graphic skewness (SK_i), and graphic kurtosis (K_G) are calculated using formulas in Folk and Ward (1957). Verbal terms of the grain sizes, sorting, skewness, and kurtosis are adapted from Udden-Wentworth grain-size scale (Udden-Wentworth, 1922) and verbal limits in Folk and Ward (1957). The grain roundness is estimated using the visual chart of roundness in Krumbein and Sloss (1951). The textural maturity and the associated textural inversion is defined on the basis of the matrix contents and degrees of sorting and roundness (Folk, 1951). As the degree of sorting of Folk and Ward (1957) has a better correlation with the standard deviation than Trask's (1932) sorting degree (Friedman, 1962), the former sorting degree is used to define textural maturity instead of the latter one.

4. RESULTS

Sandstones of Wutonggou low-order cycle are divided into three petrofacies on the basis of their relative content of quartz, feldspar, and lithic fragments (Figure 5; see

Zheng and Yang, submitted manuscript for details). The textural characteristics of each petrofacies, including the graphic mean, inclusive standard deviation, graphic skewness and kurtosis, matrix content, degree of roundness, and textural maturity and the associated textural inversion, are documented. In addition, each petrofacies is further subdivided in terms of their depositional environments to present the textural characteristics of various sandstone lithofacies.

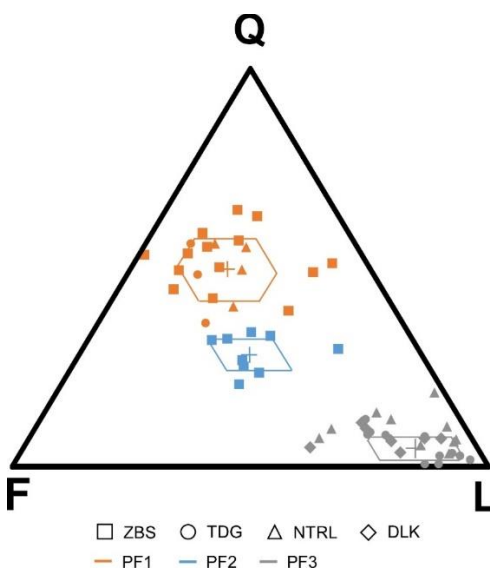


Figure 5. QFL ternary diagram and petrofacies. Petrofacies 1 has highest quartz content; petrofacies 2 has intermediate quartz content; petrofacies 3 has lowest quartz content. PF1, petrofacies 1; PF2, petrofacies 2; PF3, petrofacies 3.

4.1. TEXTURAL CHARACTERISTICS OF PETROFACIES 1

Petrofacies 1 (PF1) has a mean composition of $Q_{51}F_{30}L_{19}$ and occurs in eleven lithic arenites, nine feldspathic arenites, and one lithic wacke (Figure 5; Table 1). PF1 has an average graphic mean (Mz) of 0.88, corresponding to the grain size of coarse-sized, and includes three fine-, nine medium-, six coarse-, and three very coarse-sized

sandstones. PF1 is overall moderately well sorted with an average inclusive graphic standard deviation (σ_i) of 0.60 and is subdivided into eight well sorted-, eight moderately well sorted-, four moderately sorted-, and one poorly sorted-sandstones. PF1 is overall positively skewed with an average inclusive graphic skewness of 0.20 and contains one very negatively skewed-, one negatively skewed-, ten nearly symmetrically-, six positively skewed-, and two very positively skewed-sandstones. PF1 has an average graphic kurtosis of 1.34, corresponding to the degree of leptokurtic, and includes eighteen leptokurtic and three very leptokurtic sandstones. The average matrix content of PF1 is 1.47%, of which one sandstone contains matrix more than 5% and the rest contain matrix less than 5%. Two angular-subangular, seventeen subangular-subrounded, and two subrounded-rounded sandstones occur in PF1, of which the framework grains are overall subangular-subrounded with an average roundness of 0.39. PF1 has one immature, five submature, and fifteen mature sandstones and includes three texturally inverted submature or immature sandstones (Figures. 6, 7, 8; Table 1).

PF1 occurs in the lower 420 m, upper 220 m, and middle 50 m of Zhaobishan (ZBS), North Tarlong (NTRL), and Taodonggou (TDG) sections, respectively (Figures. 6, 7, 8). PF1 includes twelve littoral/beach, eight deltaic, and one fluvial sandstone (Figures. 6, 7, 8; Table 1). The deltaic sandstones have the average graphic mean, inclusive graphic standard deviation, inclusive graphic skewness, and graphic kurtosis of 0.78, 0.66, 0.39, and 1.40, respectively. The average matrix content and the average roundness is 1.63% and 0.42, respectively. Deltaic sandstones of PF1 include one immature, three submature, and four mature sandstones and three of them are texturally inverted. The littoral/beach sandstones have the average graphic mean, inclusive graphic

standard deviation, inclusive graphic skewness, and graphic kurtosis of 1.15, 0.58, 0.06, and 1.32, respectively. The average matrix content and the average roundness is 1.36% and 0.37, respectively. Littoral/beach sandstones of PF1 include two submature and ten mature sandstones and none of them is texturally inverted. The only one fluvial sandstone of PF1 has graphic mean, inclusive graphic standard deviation, inclusive graphic skewness, and graphic kurtosis of 0.97, 0.52, 0.25, and 1.26, respectively. This fluvial sandstone is mature and includes 1.54% matrix with the roundness of 0.37 (Table 1).

4.2. TEXTURAL CHARACTERISTICS OF PETROFACIES 2

Petrofacies 2 (PF2) has a mean composition of $Q_{28}F_{36}L_{36}$ and occurs in seven litharenites and two feldspathic arenites (Figure 5; Table 2). PF2 has an average graphic mean (M_z) of 0.96, corresponding to the coarse-sized, and includes six medium-, two coarse-, and one very coarse-sized sandstones. PF2 is overall moderately well sorted with an average inclusive graphic standard deviation (σ_i) of 0.51 and contains five well sorted- and four moderately well sorted-sandstones. PF2 is overall nearly symmetrical-positively skewed with an average inclusive graphic skewness of 0.88 and includes seven nearly symmetrically- and two positively skewed-sandstones. PF2 has an average graphic kurtosis of 1.38, corresponding to the degree of leptokurtic, and includes eighteen leptokurtic and one very leptokurtic sandstones. The average matrix content of PF2 is 0.29%, of which all sandstones contain matrix less than 5%. One angular-subangular and eight subangular-subrounded sandstones occur in PF2, of which the framework grains are

Table 1. Compositional and textural characteristics of petrofacies 1

Sample #	Section	Q	F	L	Mz	SD	Ski	KG	Matrix%	Roundness	Textural Maturity	Textural Inversion
PF1-Littoral/beach facies												
S15-31	ZBS	39	32	29	0.76	0.58	-0.08	1.29	2.00	0.38	Mature	No
S15-35	ZBS	40	39	21	1.12	0.50	0.12	1.28	0.00	0.29	Mature	No
S15-36	ZBS	34	24	41	-0.11	0.78	-0.73	1.26	3.21	0.44	Submature	No
S15-38	ZBS	37	31	32	0.83	0.91	0.19	1.21	3.00	0.38	Submature	No
S15-41	ZBS	29	49	23	1.21	0.49	-0.04	1.38	0.30	0.33	Mature	No
S15-45	ZBS	46	21	34	0.01	0.51	0.82	1.37	0.00	0.45	Mature	No
S15-49	ZBS	36	43	20	1.28	0.48	-0.02	1.58	1.00	0.31	Mature	No
S15-51	ZBS	24	37	39	1.11	0.52	0.18	1.28	0.00	0.48	Mature	No
NTR39-17	NTRL	15	34	50	1.15	0.48	0.05	1.28	4.00	0.37	Mature	No
TD128	TDG	36	37	27	2.12	0.57	0.19	1.28	2.02	0.28	Mature	No
TD131	TDG	25	42	34	2.33	0.63	0.02	1.34	0.75	0.35	Mature	No
TD137	TDG	38	36	26	2.00	0.49	0.01	1.24	0.00	0.32	Mature	No
Ave		33	35	31	1.15	0.58	0.06	1.32	1.36	0.37		
PF1-Deltaic facies												
S15-33	ZBS	30	13	57	-0.95	0.89	-0.15	1.14	0.00	0.50	Submature	Yes
S15-37	ZBS	32	17	51	1.30	0.45	2.60	1.42	3.00	0.42	Mature	No
S15-47	ZBS	36	46	18	1.95	0.46	0.04	1.40	0.00	0.42	Mature	No
S15-48	ZBS	34	7	59	-0.52	1.05	0.21	1.57	0.00	0.54	Submature	Yes
S15-52	ZBS	29	23	48	0.04	0.87	0.33	1.44	0.00	0.45	Submature	No
GW9-19	NTRL	34	23	43	0.64	0.59	0.06	1.51	2.00	0.35	Mature	No
NTR36-17	NTRL	33	27	40	1.77	0.50	-0.03	1.43	2.00	0.30	Mature	No
NTR37-17	NTRL	43	29	27	1.98	0.44	0.09	1.27	6.00	0.35	Immature	Yes
Ave		34	23	43	0.78	0.66	0.39	1.40	1.63	0.42		
PF1-Fluvial facies												
S15-40	ZBS	41	37	22	0.97	0.52	0.25	1.26	1.54	0.38	Mature	No
Overall average		33	30	37	1.06	0.59	0.28	1.36	1.40	0.39		

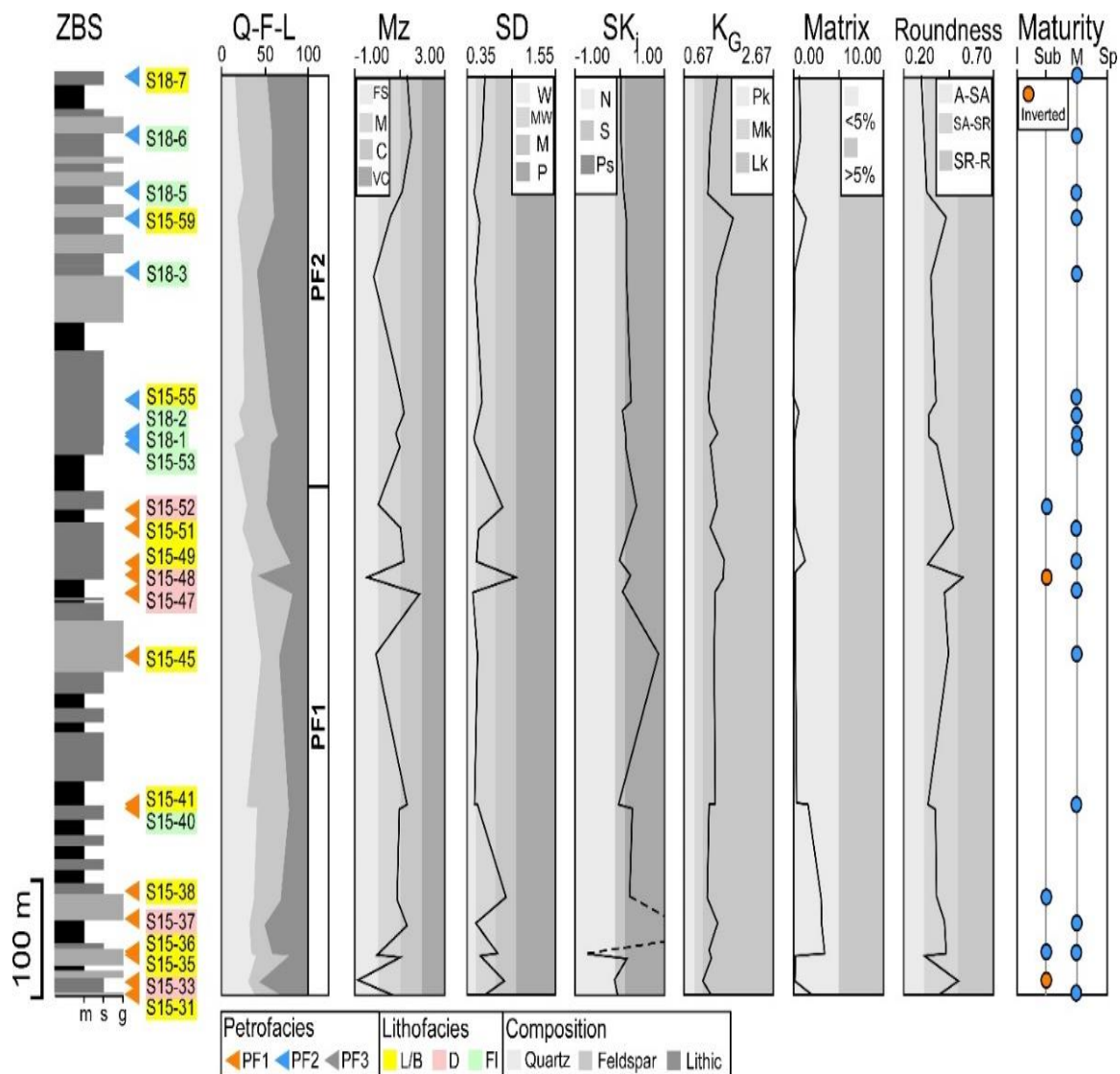


Figure 6. Simplified stratigraphic column of ZBS section showing compositions and textures of sandstones of Wutonggou low-order cycle. The triangle arrows indicate the petrofacies, and the color labeled sample numbers represent different lithofacies. In the last section, the texturally inverted sandstones are in orange color, and the normal sandstones are in blue color. PF1, petrofacies 1; PF2, petrofacies 2; PF3, petrofacies 3; L/B, littoral/beach; D, delta; Fl, fluvial; Fs, fine-sized; M, medium-sized; C, coarser-sized; VC, very coarse-sized; W, well sorted; MW, moderately well sorted; M, moderately sorted; P, poorly sorted; N, negatively skewed; S, symmetrical; Ps, positively skewed; Pk, platykurtic; Mk, mesokurtic; Lk, leptokurtic; A-SA, angular-subangular; SA-SR, subangular-subrounded; SR-R, subrounded-rounded; I, immature; Sub, submature; M, mature; Sp, supermature.

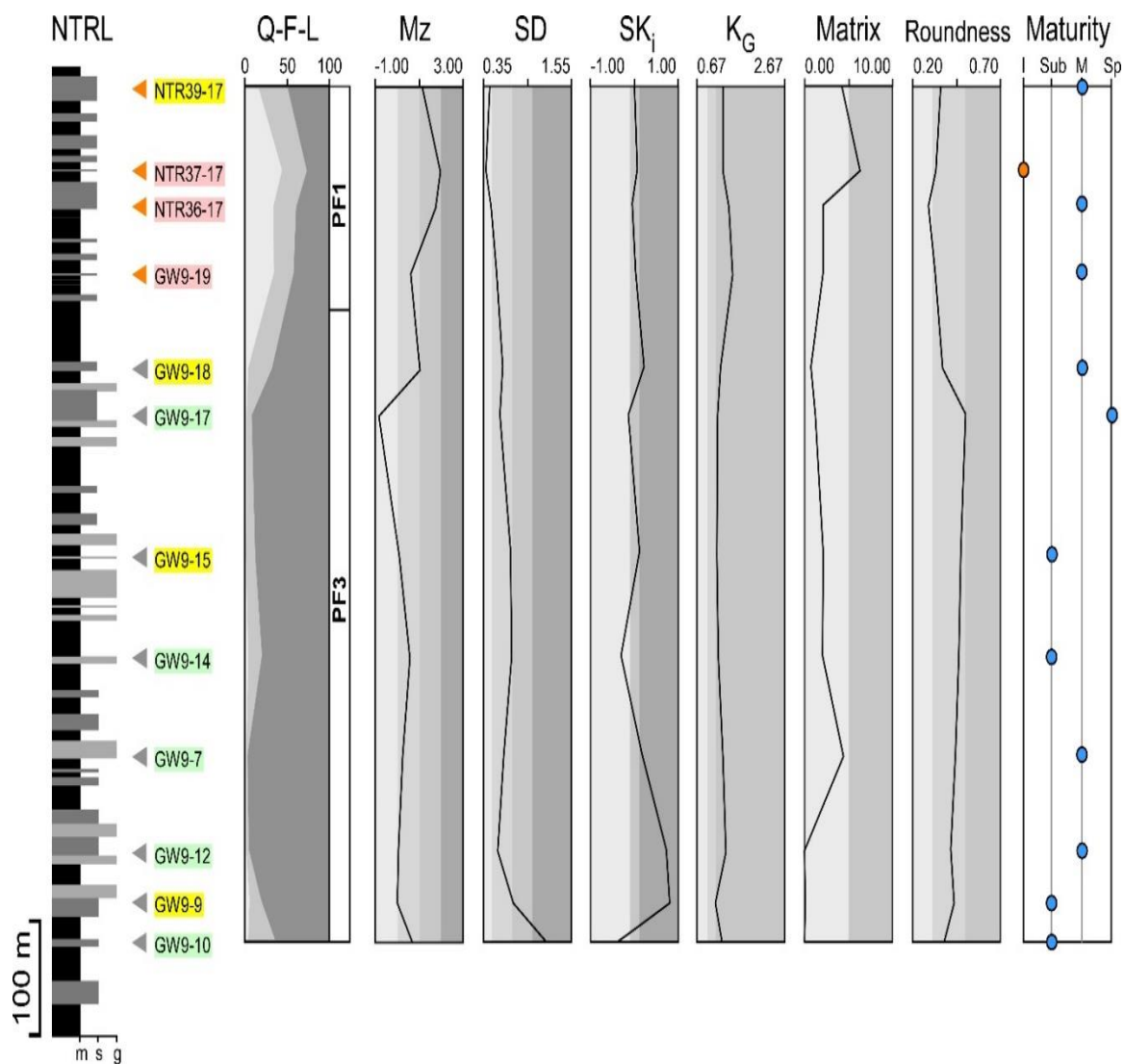


Figure 7. Simplified stratigraphic column of NTRL section showing compositions and textures of sandstones of Wutonggou low-order cycle. See figure 6 for legends and explanations of the abbreviations.

overall subangular-rounded with an average roundness of 0.35. All sandstones occur in PF2 are mature without textural inversion (Figure 7; Table 2).

PF2 occurs in the upper 350 m of Zhaobishan section and includes three littoral/beach and six fluvial sandstones (Figure 7; Table 2). The littoral/beach sandstones

have average graphic mean, inclusive graphic standard deviation, inclusive graphic skewness, and graphic kurtosis of 1.01, 0.56, 0.10, and 1.49, respectively. The average matrix content and the average roundness are 0.57% and 0.37, respectively. All these three sandstones are mature and none of them is texturally inverted. The fluvial sandstones have average graphic mean, inclusive graphic standard deviation, inclusive graphic skewness, and graphic kurtosis of 0.94, 0.49, 0.07, and 1.32, respectively. The average matrix content and the average roundness are 0.15% and 0.34, respectively. Similarly, all fluvial sandstones of PF2 are mature and none of them is texturally inverted (Figure 7; Table 2).

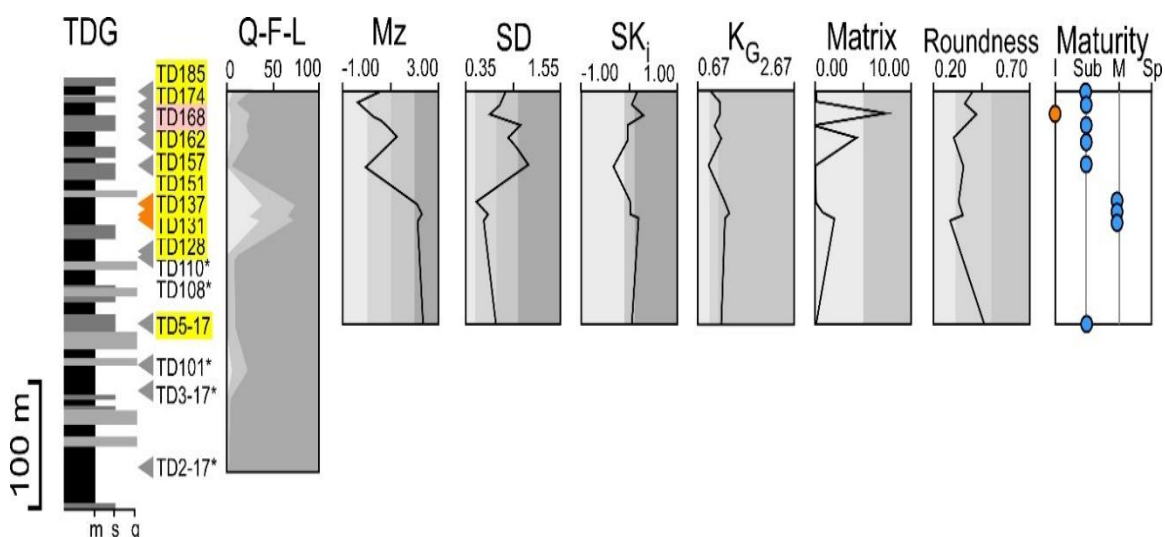


Figure 8. Simplified stratigraphic column of TDG section showing compositions and textures of sandstones of Wutonggou low-order cycle. See figure 6 for legends and explanations of the abbreviations. * samples are conglomerates, of which the textural characteristics are not discussed in this study.

4.3. TEXTURAL CHARACTERISTICS OF PETROFACIES 3

Petrofacies 3 (PF3) has a mean composition of $Q_8F_{13}L_{79}$ and occurs in twenty-one litharenites and one lithic wackes (Figure 5; Table 3). PF3 has an average graphic mean (Mz) of 0.41, corresponding to the grain size of coarse-sized, and includes six very coarse-sized, twelve coarse-sized, three medium-sized, and one fine-sized sandstones. PF3 is overall moderately sorted with an average inclusive standard deviation of 0.77 and includes three well sorted-, six moderately well sorted-, nine moderately sorted-, and four poorly sorted-sandstones. PF3 is overall positively skewed with an average graphic skewness of 0.16 and contains two very negatively skewed-, one negatively skewed-, six nearly symmetrical-, nine positively skewed-, and four very positively skewed sandstones. PF3 is overall leptokurtic with an average graphic kurtosis of 1.18 and includes one platykurtic, five mesokurtic, fourteen leptokurtic, one very leptokurtic, and one extremely leptokurtic sandstones. The average matrix content of PF3 is 1.13%, of which one sandstone contains matrix more than 5%, and the rest contain matrix less than 5%. One angular-subangular, seventeen subangular-subrounded, and four subrounded-rounded sandstones occur in PF3, of which the framework grains are overall subangular-subrounded with an average roundness of 0.44. PF3 is dominant with submature sandstones and consists of one immature, thirteen submature, six mature, and two supermature samples, of which eleven sandstones are texturally inverted (Figures. 7, 8, 9; Table 3).

PF3 occurs in the lower 600 m of North Tarlong, lower 200 m and upper 90 m of Taodonggou, and the entire Dalongkou sections. PF3 includes seven deltaic, ten littoral/beach, and five fluvial samples. The deltaic samples have average graphic mean,

inclusive graphic standard deviation, inclusive graphic skewness, and graphic kurtosis of 0.37, 0.59, 0.24, and 1.54, respectively. The average matrix content and the average roundness are 1.83% and 0.47, respectively. These samples have one immature, two submature, three mature, and one supermature sandstones, and four of the sandstones are texturally inverted. The littoral/beach samples have average graphic mean, inclusive graphic standard deviation, inclusive graphic skewness, and graphic kurtosis of 0.57, 0.89, 0.16, and 1.09, respectively. The average matrix content and the average roundness are 0.72% and 0.42, respectively. The littoral/beach samples of PF3 consist nine submature and one mature sandstones, and one of them is texturally inverted. The fluvial samples have average graphic mean, inclusive graphic standard deviation, inclusive graphic skewness, and graphic kurtosis of 0.15, 0.79, 0.05, and 1.24, respectively. The average matrix content and the average roundness are 1.42% and 0.45, respectively. This lithofacies has two submature, two mature, and one supermature sandstones, and none of them is texturally inverted (Figures. 7, 8, 9; Table 3).

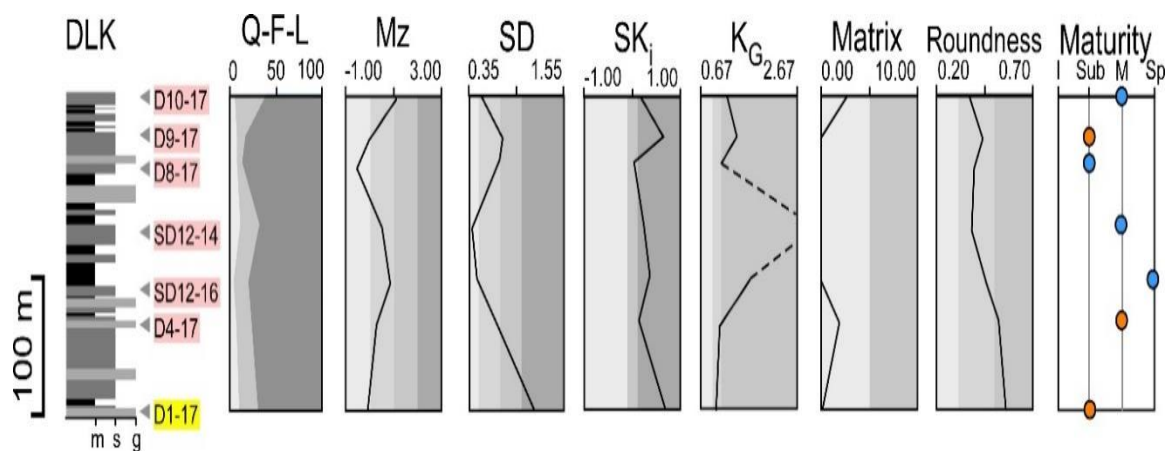


Figure 9. Simplified stratigraphic column of DLK section showing compositions and textures of sandstones of Wutonggou low-order cycle. See figure 6 for legends and explanations of the abbreviations.

Table 2. Compositional and textural characteristics of petrofacies 2

Sample #	Section	Q	F	L	Mz	SD	Ski	KG	Matrix%	Roundness	Textural Maturity	Textural Inversion
PF2-Littoral/beach lithofacies												
S15-55	ZBS	26	30	44	1.03	0.55	0.21	1.27	0.00	0.38	Mature	No
S15-59	ZBS	18	43	39	0.60	0.53	0.10	1.78	1.00	0.44	Mature	No
S18-7	ZBS	15	37	48	1.38	0.60	0.00	1.43	0.70	0.29	Mature	No
Ave		20	37	44	1.01	0.56	0.10	1.49	0.57	0.37		
PF2-Fluvial lithofacies												
S15-53	ZBS	14	43	43	1.00	0.50	0.09	1.28	0.00	0.38	Mature	No
S18-1	ZBS	26	39	35	0.83	0.46	0.09	1.44	0.00	0.34	Mature	No
S18-2	ZBS	20	39	41	1.22	0.50	0.05	1.29	0.20	0.33	Mature	No
S18-3	ZBS	23	17	59	-0.13	0.46	0.12	1.45	0.00	0.35	Mature	No
S18-5	ZBS	25	33	41	1.11	0.46	0.06	1.22	0.00	0.32	Mature	No
S18-6	ZBS	19	39	42	1.59	0.57	-0.01	1.28	0.70	0.31	Mature	No
Ave		21	35	44	0.94	0.49	0.07	1.32	0.15	0.34		
Overall average		21	35	44	0.94	0.49	0.07	1.32	0.15	0.34		

Table 3. Compositional and textural characteristics of petrofacies 3

Sample #	Section	Q	F	L	Mz	SD	Ski	KG	Matrix%	Roundness	Textural Maturity	Textural Inversion
PF3-Littoral/beach lithofacies												
gw9-9	NTRL	6	14	81	0.02	0.80	0.84	1.12	0.00	0.45	Submature	No
GW9-15	NTRL	1	11	88	0.12	0.77	0.14	1.15	2.00	0.49	Submature	No
GW9-18	NTRL	4	28	68	1.06	0.67	0.24	1.22	0.68	0.39	Mature	No
TD5-17	TDG	0	10	90	2.33	0.73	0.01	1.18	0.00	0.46	Submature	No
TD151	TDG	0	5	94	-0.10	1.15	-0.34	0.88	0.00	0.36	Submature	No
TD157	TDG	4	19	76	1.25	0.88	-0.06	1.19	4.50	0.30	Submature	No
TD162	TDG	4	17	78	0.86	1.07	-0.07	1.02	0.00	0.36	Submature	No
TD174	TDG	2	9	89	-0.41	0.78	0.06	1.15	0.00	0.35	Submature	No
TD185	TDG	7	20	72	0.60	0.85	0.17	0.97	0.00	0.41	Submature	No
D1-17	DLK	9	21	70	-0.04	1.18	0.58	1.01	0.00	0.59	Submature	Yes
Ave		4	15	81	0.57	0.89	0.16	1.09	0.72	0.42		
PF3-Deltaic lithofacies												
TD168	TDG	5	21	75	0.32	0.63	0.26	1.15	7.80	0.42	Immature	Yes
D4-17	DLK	6	17	77	0.31	0.68	0.13	1.07	2.00	0.56	Mature	Yes
SD12-16	DLK	3	16	81	0.84	0.44	0.28	1.69	0.00	0.51	Supermature	No
SD12-14	DLK	11	21	69	0.55	0.39	0.23	3.09	0.00	0.45	Mature	No
D8-17	DLK	7	6	87	-0.53	0.72	0.05	1.08	0.00	0.46	Submature	No
D9-17	DLK	7	9	84	-0.02	0.78	0.56	1.44	0.00	0.50	Submature	Yes
D10-17	DLK	4	35	61	1.12	0.50	0.15	1.24	3.00	0.42	Mature	No
Ave		6	18	76	0.37	0.59	0.24	1.54	1.83	0.47		
PF3-Fluvial lithofacies												
gw9-10	NTRL	4	32	64	0.67	1.27	-0.38	1.27	0.00	0.39	Submature	No
gw9-12	NTRL	2	3	95	0.07	0.59	0.75	1.34	0.00	0.43	Mature	No
gw9-7	NTRL	2	1	97	0.23	0.68	0.20	1.27	4.14	0.46	Mature	No
gw9-14	NTRL	4	16	80	0.59	0.80	-0.26	1.16	1.97	0.48	Submature	No
GW9-17	NTRL	2	6	92	-0.79	0.62	-0.08	1.17	1.00	0.51	Supermature	No
Ave		3	12	86	0.15	0.79	0.05	1.24	1.42	0.45		
Overall Average		5	15	80	0.29	0.75	0.16	1.32	1.26	0.46		

5. CONTROLS ON TEXTURE CHARACTERISTICS

5.1. PROVENANCE

Three petrofacies are differentiated on the basis of their grain compositions that were derived from different provenance, including the source lithology and the locations. Both petrofacies 1 (PF1) and petrofacies 2 (PF2) are interpreted as derived from the eastern North Tianshan Suture (ENTS), about 100 km south of the studied areas. Moreover, the source lithologies of PF1 and PF2 were slightly different that the main source lithology of PF1 are rhyolite, chert, and quartzite, whereas the source lithology of PF2 are dominated by rhyolite and granite, and subordinate with chert and quartzite (Zheng and Yang, submitted manuscript).

The textural characteristics of PF1 and PF2, similar to their grain compositions, show slight differences. Overall, sandstones occur in PF1 and PF2 are mainly coarse- to medium-sized, moderately well sorted, and leptokurtic. Moreover, the matrix contents of PF1 and PF2 are low and the framework grains are subangular to subrounded. Despite the great similarities between PF1 and PF2, differences in the grain size distribution and textural maturity exist. PF1 has a broad grain size ranging from -0.95 to 2.33, whereas the sizes of PF2 range from -0.13 to 1.59. Moreover, the inclusive standard deviation of PF1 ranges from 0.44 to 1.05, of which the range is also broader than the range of PF2, from 0.46 to 0.60 (Figure 10). Seventy percent of the sandstones of PF1 are mature, whereas all sandstones of PF2 are mature. These textural characteristics suggest that sandstones of PF1 are relatively worse sorted and less mature than those of PF2. The differences in textural characteristics were likely caused by their different source lithologies. Source

rocks of PF1 were the mixtures of rhyolite, granite, chert, quartzite, whereas the source rocks of PF2 were uniform and dominated by rhyolites and granites. As rhyolites and granites, and chert and quartzite were derived from the volcanic arc and the accretionary wedge and trench, respectively, these grains might have different original grain sizes. In addition, these grains might also have different degrees of resistance during transportation that chert grains were likely more stable than the volcanic and metamorphic lithic fragments (Cameron and Blatt, 1971; Abbott and Peterson, 1978). As a result, PF1 shows more variations in grain sizes and sorting degrees and has lower textural maturity than PF2.

In contrast to PF1 and PF2, the textural characteristics of sandstones of PF3 are different. The average graphic mean of PF3 is 0.41, indicating that PF3 has an overall coarser grain size than PF1 and PF2. Moreover, the inclusive standard deviation of PF3 ranges from 0.39 (well sorted) to 1.27 (poorly sorted) with an average value of 0.77 and suggests that PF3 has an overall worse sorting degree and a wider range of sorting degree than PF1 and PF2 (Figure 10). The average roundness of PF3 is 0.46, about 0.1 higher than the roundness of PF1 and PF2, indicating that the degree of roundness of PF3 is better than PF1 and PF2. Moreover, the textural maturity of PF3 is lower than the maturities of PF1 and PF2 that only 37% sandstones of PF3 are mature.

The results indicate that the provenance not only controlled grain compositions, but also greatly influenced textural characteristics. The provenance of PF3 is interpreted as including the volcanic, metamorphic and sedimentary rocks from both volcanic arc, accretionary wedge and trench of the eastern North Tianshan Suture and rift shoulders

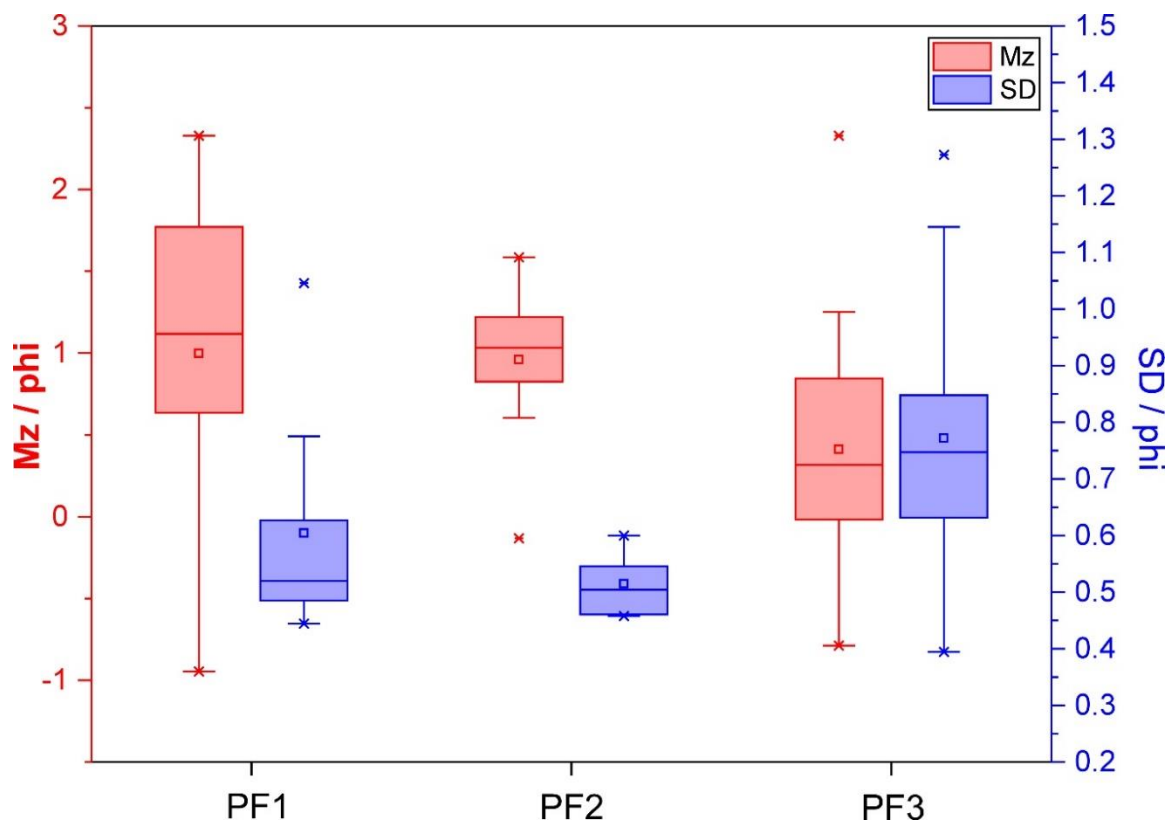


Figure 10. Box and whisker plot of graphic means and inclusive standard deviations of PF1, PF2, and PF3. Mz, graphic mean; SD, inclusive standard deviation.

(Zheng and Yang, submitted manuscript). In contrast, rocks of the eastern North Tianshan Suture were the only provenance of PF1 and PF2. Therefore, PF3 has not only more lithic fragments but also broader ranges of grain sizes and sorting degrees than PF1 and PF2. Local rock fragments from the rift shoulders without many transportations, such as the rip-up mud clasts, might be the origins of the coarse-sized clasts. In addition, as the greater Turpan-Junggar basin was a partitioned rift basin with abundant rift shoulders and complex drainage systems that local lithic fragments might experience long transportations on the gentle ramps of half-grabens within the rift basin (Soreghan and

Cohen, 1993; Obrist-Farner and Yang, 2017), thus to form the fine-sized and rounded grains.

5.2. DEPOSITIONAL ENVIRONMENTS

To discuss the influences of depositional environments, textural characteristics, including sorting degree, skewness, and textural maturity, of littoral/beach, deltaic, and fluvial sandstones are compared. As the provenance greatly affects the textural characteristics, only sedimentary facies belong to the same petrofacies are compared.

The littoral/beach, deltaic, and fluvial sandstones show limited variations in sorting degrees, skewness, and textural maturity. PF1 has eight deltaic, twelve littoral/beach, and one fluvial sandstones. As the fluvial sandstone is not statistically sufficient, it is not compared with other sandstone lithofacies. Both littoral/beach and deltaic facies are moderately well sorted and positively skewed, indicating these two facies cannot be distinguished by sorting degree and skewness (Figure 11). Moreover, these two facies are mainly dominated by submature-mature sandstones (Table 1). Similarly, the littoral/beach and fluvial sandstones of PF2 also have limited variations in sorting degrees, skewness, and textural maturity that these facies are moderately well sorted, positively skewed, and mature (Figure 12; Table 2).

In contrary to PF1 and PF2, the textural characteristics of various sedimentary facies of PF3 are more complex. Among the three facies, deltaic sandstones are characterized by highest sorting degree that they are moderately well sorted, whereas littoral/beach and fluvial sandstones are moderately sorted (Figure 13; Table 3).

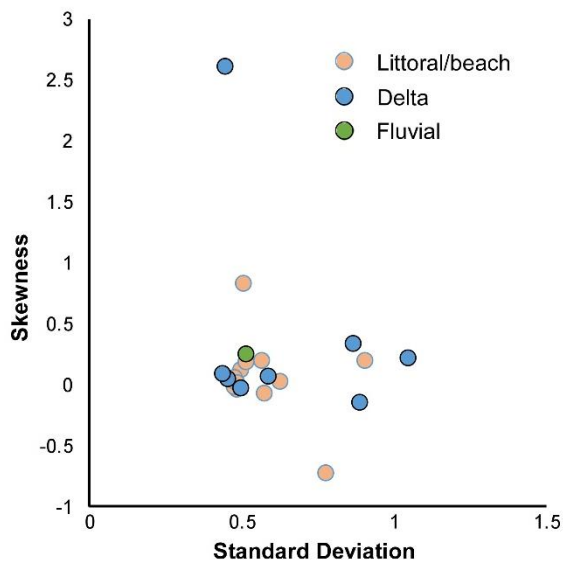


Figure 11. Bivariate plot of standard deviation versus skewness of petrofacies 1 sandstones. This diagram shows that littoral/beach, deltaic and fluvial sandstones of petrofacies 1 have similar sorting degree and skewness.

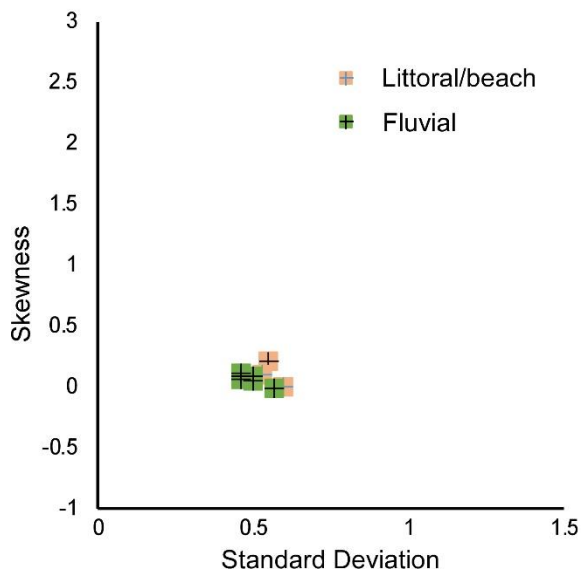


Figure 12. Bivariate plot of standard deviation versus skewness of petrofacies 2 sandstones. This diagram shows that littoral/beach and fluvial sandstones of petrofacies 2 have similar sorting degree and skewness.

In addition, littoral/beach facies are mainly submature sandstones, whereas the deltaic and fluvial facies include immature to supermature sandstones (Table 3). The overall textural maturities of deltaic and fluvial facies are relatively higher than that of littoral/beach facies.

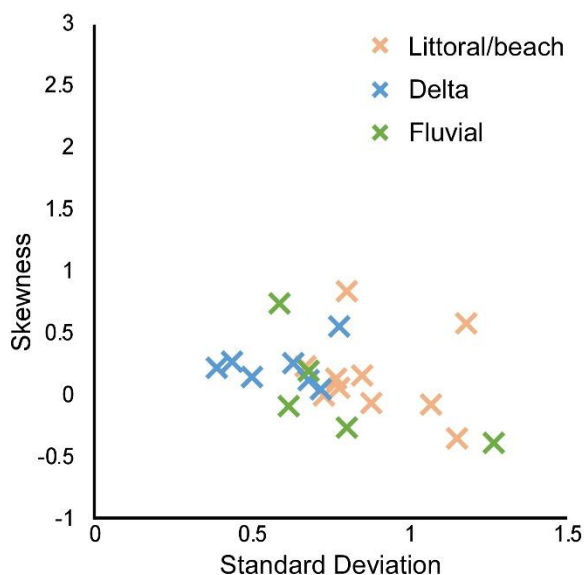


Figure 13. Bivariate plot of standard deviation versus skewness of petrofacies 3 sandstones. This diagram shows that deltaic sandstones of petrofacies 3 are relatively better sorted than littoral/beach sandstones, and fluvial sandstones have variable sorting degrees.

Previous studies demonstrate that littoral/beach sandstones in marine setting are typically well sorted, positively skewed, and mature resulting from forth and back transportation and high input energy (Folk, 1951; Folk and Ward, 1957; Friedman, 1962, 1967). However, as the littoral/beach sandstones in this study are collected from nonmarine environment, the reworking process produced by tides are absent. Moreover, the directions of waves are greatly influenced by regional factors thus may form

sandstones with distinct textural characteristics in different positions of a lake. Finally, as the frequent lake expansion and contraction in the greater Turpan-Junggar basin (Yang et al., 2007, 2010), the depositional environments may differ even within a thin interval. The depositional environments are interpreted with their broad terms, such as the littoral/beach (Yang et al., 2007, 2010), but detailed sub-environments are difficult to be obtained by the field interpretations. These sub-environments are necessary for detailed textural analysis. For example, backshore and upper shoreface are both interpreted as littoral/beach environment, but depositional processes of backshore and uppershore facies are caused by waves and tides, respectively. The result of this study indicates that textural characteristics of sandstones in nonmarine fluvial-lacustrine environments are not good criteria to distinguish different sedimentary facies.

6. CONCLUSIONS

Sandstones of the upper Permian-lowermost Triassic Wutonggou low-order cycle in Bogda Mountains, NW China are classified as three petrofacies, of which the textural characteristics are documented. Petrofacies 1 is overall coarse-sized, moderately well sorted, and submature-mature. Textural characteristics of petrofacies 2 are similar to petrofacies 1, but are slightly finer, better sorted, and more mature. In contrast to petrofacies 1 and petrofacies 2, petrofacies 3 is the coarsest-sized with a broad grain size range, worst sorted, and least mature. Variations of textural characteristics of petrofacies 1, 2, and 3 suggest that provenance, including source lithology and location, is a dominant factor in controlling sandstone textures. Moreover, each petrofacies is

subdivided into littoral/beach, deltaic, and fluvial sedimentary facies. Sandstones of different facies do not show great differences in sorting, skewness, and textural maturities, and thus are unlikely to be distinguished on the basis of their textural characteristics. The results of this study present the textural characteristics of the ancient fluvial-lacustrine sandstones and discuss the possible controlling factors of the sandstone textures.

ACKNOWLEDGEMENTS

We would like to thank Drs. J. Wang, M. L. Wan and Mr. S. W. Mei of Nanjing Institute of Geology and Paleontology of Chinese Academy of Sciences, Y. R. Lu, X. Zhan, J. Duan, J. Fredericks, Z. Y. Jue, S. X. Wu and Mr. Li for their assistance in field and funding. This research was partially supported by the student research grant from Alfred Spreng Graduate Research Grant from Geology and Geophysics Program of Missouri University of Science and Technology to Dongyu Zheng, and by a research grant (EAR-1714749) from National Science Foundation to Wan Yang.

REFERENCES

- Abbott, P. L., and Peterson, G. L., 1978, Effects of abrasion durability on conglomerate clast populations; examples from Cretaceous and Eocene conglomerates of the San Diego area, California: *Journal of Sedimentary Research*, v. 48, no. 1, p. 31-42.
- Arens, S., Van Boxel, J., and Abuodha, J., 2002, Changes in grain size of sand in transport over a foredune: *Earth Surface Processes and Landforms*, v. 27, no. 11, p. 1163-1175.

- Barndorff-Nielsen, O., 1977, Exponentially decreasing distributions for the logarithm of particle size: *Proc. R. Soc. Lond. A*, v. 353, no. 1674, p. 401-419.
- Boggs Jr, S., and Boggs, S., 2009, *Petrology of sedimentary rocks*, Cambridge university press.
- Boulton, G., 1978, Boulder shapes and grain - size distributions of debris as indicators of transport paths through a glacier and till genesis: *Sedimentology*, v. 25, no. 6, p. 773-799.
- C. Griffiths, J., 1967, *Scientific Method in Analysis of Sediments*.
- Cameron, K. L., and Blatt, H., 1971, Durabilities of sand size schist and 'volcanic' rock fragments during fluvial transport, Elk creek, Black Hills, South Dakota: *Journal of Sedimentary Research*, v. 41, no. 2, p. 565-576.
- Charvet, J., Shu, L., Laurent-Charvet, S., Wang, B., Faure, M., Cluzel, D., Chen, Y., and De Jong, K., 2011, Palaeozoic tectonic evolution of the Tianshan belt, NW China: *Science China Earth Sciences*, v. 54, no. 2, p. 166-184.
- Charvet, J., Shu, L. S., and Laurent-Charvet, S., 2007, Paleozoic structural and geodynamic evolution of eastern Tianshan (NW China): welding of the Tarim and Junggar plates: *Episodes*, v. 30, no. 3, p. 162-186.
- Dickinson, W. R., 1970, Interpreting detrital modes of graywacke and arkose: *Journal of Sedimentary Research*, v. 40, no. 2.
- Dickinson, W. R., and Suczek, C., 1979, Plate tectonics and sandstone composition: *American Association of Petroleum Geologists Bulletin*, v. 63, no. 12, p. 2164-2182.
- Dott Jr, R. H., 1964, Wacke, Graywacke and Matrix--What Approach to Immature Sandstone Classification?: *Journal of Sedimentary Research*, v. 34, no. 3.
- Ehrlich, R., and Full, W. E., 1987, Sorting out geology—unmixing mixtures: Use and Abuse of Statistical Methods in the Earth Sciences, v. 1, p. 33-46.
- Folk, R. L., 1951, Stages of textural maturity in sedimentary rocks: *Journal of Sedimentary Research*, v. 21, no. 3, p. 127-130.
- Folk, R. L., 1980, *Petrology of Sedimentary Rocks*: Hemphill Publishing Company, Austin, Texas, p. 184.
- Folk, R. L., and Ward, W. C., 1957, Brazos River bar [Texas]; a study in the significance of grain size parameters: *Journal of Sedimentary Research*, v. 27, no. 1, p. 3-26.

- Fredericks, J. G., 2017, Provenance and depositional environments of fluvial-lacustrine deposits in a non-marine rift basin, Lower-Triassic Jiucayuan and Shaofanggou low-order cycles Bogda Shan, NW China.
- Friedman, G. M., 1962, On sorting, sorting coefficients, and the lognormality of the grain-size distribution of sandstones: *The Journal of Geology*, v. 70, no. 6, p. 737-753.
- Garzanti, E., Al-Juboury, A. I., Zoleikhaei, Y., Vermeesch, P., Jotheri, J., Akkoca, D. B., Obaid, A. K., Allen, M. B., Andó, S., and Limonta, M., 2016, The Euphrates-Tigris-Karun river system: Provenance, recycling and dispersal of quartz-poor foreland-basin sediments in arid climate: *Earth-Science Reviews*, v. 162, p. 107-128.
- Gazzi, P., 1966, Le arenarie del flysch sopracretaceo dell'Appennino modenese; correlazioni con il flysch di Monghidoro: *Mineral. Petrogr. Acta*, v. 12, no. 6, p. 69-97.
- Glaister, R., and Nelson, H., 1974, Grain-size distributions, an aid in facies identification: *Bulletin of Canadian Petroleum Geology*, v. 22, no. 3, p. 203-240.
- Greene, T. J., Carroll, A. R., Wartes, M., Graham, S. A., and Wooden, J. L., 2005, Integrated provenance analysis of a complex orogenic terrane: Mesozoic uplift of the Bogda Shan and inception of the Turpan-Hami Basin, NW China: *Journal of Sedimentary Research*, v. 75, no. 2, p. 251-267.
- Guan, W., 2011, Provenance analysis of Upper Permian-basal Triassic fluviallacustrine sedimentary rocks in the greater Turpan-Junggar Basin, southern Bogda Mountains, NW China: Wichita State University.
- Hartmann, D., 2007, From reality to model: Operationalism and the value chain of particle-size analysis of natural sediments: *Sedimentary Geology*, v. 202, no. 3, p. 383-401.
- Ingersoll, R. V., Bullard, T. F., Ford, R. L., Grimm, J. P., Pickle, J. D., and Sares, S. W., 1984, The effect of grain size on detrital modes: a test of the Gazzi-Dickinson point-counting method: *Journal of Sedimentary Research*, v. 54, no. 1, p. 103-116.
- Johnson, M., 1994, Thin section grain size analysis revisited: *Sedimentology*, v. 41, no. 5, p. 985-999.
- Johnsson, M. J., 1993, The system controlling the composition of clastic sediments: *Geological Society of America Special Papers*, v. 284, p. 1-20.

- Jun, G., Maosong, L., Xuchang, X., Yaoqing, T., and Guoqi, H., 1998, Paleozoic tectonic evolution of the Tianshan Orogen, northwestern China: *Tectonophysics*, v. 287, no. 1, p. 213-231.
- Krumbein, W. C., and Sloss, L. L., 1951, *Stratigraphy and sedimentation*, LWW, v. 5.
- Laurent - Charvet, S., Charvet, J., Shu, L., Ma, R., and Lu, H., 2002, Palaeozoic late collisional strike - slip deformations in Tianshan and Altay, eastern Xinjiang, NW China: *Terra Nova*, v. 14, no. 4, p. 249-256.
- Liao, Z., Lu, L., Jiang, N., Xia, F., Sung, F., Zhou, Y., Li, S., and Zhang, Z., Carboniferous and Permian in the western part of the east Tianshan Mountains: Beijing, *in Proceedings Eleventh Congress of Carboniferous Stratigraphy and Geology, Guide Book Excursion 1987, Volume 4*, p. 50.
- M. Friedman, G., 1967, Dynamic Processes and Statistical Parameters Compared for Size Frequency Distribution of Beach and River Sands.
- Obrist-Farner, J., and Yang, W., 2016, Implications of loess and fluvial deposits on paleoclimatic conditions during an icehouse–hothouse transition, Capitanian upper Quanzijie low-order cycle, Bogda Mountains, NW China: *Palaeogeography, Palaeoclimatology, Palaeoecology*, v. 441, p. 959-981.
- Obrist-Farner, J., and Yang, W., 2017, Provenance and depositional conditions of fluvial conglomerates and sandstones and their controlling processes in a rift setting, mid-Permian lower and upper Quanzijie low order cycles, Bogda Mountains, NW China: *Journal of Asian Earth Sciences*, v. 138, p. 317-340.
- Obrist-Farner, J., Yang, W., and Hu, X.-F., 2015, Nonmarine time-stratigraphy in a rift setting: An example from the Mid-Permian lower Quanzijie low-order cycle Bogda Mountains, NW China: *Journal of Palaeogeography*, v. 4, no. 1, p. 27-51.
- Odom, I. E., Doe, T. W., and Dott, R. H., 1976, Nature of feldspar-grain size relations in some quartz-rich sandstones: *Journal of Sedimentary Research*, v. 46, no. 4, p. 862-870.
- Passega, R., 1957, Texture as characteristic of clastic deposition: *AAPG Bulletin*, v. 41, no. 9, p. 1952-1984.
- Peng, X., 2016, Provenance and depositional environments of fluvial-lacustrine sandstones of lower Permian Lucaogou low-order cycle, Bogda Mountains, NW China: *Missouri University of Science and Technology*.
- Pettijohn, F. J., Potter, P. E., and Siever, R., 2012, *Sand and sandstone*, Springer Science & Business Media.

- Shao, L. E. I., Stattegger, K., and Garbe-Schoenberg, C. D., 2001, Sandstone petrology and geochemistry of the turpan basin (nw china): Implications for the tectonic evolution of a continental basin: *Journal of Sedimentary Research*, v. 71, no. 1, p. 37-49.
- Shu, L., Wang, B., Zhu, W., Guo, Z., Charvet, J., and Zhang, Y., 2011, Timing of initiation of extension in the Tianshan, based on structural, geochemical and geochronological analyses of bimodal volcanism and olistostrome in the Bogda Shan (NW China): *International Journal of Earth Sciences*, v. 100, no. 7, p. 1647-1663.
- Shu, L. S., Zhu, W., Wang, B., Faure, M., Charvet, J., and Cluzel, D., 2005, The post-collision intracontinental rifting and olistostrome on the southern slope of Bogda Mountains, Xinjiang: *Acta Petrologica Sinica*, v. 21, p. 1, 25-36.
- Soreghan, M. J., and Cohen, A. S., 1993, The effects of basin asymmetry on sand composition: examples from Lake Tanganyika, Africa: *SPECIAL PAPERS-GEOLOGICAL SOCIETY OF AMERICA*, p. 285-285.
- Suttner, L. J., 1974, Sedimentary petrographic provinces: an evaluation.
- Thomas, S. G., Tabor, N. J., Yang, W., Myers, T. S., Yang, Y., and Wang, D., 2011, Palaeosol stratigraphy across the Permian-Triassic boundary, Bogda Mountains, NW China: Implications for palaeoenvironmental transition through earth's largest mass extinction: *Palaeogeography, Palaeoclimatology, Palaeoecology*, v. 308, no. 1-2, p. 41-64.
- Trask, P. D., 1932, Origin and environment of source sediments of petroleum: Houston: Texas: Gulf Publication Company, 323p.
- Visher, G. S., 1969, Grain size distributions and depositional processes: *Journal of Sedimentary Research*, v. 39, no. 3.
- Wartes, M. A., Carroll, A. R., and Greene, T. J., 2002, Permian sedimentary record of the Turpan-Hami basin and adjacent regions, northwest China: Constraints on postamalgamation tectonic evolution: *Geological Society of America Bulletin*, v. 114, no. 2, p. 131-152.
- Wentworth, C. K., 1922, A scale of grade and class terms for clastic sediments: *The journal of geology*, v. 30, no. 5, p. 377-392.
- Xia, L.-Q., Xu, X.-Y., Xia, Z.-C., Li, X.-M., Ma, Z.-P., and Wang, L.-S., 2004, Petrogenesis of Carboniferous rift-related volcanic rocks in the Tianshan, northwestern China: *Geological Society of America Bulletin*, v. 116, no. 3-4, p. 419-433.

- Xiao, W.-J., Zhang, L.-C., Qin, K.-Z., Sun, S., and Li, J.-L., 2004, Paleozoic accretionary and collisional tectonics of the Eastern Tianshan (China): implications for the continental growth of central Asia: *American Journal of Science*, v. 304, no. 4, p. 370-395.
- Xiao, W., Windley, B. F., Allen, M. B., and Han, C., 2013, Paleozoic multiple accretionary and collisional tectonics of the Chinese Tianshan orogenic collage: *Gondwana Research*, v. 23, no. 4, p. 1316-1341.
- Yang, W., Crowley, J., Obrist-Farner, J., Tabor, N., Feng, Q., and Liu, Y., A marine back-arc origin for the Upper Carboniferous basement of intracontinental greater Turpan-Junggar basin-Volcanic, sedimentary, and geochronologic evidence from southern Bogda Mountains, *in Proceedings NW China: Geological Society of America Annual Meeting, GSA Abstract with Programs 2013, Volume 45*.
- Yang, W., Feng, Q., Liu, Y., Tabor, N., Miggins, D., Crowley, J. L., Lin, J., and Thomas, S., 2010, Depositional environments and cyclo- and chronostratigraphy of uppermost Carboniferous–Lower Triassic fluvial–lacustrine deposits, southern Bogda Mountains, NW China — A terrestrial paleoclimatic record of mid-latitude NE Pangea: *Global and Planetary Change*, v. 73, no. 1–2, p. 15-113.
- Yang, W., Liu, Y., Feng, Q., Lin, J., Zhou, D., and Wang, D., 2007, Sedimentary evidence of Early–Late Permian mid-latitude continental climate variability, southern Bogda Mountains, NW China: *Palaeogeography, Palaeoclimatology, Palaeoecology*, v. 252, no. 1, p. 239-258.
- Zhang, X., 1981, Regional stratigraphic chart of northwestern China, branch of Xinjiang Uygur Autonomous Region, Beijing, Geological Publishing House.

SECTION

2. CONCLUSIONS

The integrated petrographic and field studies of sandstones of Wutonggou low-order cycle, exposed in the northern and southern foothills of Bogda Mountains, NW China provide clues to interpret the provenance, the unroofing history of the eastern North Tianshan Suture, and investigate the influences of provenance and depositional environments on sandstone textures. Based on the stratigraphic distribution of the identified three petrofacies, conglomerate composition, and paleocurrent direction, the provenance of sandstones in Bogda Mountains are interpreted. The provenance of Zhaobishan (ZBS) section changed from the undissected volcanic arc, accretionary wedge, and trench to dominant transitional volcanic arc. The provenance of North Tarlong (NTRL) and Taodonggou (TDG) sections changed from the undissected volcanic arc and rift shoulders to the transitional volcanic arc, accretionary wedge, and trench. The provenance of Dalongkou (DLK) section unchanged and was the undissected volcanic arc and rift shoulders. The differences in petrofacies distributions in ZBS and NTRL-TDG sections suggest two unroofing trends existed in the eastern North Tianshan Suture (ENTS). ENTS was an amalgamated complex of volcanic arc, accretionary wedge, and trench with spatial and temporal variations in lithology during late Permian-earliest Triassic.


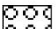






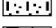
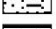


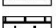

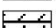

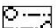


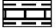
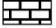
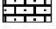
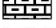
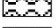
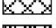

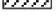

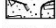

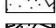
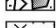
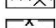






The textural characteristics of the three petrofacies are documented that petrofacies 2 is slightly better sorted and more mature than petrofacies 1, and petrofacies

3 is coarser in grain size, worse sorted and less mature than petrofacies 1 and 2. The provenance greatly influence the textural characteristics of these sandstones. Moreover, the three petrofacies are subdivided into littoral/beach, deltaic, and fluvial sedimentary facies. These facies show limited variations in sorting, skewness, and textural maturity, thus they are difficult to be distinguished by textural characteristics.


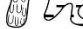





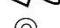


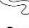

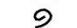

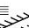





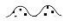


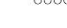








This work demonstrates that sandstones of ancient rift basins bordered by suture zones are derived from both suture zones and rift basins. In addition, this work provides a detailed provenance study to reconstruct a key element of one of the largest accretionary orogenic belts on Earth and to understand the nature and unroofing process of the ancient suture zone that shows great heterogeneity in lithology spatially and temporally. Finally, this work indicates that provenance is the major control on composition and textural of sandstones, and the influence of depositional environments for fluvial-lacustrine sandstones is likely limited. The results of this work can serve as an analogy for provenance studies of other suture zones and enrich our understanding of the controlling factors on sandstones.

APPENDIX A.
ZHAOBISHAN SECTION

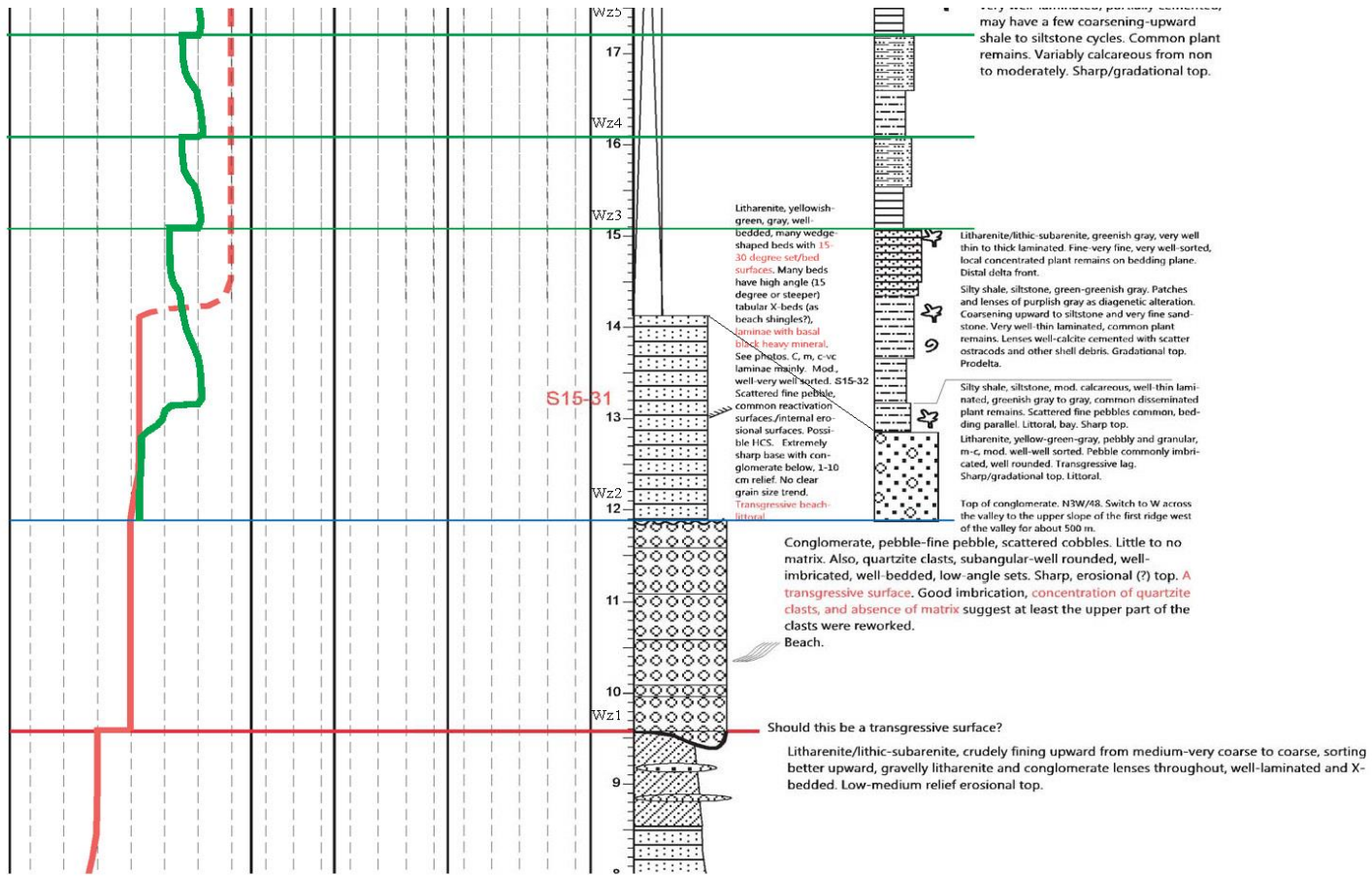
LITHOLOGY

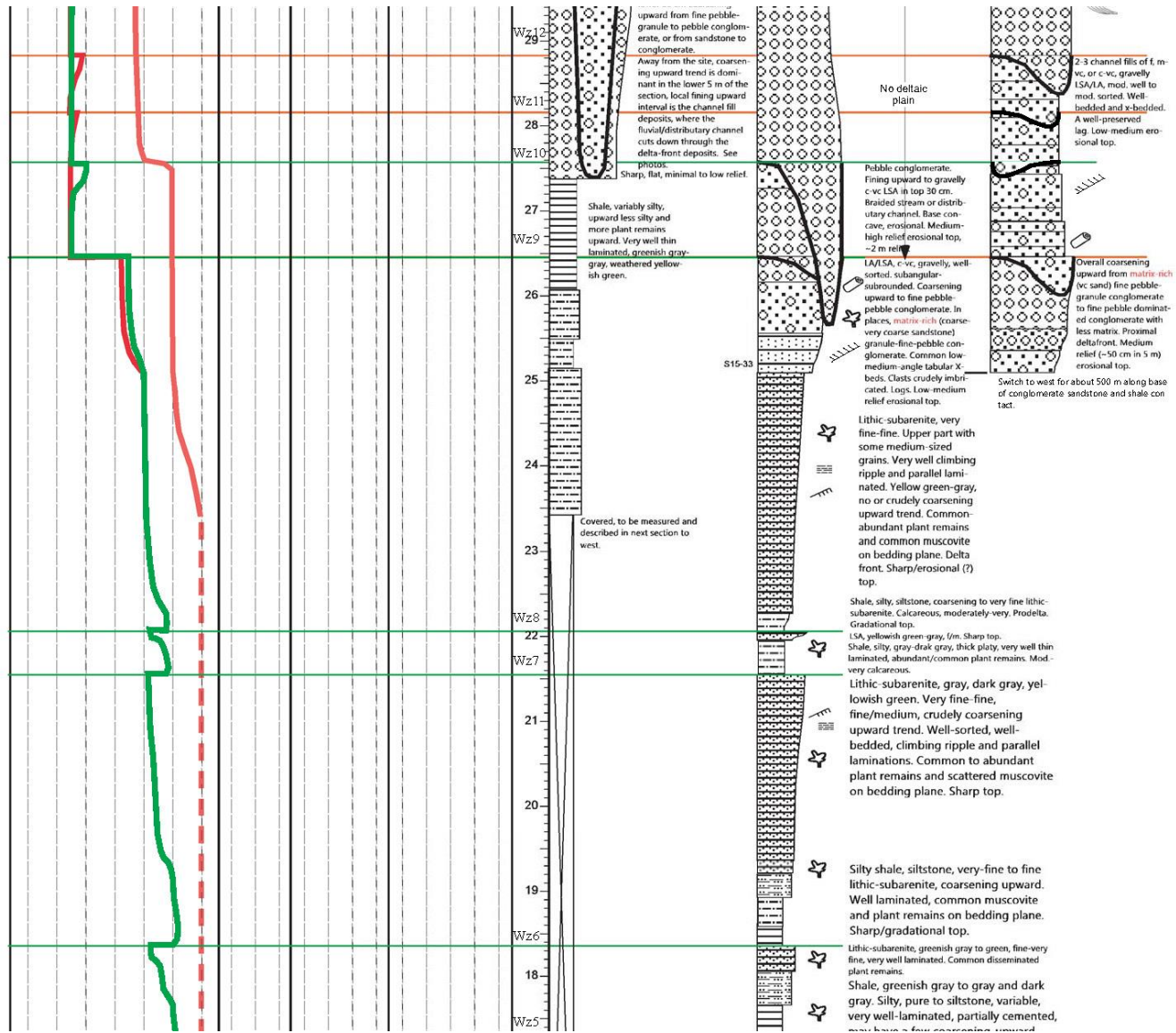
	Normal graded conglomerate or sandstone
	Reverse graded conglomerate or sandstone
	Clast-supported conglomerate
	Matrix-supported conglomerate
	Sandstone
	Well-bedded sandstone
	Well-laminated sandstone
	Cross-bedded sandstone
	Conglomeratic sandstone
	Calcareous sandstone
	Muddy sandstone
	Interbedded sandstone and shale/siltstone
	Shale
	Silty shale
	Calcareous shale or mudstone
	Dolostone
	Shale, dolomitic.
	Mudstone
	Conglomeratic mudstone
	Calcrete or altered palustrine limestone
	Paleosol
	Limestone with shale partings
	Limestone
	Arenaceous limestone
	Argillaceous limestone
	Oolitic packstone/grainstone
	Pyroclastic breccia
	Extrusive igneous rocks
	Modern salt accumulation
	Intrusive igneous rocks
	Pillow basalt
	Mafic porphyry
	Felsic porphyry
	Breccia
	Tuffaceous sandstone
	Tuffaceous shale
	Oolitic sandstone
	Gypsiferous sandstone
	Bedded halite
	Bedded gypsum
	Gypsum and shale inter-laminite

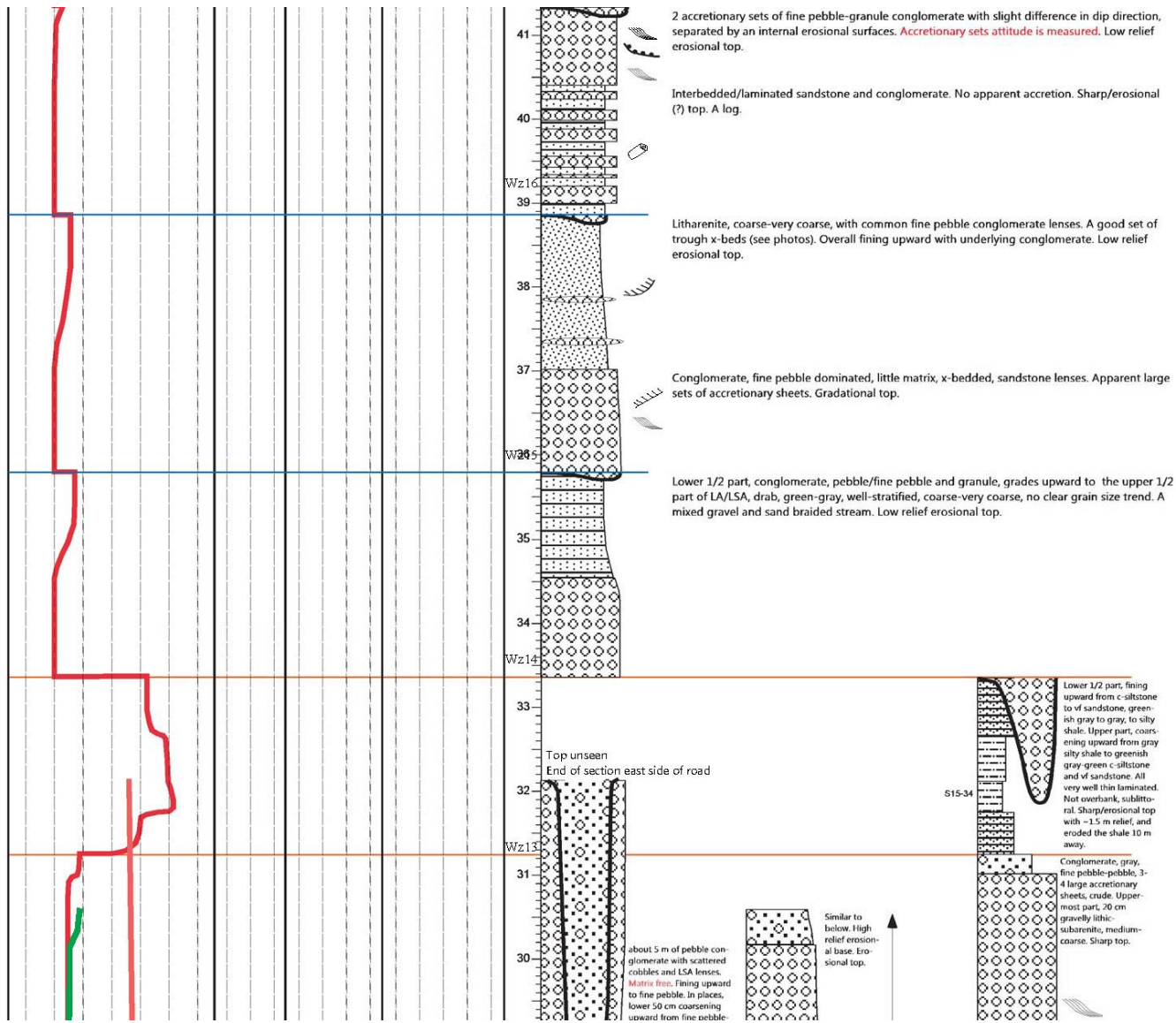
SEDIMENTARY TEXTURE AND STRUCTURE

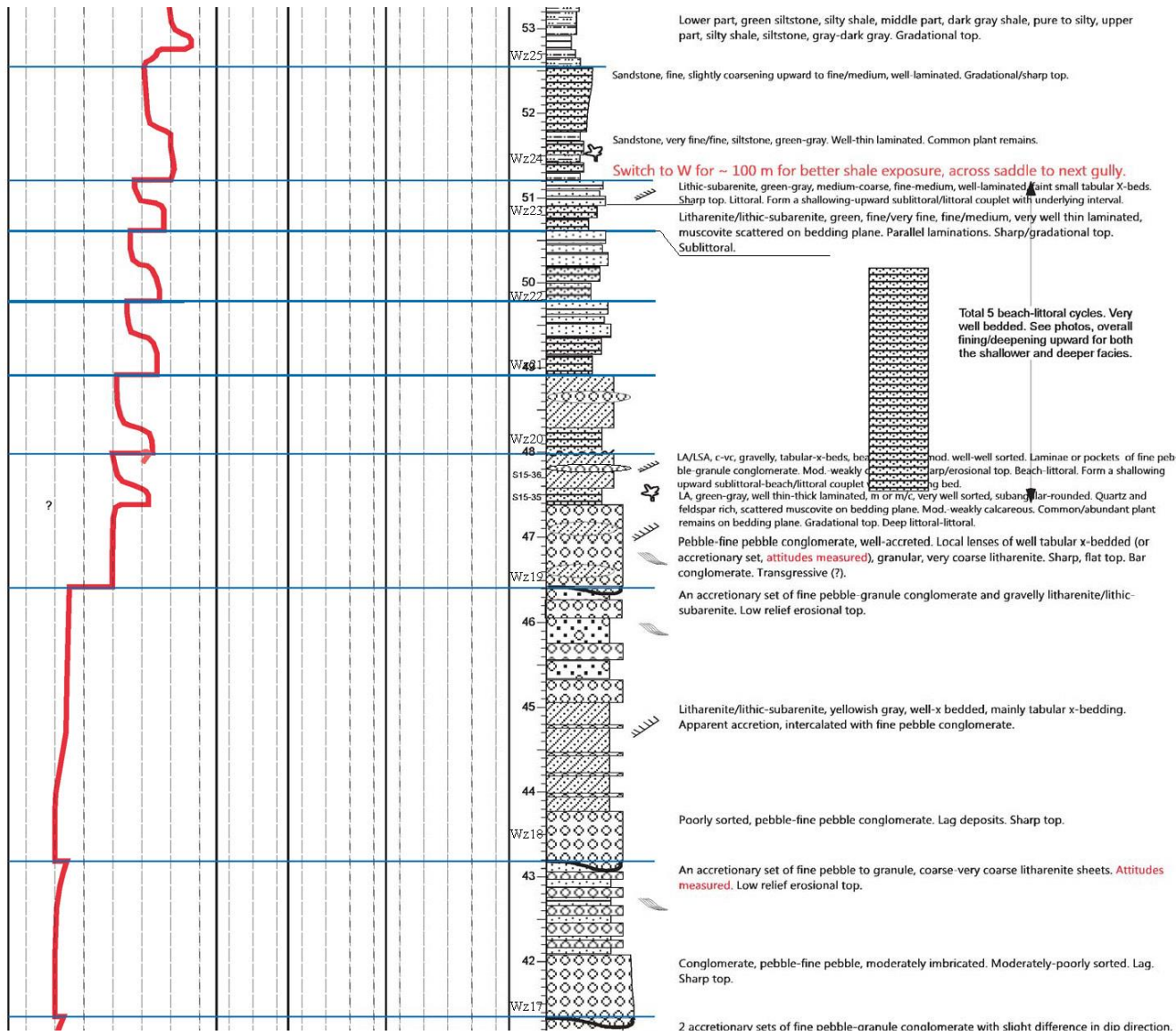
	Soil slickensides
	Illuviated muddy sediments
	Root mold, silicified/calcareous stumps or branches
	Calcareous claystone and sandstone nodules, commonly root mottled
	Rhizoconcretion or calcitic nodules
	Limonitic clayey soil pisoid
	Mud cracks
<hr/>	
	Mud chips, rip-up clasts
	Pisoids
	Ooids and superficial ooids
	Invertebrate bone fossils
	Trace fossils
	Plants and plant debris
	Fish or fish scale fossils
	Shell fragments
	Burrows, mottling structure
<hr/>	
	Planar, tabular, and/or trough x-bedding
	Erosional surface
	Internal erosional surface
	Ripple and climbing ripple laminations
	Hummocky cross stratification (HCS)
	Contorted bedding
	Cryptalgal lamination
	Symmetrical ripple marks
	Vesicles filled with calcite or other minerals
	Normal graded bedding
	Reverse graded bedding
	Algal coated pisoid and oncoid
	Petrified wood
	Microfaults
	Dissolution cavities/vugs
	Extensive brecciation structure

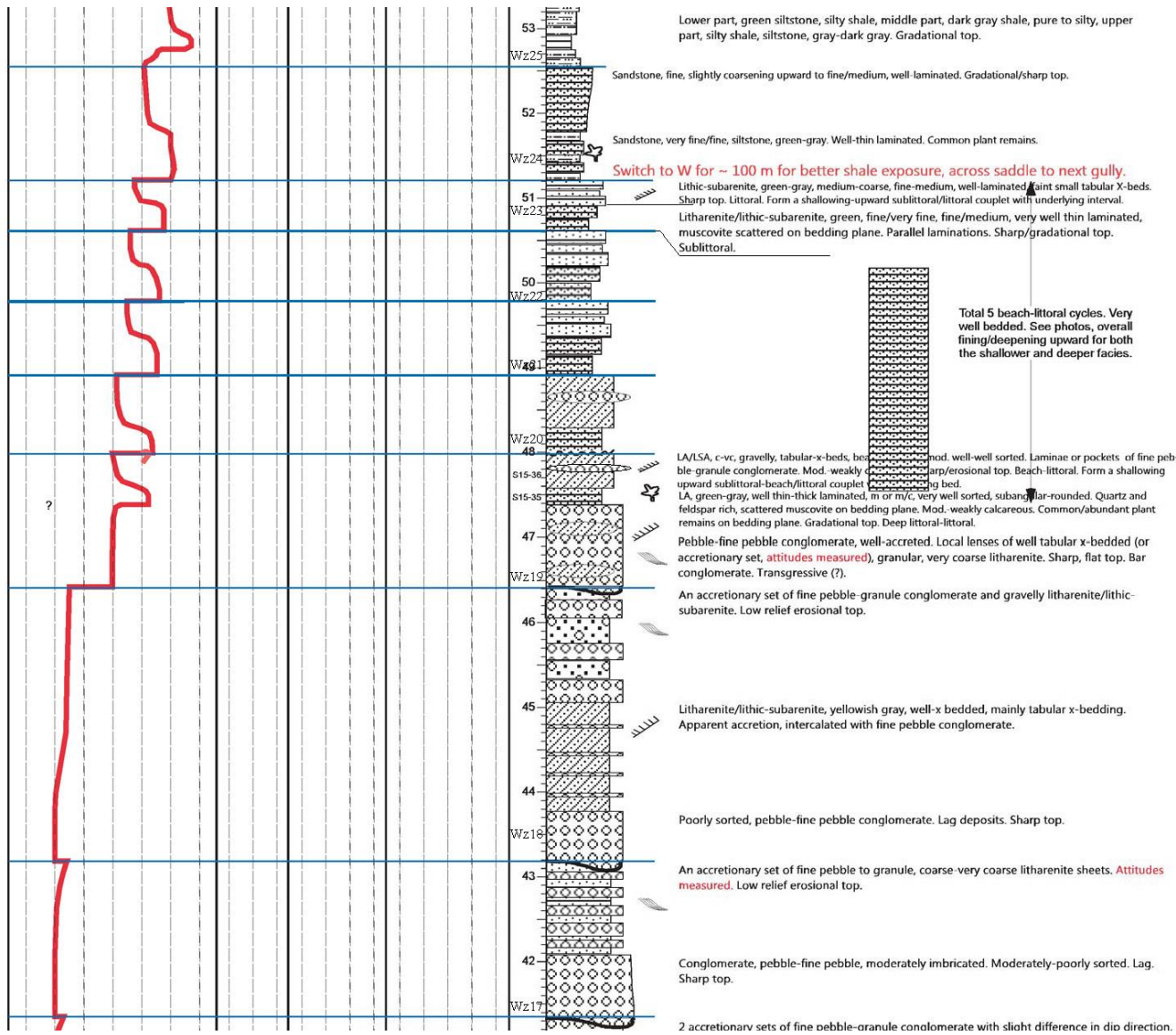
LA - Lithic arenite
 LSA - Lithic subarenite
 LW - Lithic wacke
 CRL - Climbing ripple laminations

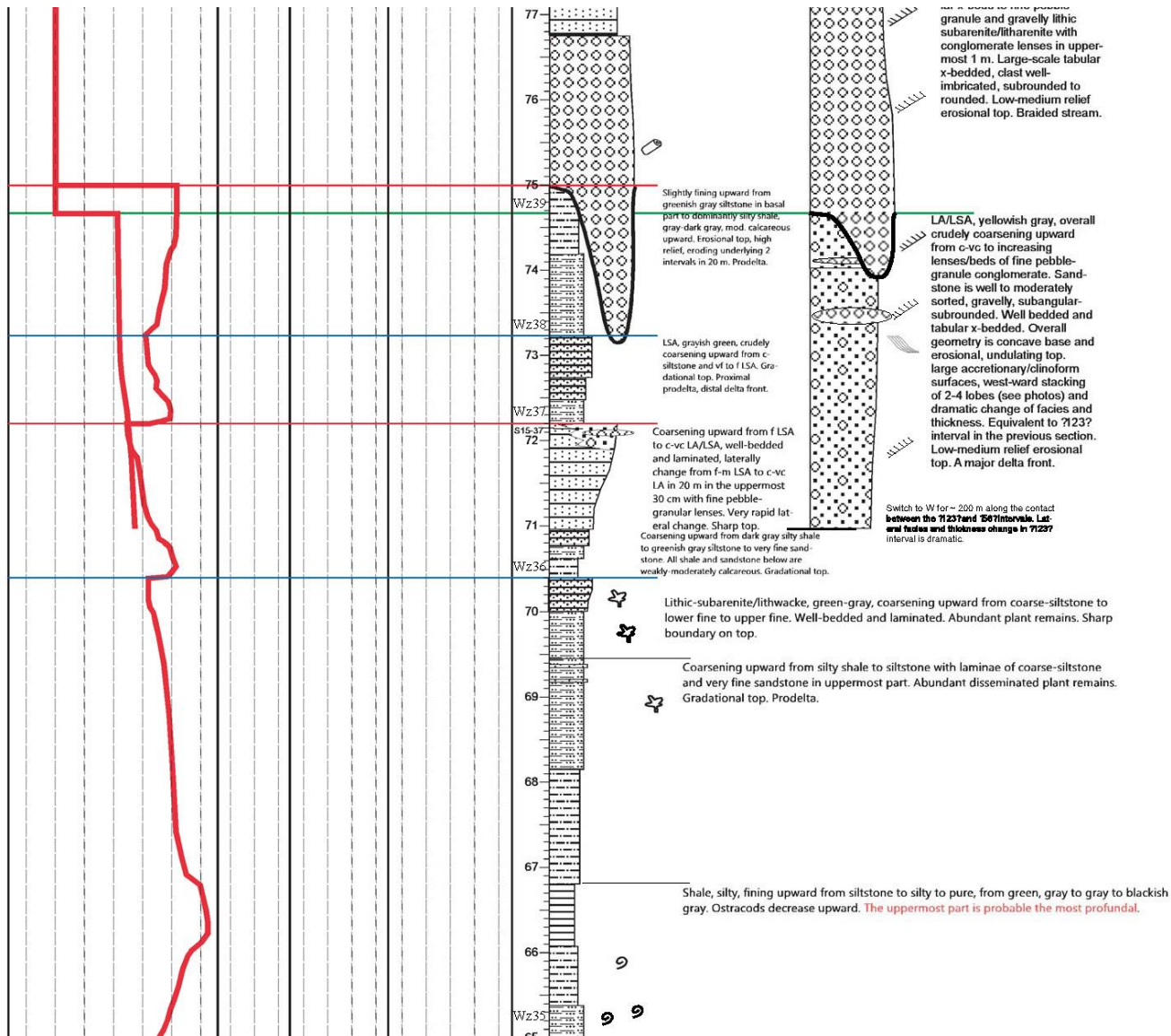


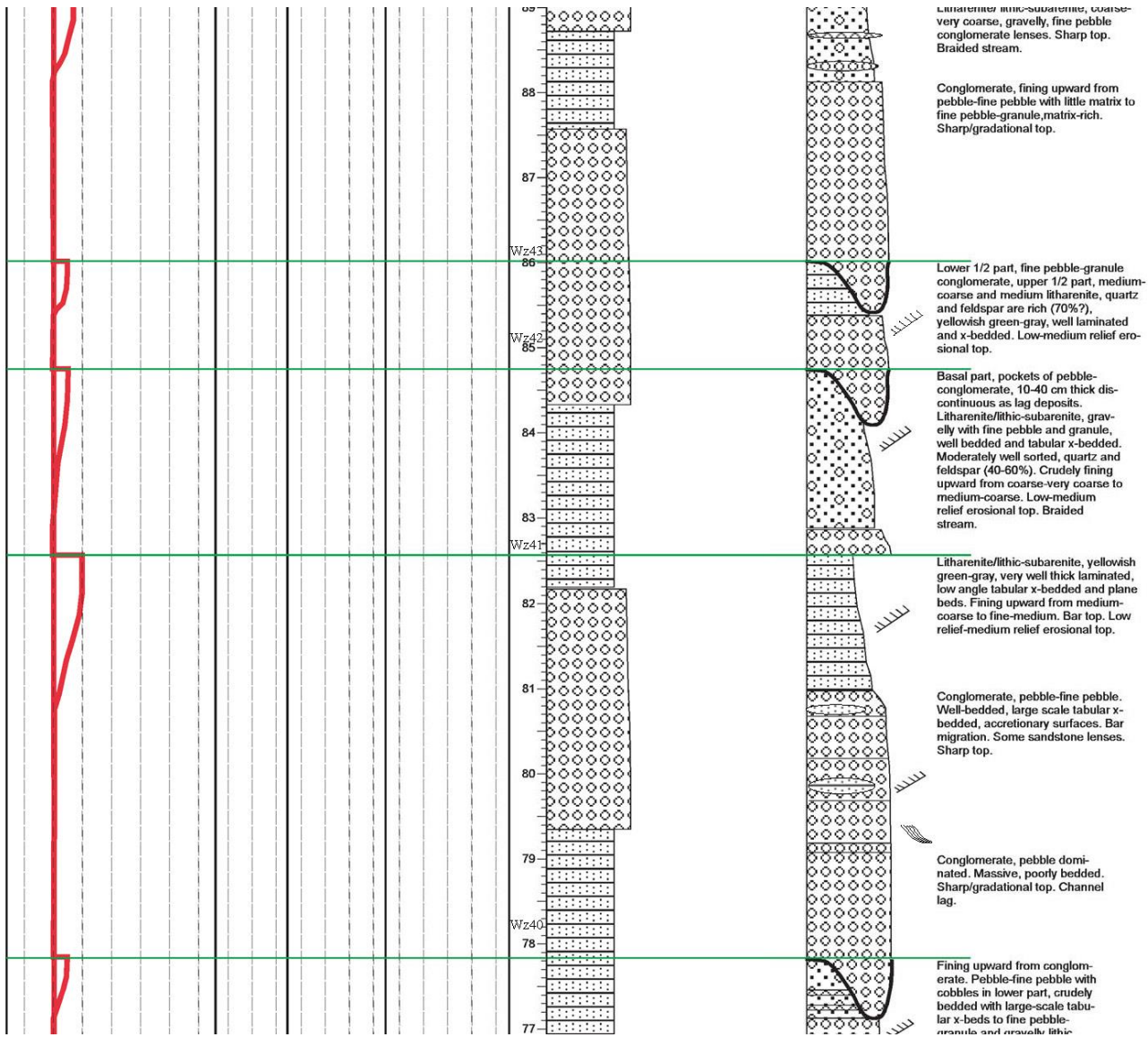


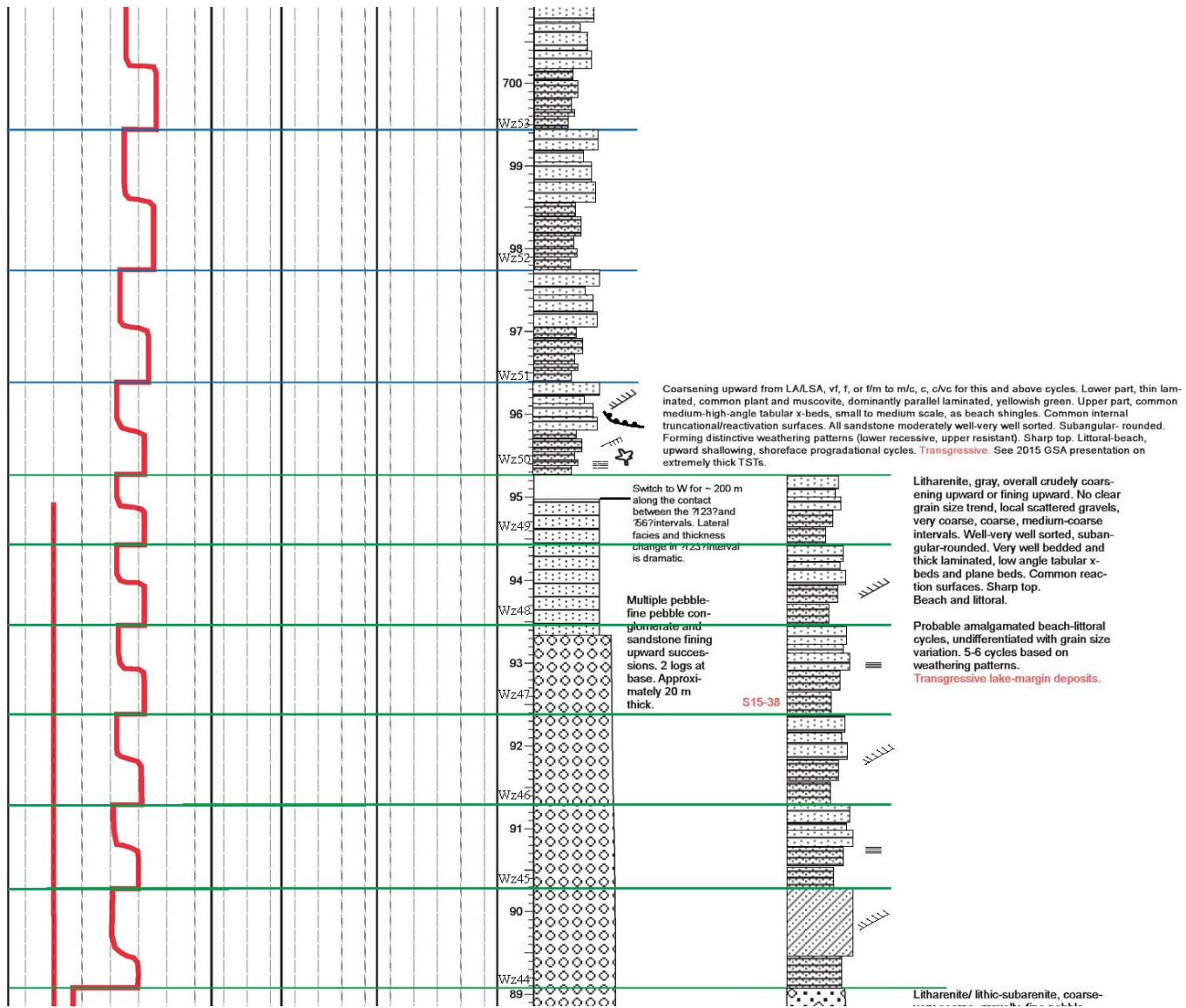


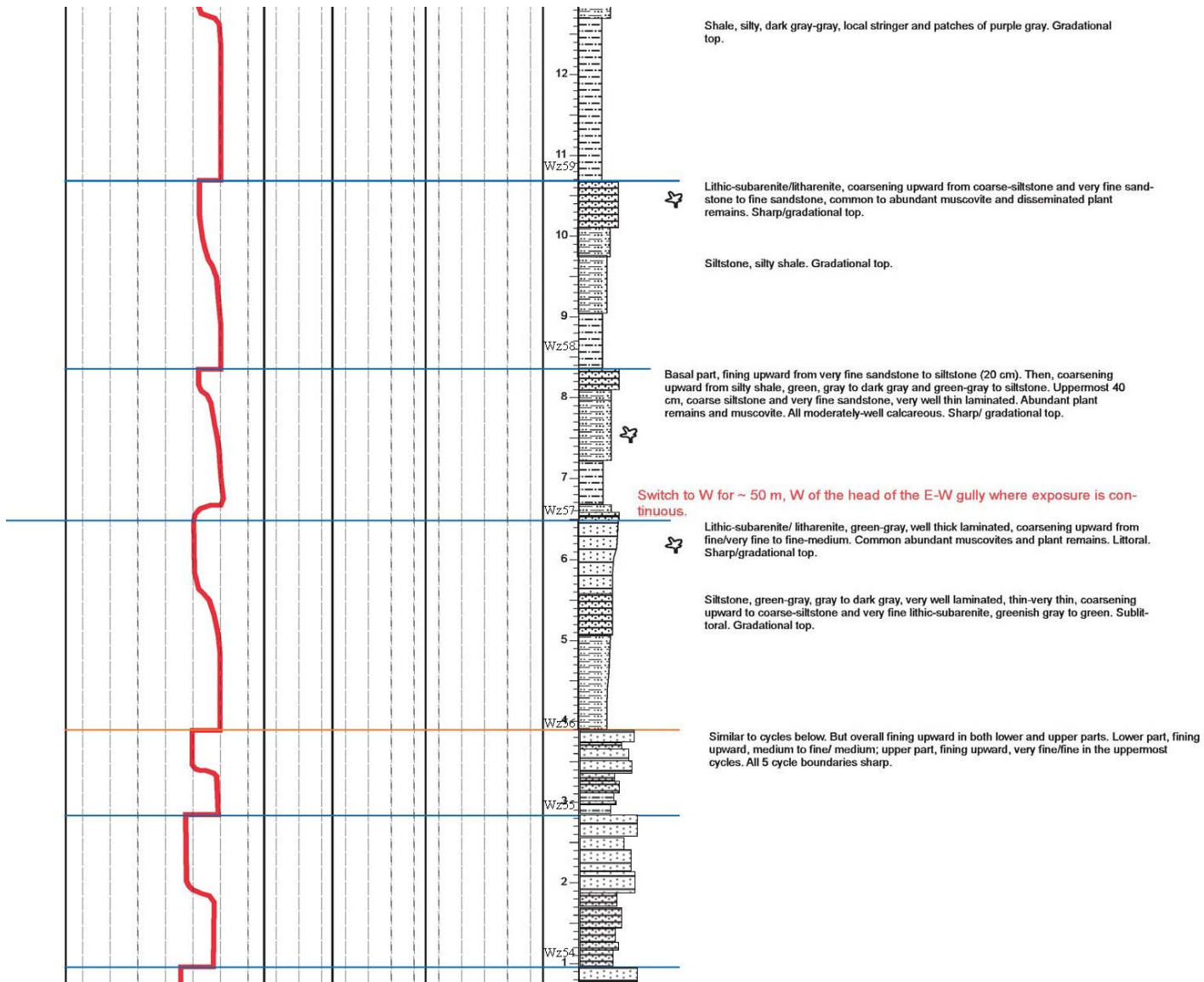


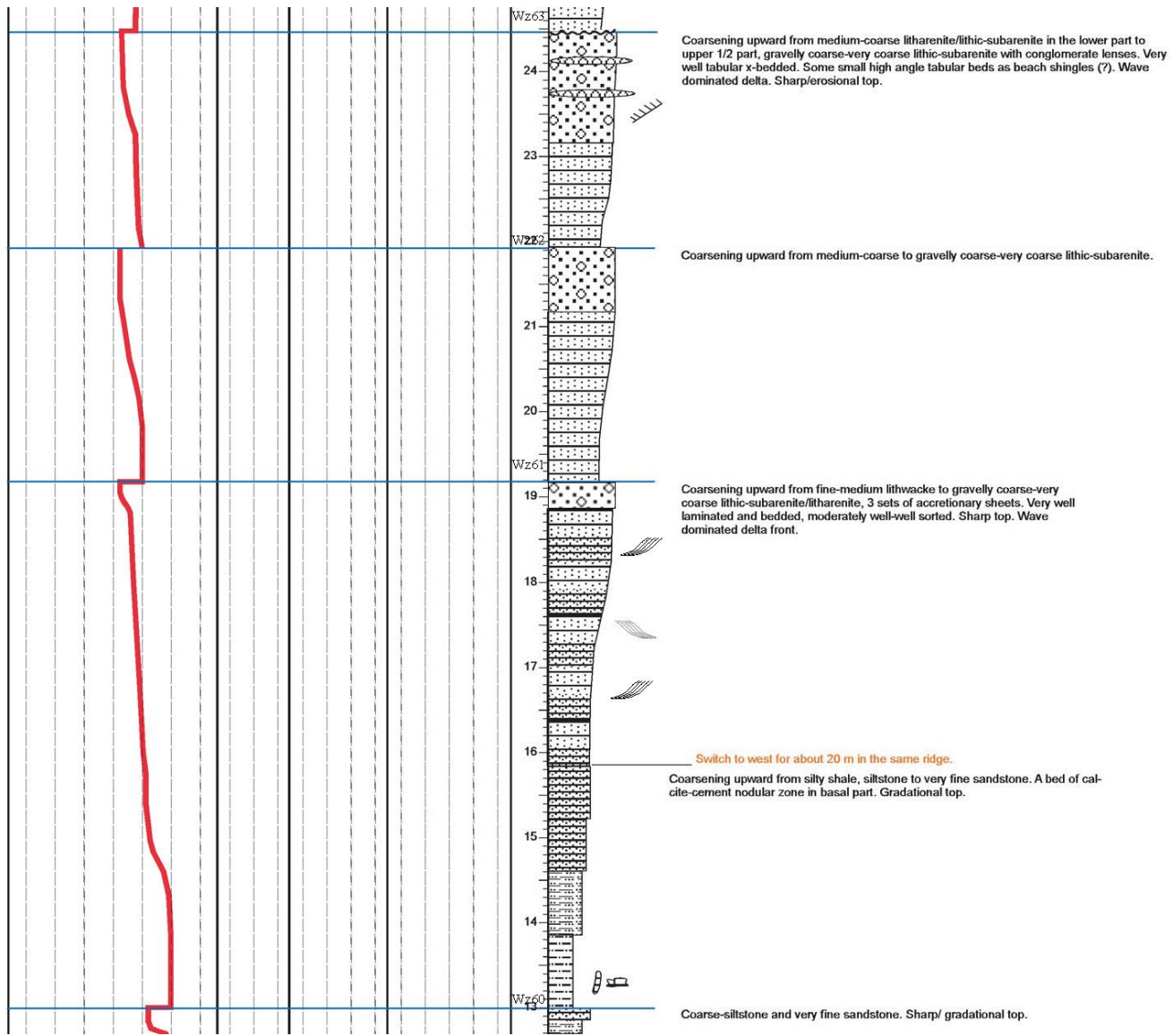


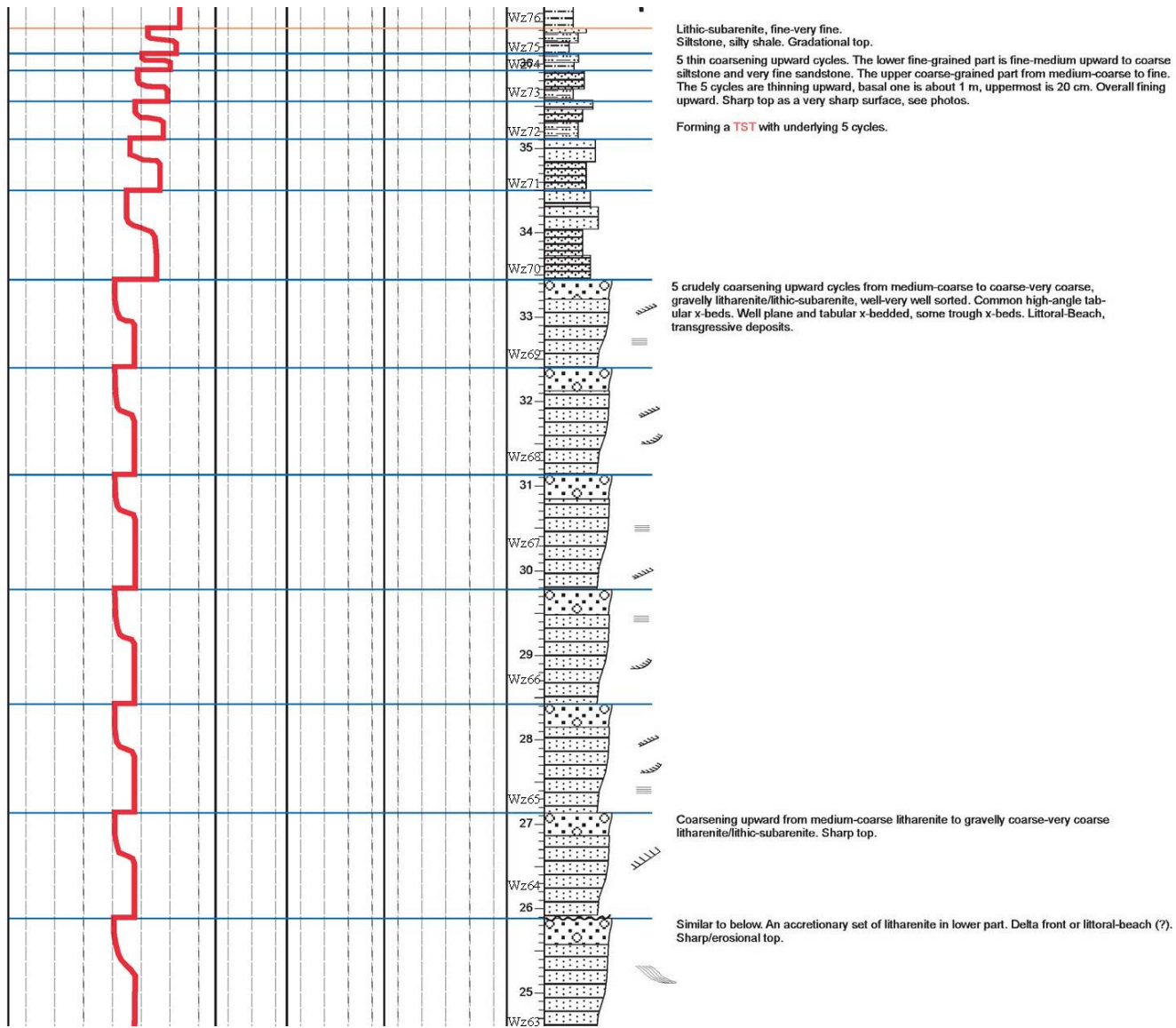


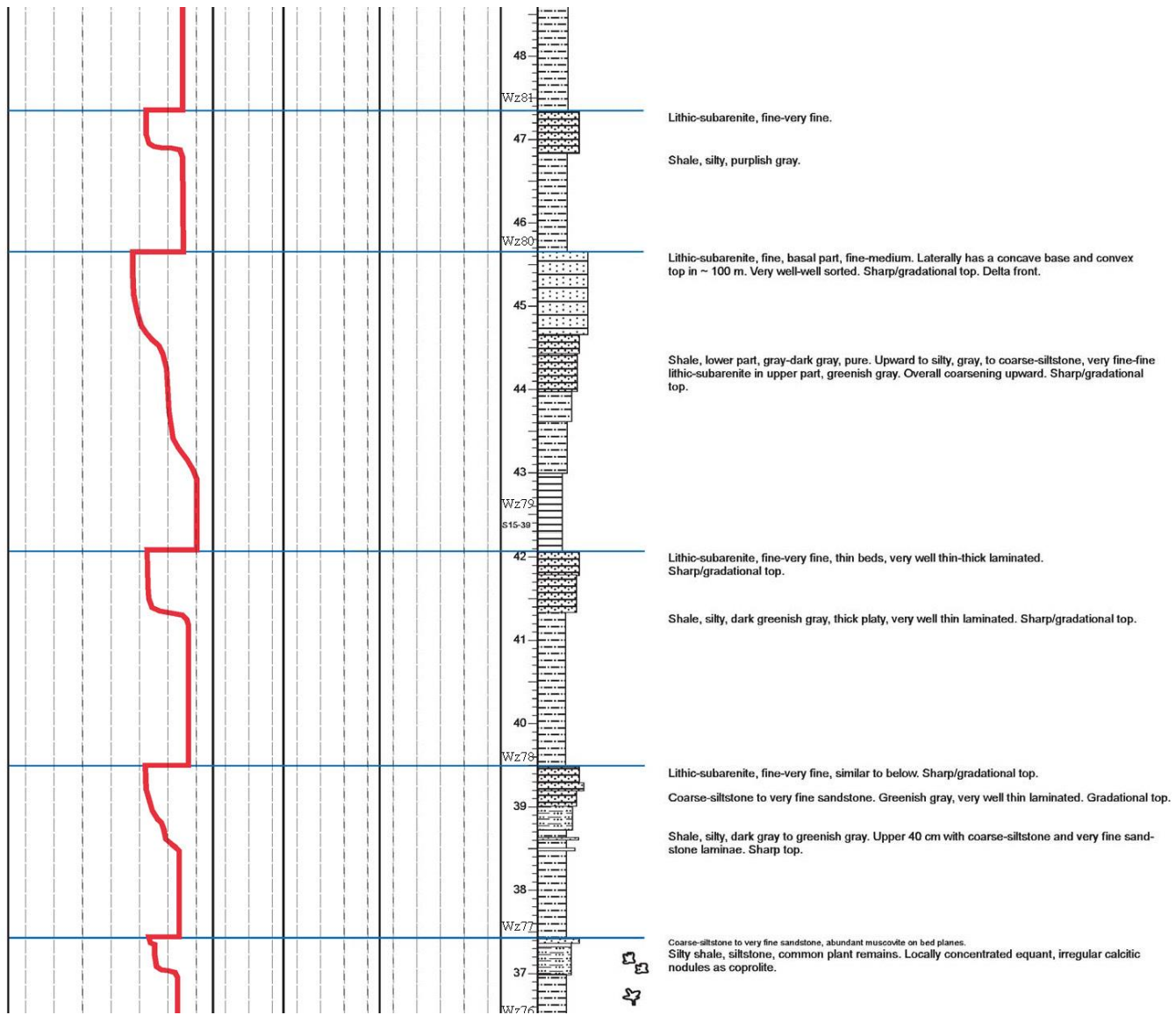


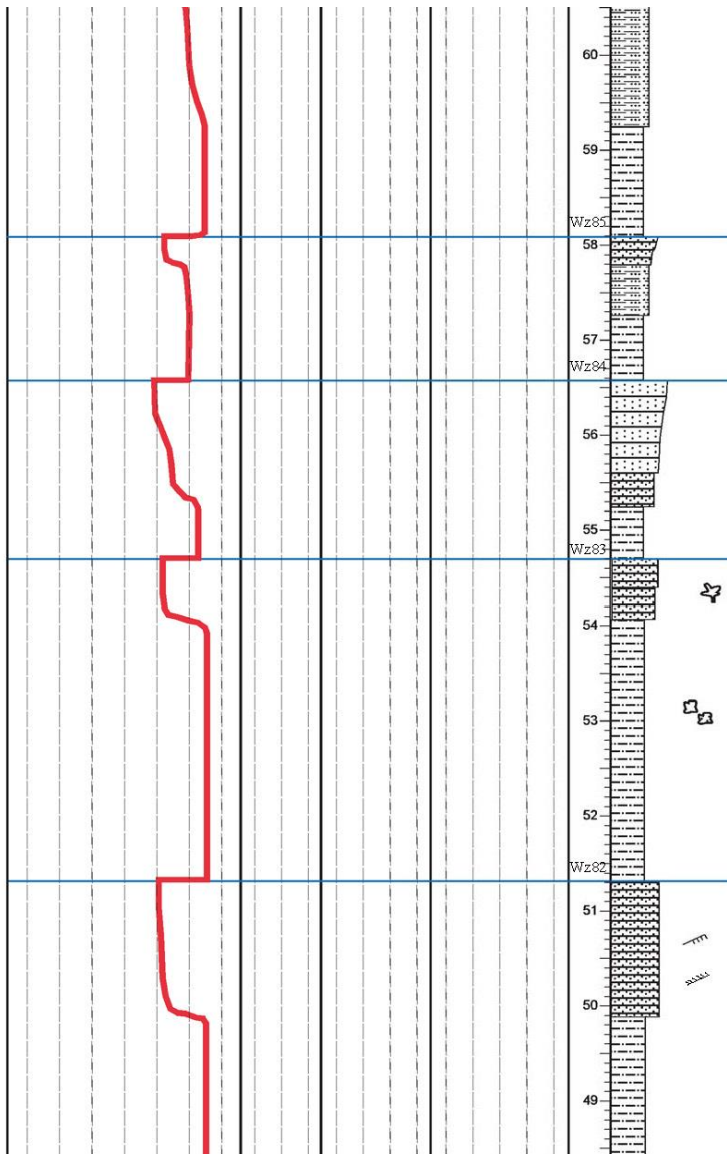












Silty shale and siltstone, coarsening upward.

60

59

Wz85

58

Coarsening upward from very fine-fine lithic-subarenite.
Shale, silty, greenish gray upward to siltstone.

57

Wz84

Coarsening upward from fine to medium lithic subarenite. Gradational/sharp top.

56

Coarsening upward from silty shale to very fine sandstone.

55

Wz83

Lithic-subarenite, fine-very fine, greenish gray, well-thin laminated. Common plant remains and muscovite.

54

Shale, silty, purplish gray. Stringers of discontinuous, 1-10s cm, calcitic nodules, diagenetic. Gradational top.

53

52

Wz82

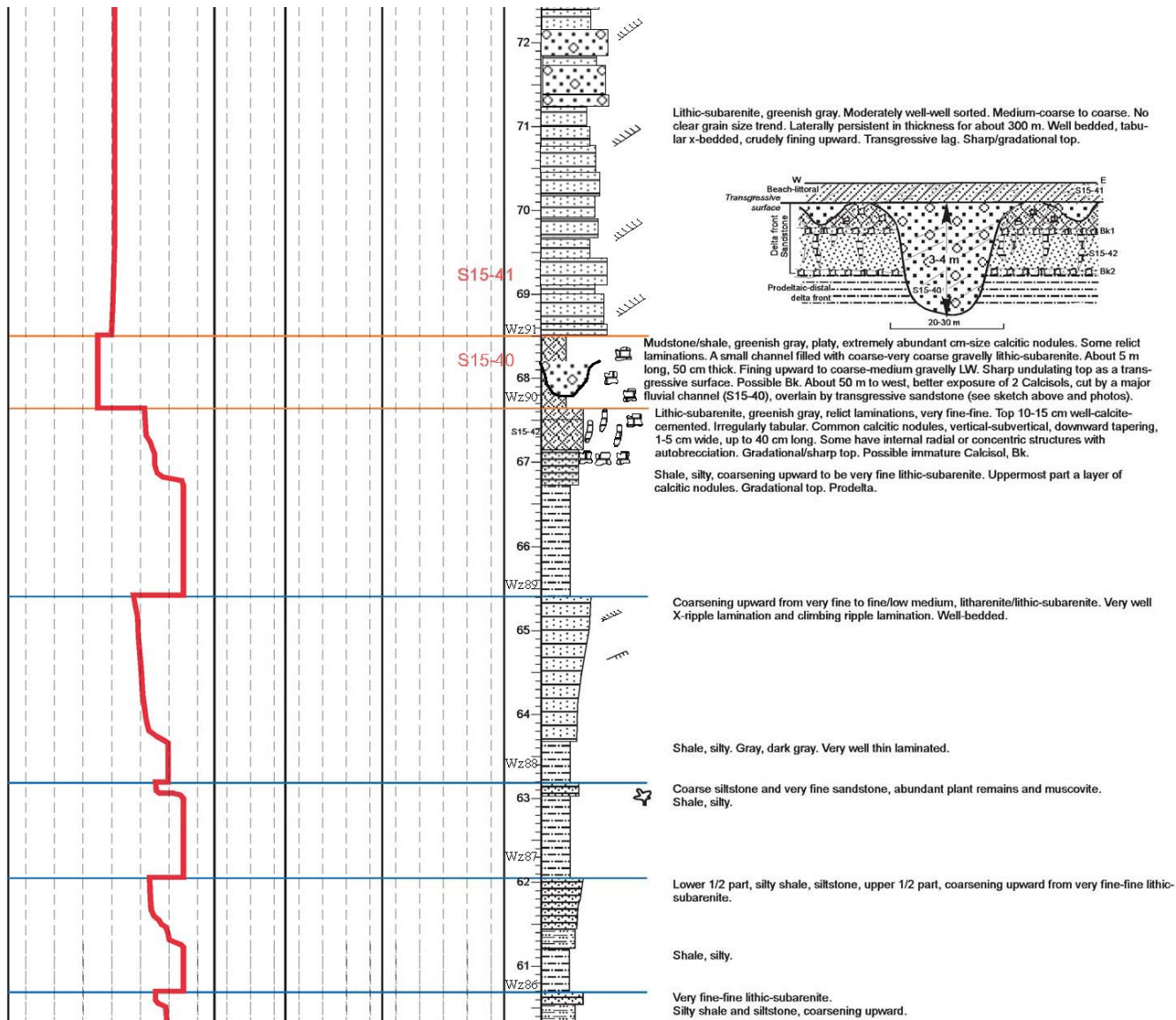
Lithic-subarenite, fine-very fine, X-ripple-laminations and climbing-ripple-laminations and parallel laminations.

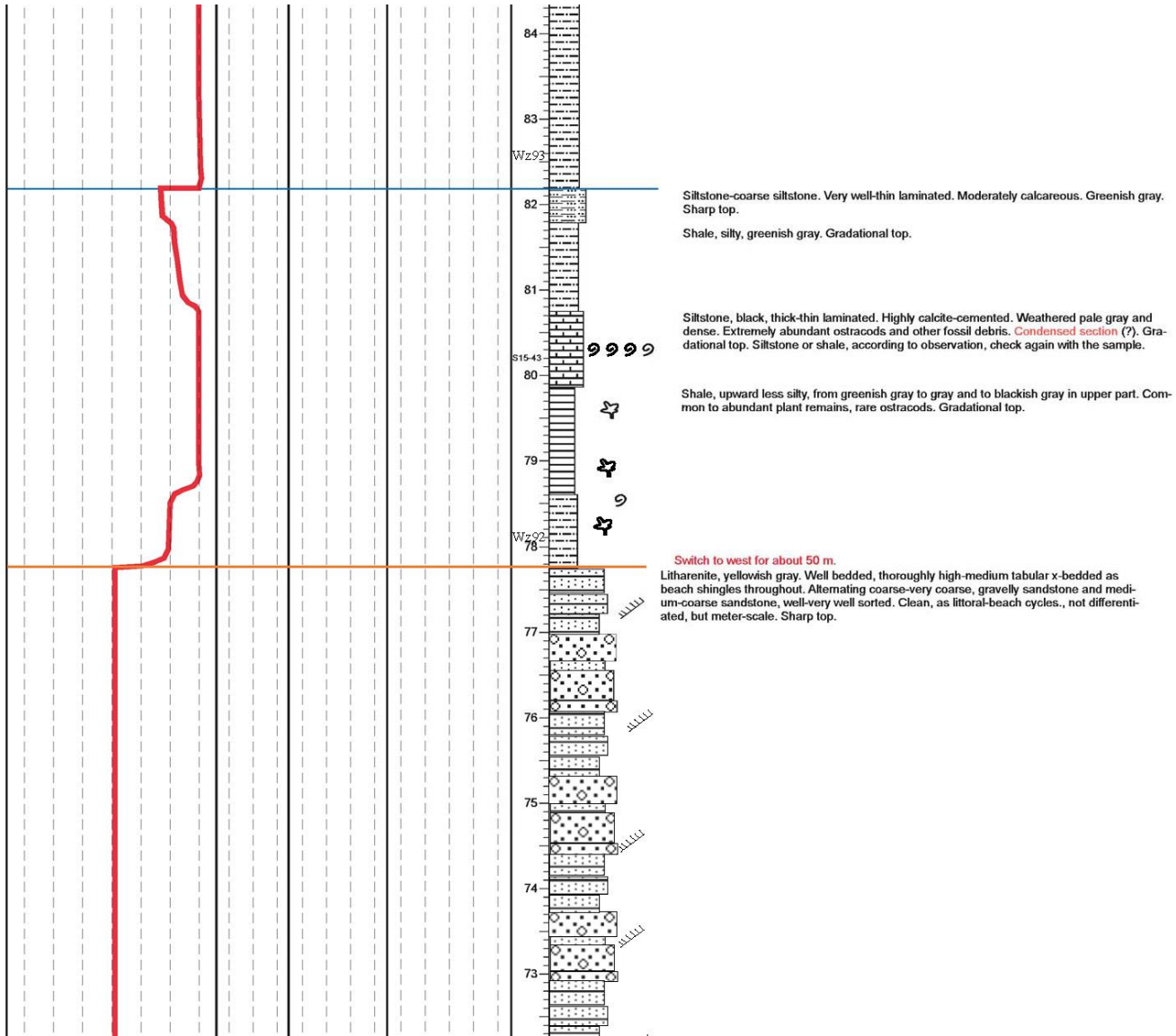
51

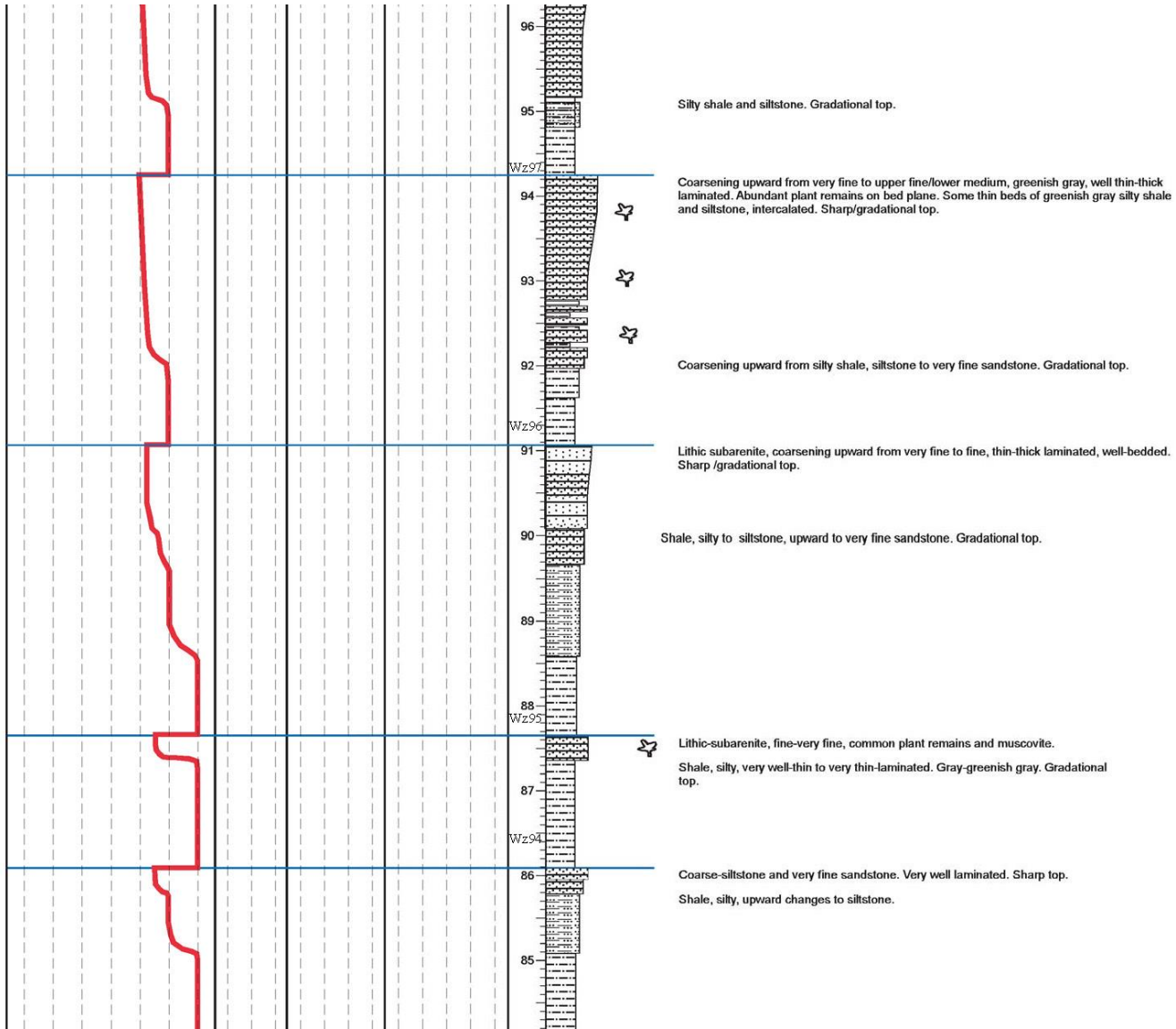
50

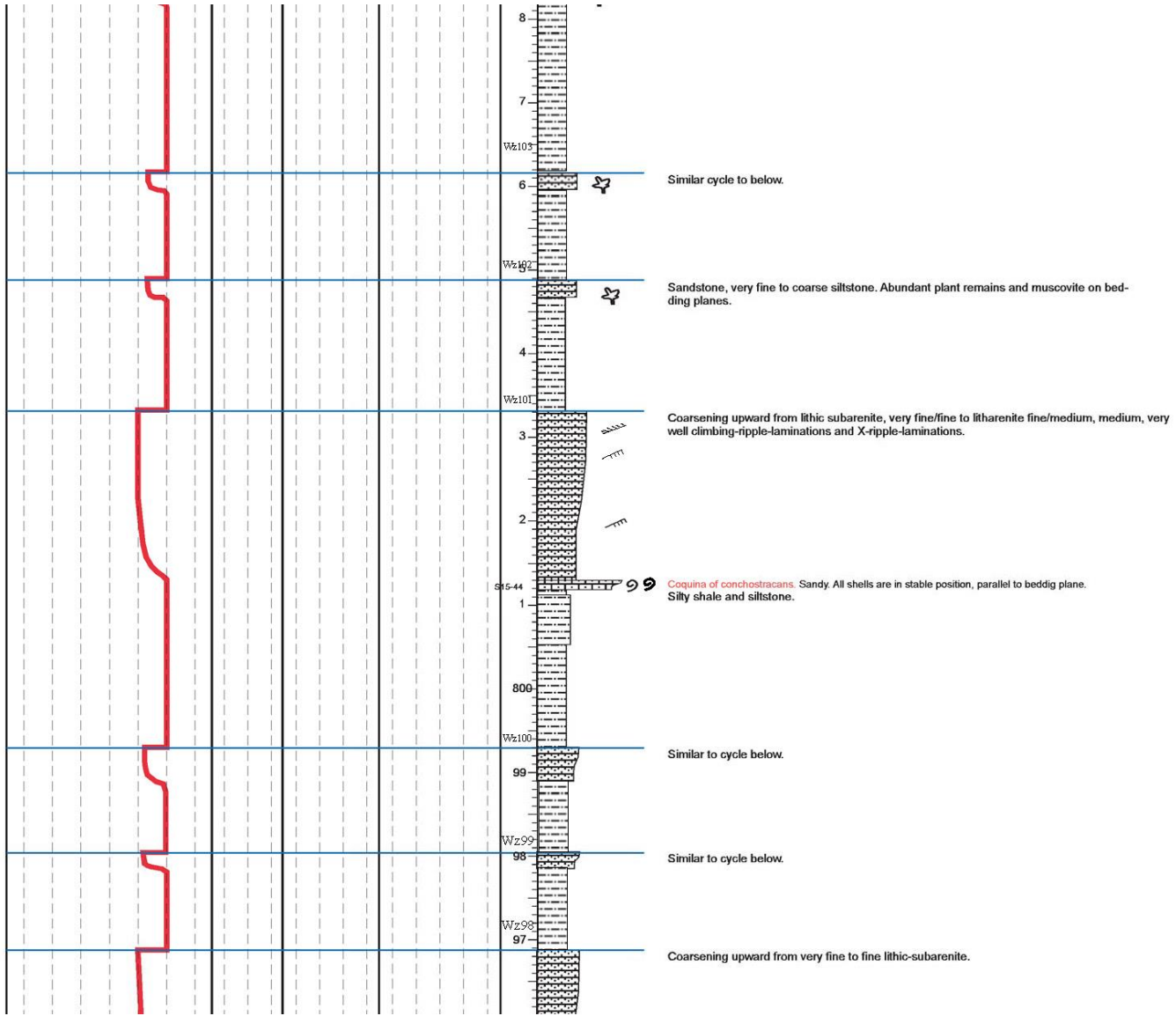
Shale, silty, purplish gray.

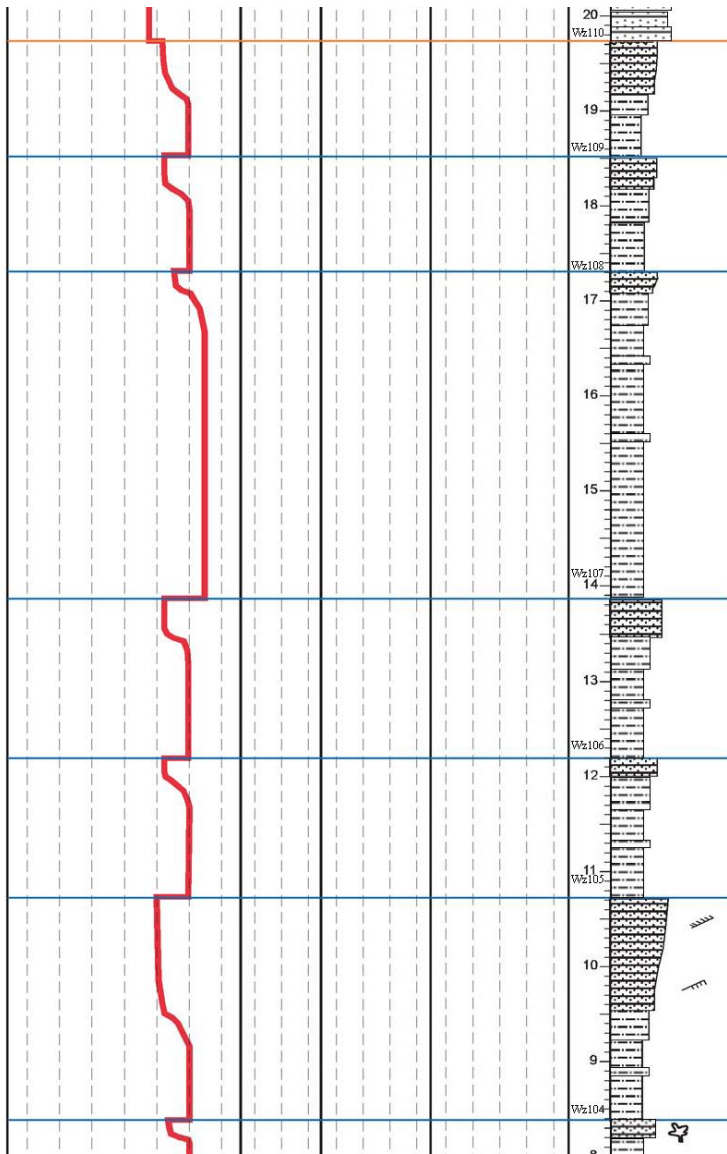
49











sequence boundary. The coarse delta front deposits were not deposited here. This location is probably an interdeltic bay. Coarsening upward from silty shale, siltstone in lower 1/2 part to very fine and fine lithic subarenite in upper part. Sharp/erosional top.

Lithic subarenite/litharenite, very fine/fine. Coarsening upward from silty shale, siltstone to very fine sandstone. Sharp/gradational boundary on top.

Lithic subarenite, very fine/fine.

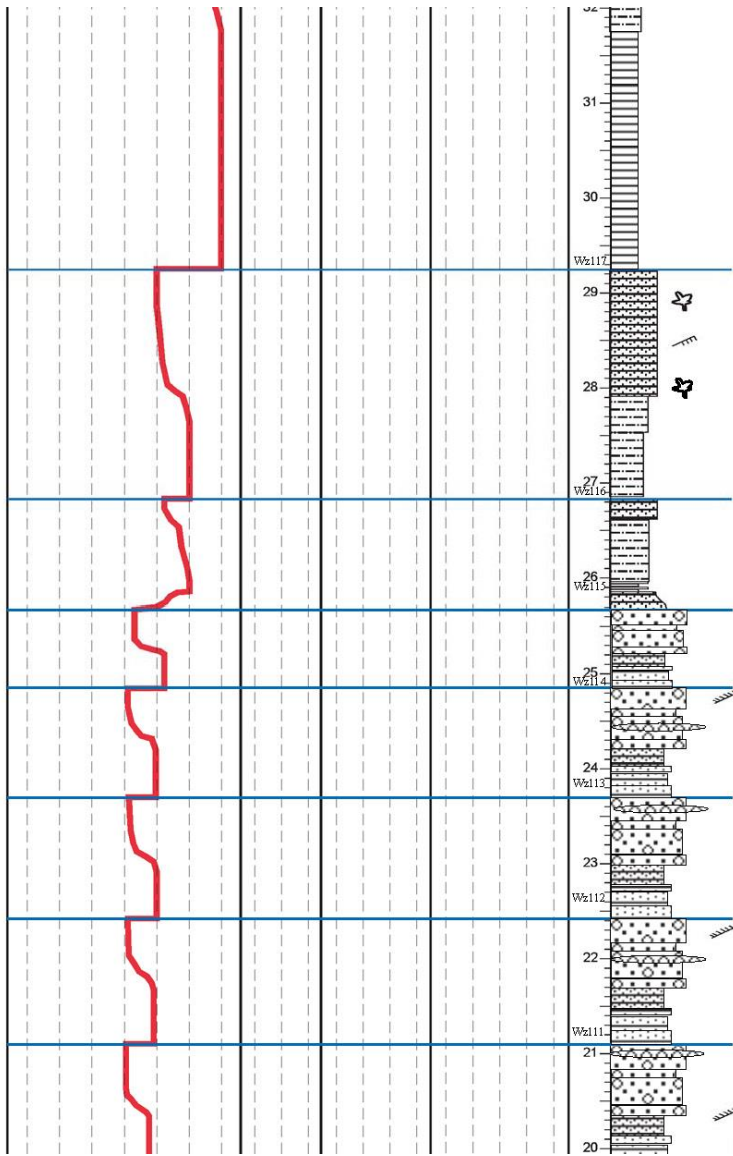
Litharenite/lithic-subarenite, upper fine/lower medium.

Lithic subarenite, fine. Gradational top.

Lithic-subarenite/litharenite, greenish gray, coarsening upward from very fine to upper fine/lower medium, climbing-ripple-laminations, X-ripple-laminations, rare small-medium tabular x-beds.

Shale, silty, siltstone, gray to greenish gray.

Similar cycle to below.



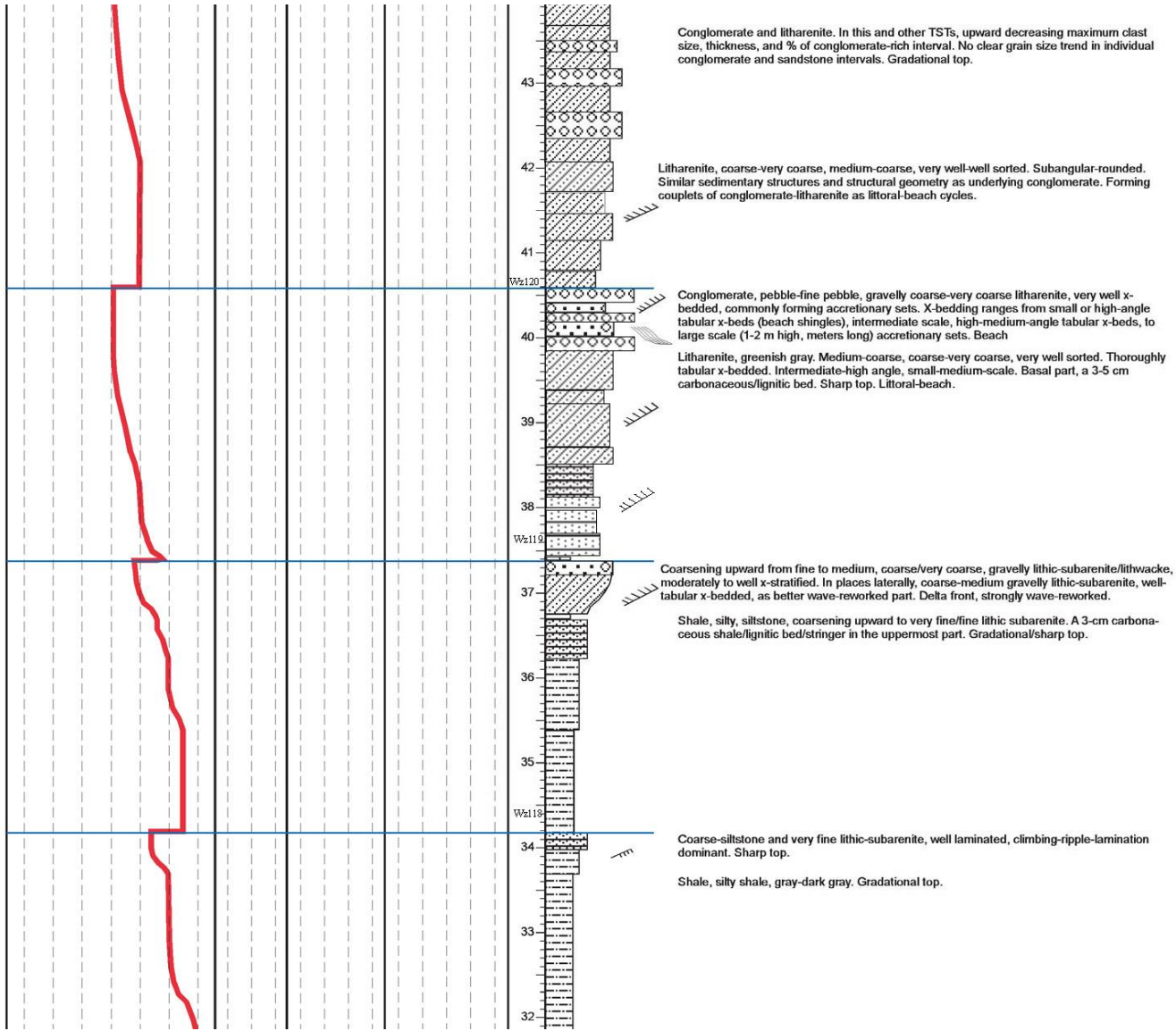
29 Lithic-subarenite/litharenite, yellowish green-gray. Thin-thick laminated. Climbing ripple laminations. Common/abundant plant remains and muscovite. Sharp top.

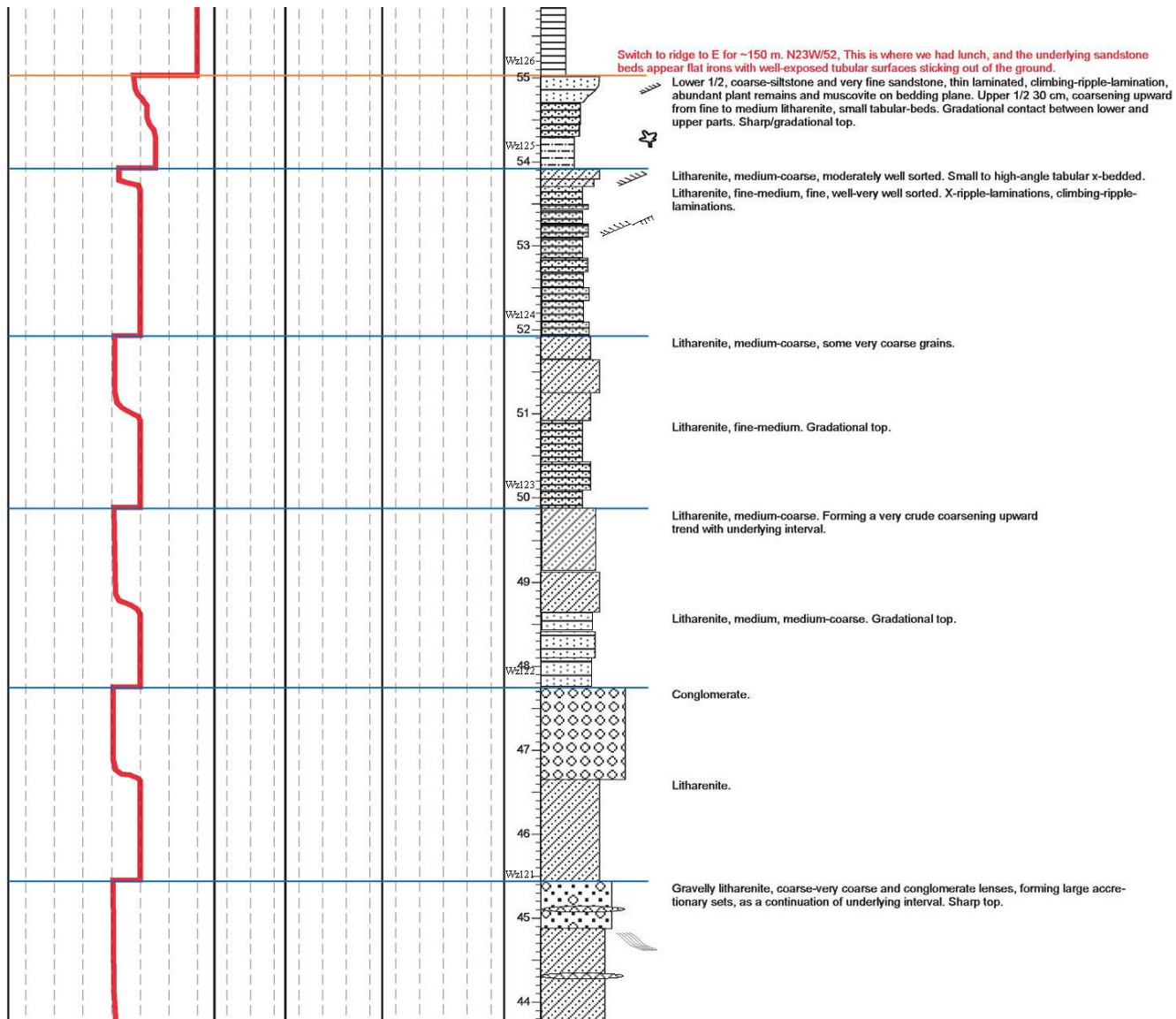
28 Shale, silty to siltstone.

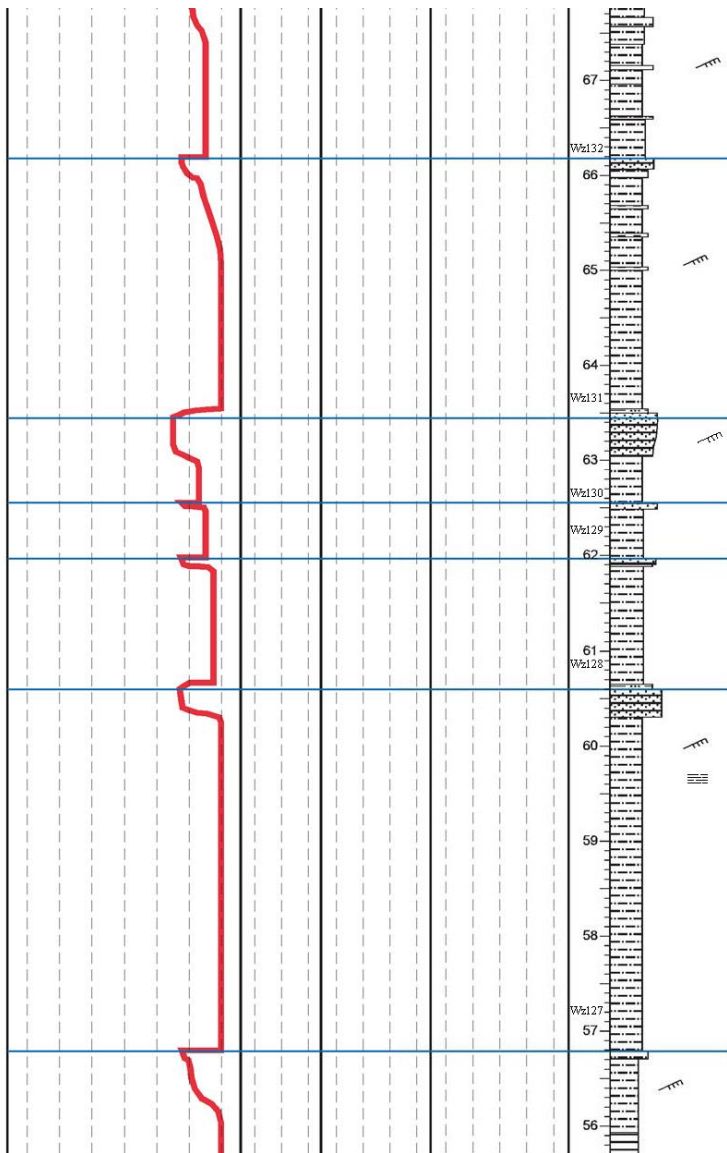
27 Coarsening upward from coarse-siltstone to very fine/fine lithic-subarenite. Distal delta front. Sharp boundary on top.

26 Interlaminated silty shale, siltstone, gray to dark gray. Prodelta. Fining upward from medium, medium-fine/very fine lithic-subarenite. LA, coarse-very coarse, gravelly, and LA, fine-medium and medium-coarse, intercalated with conglomerate lenses and laminae of fine pebble-granule with scattered pebbles. Probably 5-6 coarsening upward littoral-beach cycles of fine-medium/medium-coarse LA overlain by coarse-very coarse LA based on weathering patterns. No overall grain size trend, maximum clast size decreases upward to fine pebble. Very well tabular x-bedded, high-medium angle, small to intermediate scale, moderately well-sorted, subangular-rounded. Common reactivation surfaces. Sharp top.

20 Sharp, undulating surface, contrasting very fine sandstone and coarse-siltstone, below with coarse-very coarse litharenite and conglomerate above. **Probable first transgressive surface or sequence boundary.** The coarse delta front deposits were not deposited here. This







Interbedded coarse siltstone and silty shale, upward increasing siltstone and thickening of siltstone beds from 1 to 10 cm. Coarse siltstone climbing ripple laminated.

Laterally in 5-10 m, change to 1.5 m delta front sandstone body with concave base and convex top. See photos.

Coarse siltstone to very fine sandstone. Sharp/gradational top. Shale, silty with siltstone beds. Gradational top.

Very fine sandstone-coarse siltstone (5 cm). Slightly coarsening upward from very fine to fine lithic subarenite/lithwacke, greenish gray. Sharp/gradational top. Shale, silty.

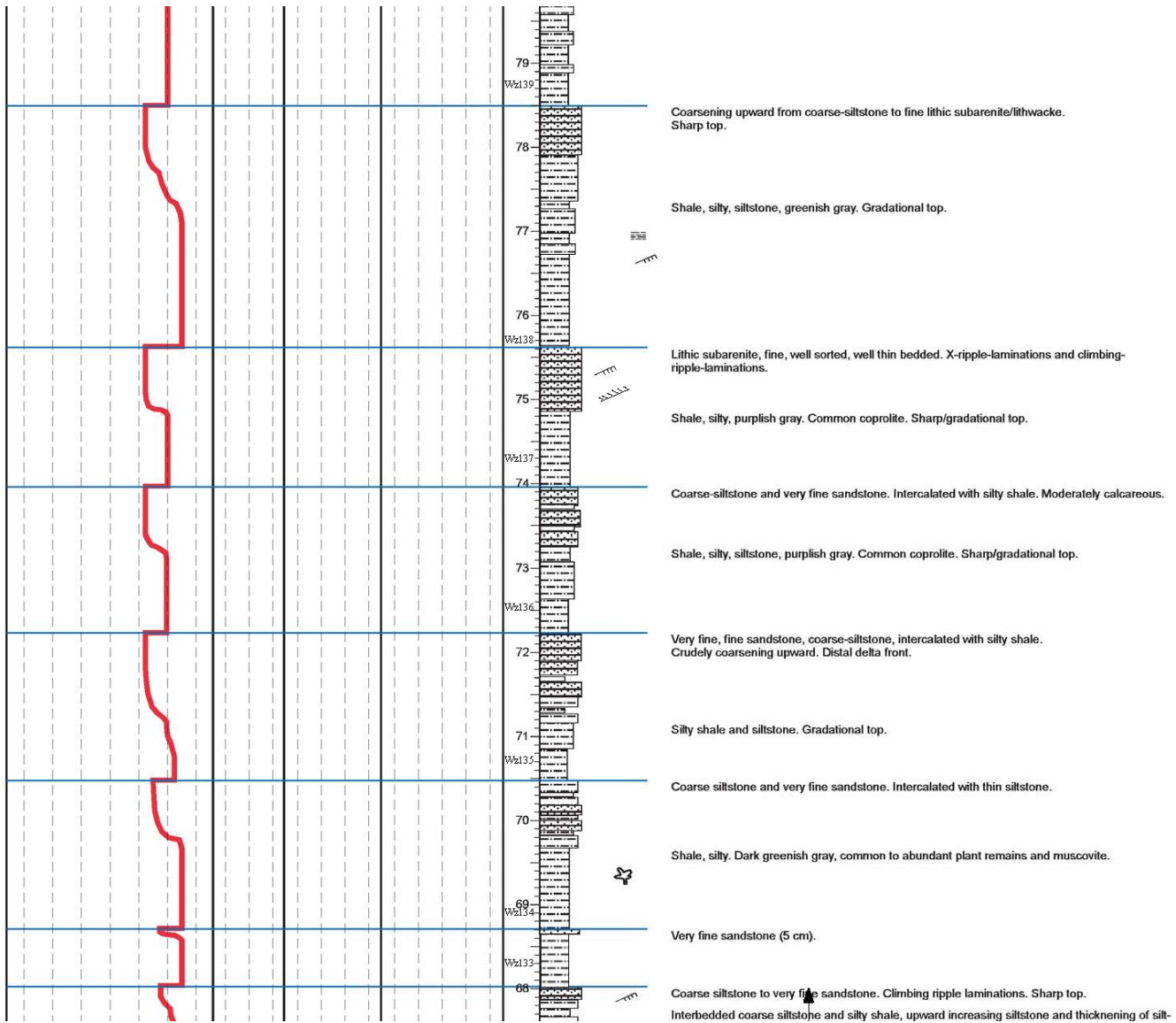
Very fine sandstone (5 cm). Shale, silty.

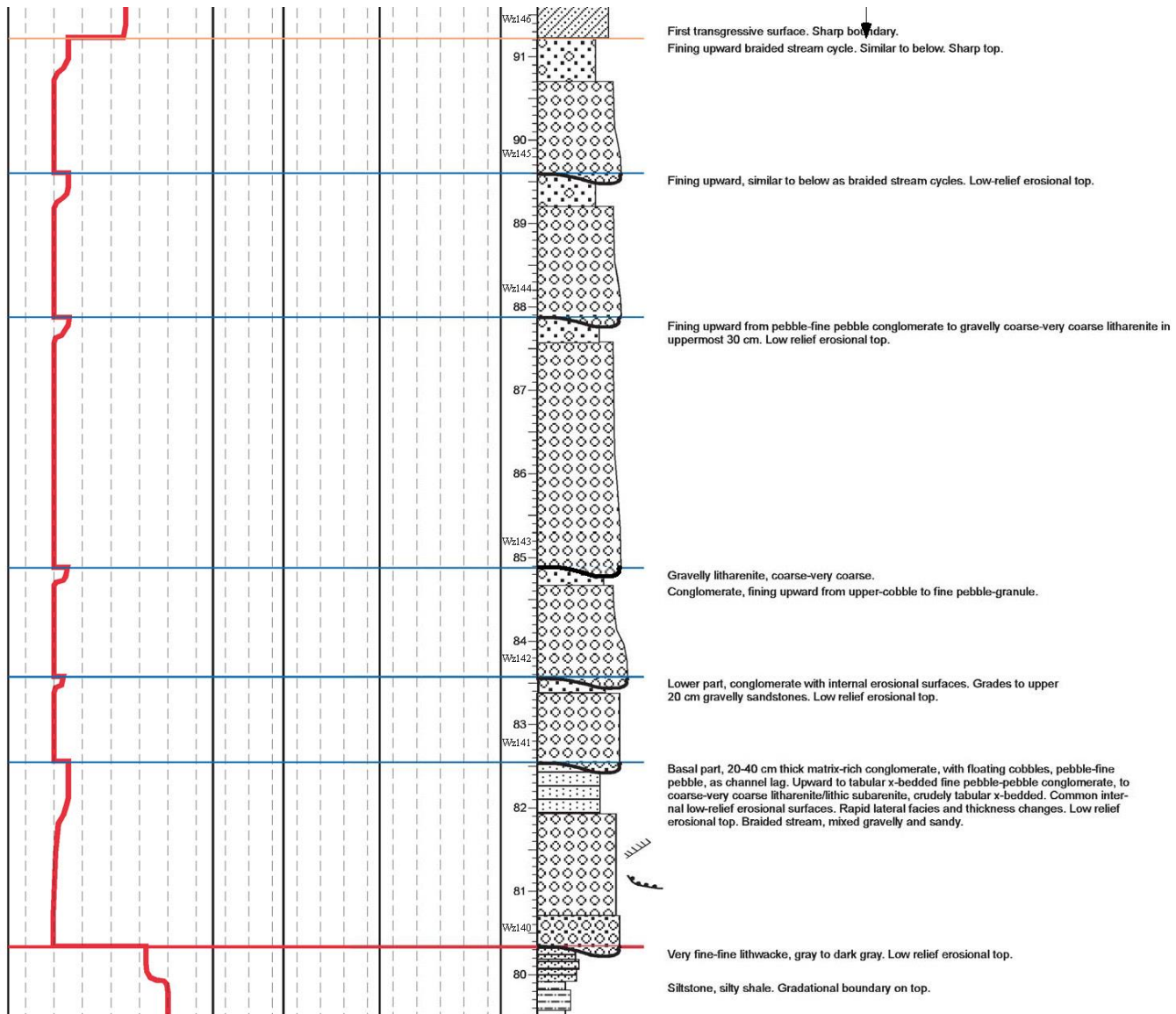
Coarse siltstone and very fine sandstone (5 cm). Shale, silty, dark gray to gray.

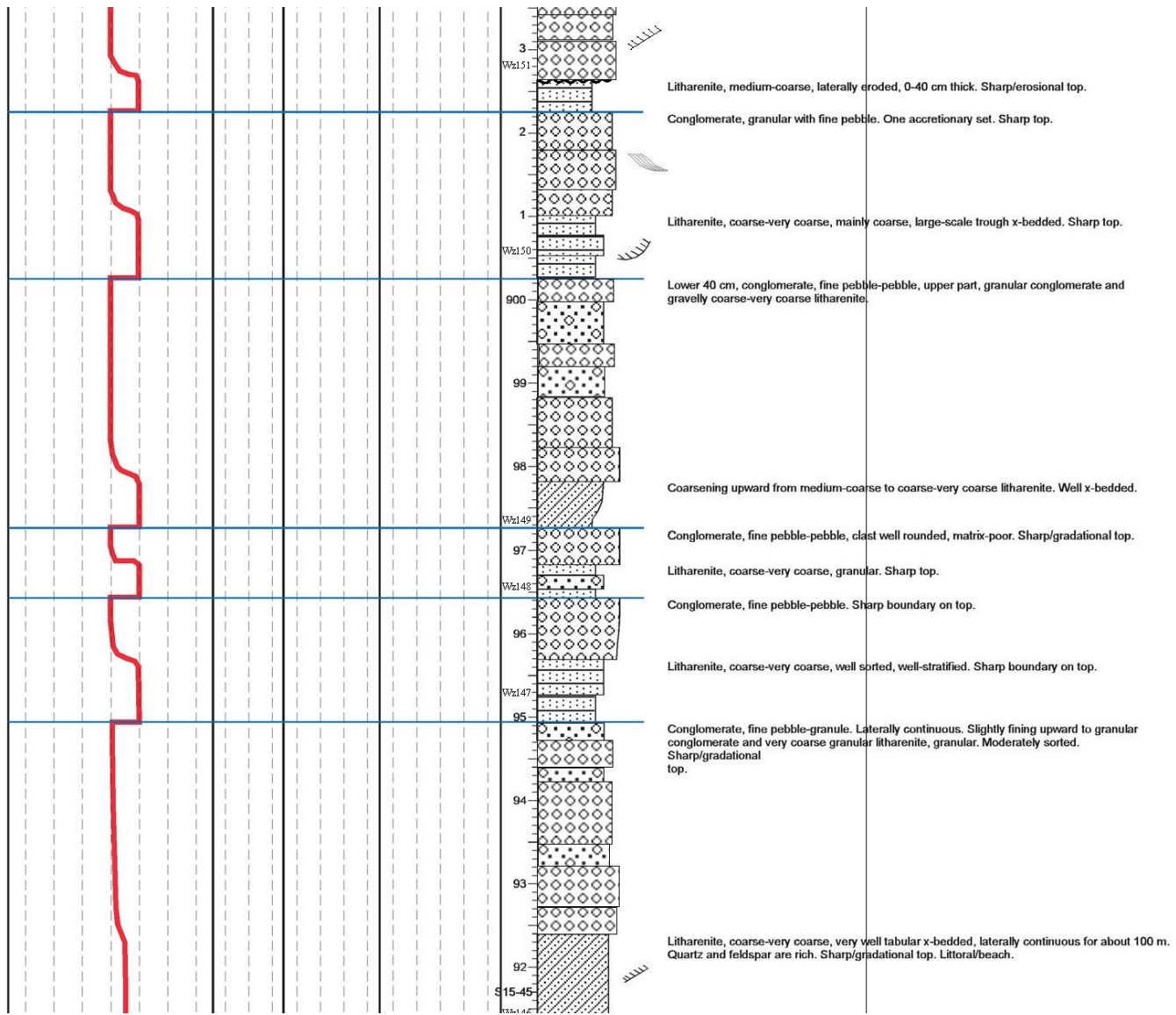
Coarse-siltstone (5 cm thick), as a transgressive deposits, common in the transition between delta front and prodelta. Slightly coarsening upward from coarse-siltstone to very fine and fine lithic-subarenite. Well climbing ripple laminations, and parallel laminations. Sharp/gradational top.

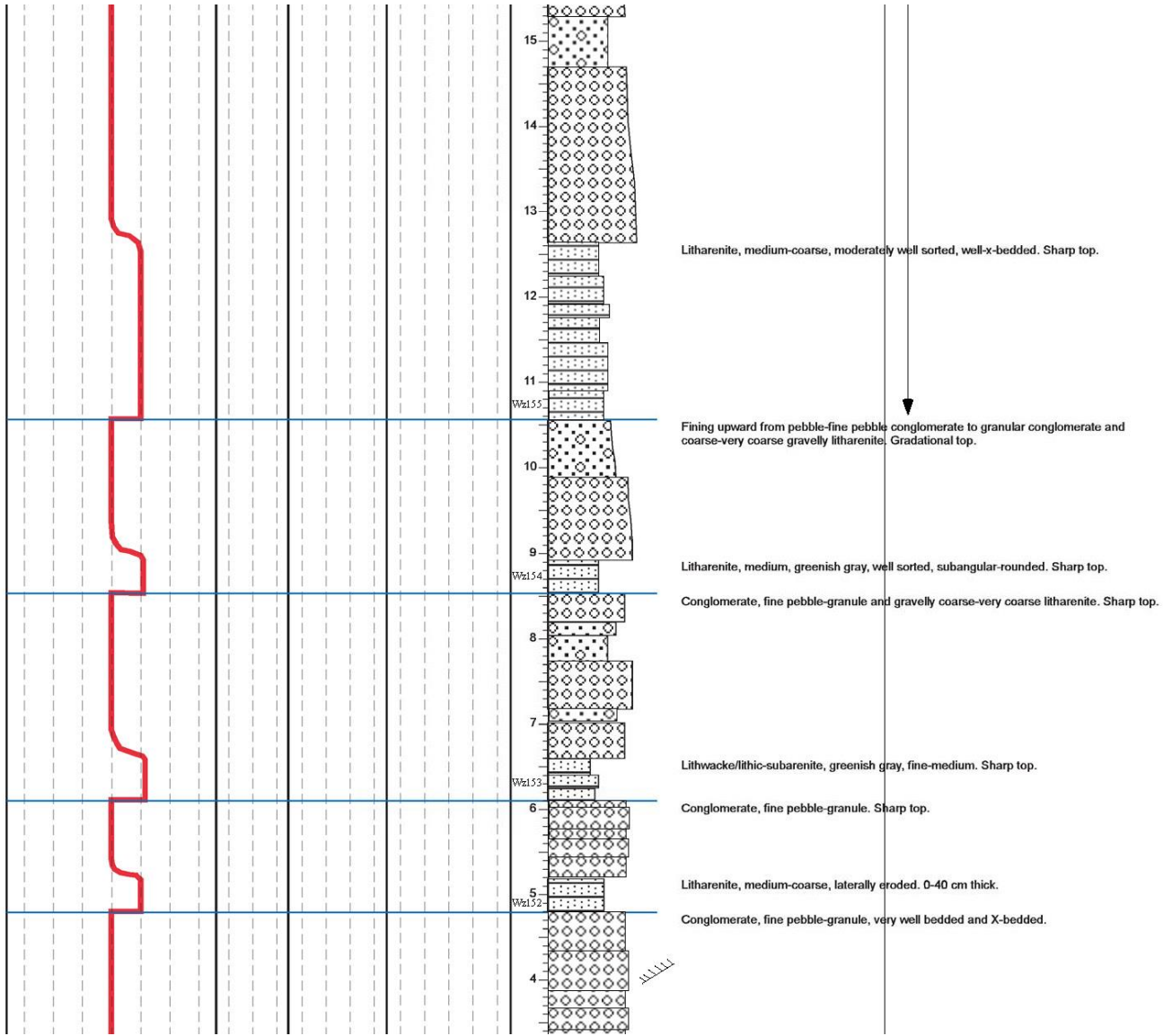
Shale, silty.

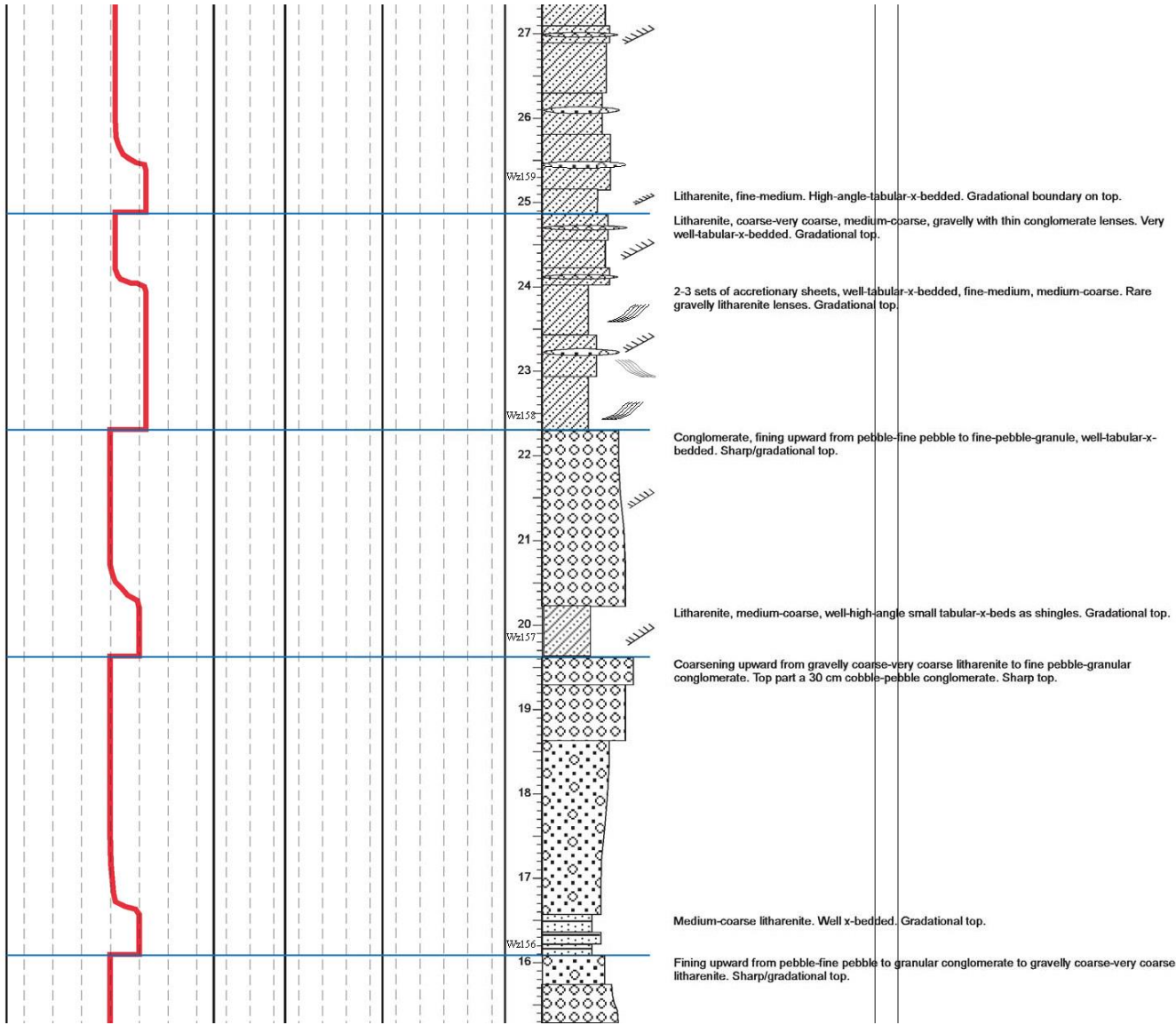
Shale, silty or pure. Some with starved ripples. Coarsening upward. Coarse-siltstone (2 cm thick) on top. Gradational top.

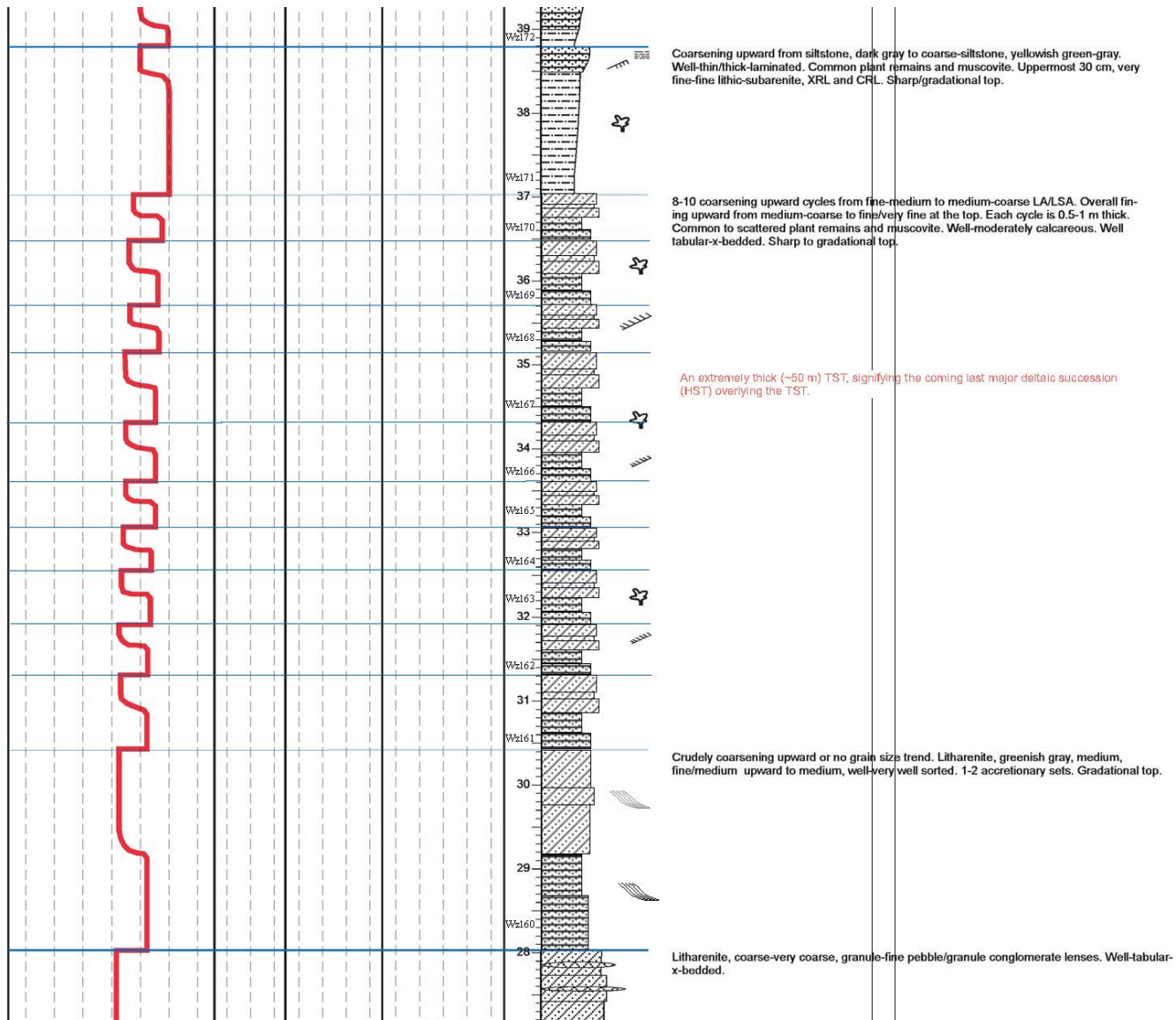


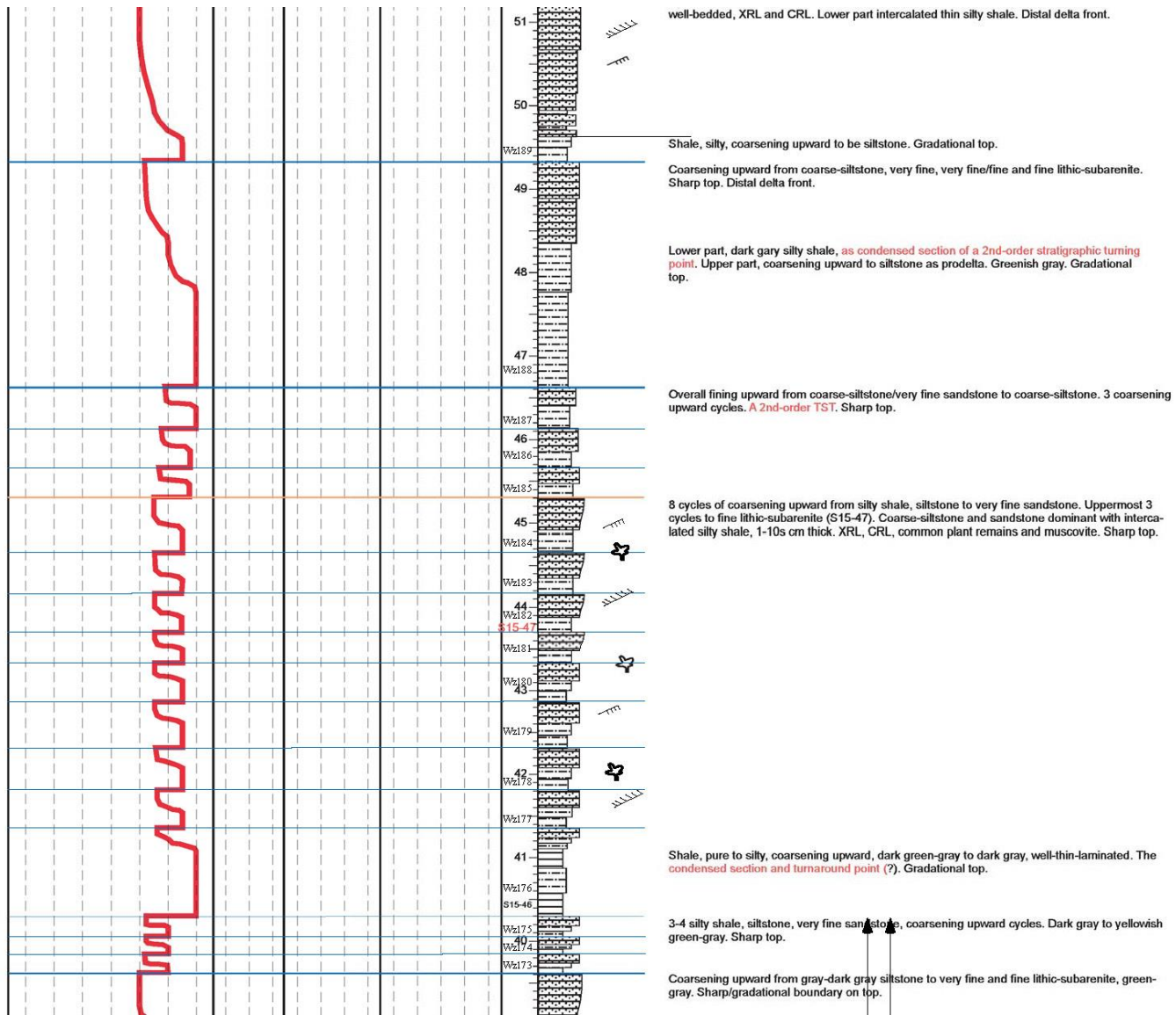


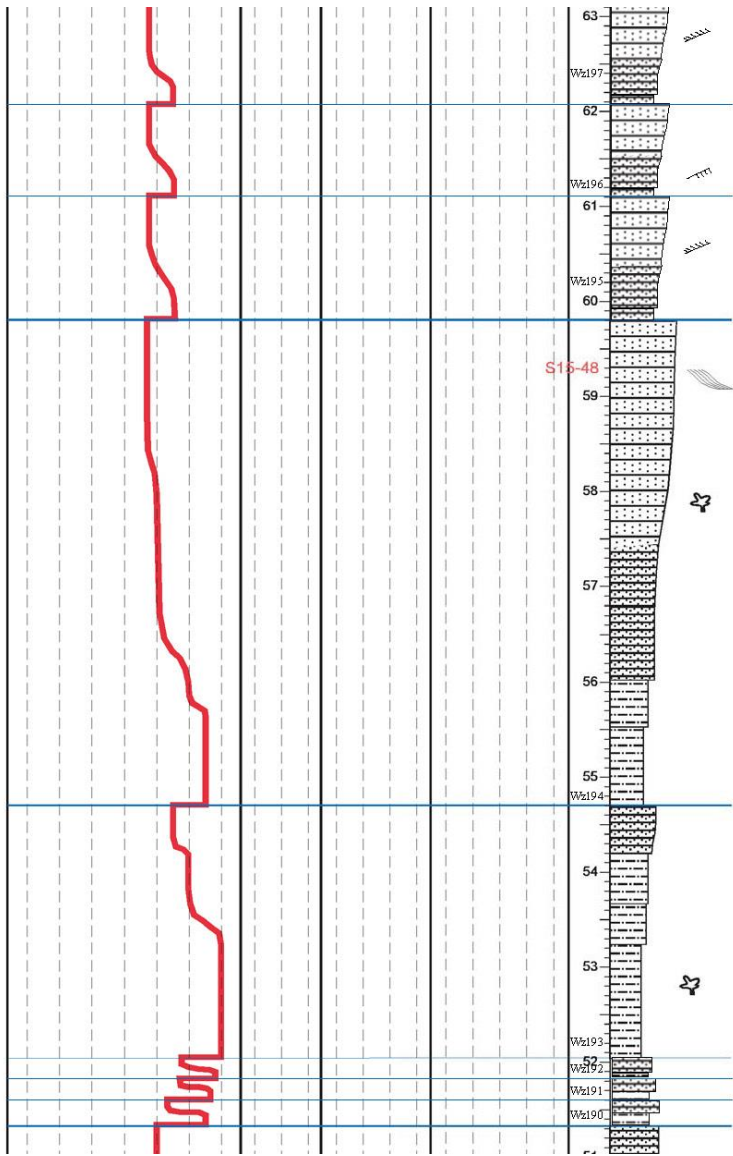












Lithwacke, coarsening upward from very fine/fine to medium-coarse, well-bedded, upper part, an accretionary set about 1 m thick. Scattered muscovite and plant remains. Not well-x-bedded in lower 1.5 m. Gradational (?) top. Delta front.

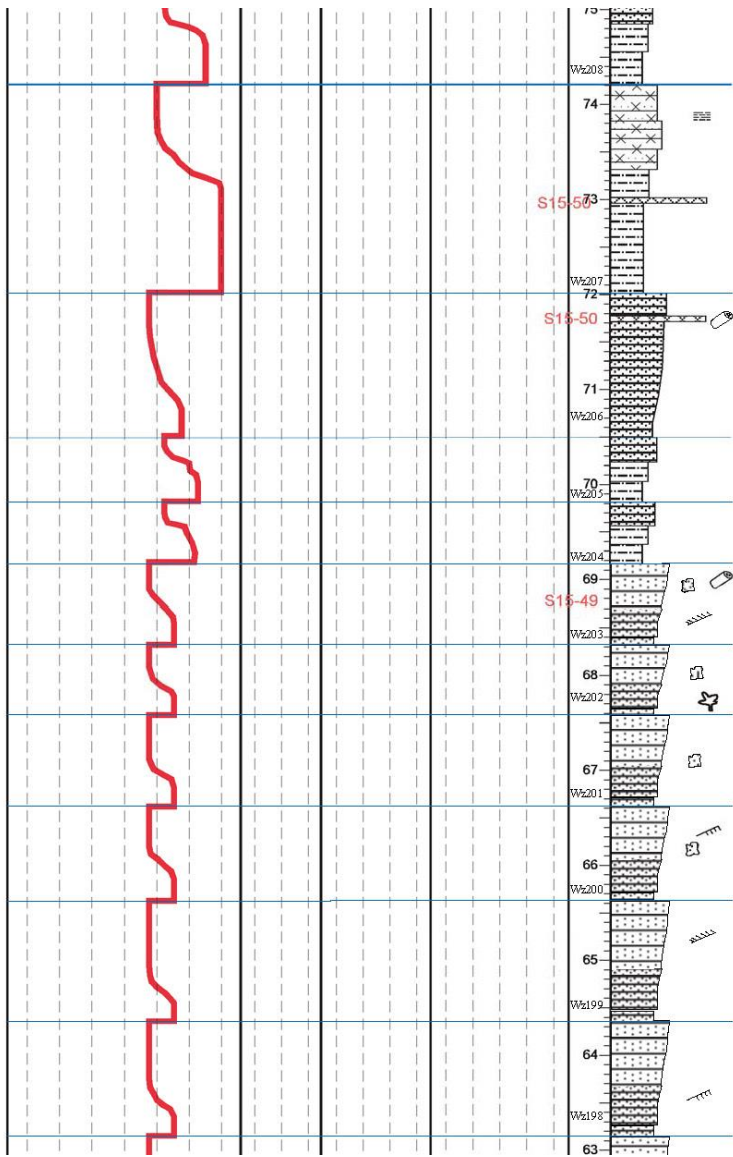
Shale, silty, siltstone, greenish gray to dark bluish gray. Coarsening upward to siltstone. Sharp top, slightly undulating.

Lithic-subarenite/lithwacke, yellow green-gray, crudely coarsening upward from coarse-siltstone to very fine sandstone. Sharp/gradational boundary on top.

Lower part dark gray silty shale with purplish gray stringers. Common plant remains, very well thin laminated. Condensed section. Upper part, dark gray-gray, silty shale, coarsening upward to siltstone. Gradational top. Prodelta.

Coarsening upward cycles with thin very fine/fine to coarse-siltstone, forming an overall fining upward trend. Sharp/gradational top.

Coarsening upward from coarse-siltstone, very fine, very fine/fine and fine lithic subarenite, well-bedded, XRL and CRL. Lower part intercalated thin silty shale. Distal delta front.



75
Wz208
Silty shale and siltstone, coarsening upward to coarse-siltstone in the uppermost 20 cm. Sharp/gradational top.

74
Lithwacke, gray, fine-very fine, tuffaceous, well-bedded and parallel laminated. Sharp/gradational top.

S15-57
Siltstone, silty shale, well-laminated, gray to greenish gray. A 2-cm thick pink tuff or tuffaceous siltstone. Gradational top.

72
Wz207
S15-50
Lithwacke, very fine to fine, greenish gray, well-laminated, moderately calcareous. A 3 cm, calcite-cemented layer of tuffaceous siltstone, where burnt branch founded. Distal delta front. Sharp/gradational top.

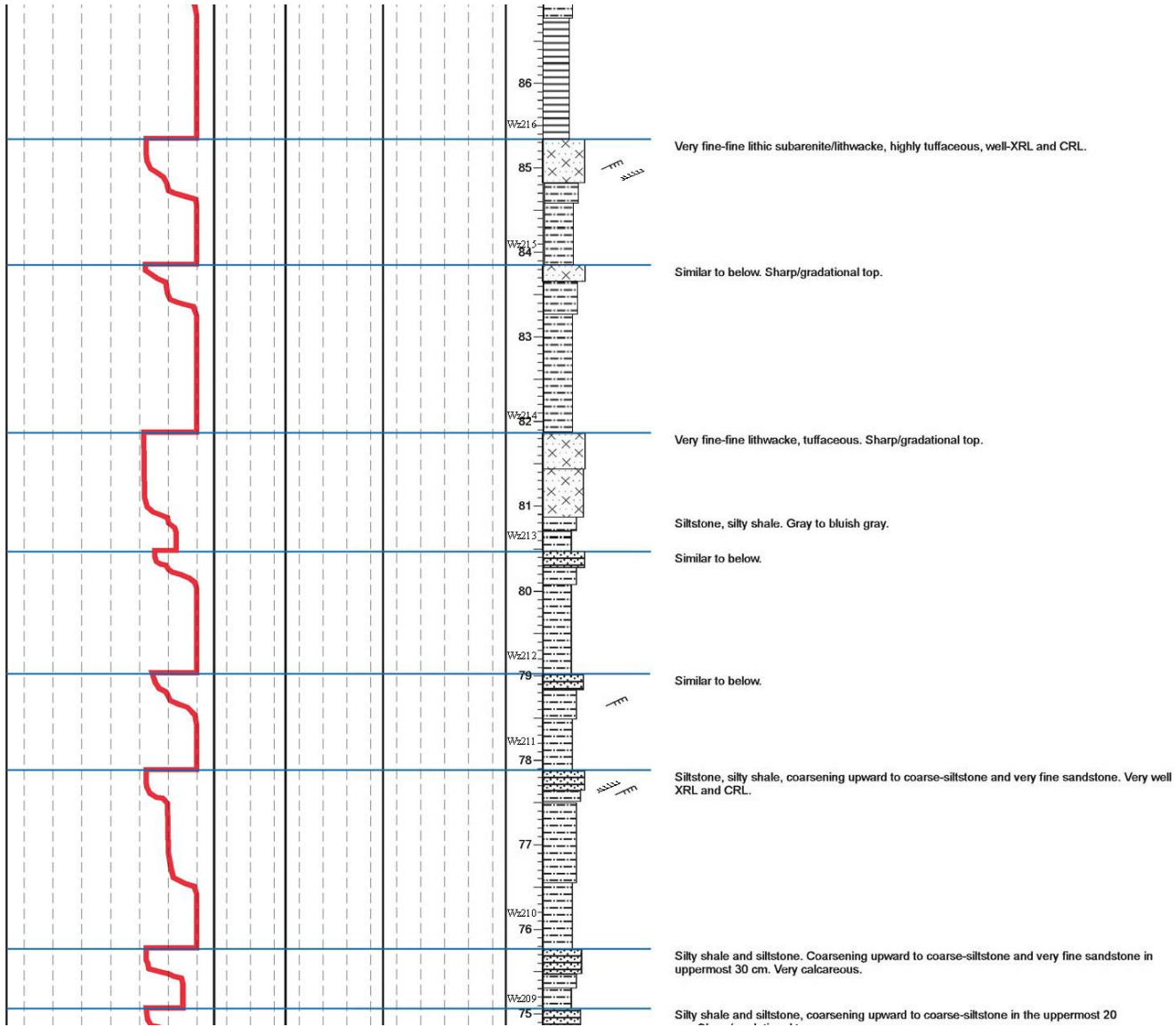
71
Wz206
2 thin coarsening upward cycles from silty shale and siltstone to very fine sandstone. Continuation of the underlying TST. Moderately calcareous. Common to abundant muscovite on bedding plane. Gradational top.

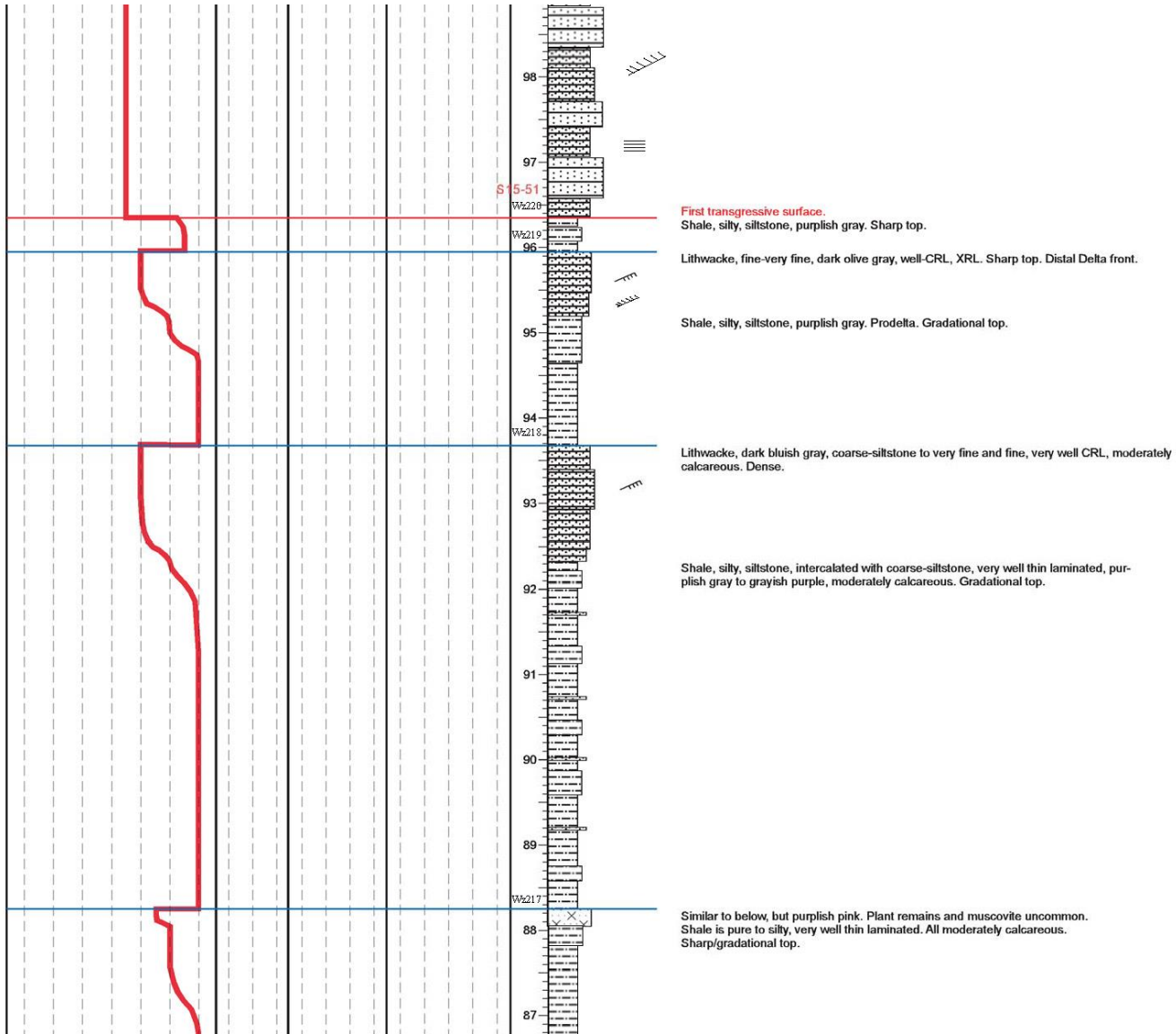
70
Wz205
An undifferentiated interval of sandstone, possibly containing meter to sub-meter coarsening upward successions from very fine/fine to medium lithwacke. Rare arenite and subarenite. Very calcareous, mostly lithwacke. Scattered muscovite and plant remains. But common black heavy minerals forming black laminae (S15-49). Uncommon tabular x-beds, mostly planar/parallel laminations, XRL and CRL. Abundant calcitic sandstone nodules in middle and upper parts. No very coarse sandstone and conglomerate present. One log in uppermost part, parallel to bedding.

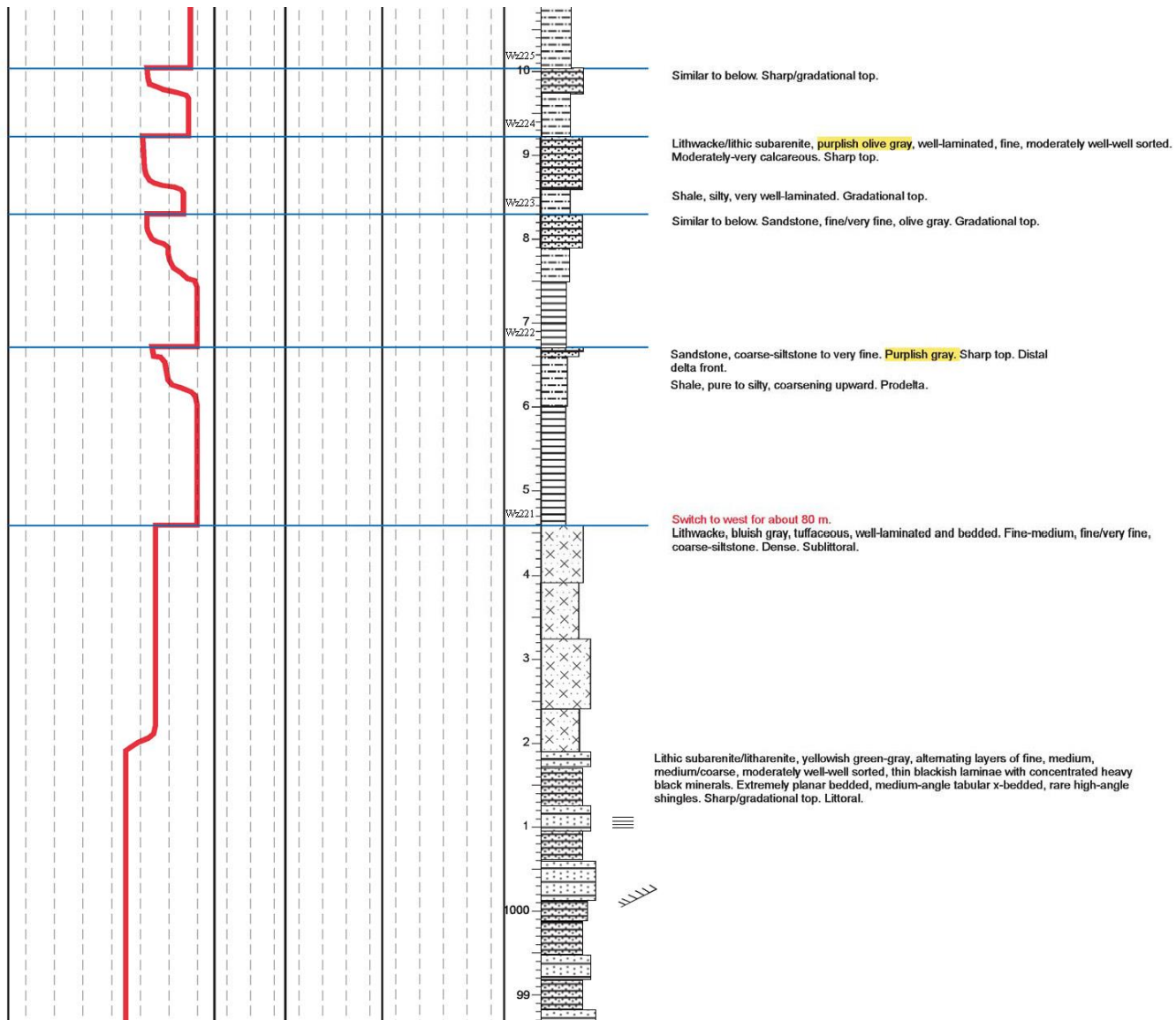
69
S15-49
Wz203
Major difference from beach-littoral sandstone below: 1. No conglomerate and very coarse sandstone. Fine sandstone dominated, some medium; 2. Rare high-angle tabular x-beds and accretionary sets; 3. Most lithwacke; 4. Common black minerals and laminae (not sure of the origin). Common to both: coarsening upward, no shale, overall fining upward.

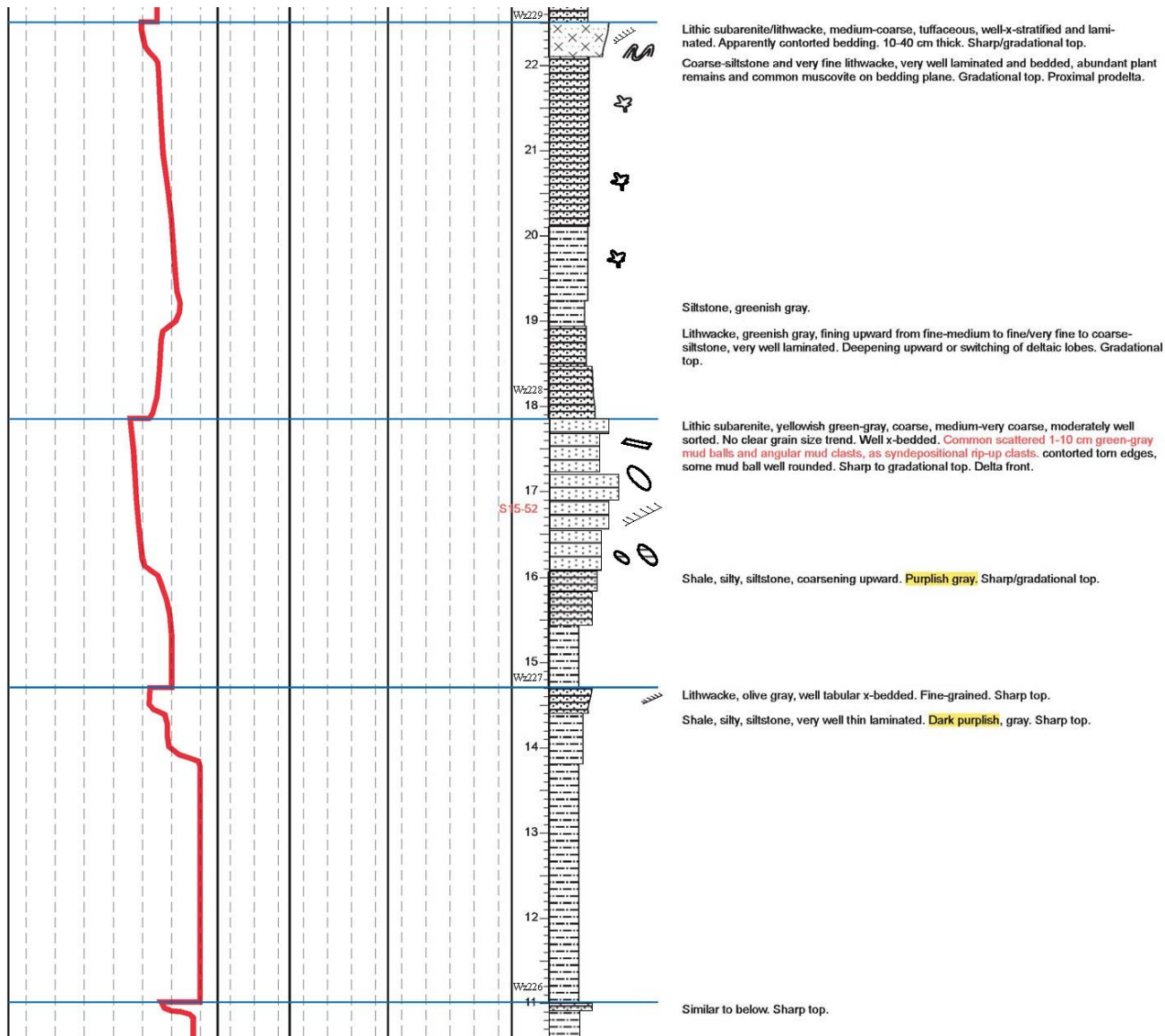
68
Wz202
Beach-littoral-sublittoral (should be prodelta to delta front?). A major change in provenance, tectonic, lake, or climatic conditions.

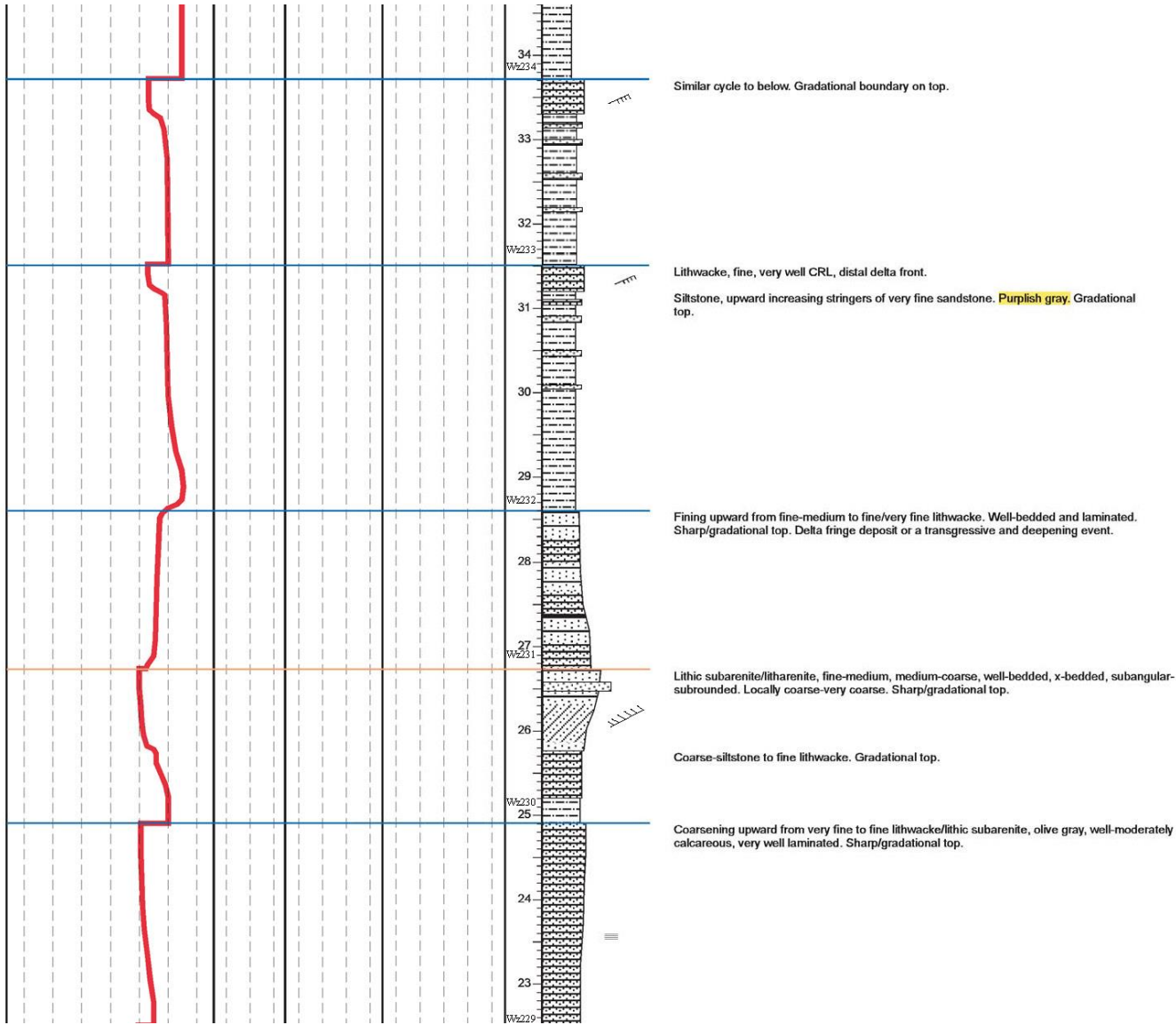
67
Wz201
66
Wz200
65
Wz199
64
Wz198
63

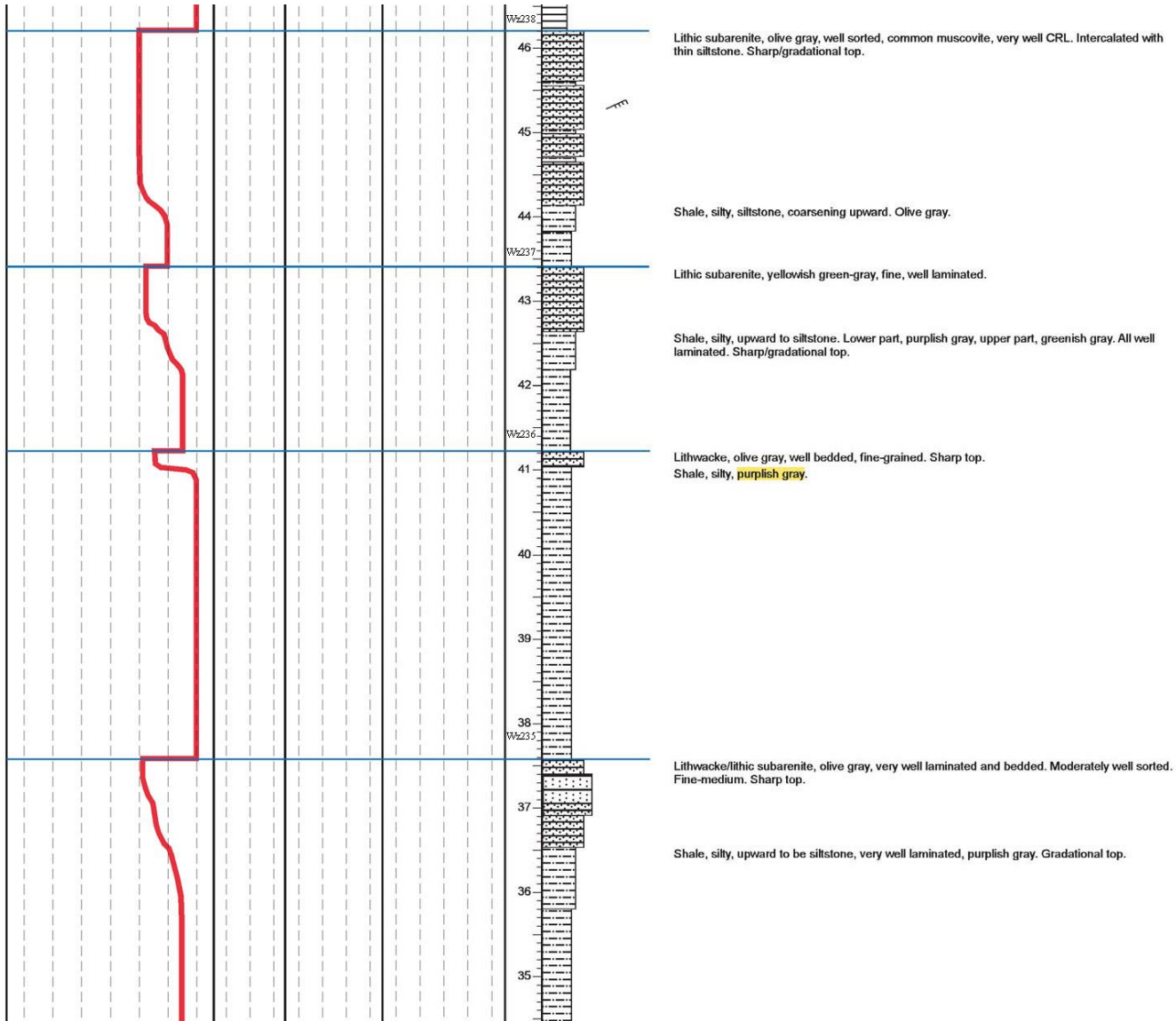


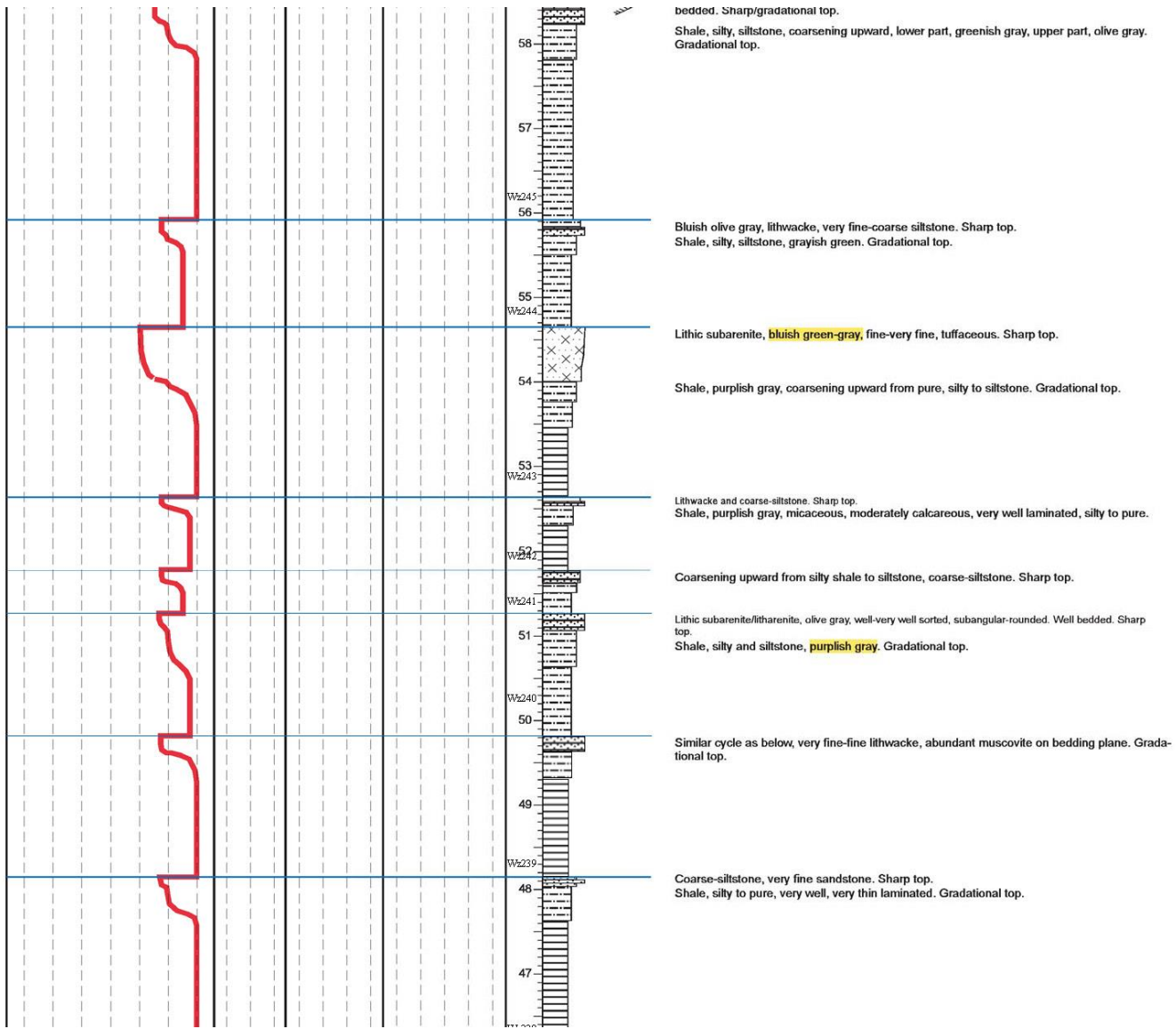


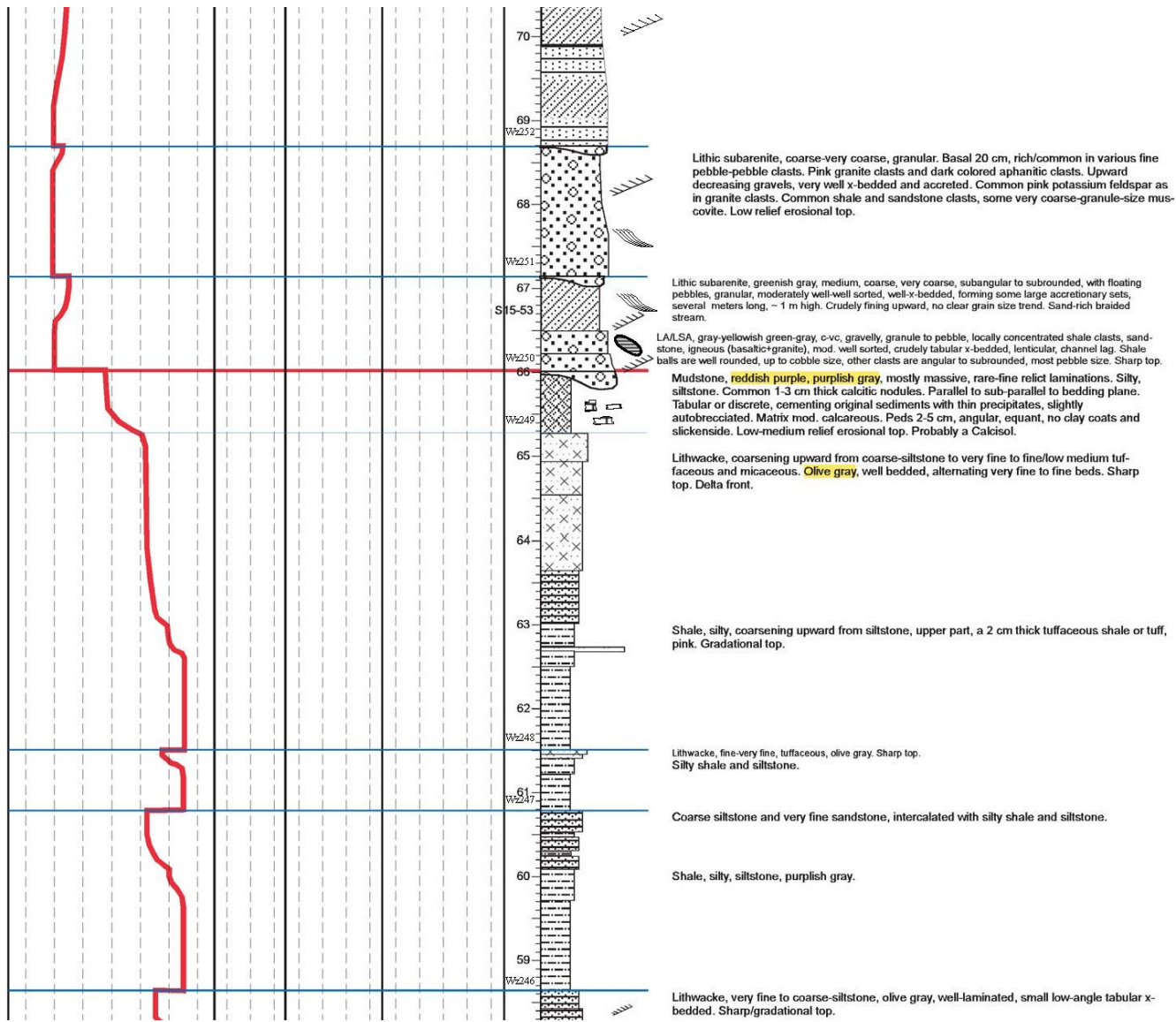


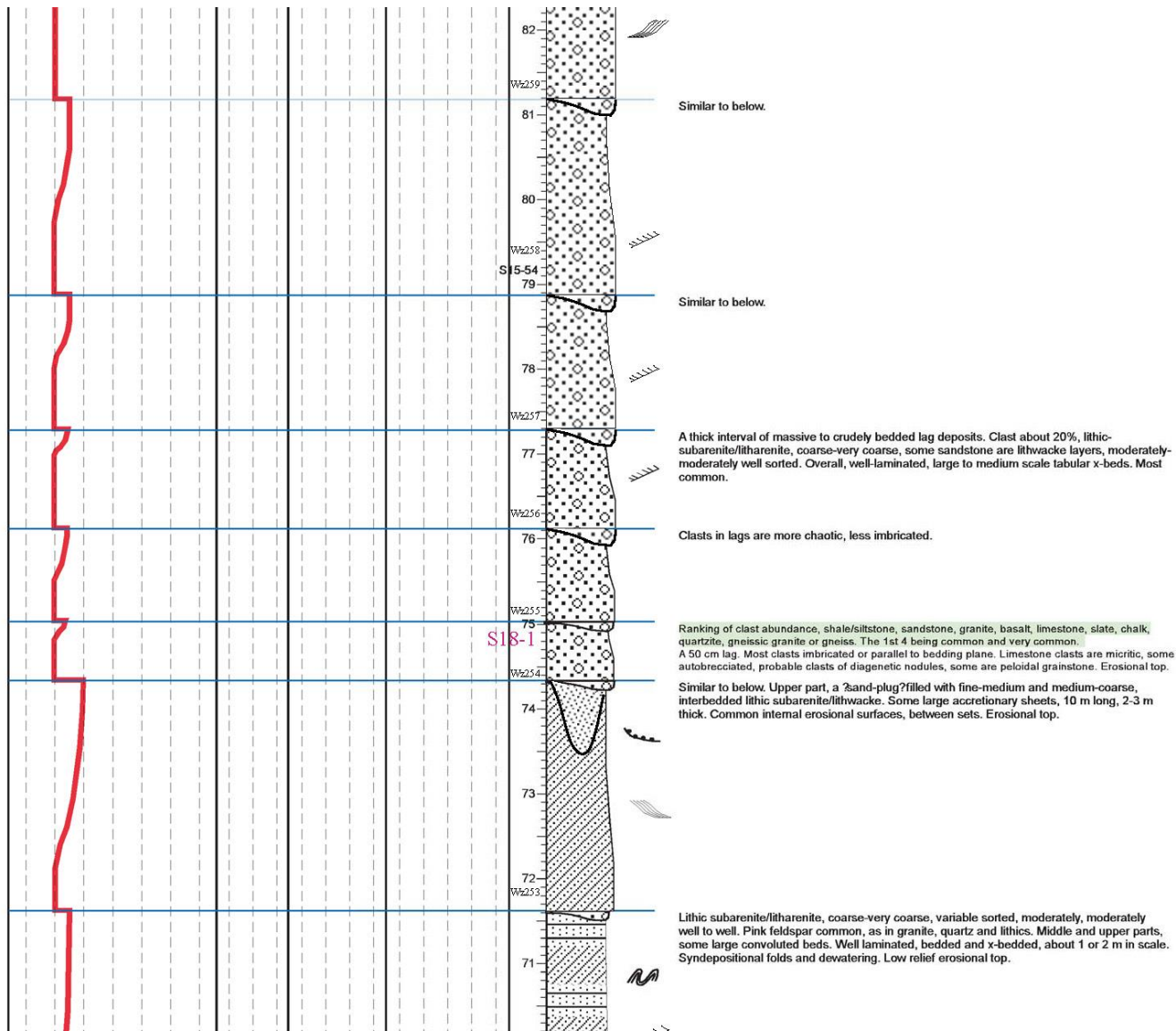


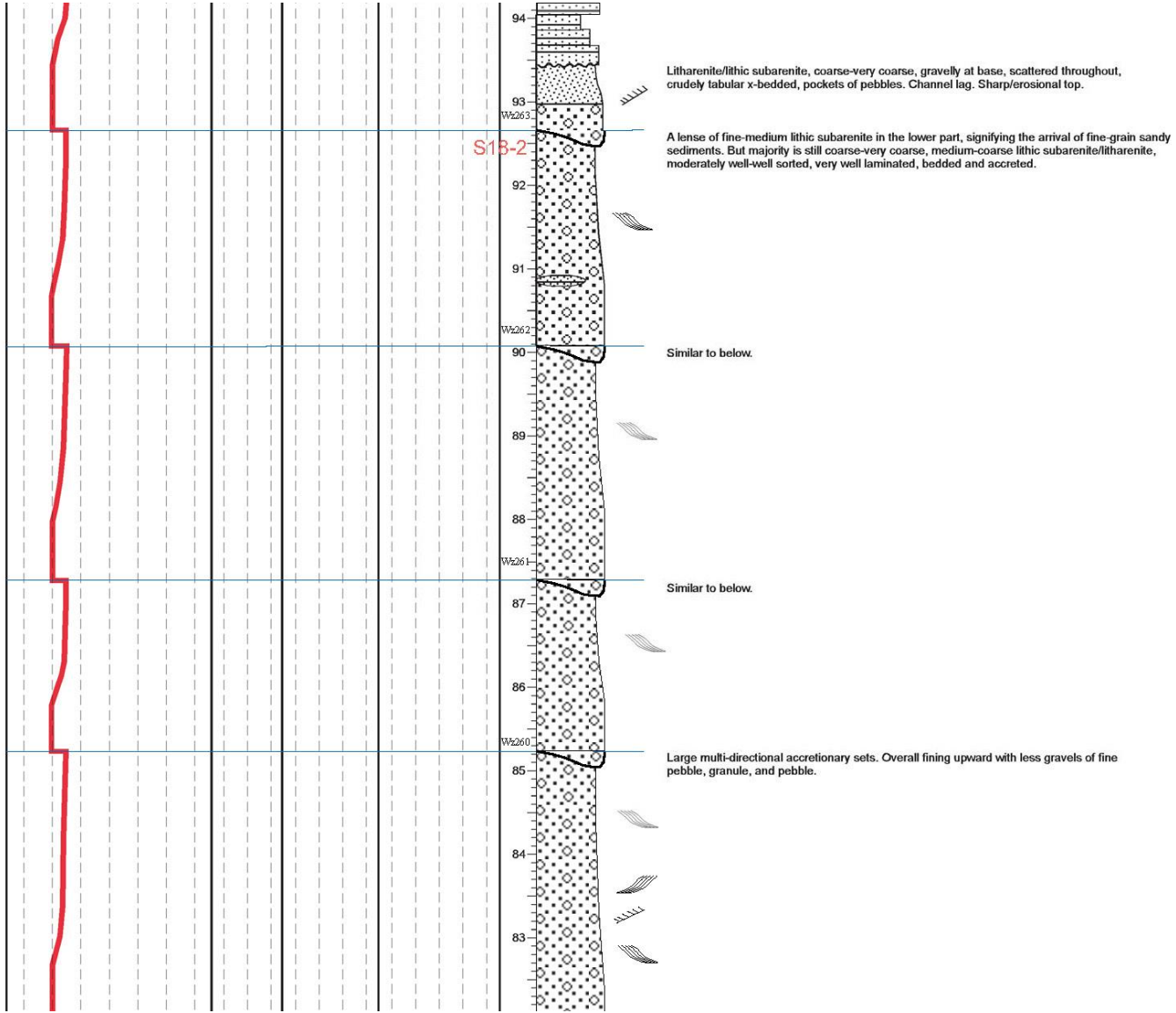


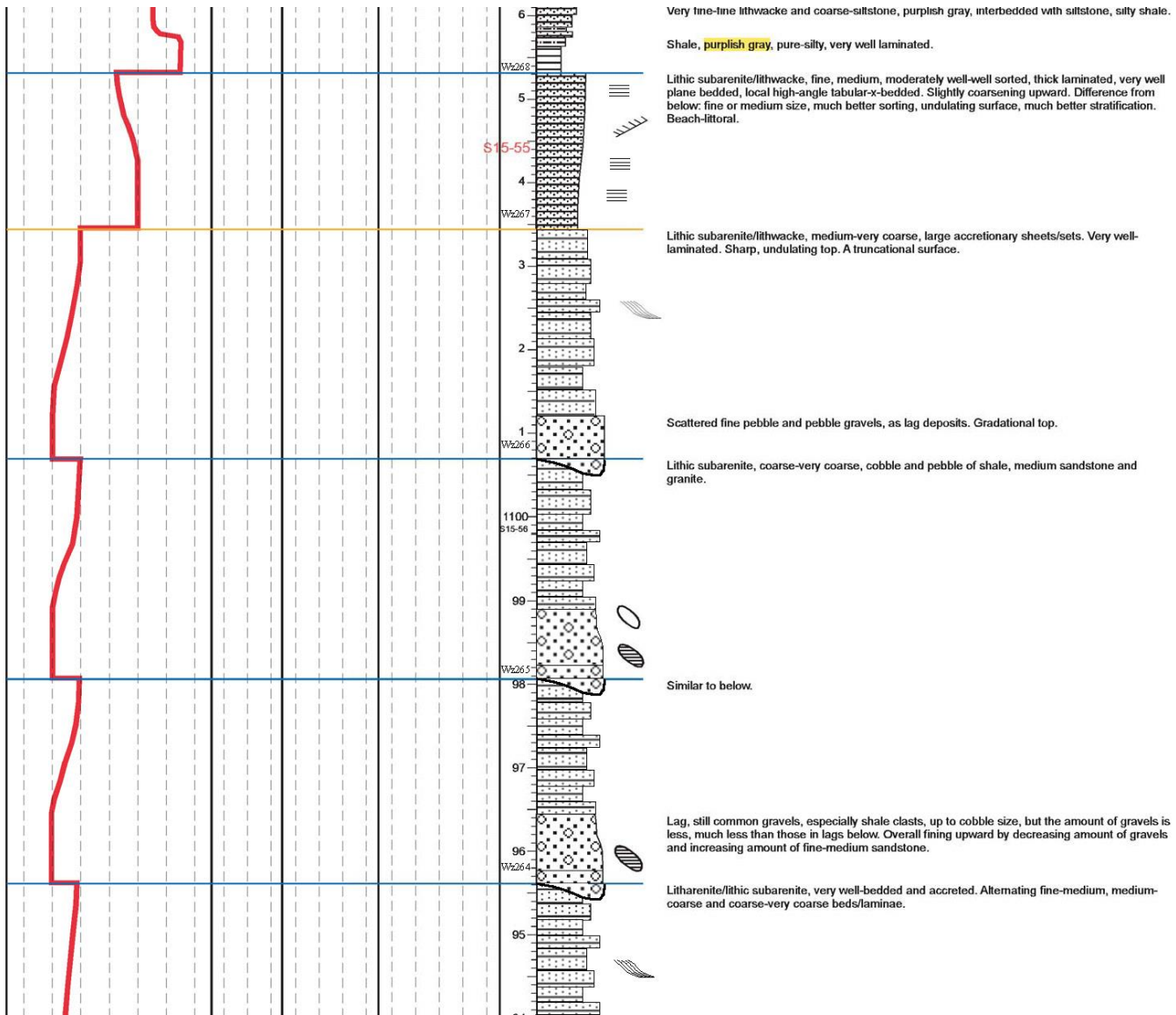


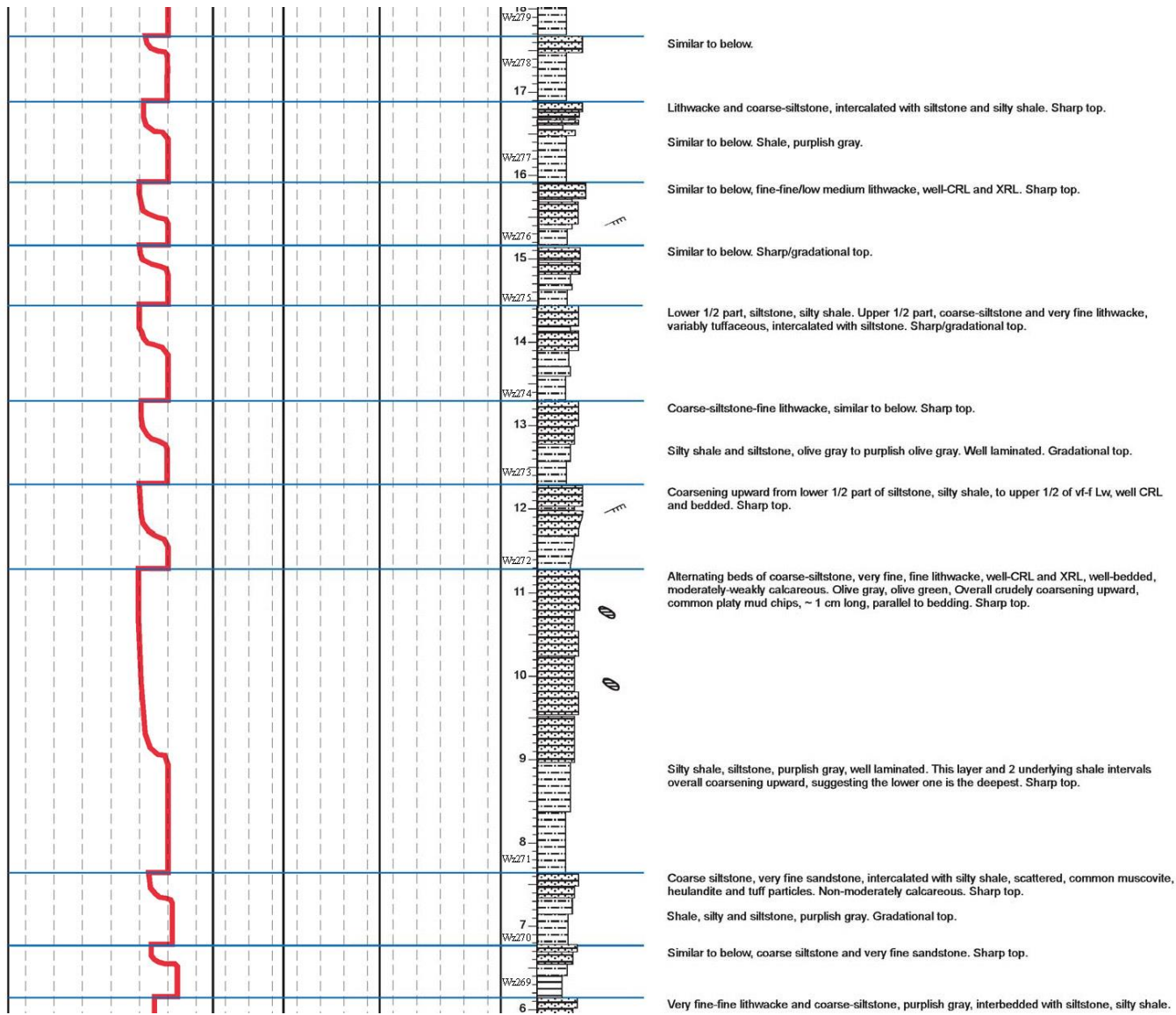


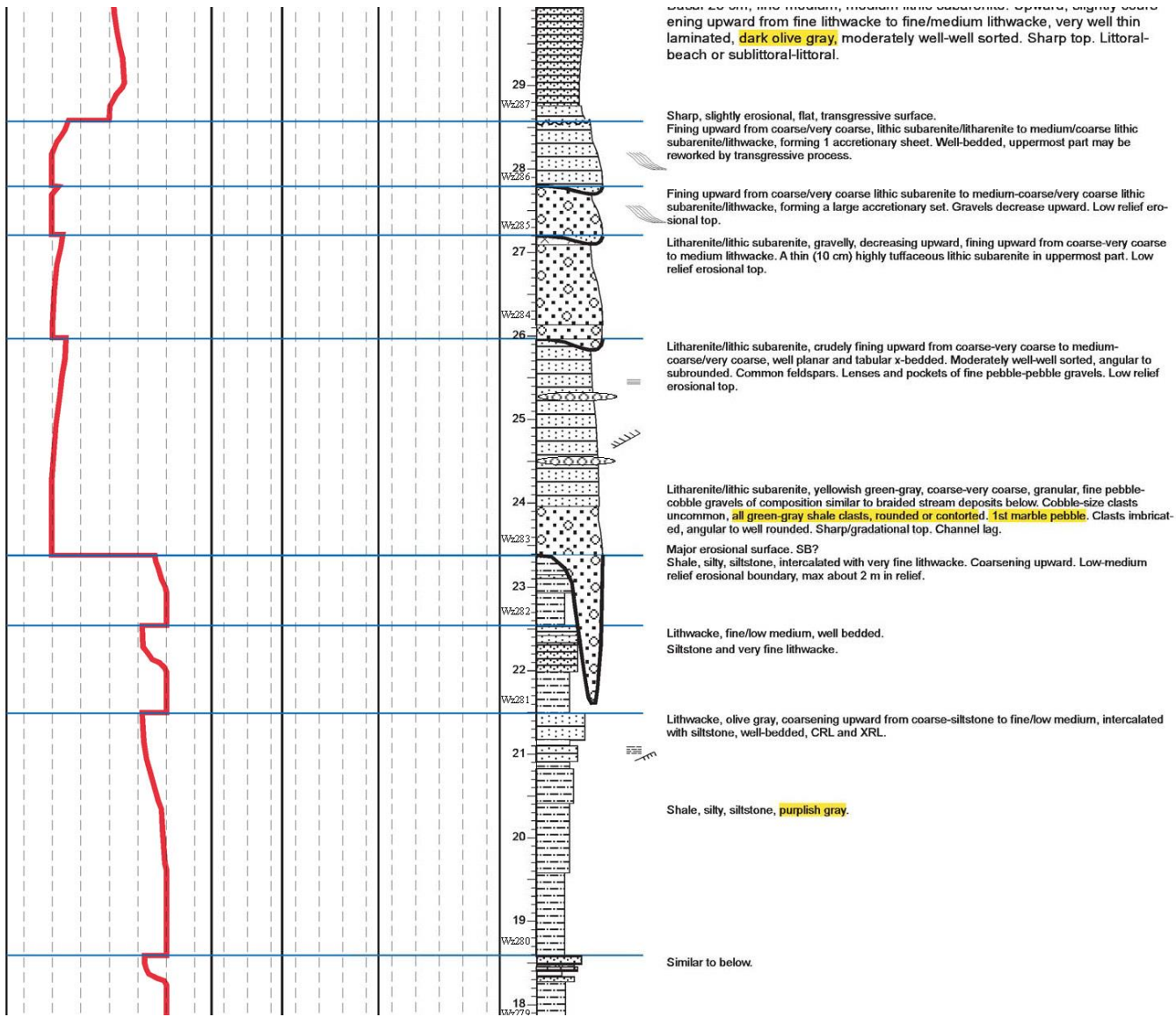


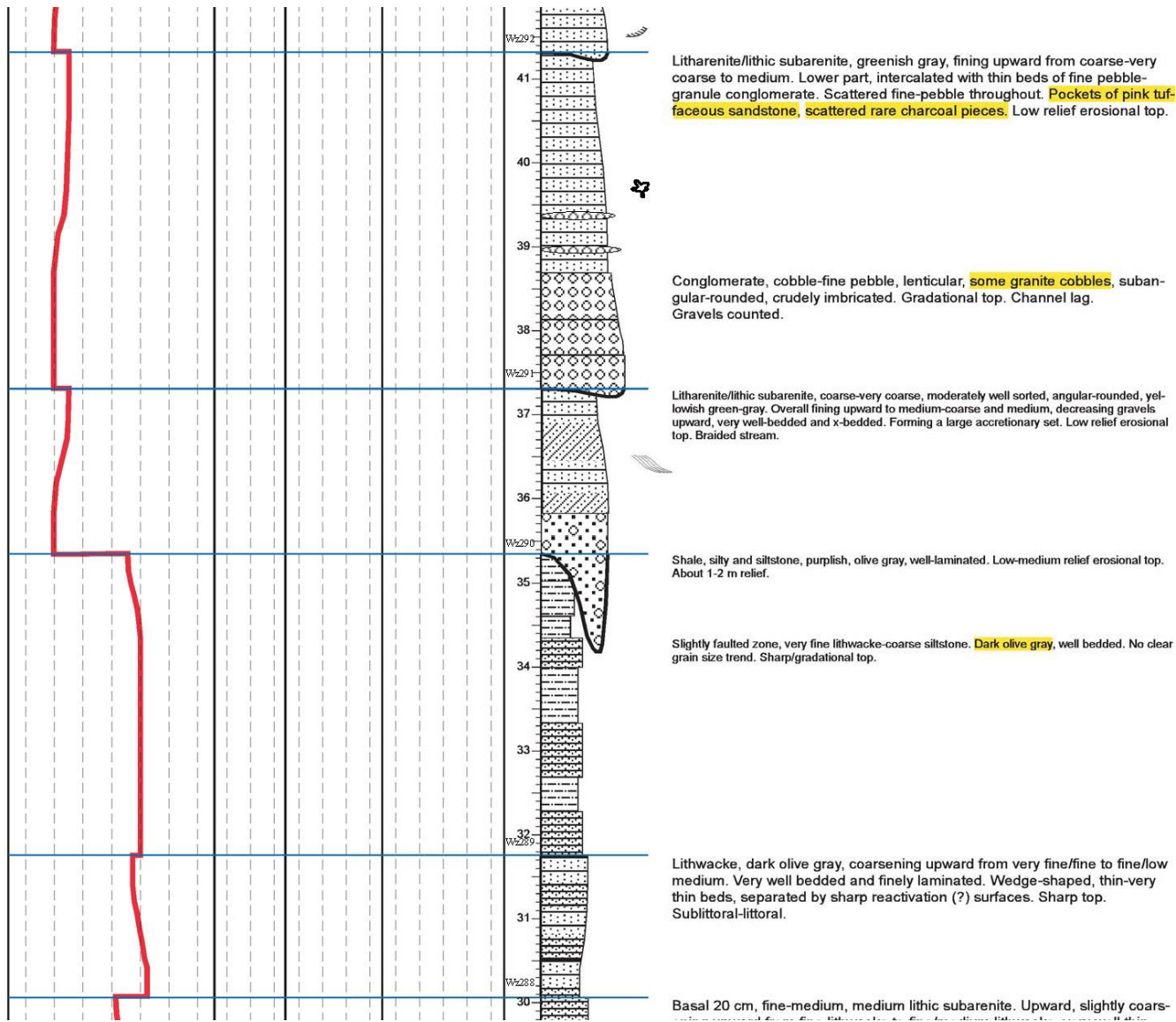


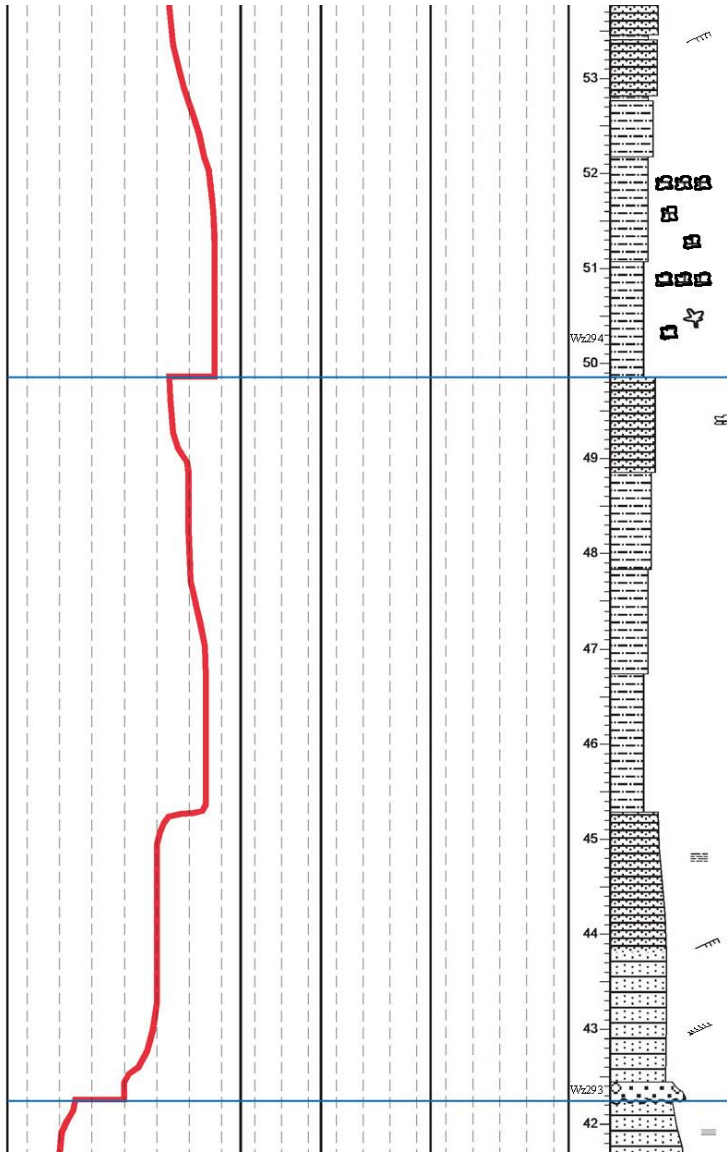












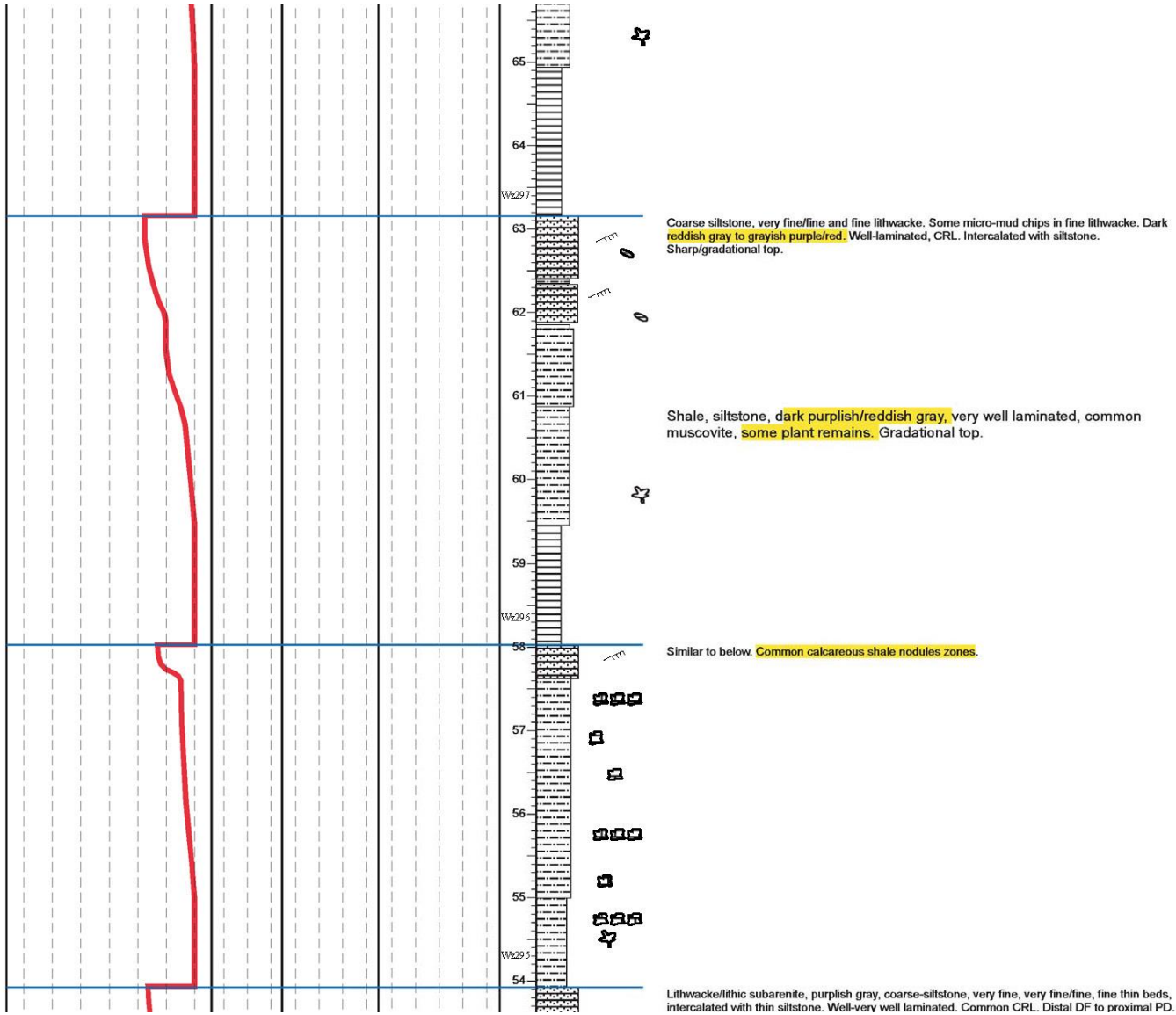
intercalated with thin siltstone. Well-very well laminated. Common CRL. Distal DF to proximal PD.

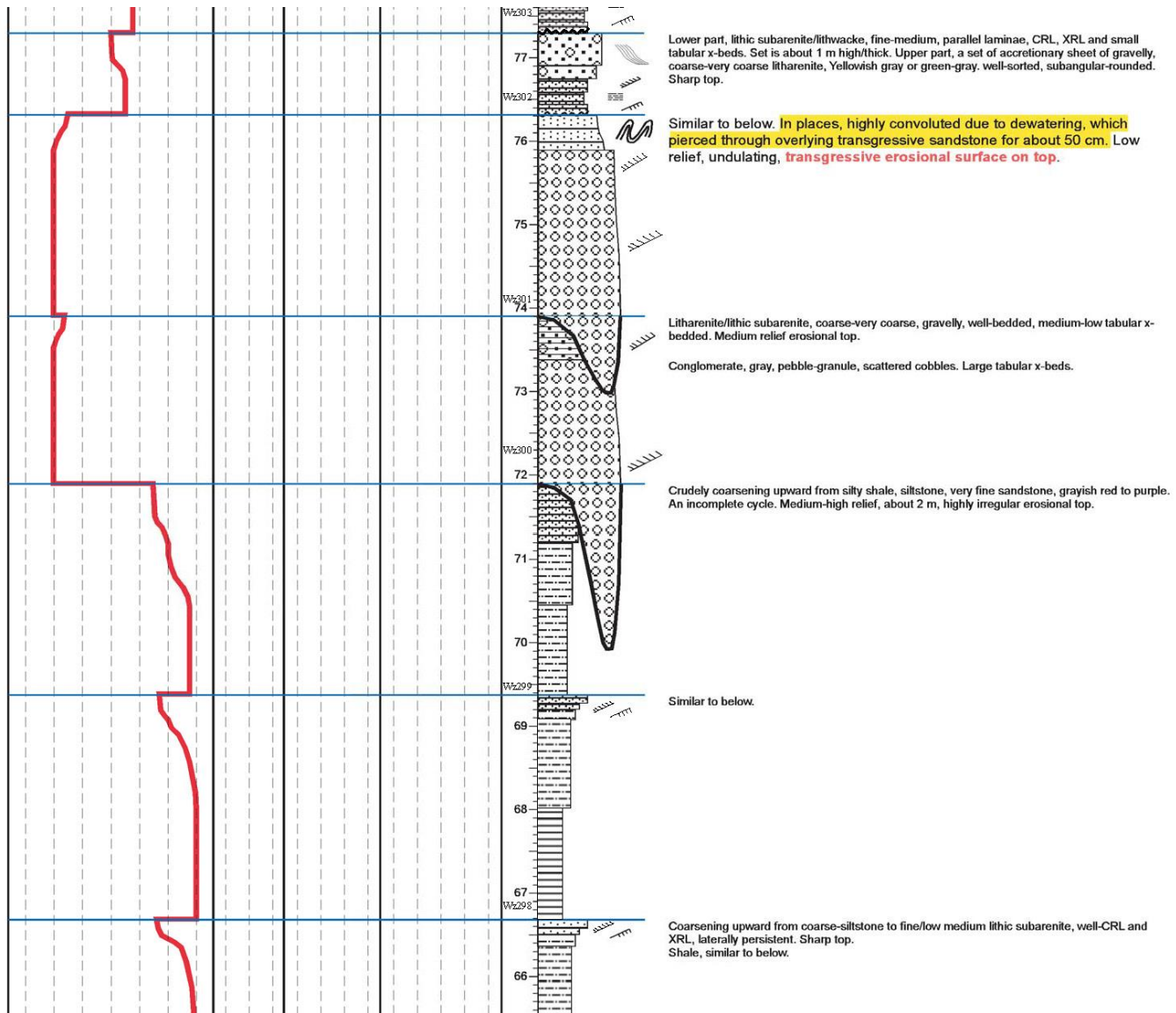
Shale, silty, siltstone, purplish gray to reddish purple, well-laminated, some scattered plant remains. Equant, irregular calcareous nodules. 1-10 cm, scattered throughout or coalesce forming bedding parallel zoning of nodules, beds. Moderately calcareous. Gradational top. Sublittoral, proximal PD.

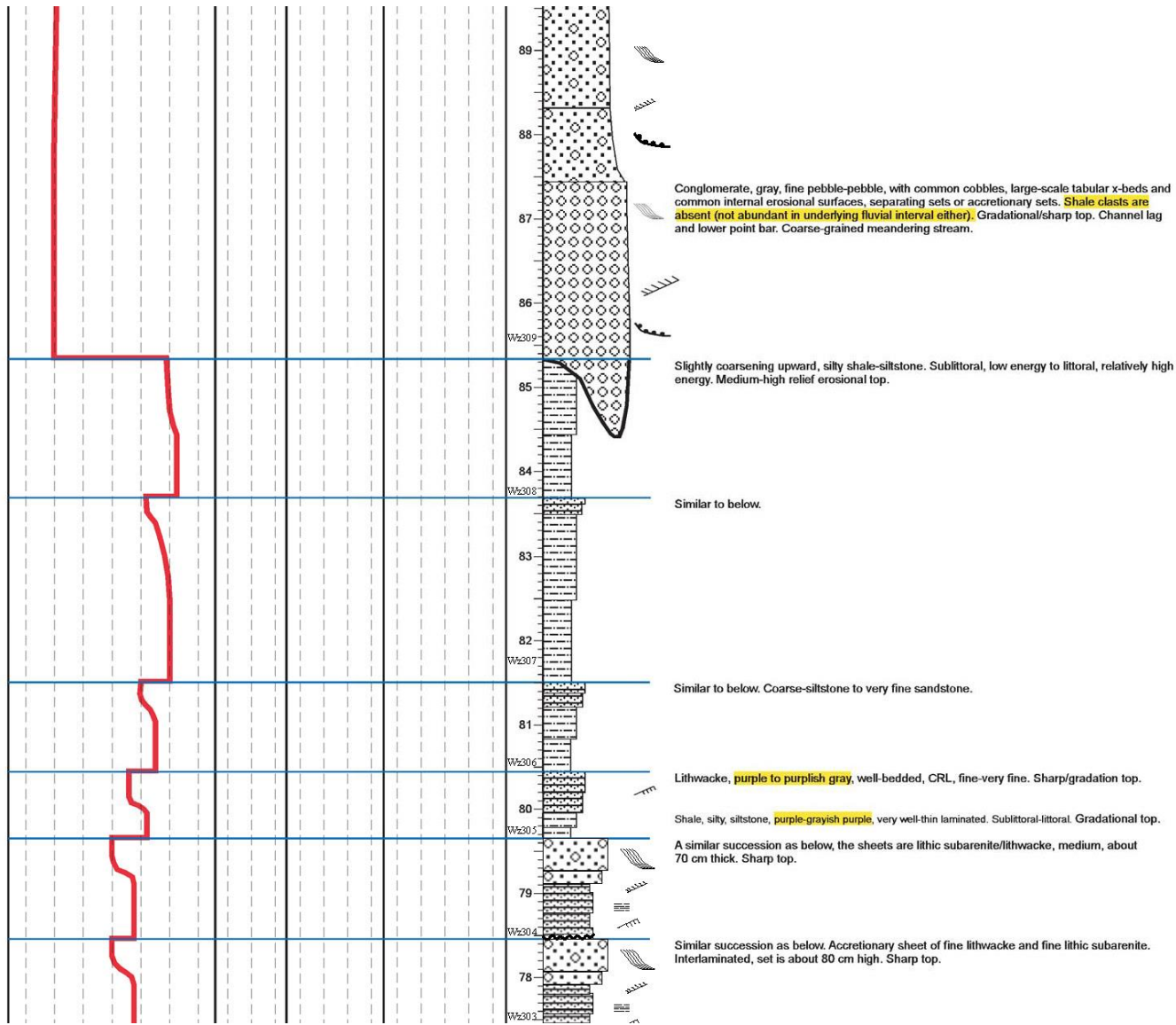
Silty shale, siltstone, coarse-siltstone, very fine sandstone, dark purplish olive gray, overall crudely coarsening upward to very fine sandstone. Very well laminated, fine to thin. Upper part, irregular calcitic nodules of roughly tabular form, parallel to bedding, as preferentially cemented shale, diagenetic. In some laminae/beds, common micro mud clasts. Gradational top. Sublittoral.

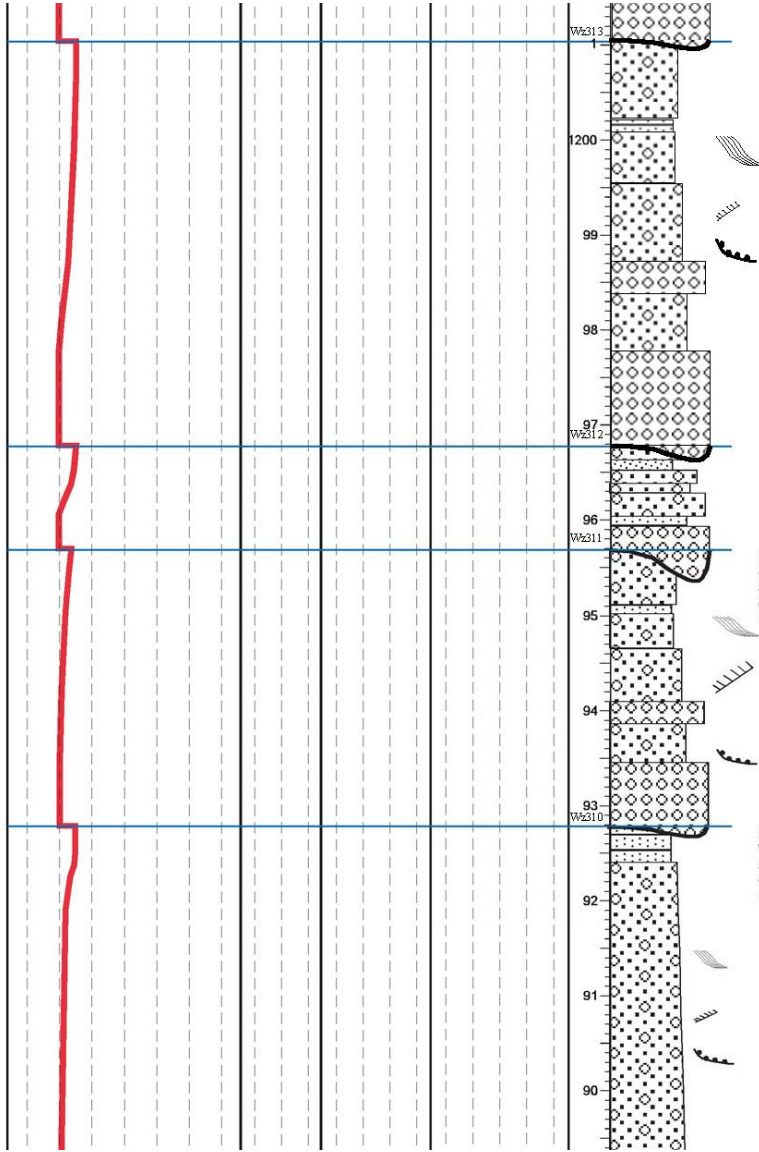
Lithwacke/lithic subarenite, fine-medium, dominated. Upper part, fine-very fine lithwacke, overall fining upward, moderately well-sorted, subangular-subrounded-rounded, locally tuffaceous and micaceous. Very well thin or finely laminated throughout, parallel, CRL, XRL. Gradational top. Deepening upward TST.

Pockets and lenses of pebble-cobble conglomerate, encased in medium-coarse, coarse-very coarse litharenite, laterally persistent. Sharp top. Transgressive lag, high-energy. Litharenite/lithic subarenite, fining upward from coarse-very coarse to medium-coarse, well planar and tabular x-bedded. Erosional/sharp top. Braided stream.



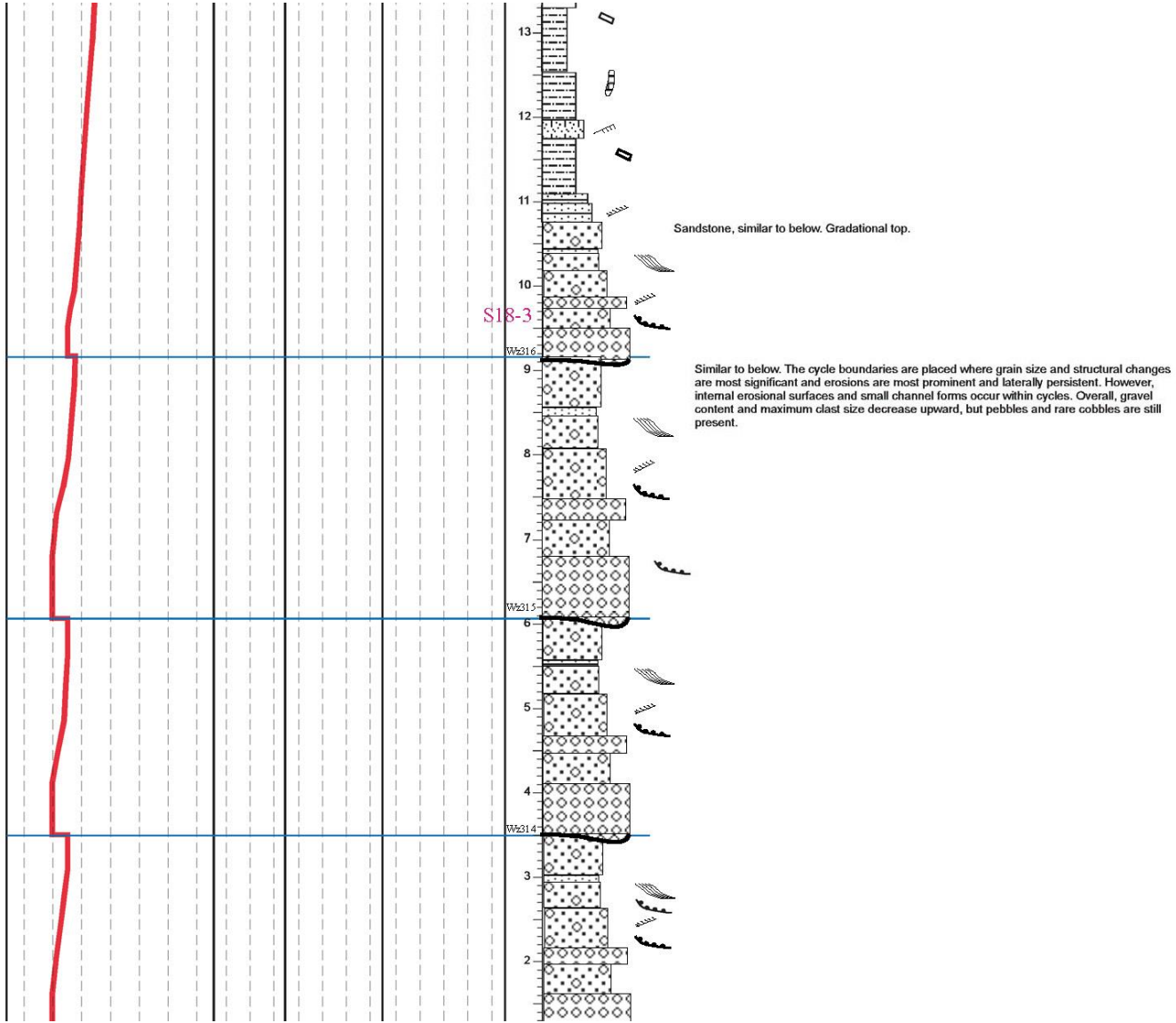


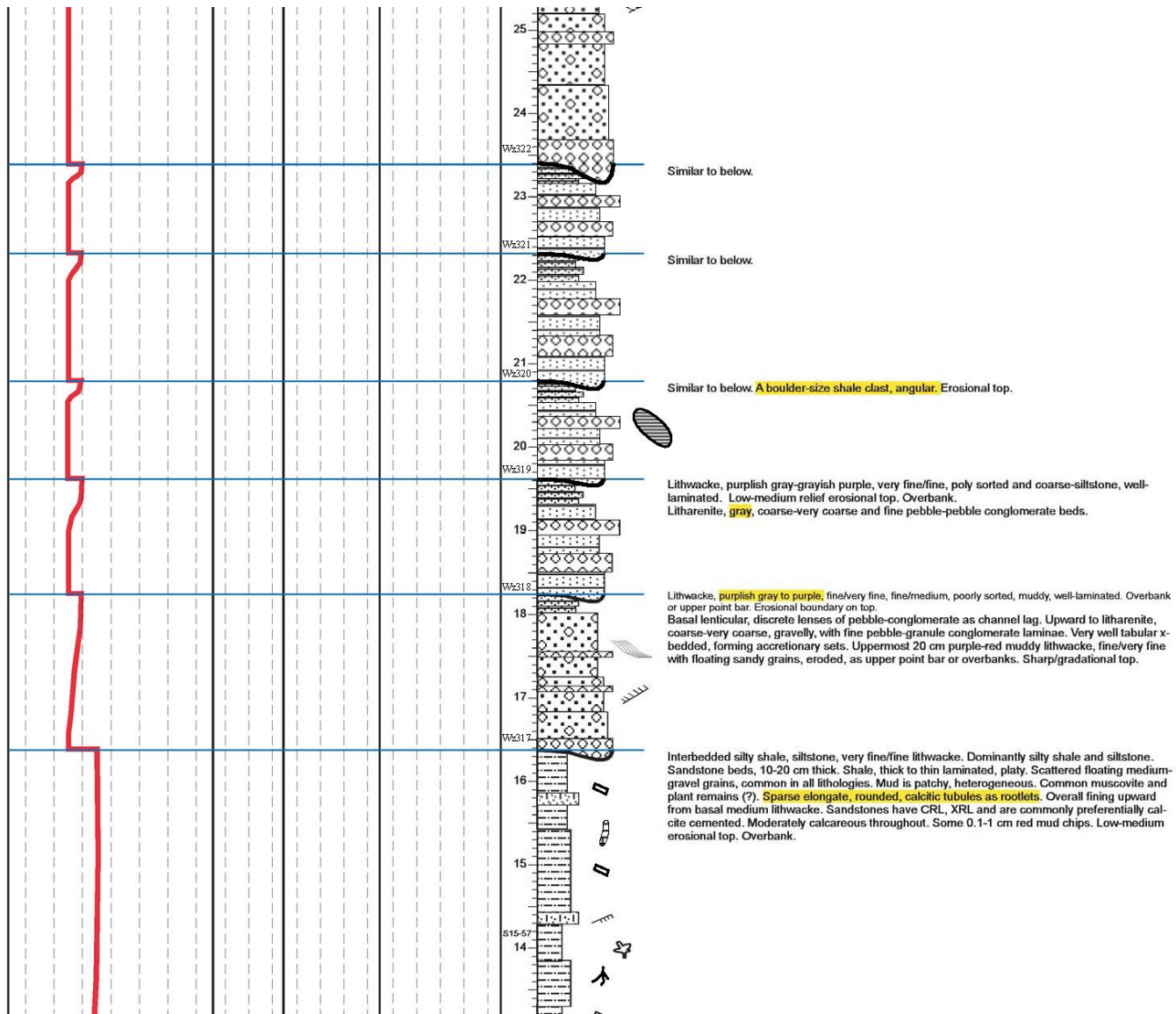


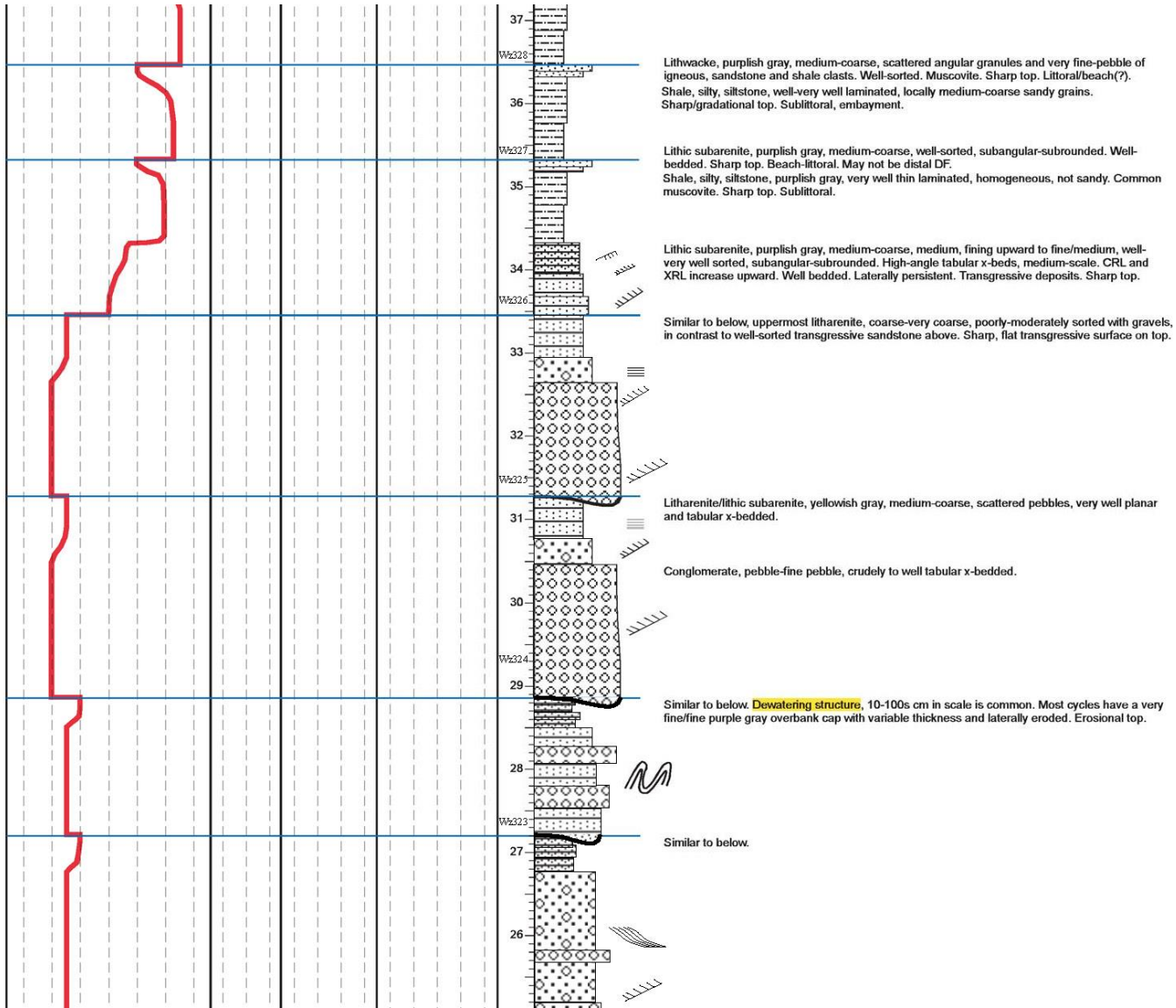


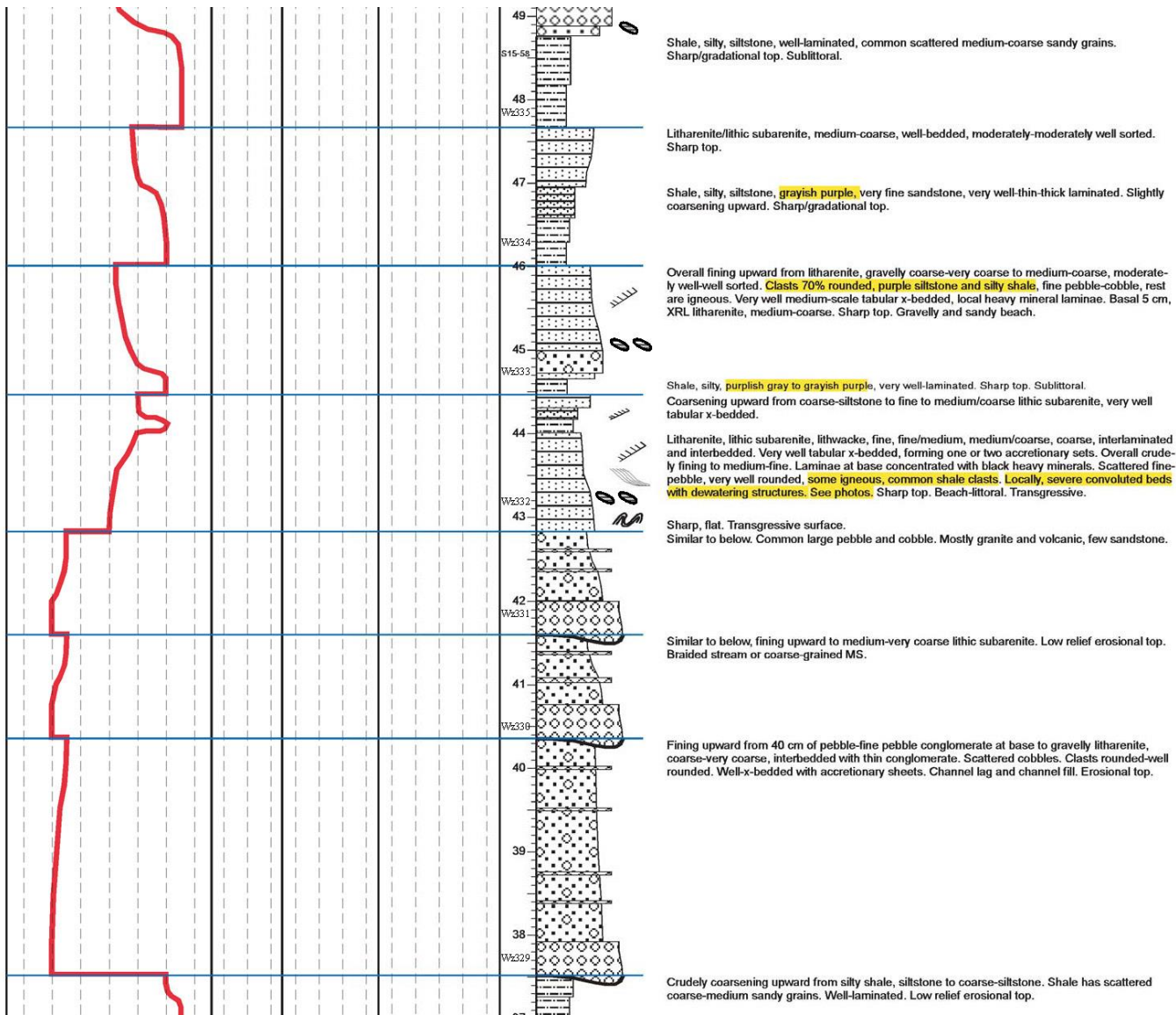
Fining upward from interbedded fine pebble-pebble conglomerate and litharenite/lithic subarenite, coarse-very coarse to less gravels and conglomerate lenses, rare medium, medium/coarse beds. Sets of large-scale tabular x-beds and accretionary sets. Gravels throughout, imbricated, decrease upward in amount and size. Common internal erosional surfaces. **No shale clast.** Low-middle relief erosional top.

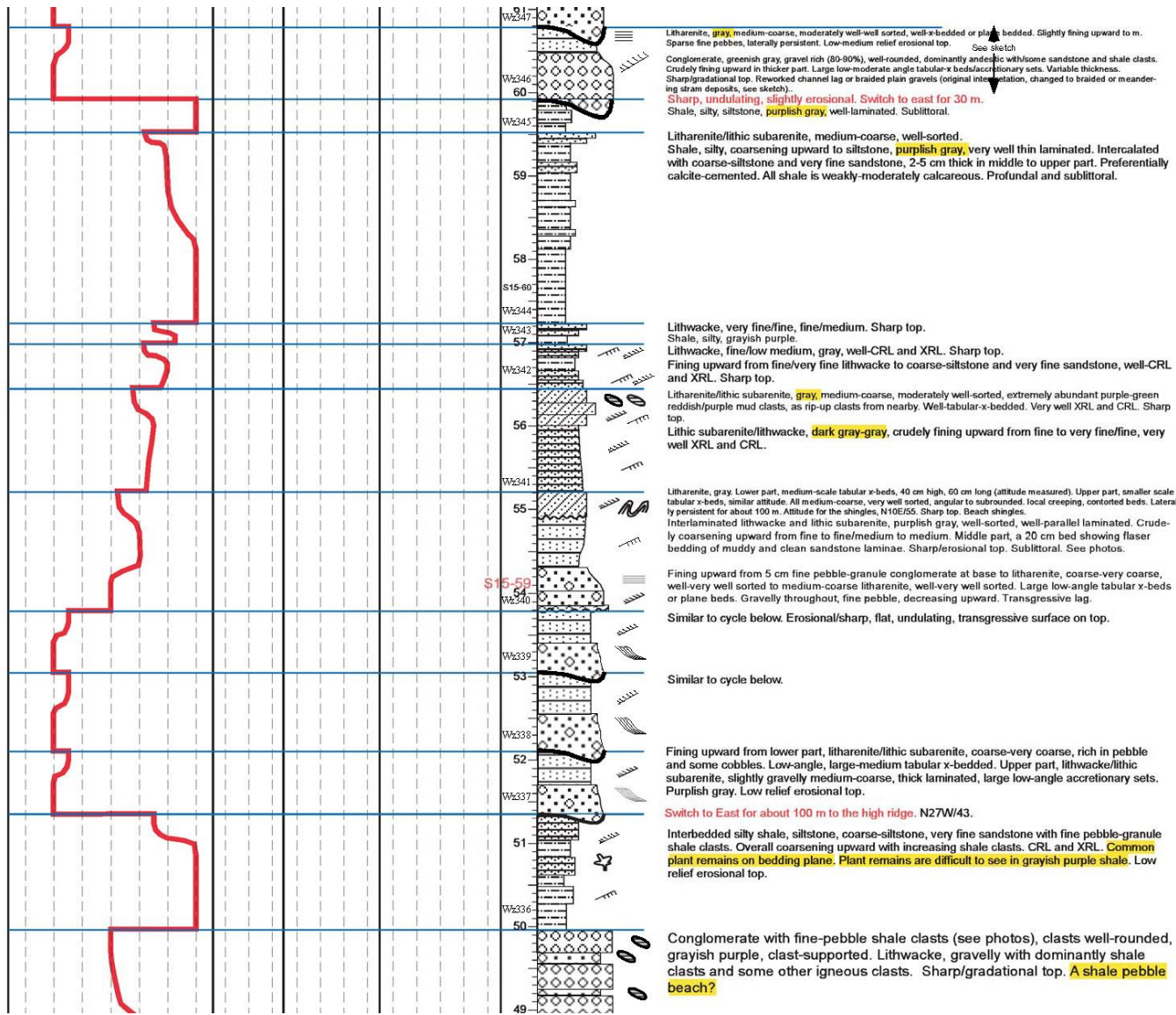
Litharenite/lithic subarenite, gray, coarse-very coarse, granular and common pebble-fine pebble. Well-cross-stratified. Common internal erosional surfaces between large-scale x-bedding sets and accretionary sets. Overall, crudely fining upward, less gravels and smaller clasts, medium-coarse lithic subarenite beds at top part. Fining upward with underlying conglomerate. Low-medium relief erosional top.

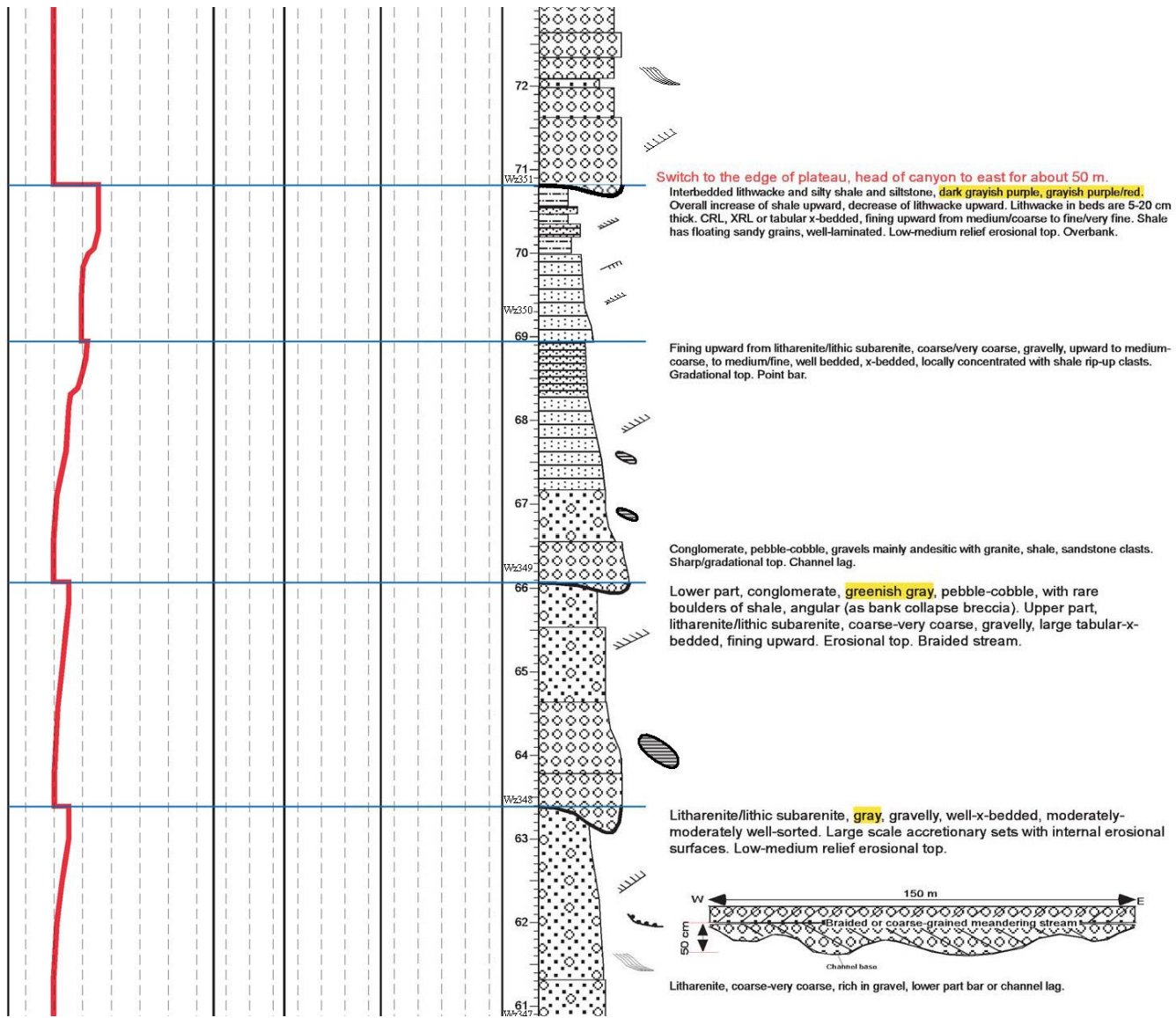


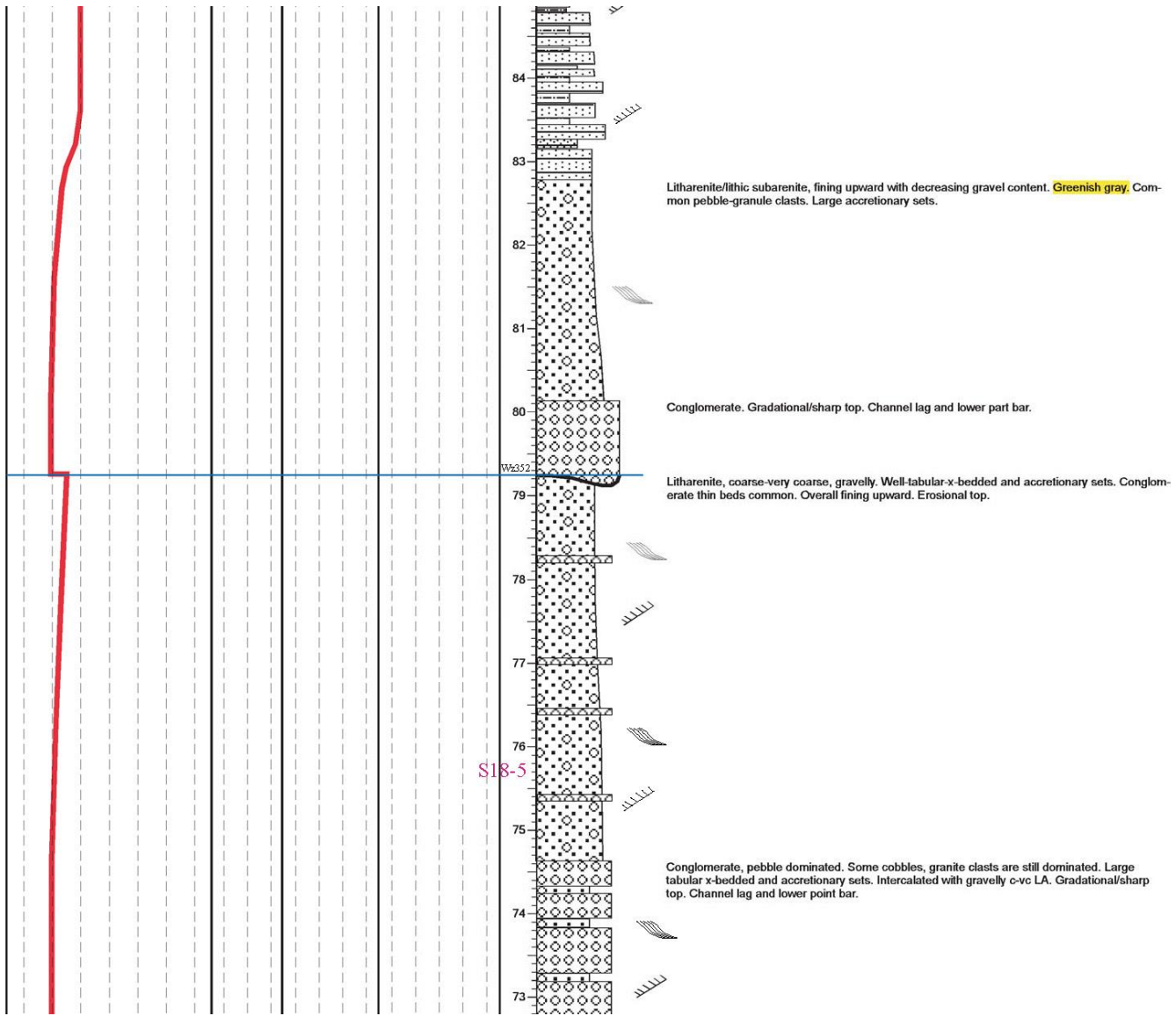


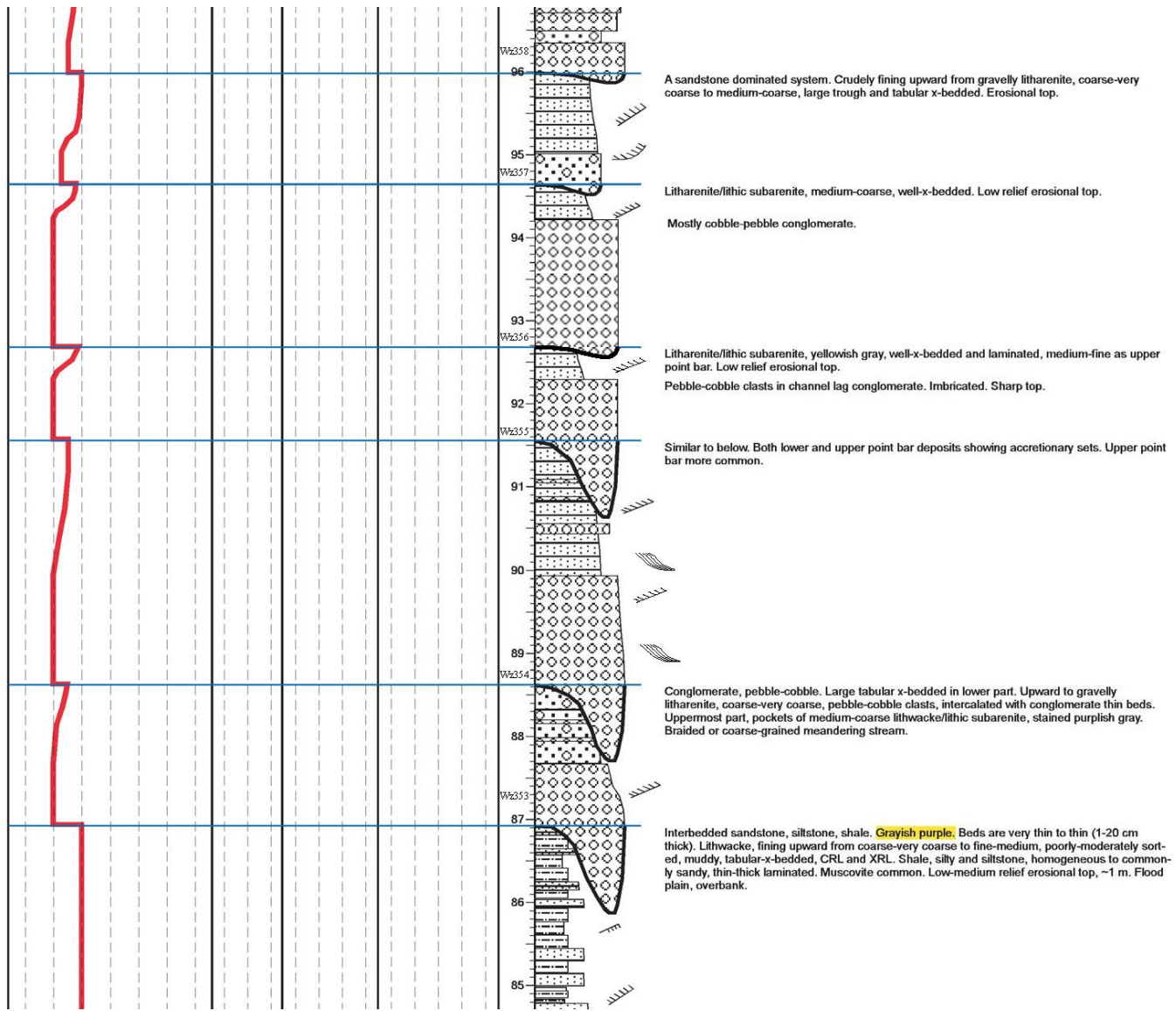


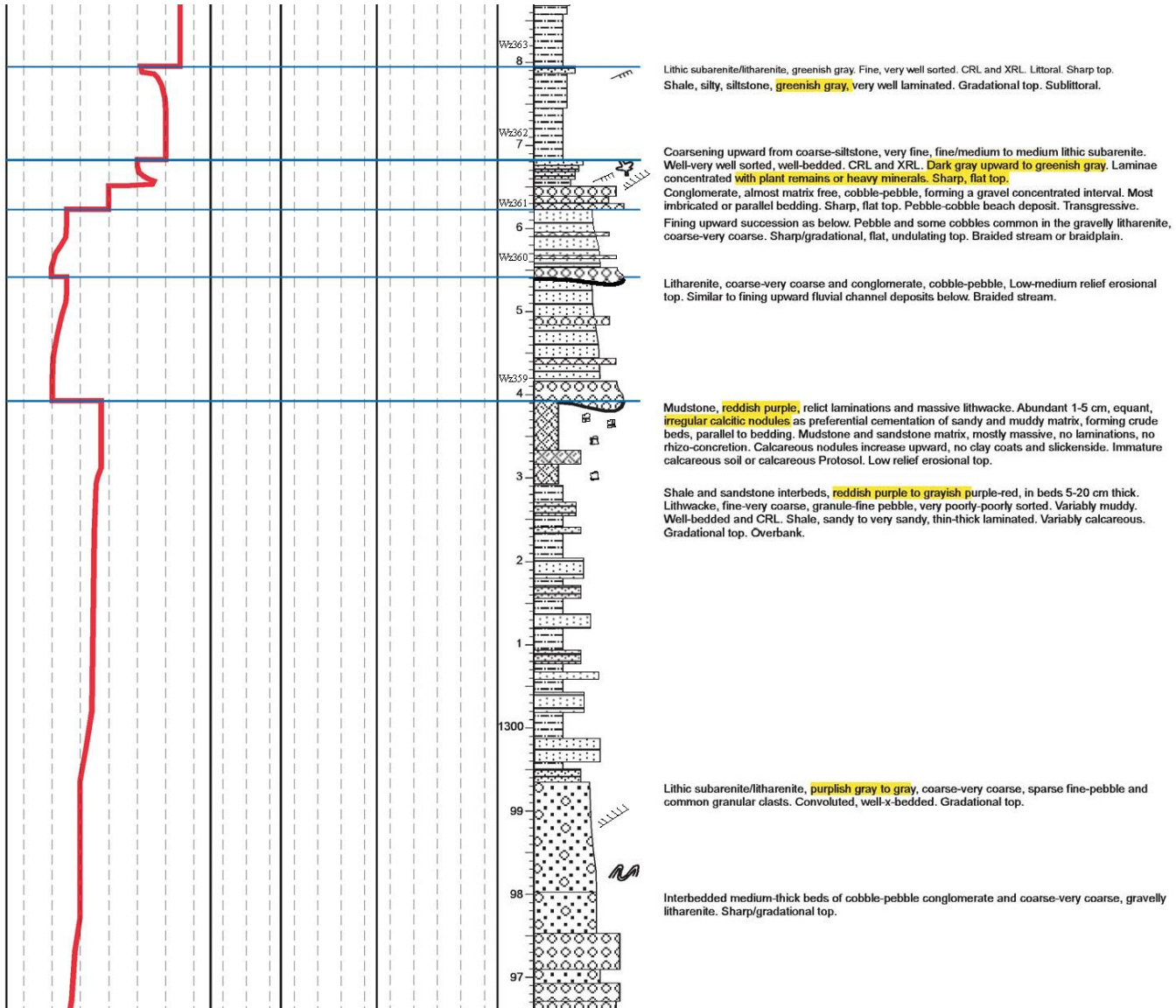


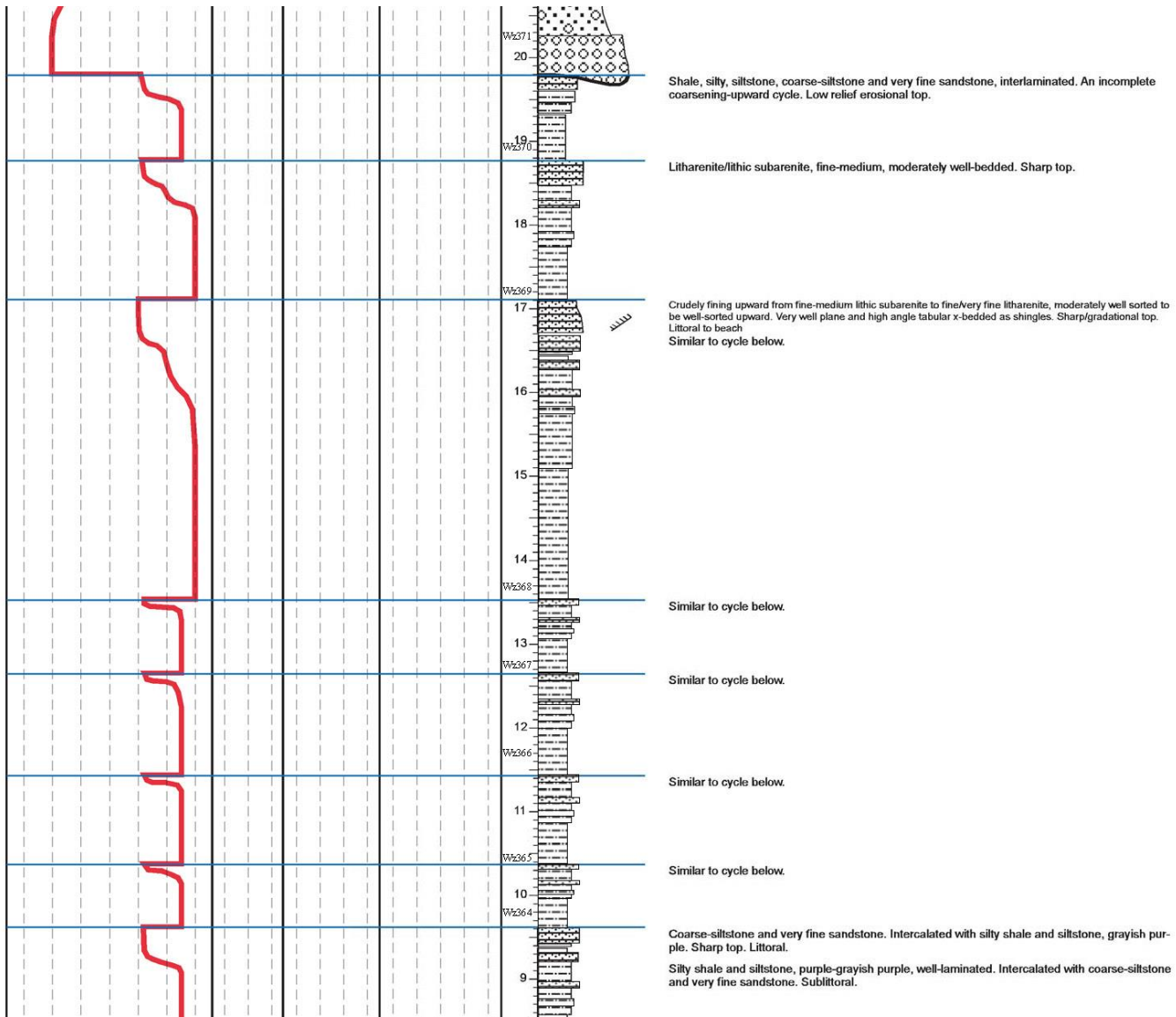


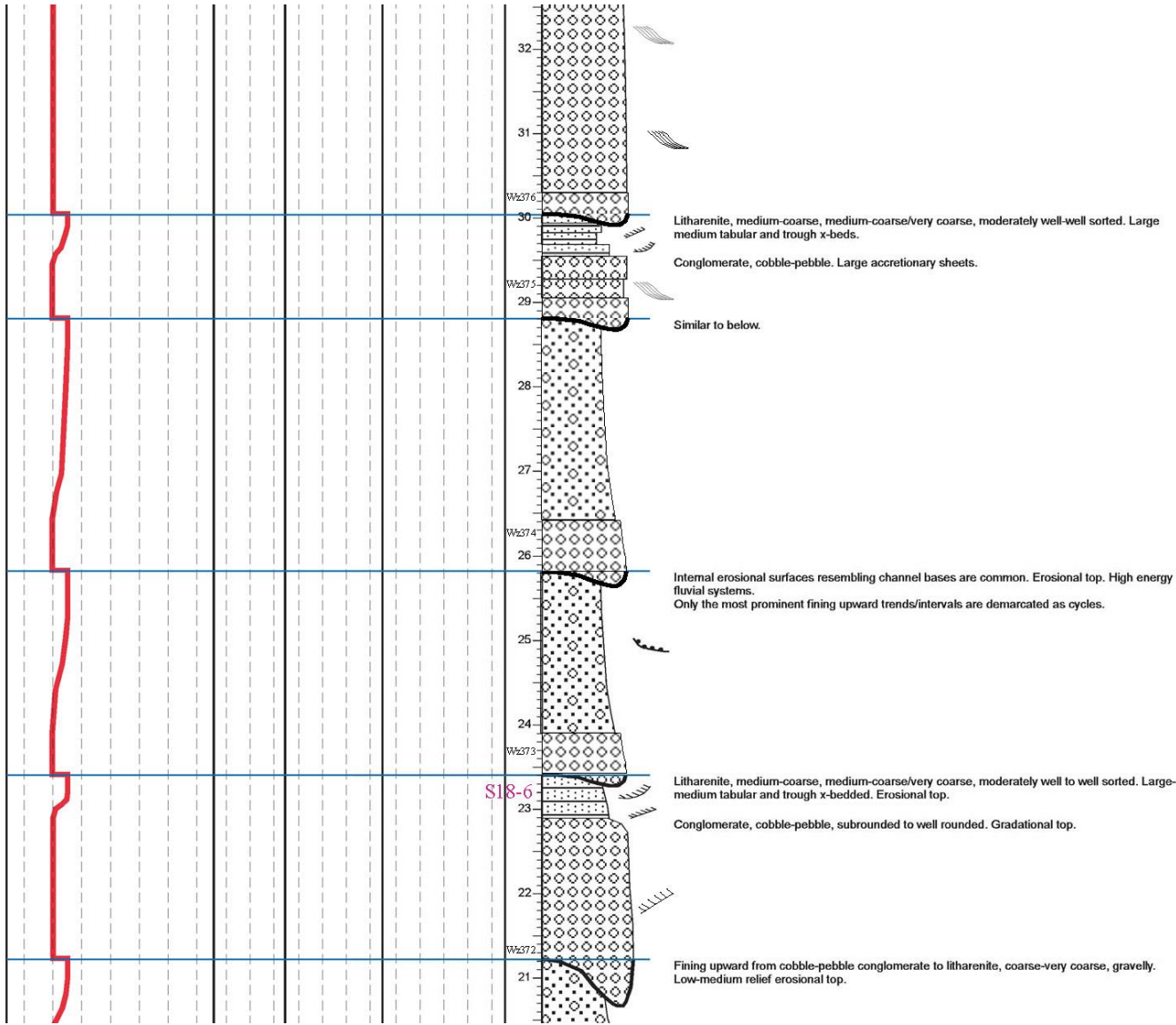


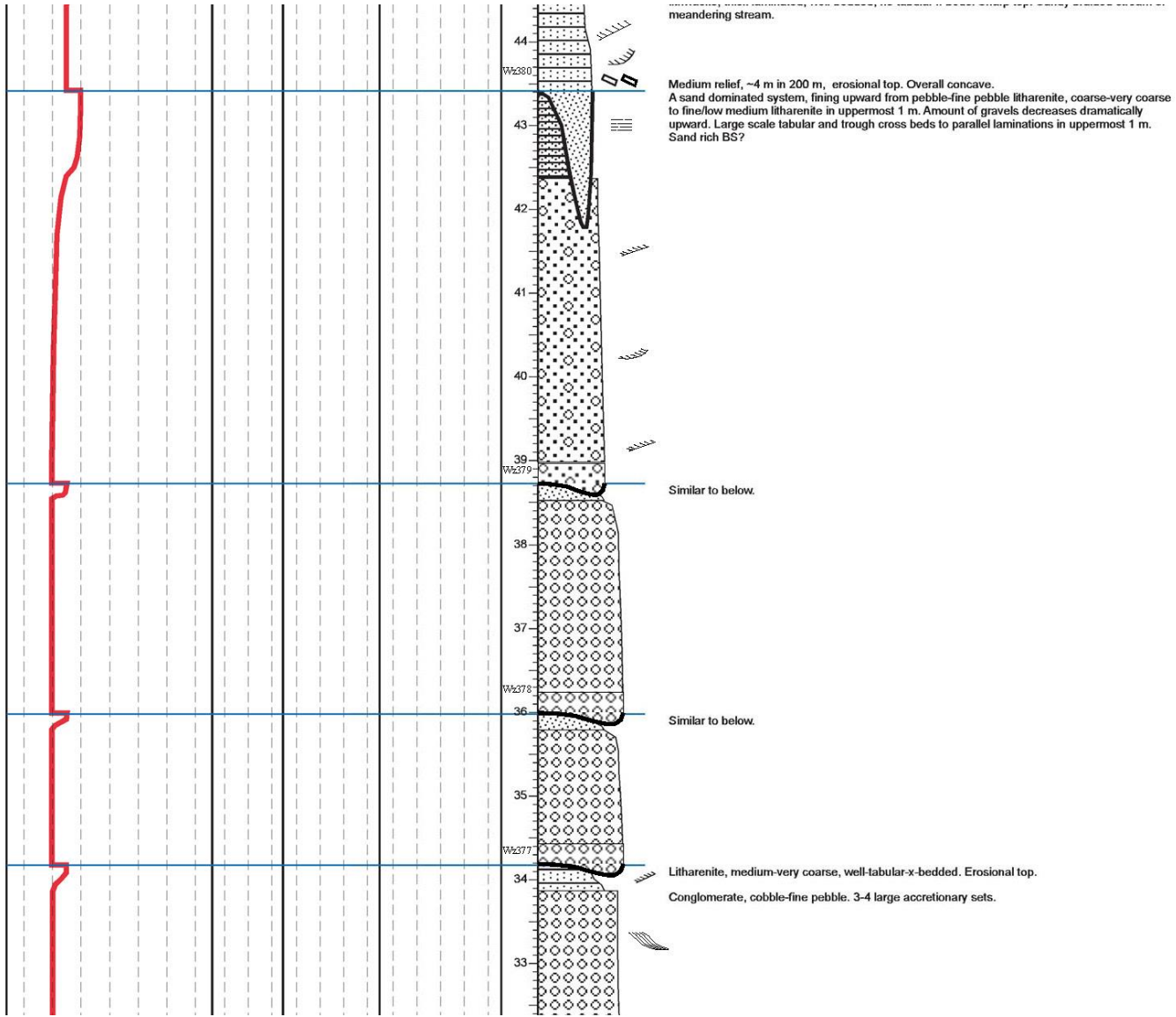


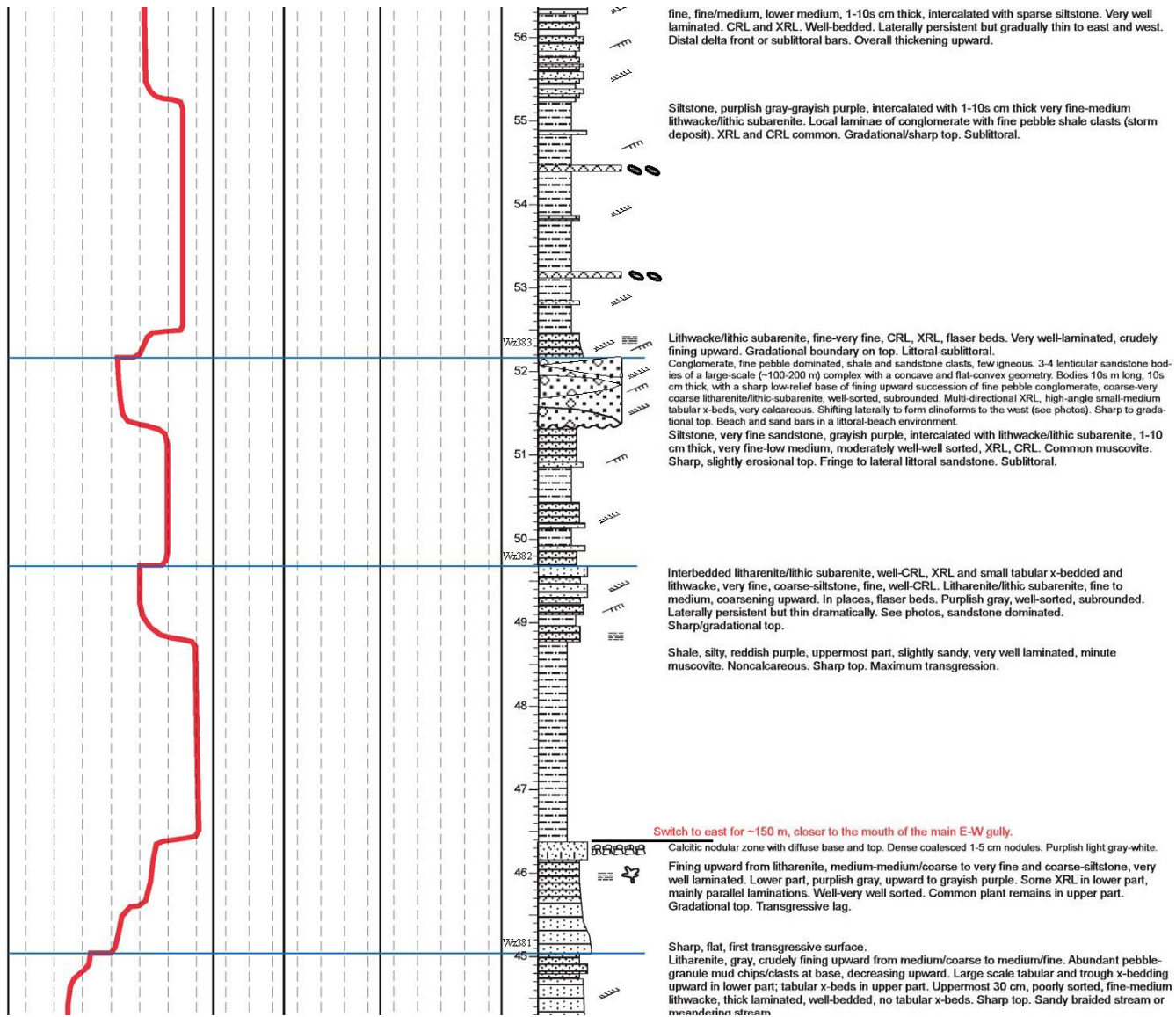


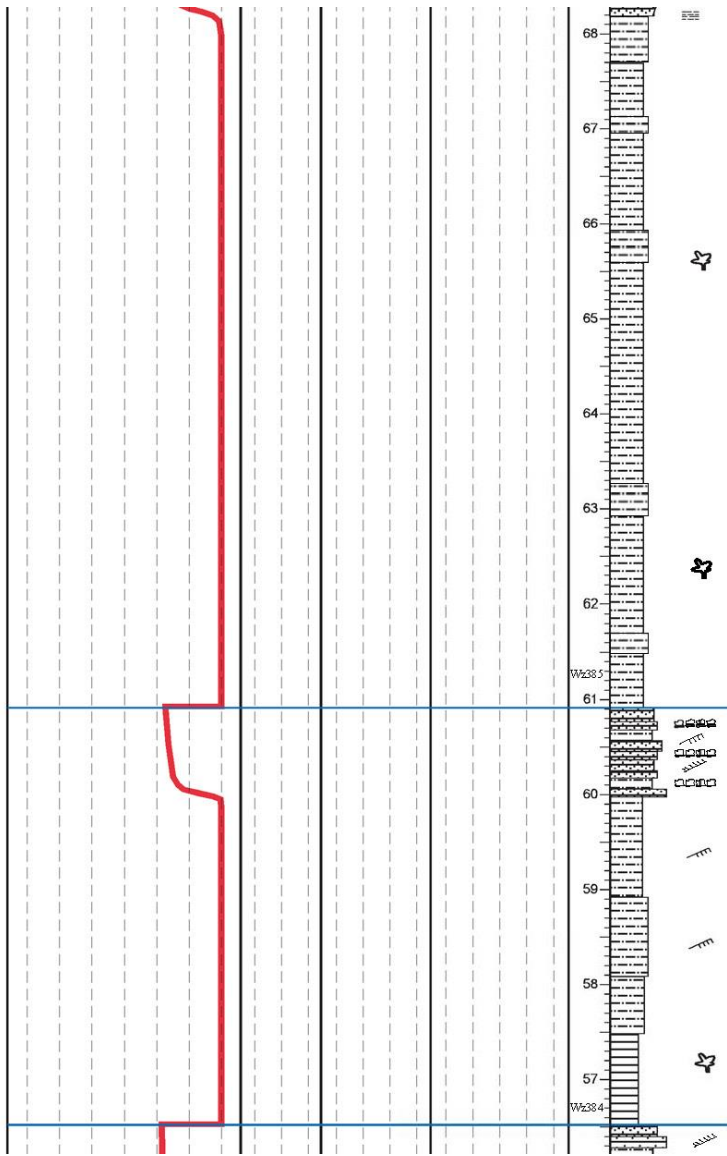










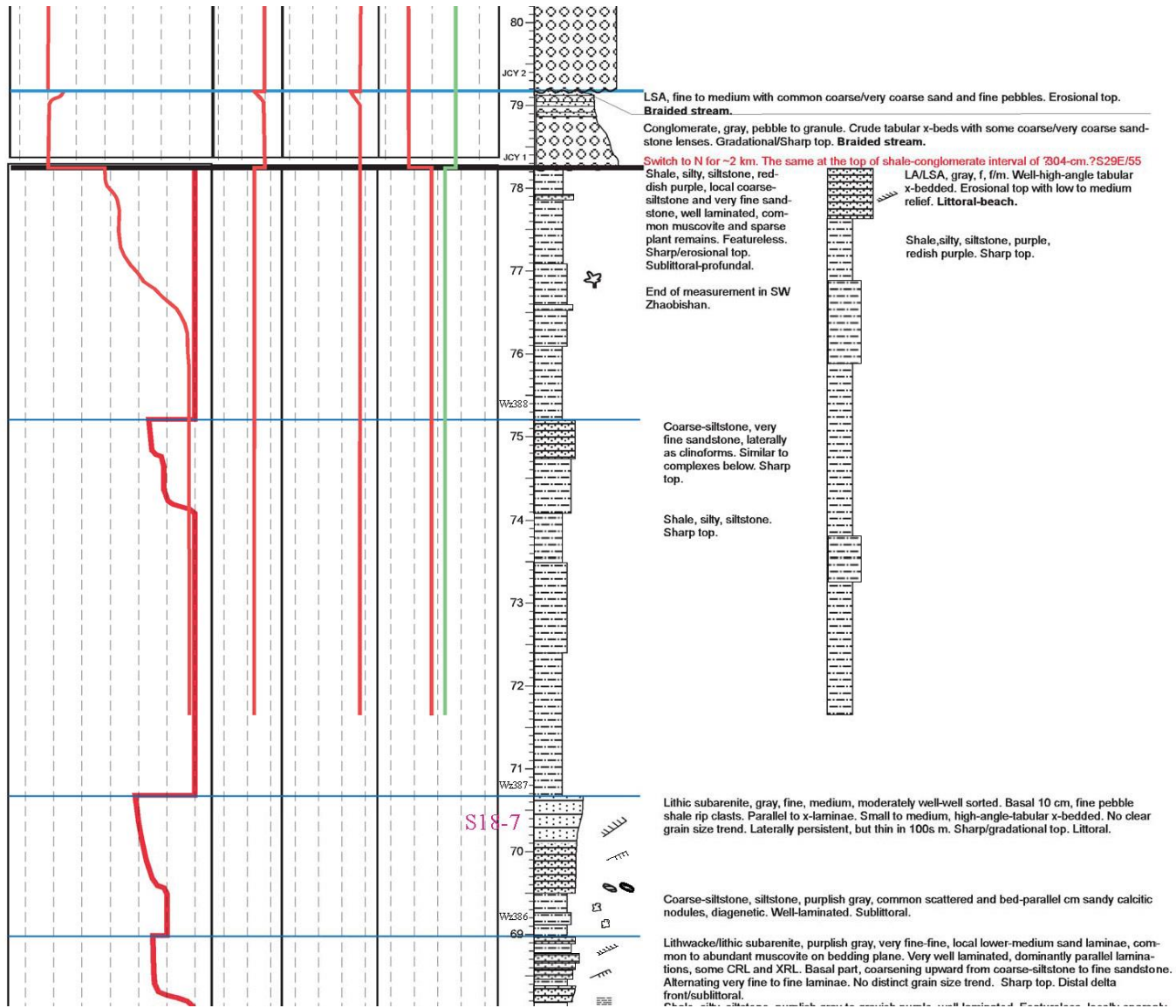


IRON/SUBIRON
 Shale, silty, siltstone, purplish gray to grayish purple, well-laminated. Featureless, locally sparsely sandy, common muscovite, scattered sparse plant remains. Uppermost part, siltstone. Gradational top. Profundal.

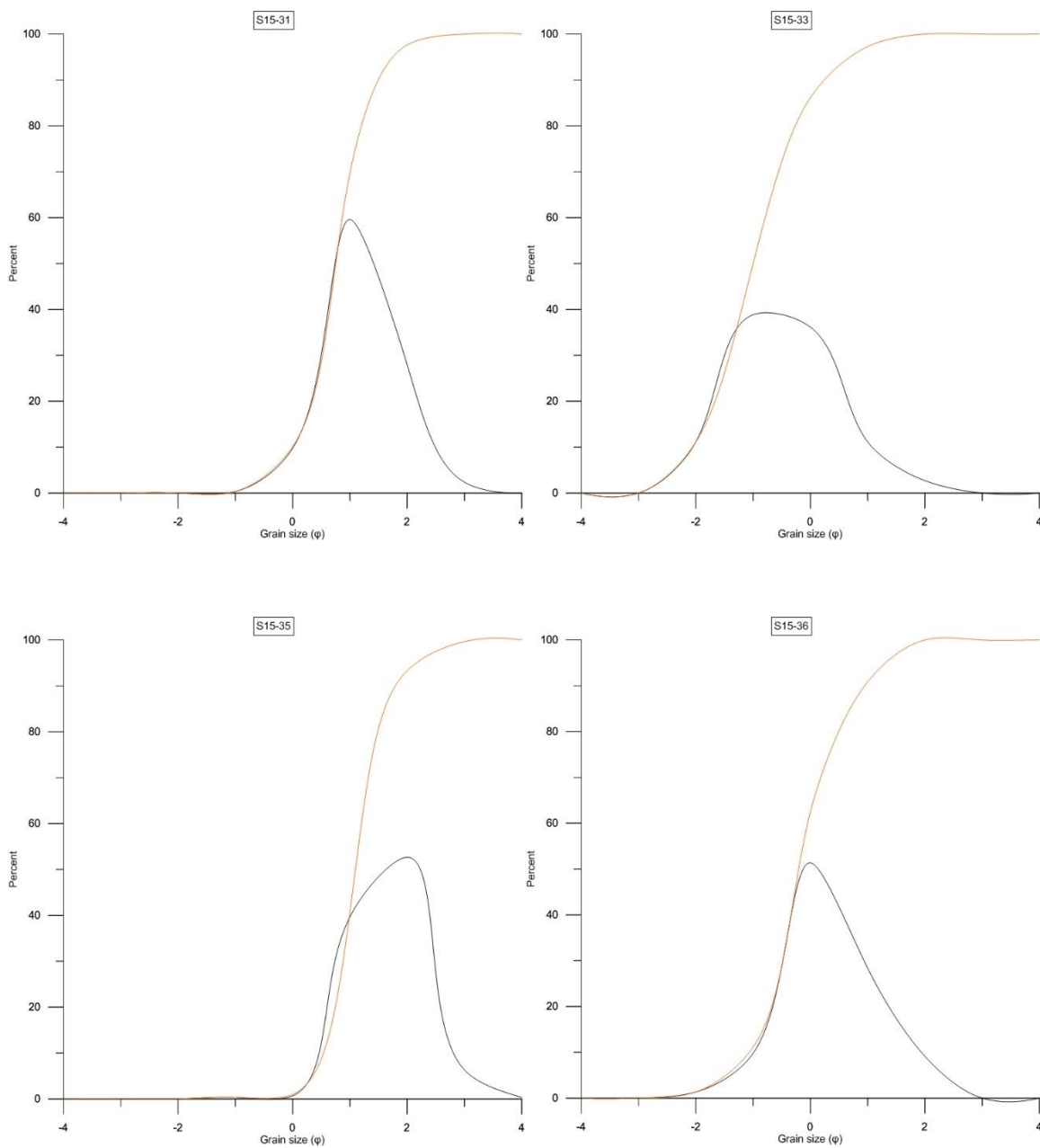
Interbedded thin very fine sandstone and coarse-siltstone and fine lithic subarenite/lithwacke thin beds. Grayish purple, well-thin bedded, CRL and XRL. Laterally persistent. 3-4, 1-5 cm thick calcitic nodular zones, composed of coalesced cm-size sandy nodules, as diagenetic cemented beds. Some scattered calcitic nodules, resembling coprolites. Distal bar or delta front.

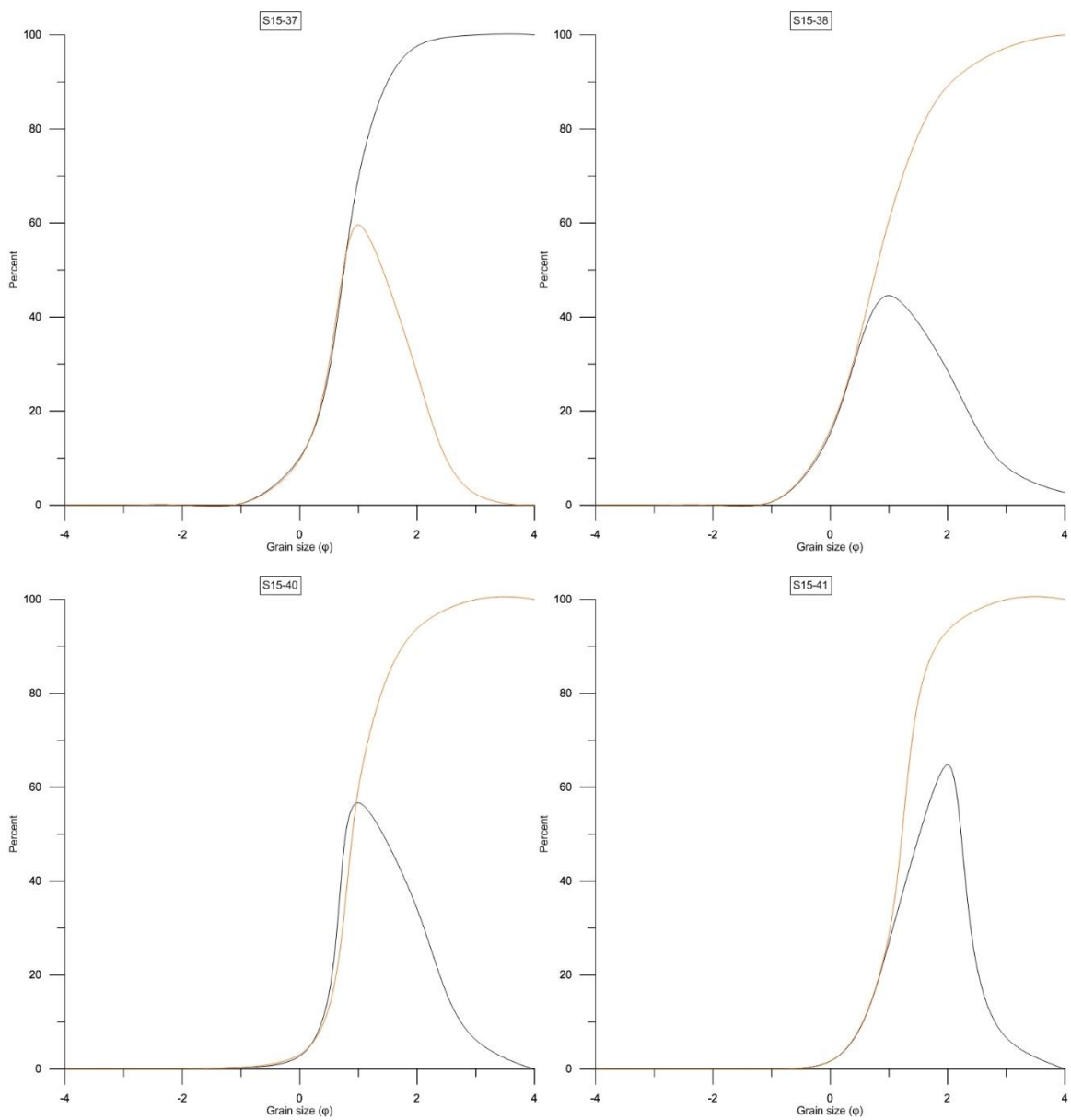
Shale, silty, siltstone, grayish-purple brown, pure to silty, common muscovite, sparse plant remains. Very well laminated, thin to medium, CRL in places. Sharp/gradational top. Sublittoral to profundal.

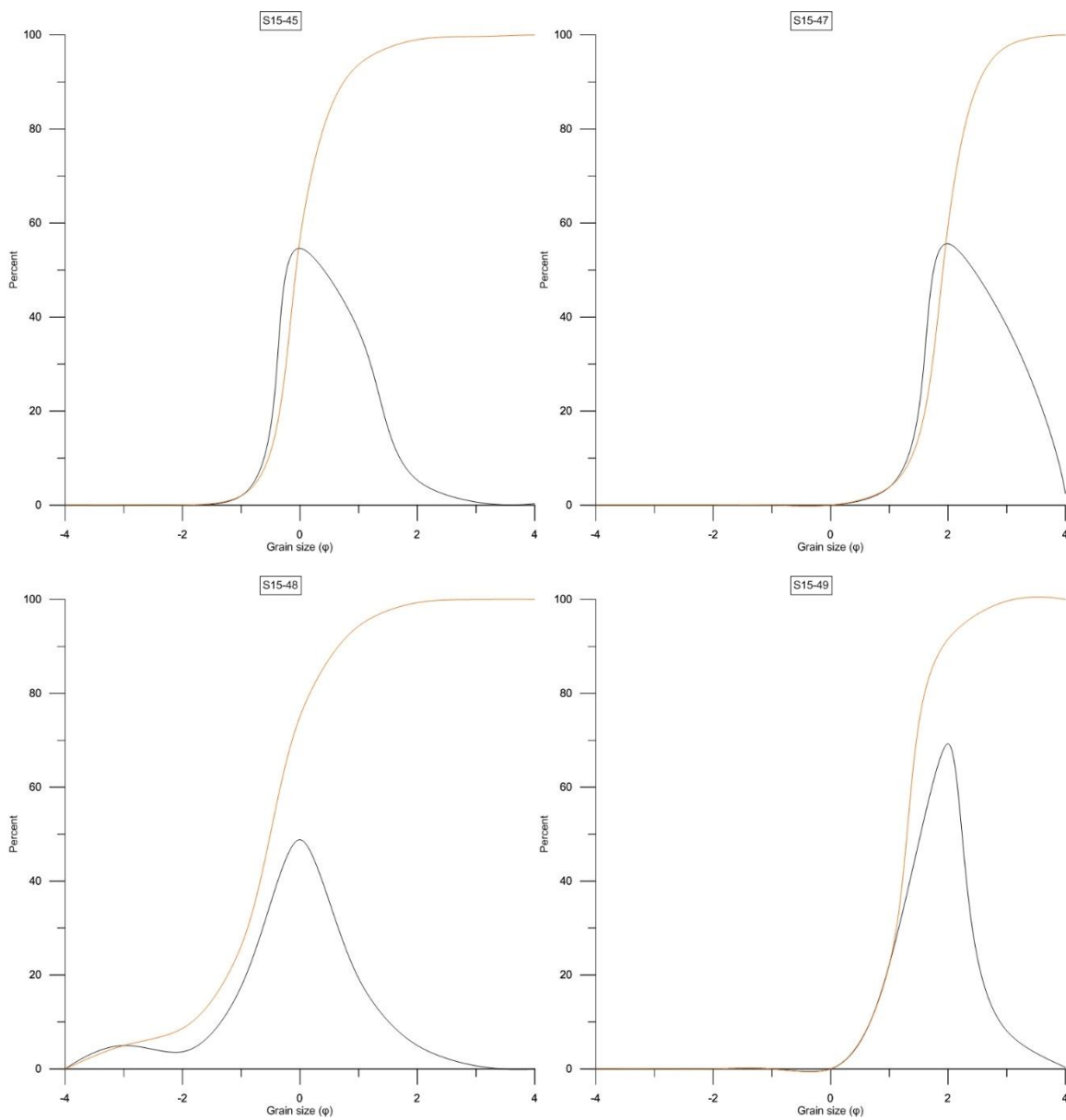
Interbedded coarse-siltstone and very fine sandstone and lithwacke/lithic subarenite/litharenite, fine, fine/medium, lower medium, 1-10s cm thick, intercalated with sparse siltstone. Very well

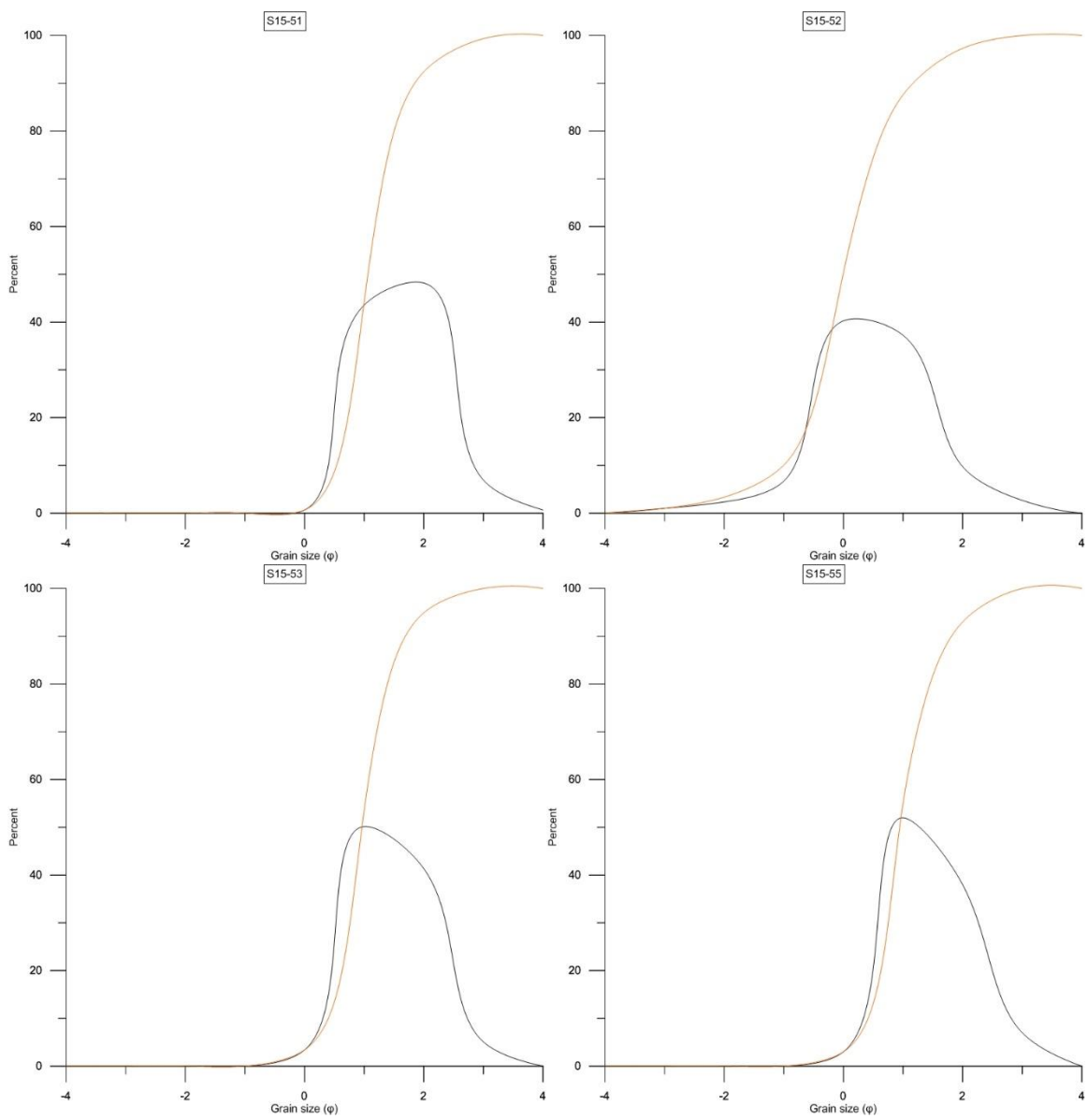


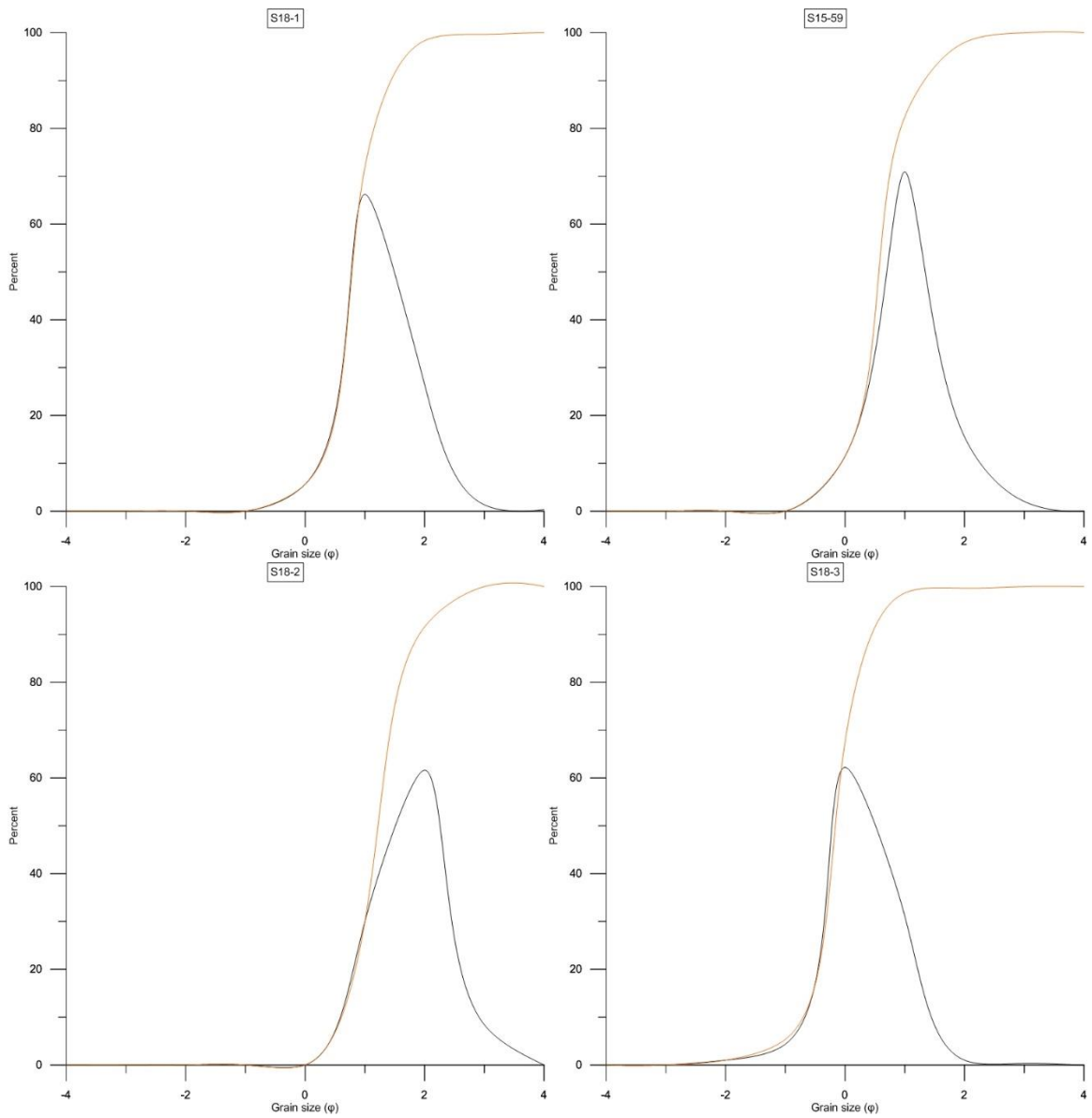
APPENDIX B.
GRAIN SIZE DISTRIBUTION

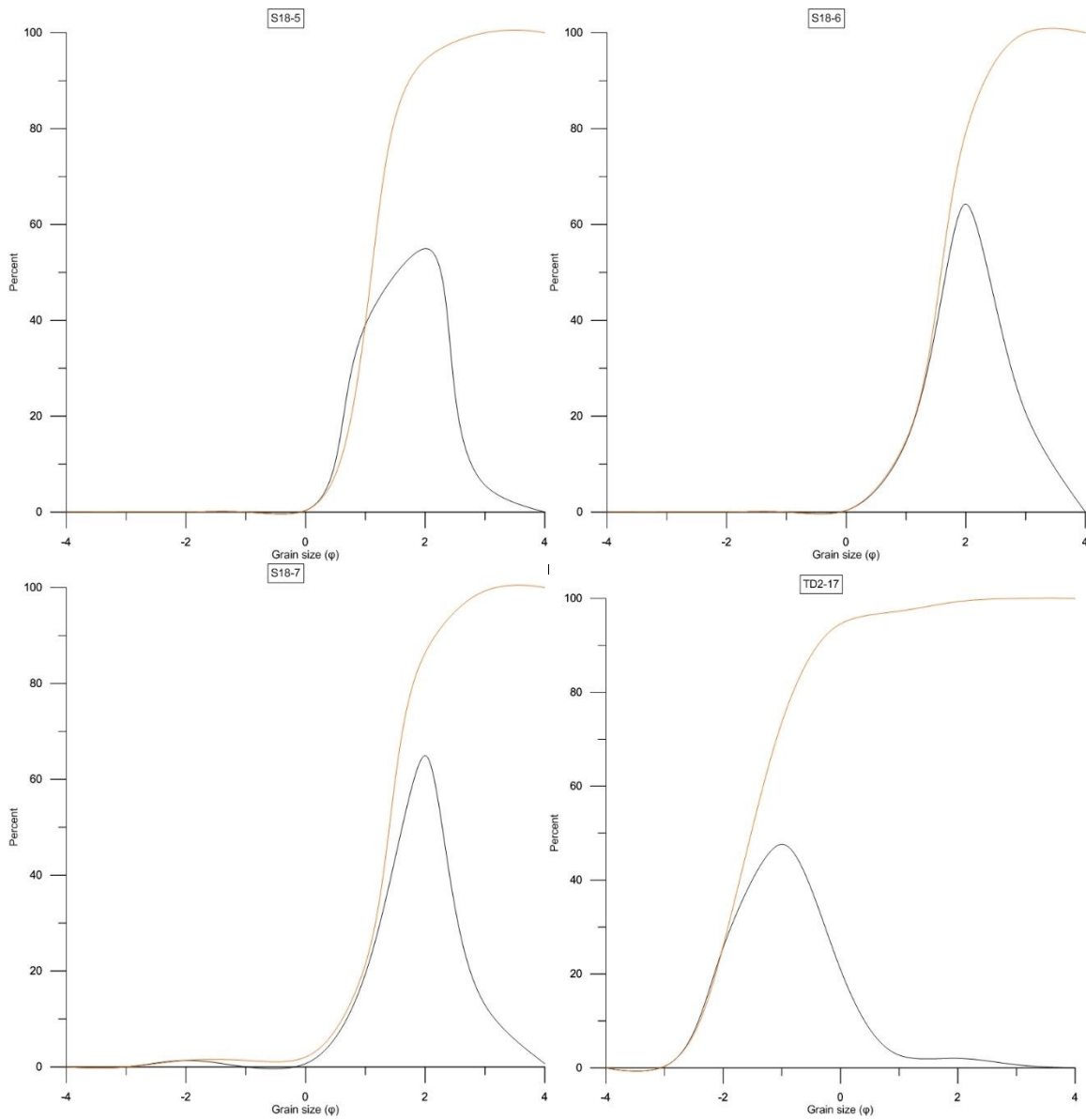


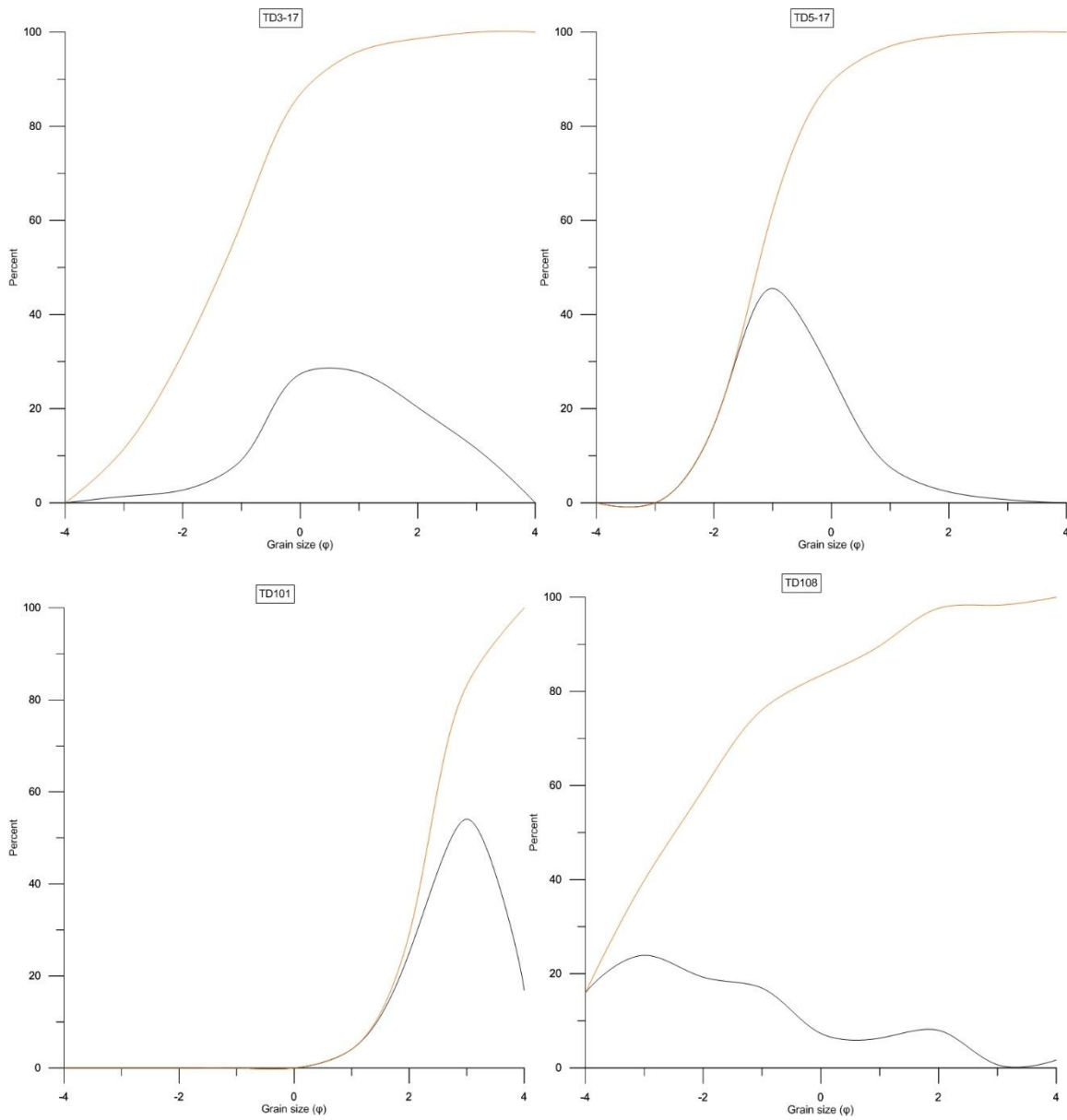


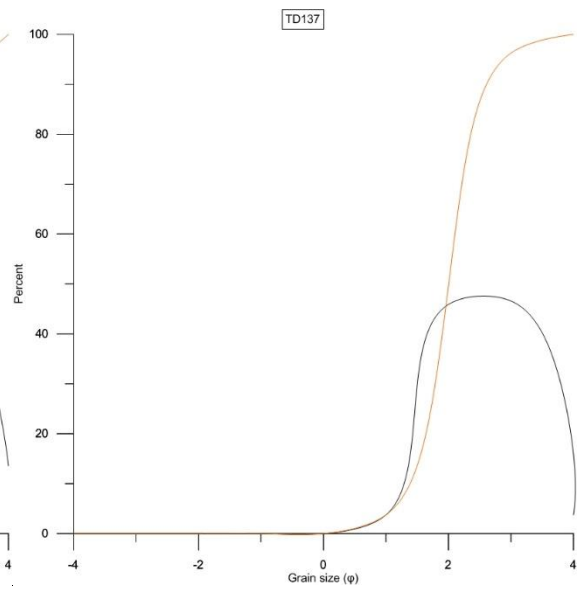
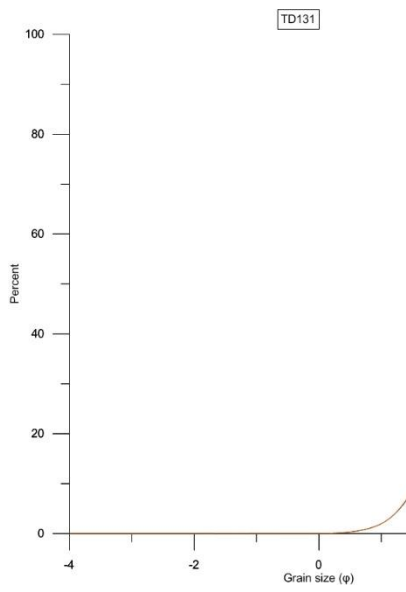
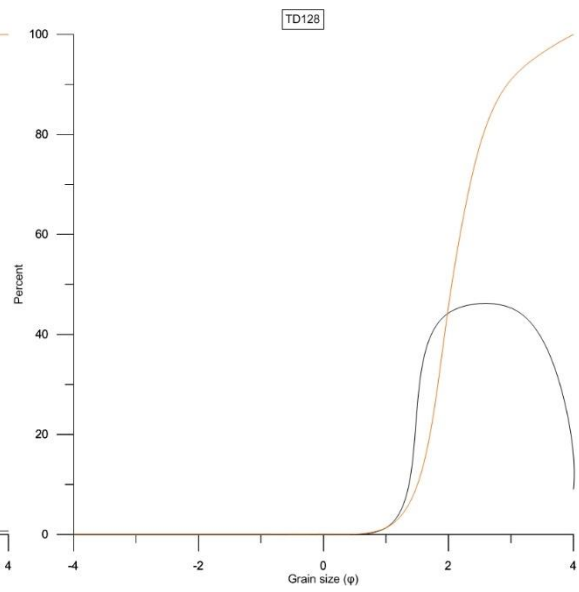
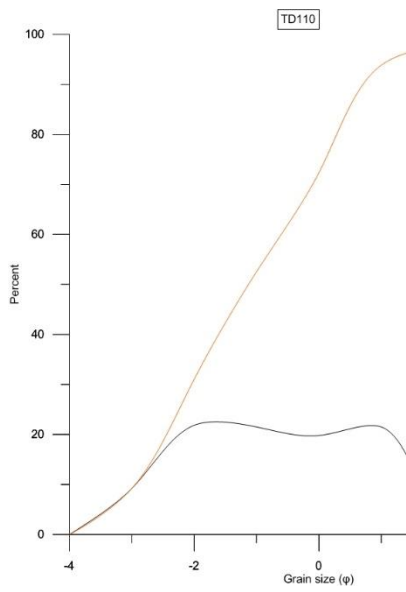


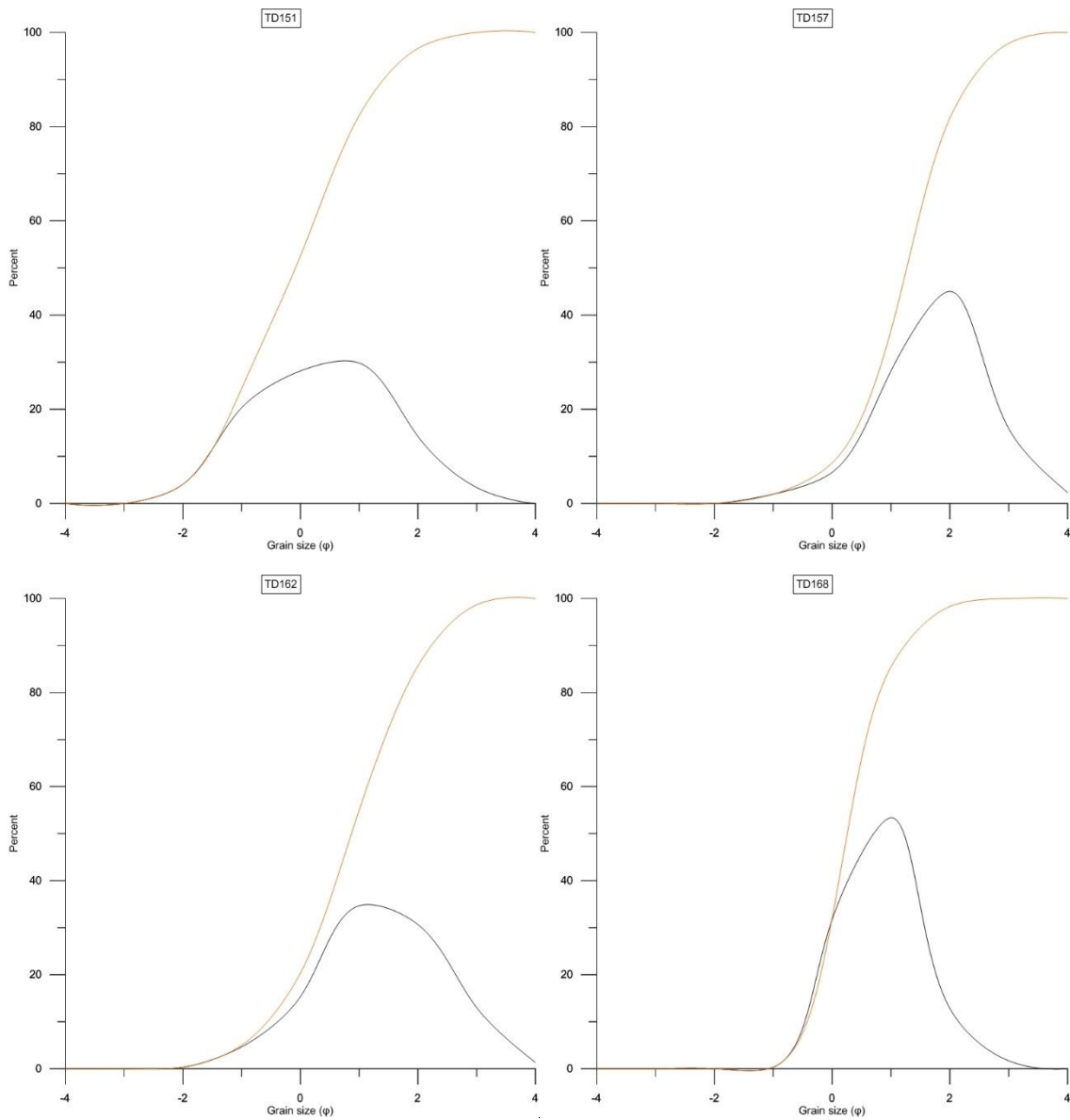


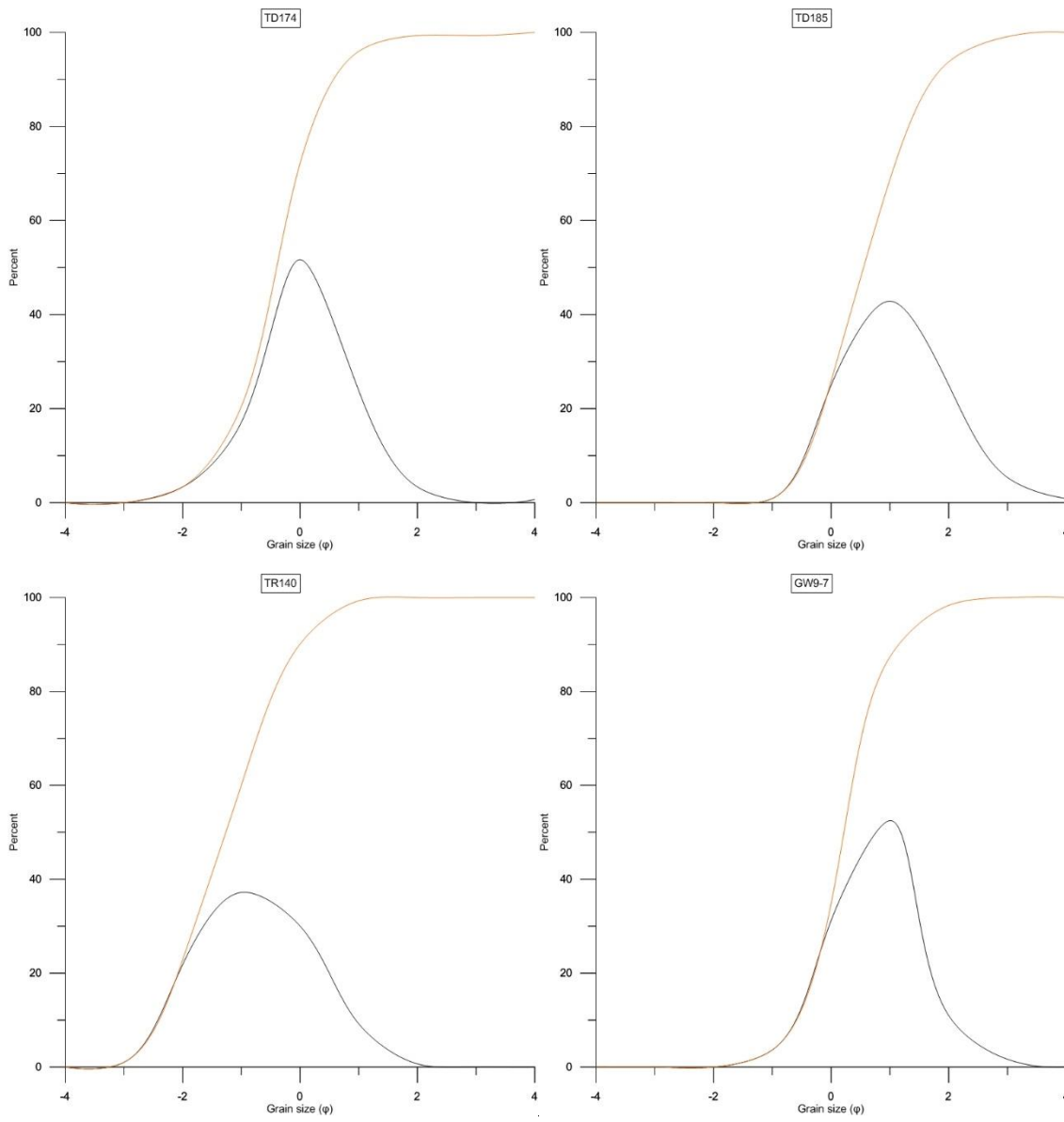


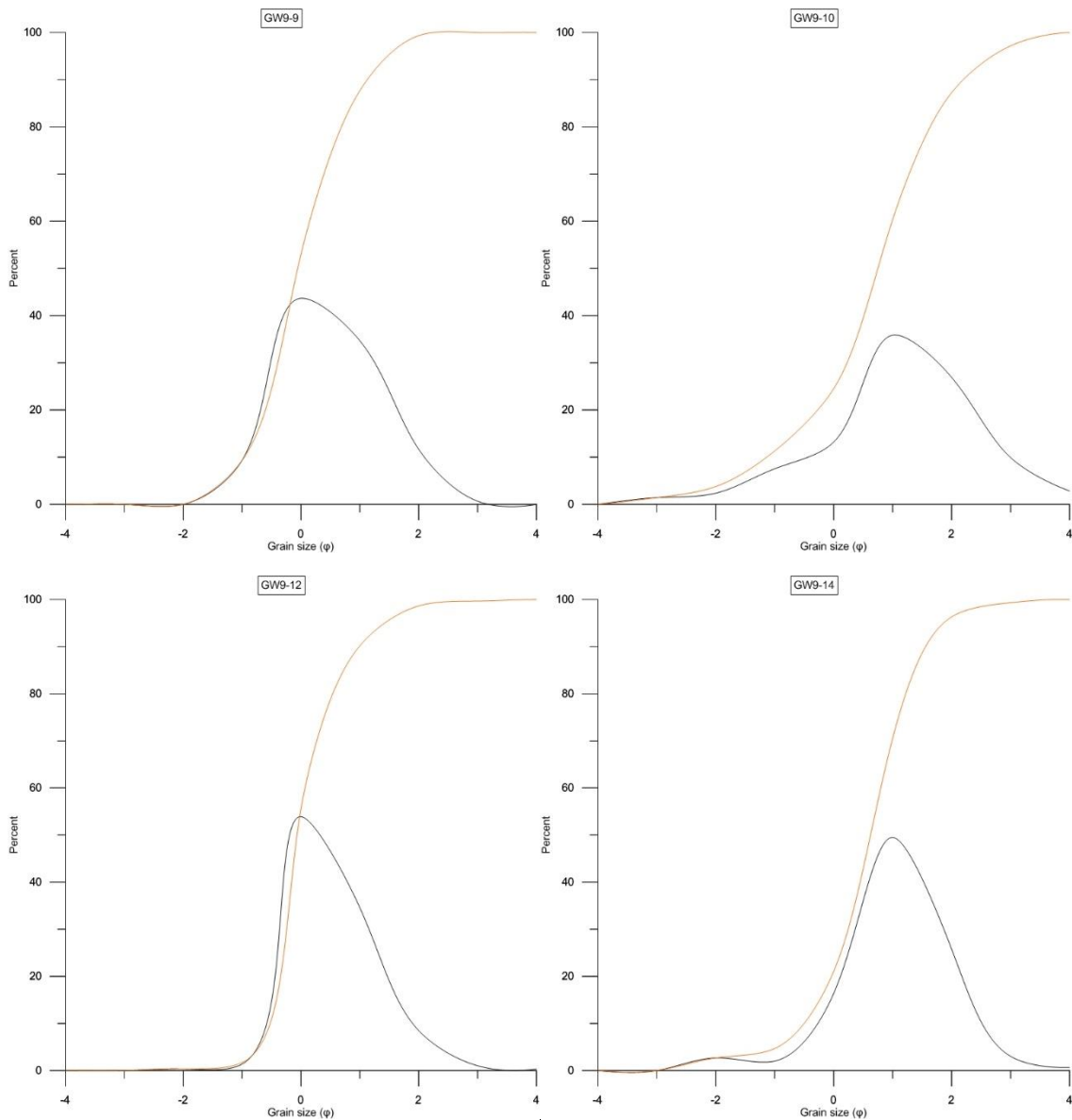


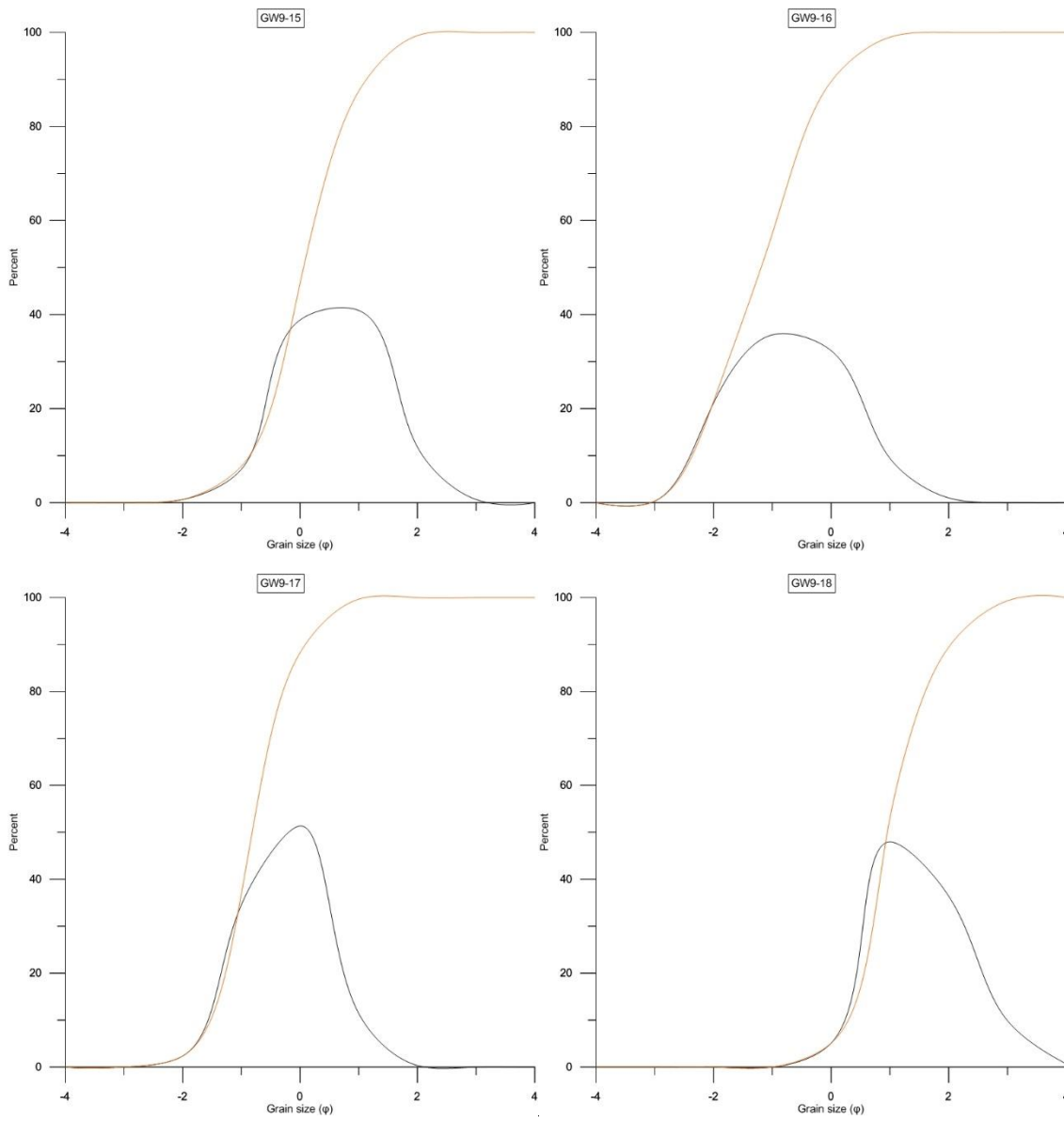


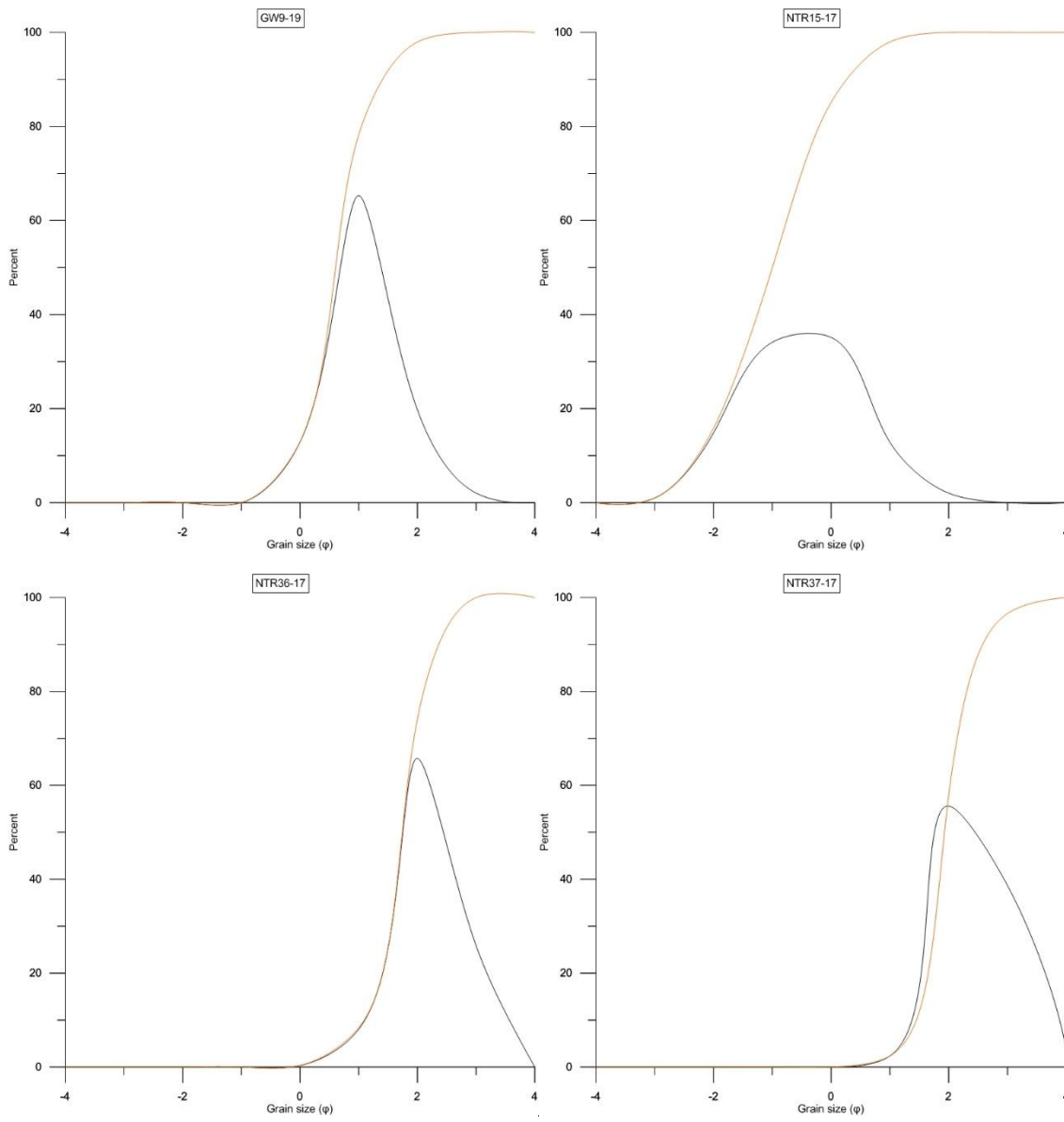


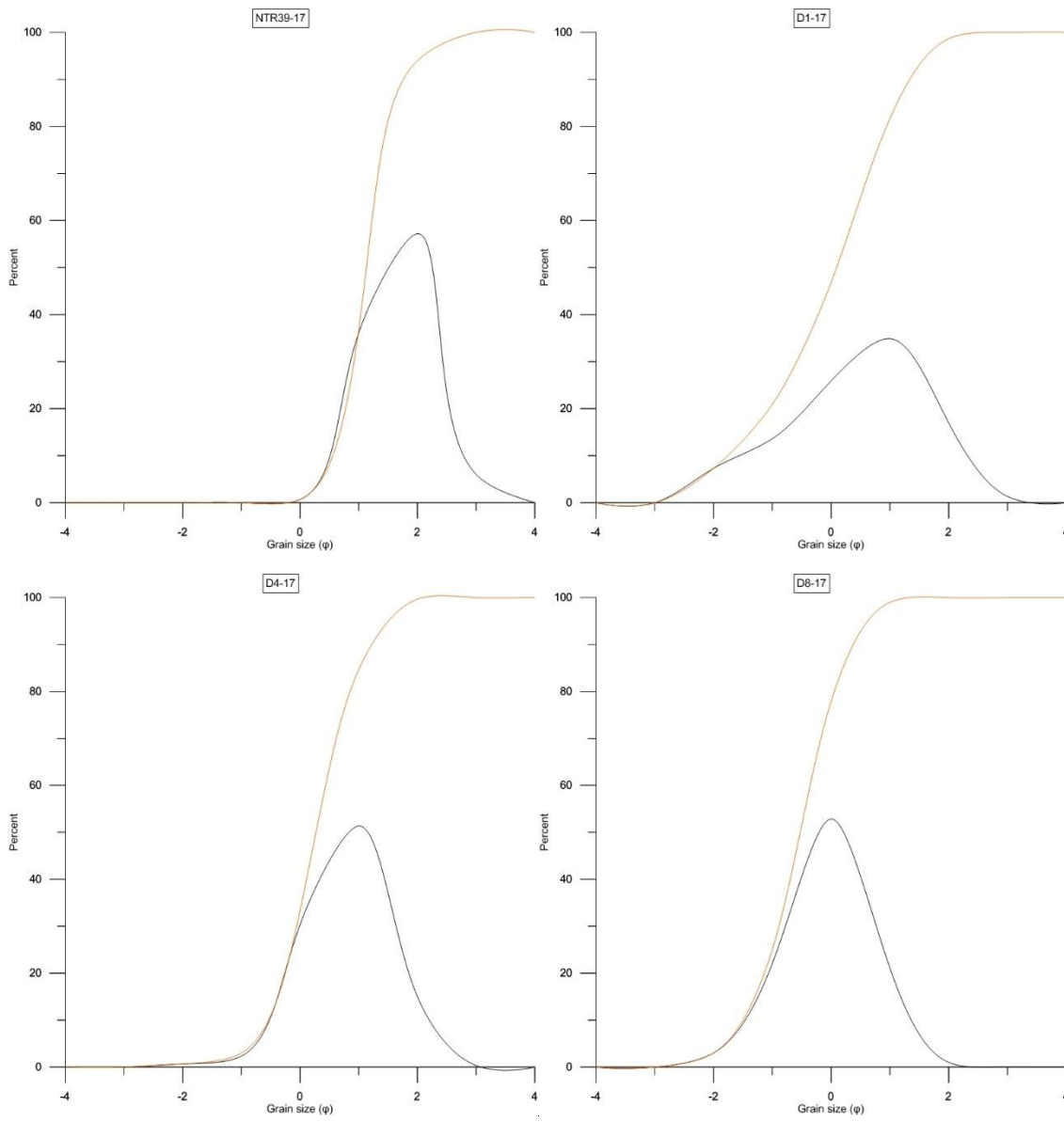


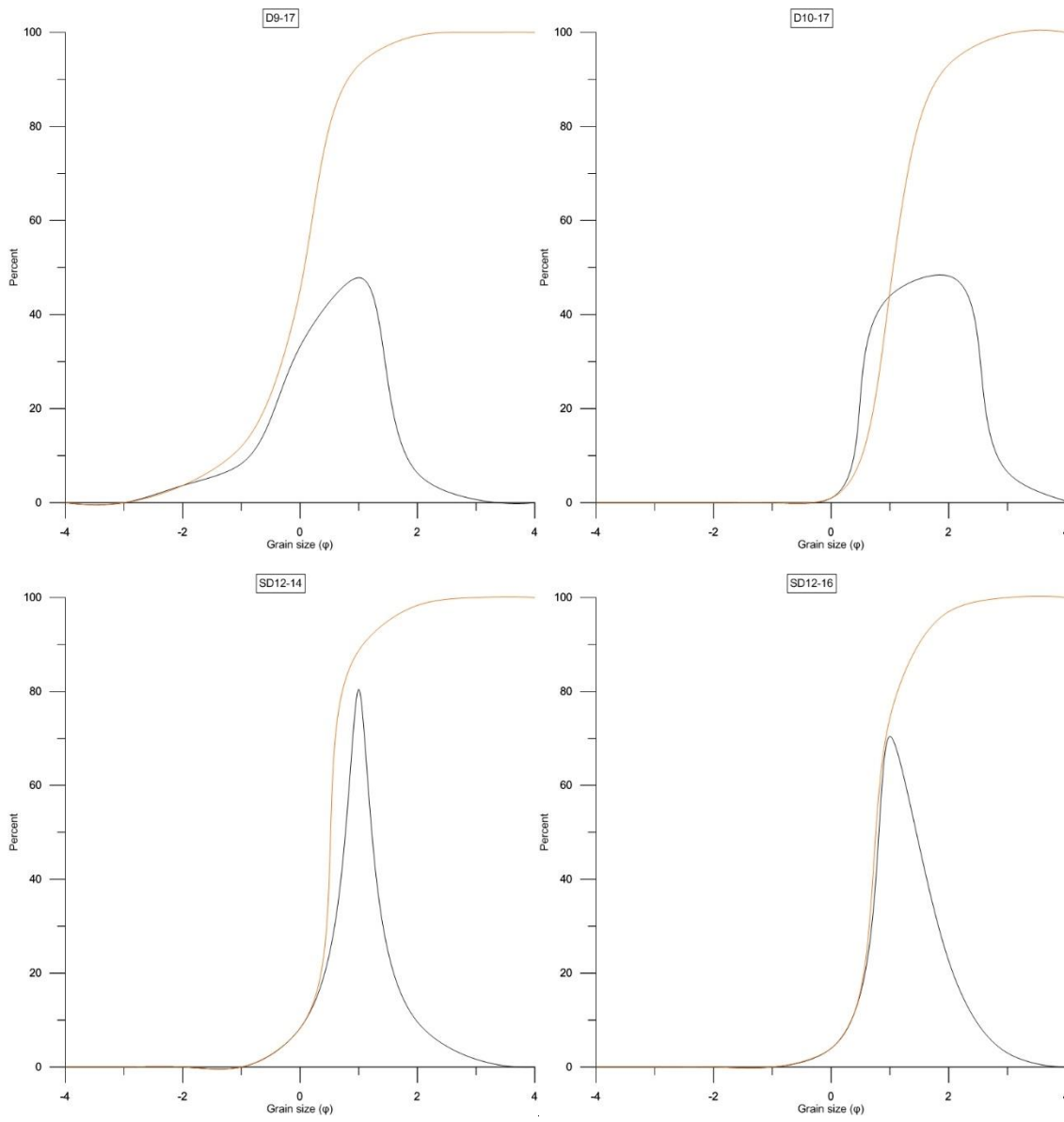












BIBLIOGRAPHY

- Allen, M. B., Windley, B. F., and Zhang, C., 1993, Palaeozoic collisional tectonics and magmatism of the Chinese Tien Shan, central Asia: *Tectonophysics*, v. 220, no. 1, p. 89-115.
- Carroll, A., Graham, S., Hendrix, M., Ying, D., and Zhou, D., 1995, Late Paleozoic tectonic amalgamation of northwestern China: sedimentary record of the northern Tarim, northwestern Turpan, and southern Junggar basins: *Geological Society of America Bulletin*, v. 107, no. 5, p. 571-594.
- Charvet, J., Shu, L., Laurent-Charvet, S., Wang, B., Faure, M., Cluzel, D., Chen, Y., and De Jong, K., 2011, Palaeozoic tectonic evolution of the Tianshan belt, NW China: *Science China Earth Sciences*, v. 54, no. 2, p. 166-184.
- Ehrlich, R., 1983, Size analysis wears no clothes, or have movements come and gone?: *Journal of Sedimentary Research*, v. 53, no. 1, p. 1-1.
- Ehrlich, R., and Full, W. E., 1987, Sorting out geology—unmixing mixtures: Use and Abuse of Statistical Methods in the Earth Sciences, v. 1, p. 33-46.
- Folk, R. L., and Ward, W. C., 1957, Brazos River bar [Texas]; a study in the significance of grain size parameters: *Journal of Sedimentary Research*, v. 27, no. 1, p. 3-26.
- Friedman, G. M., 1962, On sorting, sorting coefficients, and the lognormality of the grain-size distribution of sandstones: *The Journal of Geology*, v. 70, no. 6, p. 737-753.
- Greene, T. J., Carroll, A. R., Wartes, M., Graham, S. A., and Wooden, J. L., 2005, Integrated provenance analysis of a complex orogenic terrane: Mesozoic uplift of the Bogda Shan and inception of the Turpan-Hami Basin, NW China: *Journal of Sedimentary Research*, v. 75, no. 2, p. 251-267.
- Guan, W., 2011, Provenance analysis of Upper Permian-basal Triassic fluviallacustrine sedimentary rocks in the greater Turpan-Junggar Basin, southern Bogda Mountains, NW China: Wichita State University.
- Guan, W., Yang, W., Jeffrey, B., Feng, Q., Liu, Y., Zhao, W., and Wang, Q., Distinguishing source areas of Upper-Permian fluvial-lacustrine deltaic sediment fills of a half graben through petrographic study, southern Bogda Mountains, the Greater Turpan-Junggar basin, NW China: Abstract Volume, Am. Asso. Petrol, *in* Proceedings Geologists Annual Meeting, New Orleans 2010.

- Hartmann, D., 2007, From reality to model: Operationalism and the value chain of particle-size analysis of natural sediments: *Sedimentary Geology*, v. 202, no. 3, p. 383-401.
- Ingersoll, R. V., Bullard, T. F., Ford, R. L., Grimm, J. P., Pickle, J. D., and Sares, S. W., 1984, The effect of grain size on detrital modes: a test of the Gazzi-Dickinson point-counting method: *Journal of Sedimentary Research*, v. 54, no. 1, p. 103-116.
- Johnsson, M. J., 1993, The system controlling the composition of clastic sediments: *Geological Society of America Special Papers*, v. 284, p. 1-20.
- Jun, G., Maosong, L., Xuchang, X., Yaoqing, T., and Guoqi, H., 1998, Paleozoic tectonic evolution of the Tianshan Orogen, northwestern China: *Tectonophysics*, v. 287, no. 1, p. 213-231.
- M. Friedman, G., 1967, Dynamic Processes and Statistical Parameters Compared for Size Frequency Distribution of Beach and River Sands.
- Şengör, A., Natal'in, B., and Burtman, V., 1993, Evolution of the Altaid tectonic collage and Palaeozoic crustal growth in Eurasia: *Nature*, v. 364, no. 6435, p. 299.
- Sengor, A., and Natalin, B., 1996, Paleotectonics of Asia: fragments of a synthesis.
- Shao, L. E. I., Stattegger, K., and Garbe-Schoenberg, C. D., 2001, Sandstone petrology and geochemistry of the turpan basin (nw china): Implications for the tectonic evolution of a continental basin: *Journal of Sedimentary Research*, v. 71, no. 1, p. 37-49.
- Suttner, L. J., 1974, Sedimentary petrographic provinces: an evaluation.
- Windley, B. F., Alexeiev, D., Xiao, W., Kröner, A., and Badarch, G., 2007, Tectonic models for accretion of the Central Asian Orogenic Belt: *Journal of the Geological Society*, v. 164, no. 1, p. 31-47.
- Xiao, W.-J., Zhang, L.-C., Qin, K.-Z., Sun, S., and Li, J.-L., 2004, Paleozoic accretionary and collisional tectonics of the Eastern Tianshan (China): implications for the continental growth of central Asia: *American Journal of Science*, v. 304, no. 4, p. 370-395.
- Xiao, W., Windley, B. F., Allen, M. B., and Han, C., 2013, Paleozoic multiple accretionary and collisional tectonics of the Chinese Tianshan orogenic collage: *Gondwana Research*, v. 23, no. 4, p. 1316-1341.

Xiao, W. J., Windley, B. F., Huang, B. C., Han, C. M., Yuan, C., Chen, H. L., Sun, M., Sun, S., and Li, J. L., 2009, End-Permian to mid-Triassic termination of the accretionary processes of the southern Altaids: implications for the geodynamic evolution, Phanerozoic continental growth, and metallogeny of Central Asia: *International Journal of Earth Sciences*, v. 98, no. 6, p. 1189-1217.

VITA

Dongyu Zheng was born in Shangrao, Jiangxi, China. He received his Bachelor of Science degree in geology in July 2014 from the Department of Earth Sciences at Jilin University. He received his Doctor of Philosophy in Geology and Geophysics from Missouri University of Science and Technology in May 2019. He worked as a Graduate Teaching Assistant at Missouri University of Science and Technology from 2014 to 2018.